DOE/NASA/2749-79/1 Vol 1
NASA CR-159670
C00-2749-42

Baseline Automotive Gas Turbine Engine Development Program Final Report

Edited By
C. E. Wagner and R. C. Pampreen
Chrysler Corporation
Detroit, Michigan 48288

April 1979

Prepared for
National Aeronautics and Space Administration
Lewis Research Center
Under Contract EY-76-C-02-2749.A011

for
U.S. Department of Energy
Office of Conservation and Solar Applications
Division of Transportation Energy Conservation

DOE/NASA/2749-79/1 Volume 1
NASA CR-159670
COO-2749-42

Baseline Automotive Gas Turbine Engine Development Program Final Report

Edited By
C.E. Wagner and R.C. Pampreen
Chrysler Corporation
Detroit, Michigan 48288

April, 1979

Prepared for
National Aeronautics and Space Administration
Lewis Research Center
Cleveland, Ohio 44135
Under Contract EY-76-C-02-2749

For
U.S. Department of Energy
Office of Conservation and Solar Applications
Division of Transportation Energy Conservation
Washington, D.C. 20545

Under Interagency Agreement EC-77-A-31-1040

Acknowledgement

This report covers all work performed under DOE Contract No. EY-76-C-02-2749.A011 from November, 1972, to June, 1979. The contract was initiated by the U.S. Environmental Protection Agency, was subsequently transferred to the Energy Research and Development Administration, and was finally transferred to the Heat Engine Systems Branch, Division of Transportation Energy Conservation of the U.S. Department of Energy. Mr. Charles E. Wagner was the Chrysler Corporation Program Manager. Mr. Paul T. Kerwin, NASA-Lewis Research Center, has been the Project Officer since 1977. Previous Project Officers were David G. Evans, NASA-Lewis Research Center, and Thomas M. Sebestyen, EPA. Mr. Robert A. Mercure, DOE - Division of Transportation Energy Conservation, has been the Project Coordinator since the technical management was turned over to NASA-Lewis Research Center through an interagency agreement. This program was originally proposed, awarded, structured, and launched at Chrysler under the direction of George J. Huebner, Jr., Director of Research, and James P. Franceschina, Chief Engineer of Power Plant Research.

Contributors to this report were: A. Billington, T. Golec, J.V. Gross, H.P. LeFevre, E.M. Kohl, J.J. Lewakowski, C.H. Mader, T.D. Nogle (Laboratory Personnel), F. Dosenberger, P.K. Jain, R.A. Kost, D S. Musgrave, R.C. Pampreen, N.W. Sparks, R. Swiatek (Design and Analysis), C. Belleau, W.F. Bertrand, J.M. Corwin, F.A. Hagen, J.R. Kirberg, A. Roy, P.J. Willson (High Temperature Materials), C.M. Elliott (Continuously Variable Transmission), and W.D. Bastow, O.K. Thiel (Piston-Engine Performance Analysis).

TABLE OF CONTENTS

TABLE OF CONTENTS (continued)

Abstract

This is the first of four volumes of the contract final report, which summarizes all of the work performed in a government-sponsored Automotive Gas Turbine Development Program (DOE Contract No. EY-76-C-02-2749.A011). In this first volume of the contract final report, results are presented from tests which were conducted on a Baseline Engine to document the Automotive Gas Turbine State-of-the-Art at the start of the program and to evaluate certain component improvement concepts. The documentation consisted of defining the performance characteristics of the engine and of a vehicle powered by this engine.

Component improvements in the Baseline Engine were to be evaluated on engine dynamometer tests, in the complete vehicle on a chassis dynamometer, and on road tests. These concepts included: advanced combustors, ceramic regenerators, an integrated control system, low-cost turbine material, a continuously variable transmission, power-turbine-driven accessories, power augmentation, and linerless insulation in the engine housing. Successful verification of improvements was to be the basis of upgrading the engine by incorporating these technology advancements in a new design called the Upgraded Engine.

1.0 SUMMARY

The Chrysler sixth-generation engine was used to document existing automotive gas turbine state-of-the-art and was identified as the contract Baseline Engine. The documentation consisted of defining the performance characteristics of the engine itself and of a vehicle powered by this engine. Subsequently, an extensive component-improvement program was carried out on the Baseline Engine for the purpose of evaluating certain concepts which, if proved beneficial, would be incorporated into the design of the Upgraded Engine. These concepts included:

1. Advanced combustor systems
2. Ceramic regenerator
3. Integrated control system
4. Low-cost turbine rotors
5. Engine/control oil supply system
6. Hydromechanical transmission
7. Power-turbine-driven accessories
8. Power augmentation:
   - Water injection
   - Variable inlet guide vanes
9. Higher cycle temperature
10. Linerless insulation

Where applicable, vehicular evaluation of these concepts was identified as Task 6.

On a standard automotive day (85°F Temp., 29.92" Hg. Press.) the Baseline Engine delivered 150 HP at design speed and at a design-speed turbine-inlet-temperature of 1850°F. The design pressure ratio is 4.1:1 at a mass flow rate of 2.3 lbs/sec and a rotational speed of 44,610 rpm. Design-speed SFC is 0.54 lbs./hp-hr; idle-power SFC is 1.90. Vehicle testing showed a combined-cycle fuel economy of 8.0 mpg (gasoline) and 8.8 mpg (diesel) with a zero-60 mph acceleration time of 11 seconds in a 4500-lb vehicle.

The following summarizes the testing carried out on the different advanced concepts.

- A variety of combustor configurations were investigated: pre-mixed/pre-vaporized, droplet-diffusion, dual-stage, torch ignitor and variable geometry. The configuration with pre-mixed/pre-vaporized combustion combined with a torch ignitor yielded the lowest emission values (0.41 gram/mile HC, 3.4 grams/mile CO, and 3.1 grams/mile NOx) and was best suited to vehicle driveability.

- Three ceramic core configurations were investigated for the regenerator. Within the range of specific flow required for the Upgraded Engine, a configuration with a triangular shape yielded values of effectiveness as much as 4 points higher than values for the metallic core used as reference

- Testing showed that engine controls must be more sophisticated than the original controls used on the Baseline Engine. A closed-loop control on turbine exit temperature was successfully applied to the Baseline Engine.

- Two new manufacturing processes were explored for potential for low-cost production of turbine rotors. Both the reusable pattern process by the AiResearch Casting Division of the Garrett Corporation (AiRefrac) and the superplastic forging technique (Gatorizing) by the Pratt & Whitney Aircraft group showed some promise.

- Tests conducted on the hydromechanical continuously variable transmission (CVT) revealed little gain in fuel economy with this type of CVT. Other types, such as belt-drive, were recommended for investigation.

- The arrangement of driving engine accessories from the power turbine instead of the gas generator was shown to be more practical and of lower cost

- Power augmentation with water injection was successfully demonstrated, but the results showed a strong need for erosion protection for the compressor. Augmentation of compressor performance with variable inlet guide vanes (VIGV) was demonstrated, although the increase in design-speed

pressure ratio was 5.4% versus the goal of 7.8%. Power augmentation with VIGV was 4% versus the goal of 12%. For the amount of compressor augmentation achieved, the engine power augmentation should have been 8%. The miss in achievable augmentation was caused by deteriorated turbine efficiency at maximum compressor augmentation. Aerodynamic design parameters would have to be revised to employ augmentation on the Upgraded Engine.

- Two high-temperature alloys were investigated for the Upgraded Engine compressor-turbine rotor: IN-792/Hf and MAR-M-246. Rotors made of MAR-M-246 were cast successfully in the AiRefrac process. No sound castings were made of IN-792/Hf with this process.

- The use of linerless insulation was successfully demonstrated.

All the advanced concepts, except for items 4 and 6 above were applied to the design of the Upgraded Engine. The development effort carried out on the Baseline Engine and the test results are described in this volume.

2.0 INTRODUCTION

This part of the contract consisted of four distinct areas of work which were carried out under five program tasks. These areas consisted of:

1. Documentation of Baseline Engine performance chacteristics (Task 1.0)
2. Documentation of vehicle performance with Baseline Engine (Task 2.0)
3. Evaluation, on Baseline Engine, of advanced concepts to be applied to the Upgraded Engine (Tasks 4, 5)
4. Where applicable, evaluation of advanced concepts with vehicular testing (Task 6)

The Chrysler sixth-generation engine was selected as the Baseline Engine. 4-door sedans weighing about 4,500 lbs. were used to evaluate vehicle performance with the Baseline Engine as originally designed and as modified by the different advanced concepts. The advanced concepts which were evaluated consisted of:

1. Advanced combustor systems (Task 5.1)
2. Ceramic regenerator (Task 5.2)
3. Integrated control system (Task 5.3)
4. Low-cost turbine rotors (Task 5.4)
5. Engine/control oil supply system (Task 5.6)
6. Hydromechanical transmission (Task 5.7)
7. Power-turbine-driven accessories (Task 5.8)
8. Power augmentation:
   Water injection (Task 5.9)
   Variable inlet guide vanes (Task 5.10)
9. Higher cycle temperature (Task 5.11)
10. Linerless insulation (Task 5.12)

3.0 BASELINE-ENGINE TESTING

The Baseline Engine, Figures 1 and 2, was released in January, 1965. The engine was originally targeted for a 3600-lb. vehicle exhibiting fuel economy and performance comparable to vehicles of that date. Principal design goals were: improved rotor response, cost reduction, and capability of driving production type vehicle accessories, specifically air conditioning and power steering from the power turbine. Exhaust emissions, particularly NOx, were not a consideration in the design of the combustion system although CO and HC were controlled to achieve a burner efficiency approaching 100% with minimum odor, carbon formation, et cetera. Power plant weight and geometric configuration were determined by requirements to have reasonable mass and to fit an existing vehicle.

The engine is a 4:1 pressure ratio, regenerative, free power-turbine design. It incorporates a single-stage centrifugal compressor, two axial turbine stages and variable power turbine nozzle vanes.

3.1 Engine Performance

Pertinent 85°F full-power characteristics along with other descriptive data are itemized on Table 1. Ten of these engines as well as three 1973 intermediate-size vehicles were built as baseline hardware for this program. Engine characterization is shown in Table 2, and station notation references are shown on Figures 3 and 4. Typical engine performance is shown in Figures 5, 6, 7, 8, and engine exhaust emissions on Figure 9. Vehicle exhaust emission levels, CO and NOx, were lower than those required to meet the 1975 standards (0.4 gram/mile HC, 3.4 grams/mile CO and 3.1 grams/mile NOx).

3.2 Engine Endurance Testing

Evaluation of Baseline Engine durability relied principally on dynamometer testing. Two endurance cycles were used which were designed to subject turbine components to an accelerated life test through the use of a transient-type cycle rather than the steady-state mode.

The initial cycle evolved from years of test experience from the Contractor's proving grounds, the highways of this country and accumulated knowledge of various test-cell endurance schedules. Since steady state operation in a vehicle is the exception rather than the rule, an all-encompasing test cycle, including several starts, part-and full-throttle accelerations and a shutdown period to expose rotor bearings to soak back temperatures, was chosen.

The cycle for the Baseline Engine was of one hour duration and included:

- 9 starts
- 15 wide-open-throttle accelerations
- 4 part-throttle accelerations
- 14.5 minutes total shutdown time (includes 10.5 minute soak period).

This was equivalent to an average vehicle speed of 49 MPH (assuming typical axle ratio, tire size, etc.). An automatic programmer controlled the engine over the one hour cycle. Safeties were provided for overtemperature, overspeed, low oil pressure, no start condition, et cetera. Strip-chart recorders provided a continuous record of events. Typical speed recordings which characterize the cycle are shown in Figure 10. Failed or malfunctioning parts were repaired or replaced as necessary.

A Baseline Engine was tested on this cycle for total of 4653.7 hours. Total test time on some of the significant components at final teardown is shown on Table 3. Where applicable, total test hours are also shown on components replaced at earlier teardown inspections because of part failure or update as indicated.

Final teardown revealed that the most significantly distressed components were located in the burner section although the only non-useable part was the burner tube. Figures 11 and 12 display the first-stage turbine rotor and nozzle, respectively. Note slight erosion at the leading edge. Metallurgically the components were considered acceptable for further testing.

The second endurance cycle, shown on Figure 13, alternately subjects the matrix to 1400°F at high-power conditions, followed by rapid cool-down to 900°F at idle. The thermal transients in this test sequence are far more extreme than any anticipated vehicular duty cycle, and they are designed to screen various matrix configurations for susceptibility to thermal fatigue cracking. See Figure 14. An acceleration from 60% to 100% speed was included to subject the elastomeric core ring-gear attachment system to high torque conditions.

4.0 BASELINE VEHICLE TESTING

4.1 Vehicle Performance

Three 1973 intermediate-size, 4-door sedans were modified to accept the Baseline Engine. The modifications included:

- Widen front track of chassis.
- Modify front cross-member.
- Relocate suspension-system torsion-bar rear anchors, revise rear-frame cross-memb· odify underbody to provide clearance for exhaust ducts.
- Relocate steering gear and modify steering linkage and column.
- Modify radiator yoke to receive air conditioning condensor, electric fan and engine and transmission oil coolers.
- Modify front-fender sheet-metal to accept engine inlet ducting; install in-tank fuel pump and return-line.
- Install hydraulic brake booster and accumulator.
- Modify transmission linkage.
- Revise car comfort system—install hot-gas/water heat-exchanger and air-conditioning compressor (axial type).
- Revise wiring harness as required.

Figure 15 shows a cross section and Figure 16 a fully assembled vehicle.

Vehicle performance with the Baseline Engine was documented for several configurations at the proving grounds using esta .ished test procedures. Driveability was evaluated during several road trips and ride/drive demonstrations.

Figure 17 shows the uncorrected speed-time and distance trace for two vehicles Their weights and ambient-temperature test conditions are noted. The speed-time values are also shown with and without air conditioning corrected to a 85°F day. Performance was judged satisfactory—0-60 MPH in 11 seconds. Figure 18 shows the engine/vehicle braking capability which compared favorably to the current conventional vehicles The braking position was fixed by the control system, and the full engine braking potential could not be realized due to linkage limitations.

Figure 19 shows the fuel economy for varying road-load speeds to 90 MPH, at turbine exhaust temperatures of 1300°F (corrected for standard day) and 1300°F (actual) for ambient temperatures of 33-38°F. Metal regenerator cores were utilized for these tests. An indicated, fuel economy – particularly at low speed – would be less than with a comparable spark-ignition reciprocating engine. These tests were supplemented by vehicle evaluations at the EPA facility in Ann Arbor, Michigan, and are discussed in Reference 1. Combined fuel economies of 8.0 mpg (gasoline) and 8.8 mpg (diesel) were measured.

These data were documented using an open-loop hydromechanical control and, as a result, operating conditions were not optimized. The introduction of the integrated electronic control system (closed-loop on power turbine exhaust temperature) was expected to optimize vehicle operation in the drive and braking modes and to result in improved fuel economy and reduced emissions as described further in this report.

In summation, the majority of the evaluators who drove the vehicles judged the vehicle response as acceptable Most evaluators were totally satisfied with vehicle noise levels and driveability Overall comments by technically knowledgeable personnel were favorable.

Table 4 describes the vehicles and summarizes the test hours and miles at the close of the program The fourth vehicle (Car 618) is a Chrysler-funded project that contributed extensively to the development of the combustor and electronic control systems.

4.2 Noise Control

Principal noise sources of gas turbine powerplants are:

1. airborne intake high-frequency noise.
2. airborne exhaust noise.
3. rotor noise.
4. high speed gear noise.

Airborne intake noise can be readily attenuated by directing the inlet air through a minimum of two duct bends of maximum allowable size and lined with a suitable acoustic material. Exhaust noise is treated in a similar manner. Additionally, as a general rule, minimization of noise at the exhaust terminus requires a diffusion section which reduces gas velocity to 100 ft./sec. at rated power.

Rotor-generated noise attributed to rotor imbalance and shaft bending can be negated by isolating the rotor sleeve bearings from the bearing carrier via oil film damping, et cetera. This technique was successful in the Baseline Engines. Noise control of high-speed gearing required: precise manufacture of the involute surfaces, modification of the involute (crowning, surface finish and treatment, such as Tufftriding), oil film-thickness control, et cetera. Gear-tooth-generated noise under lightly loaded conditions in drive-to-braking-mode of operation can be controlled by bonding aluminum dampers fabricated of fully annealed material (0.06-inch thick) to the gear disc with a suitable adhesive.

Baseline-vehicle proving-grounds tests for compliance with SAE Standard J986a (wide-open throttle acceleration from 30 mph at 50 ft.) indicated sound levels of 75.1 and 75.0 dBA for the right and left sides respectively. By comparison, the EPA Prototype Vehicle Standard is 77 dBA, the legal standard is currently 86 dBA and equivalent reciprocating engines were measured at levels of 81-82 dBA. Static noise evaluations of a baseline vehicle and a 1974 conventional vehicle powered by a V8 engine are compared on Table 5.

Further improvements were made to the noise control of a second vehicle and were documented at an independent test facility by EPA personnel. Discreet frequencies were taken, and the required A-weighting was applied to arrive at the results in Table 6. Thus, the noise level for the vehicle is 73 decibels, which is the highest average value recorded. The data in Table 6 were taken to obtain additional information on the vehicle. Turbine whine was noticeable but not objectionable inside the vehicle between 35 and 55 mph.

4.3 Inlet and Exhaust Ducting

An important consideration of gas-turbine/vehicle installation is the provision of adequate engine inlet ducting for the air filter capacity as well as noise control. Inlet restriction as well as exhaust restriction have an adverse and appreciable effect on engine perfomance. An exhaust pressure-loss of 1.0" H_2O results in a loss of 1 HP at design speed, as shown in Figure 20. Restrictions generated in the inlet-ducting/filter system manifest themselves in a similar loss of performance

4.4 Vehicle Comfort Systems

The use of an intermediate gas-to-water heat exchanger was predicated on two basic factors:

- The possible toxic-gas effect of exposing Freon 12 to high temperature.
- The ease of adapting the heat exchanger to the production configuration of a passenger compartment heating and air conditioning system and associated controls.

In this system, power turbine exhaust gas is passed through a gas-to-liquid heat exchanger containing conventional coolant (50% water/ethylene glycol), which is circulated through the standard vehicle passenger-compartment heater-core. A pump driven by a 12-Volt DC motor circulates the coolant through both the heat exchanger and the heater core. Thus, the passenger-compartment heater-core configuration retains the desirable reheat feature for the air conditioning system and eliminates any possibility of the decomposition of Freon due to contact with a high-temperature surface. Figure 21 is a schematic of this system. Production louver-controls are actuated from a vacuum reservoir which is integral with a trunk-mounted vacuum pump. Heater-system evaluation at -10°F demonstrated performance superior to that of systems installed in conventional vehicles.

4.5 Vehicle Operation Log

Vehicle running time/use cycle was automatically registered on a bank of pressure-sensitive timers installed in the vehicle's trunk, Figure 22. The timers were actuated via calibrated pressure switches and sensed engine compressor pressure. The engine pressure signal approximated engine speed.

Figure 23 summarizes the engine duty cycle. Note that 46% of the total engine run time is at idle. A majority of operating time is at speeds less than 80% gas generator speed.

The relationship between engine output power and accelerator pedal, also shown on Figure 23, was designed to simulate that of a conventional vehicle, e.g., 25% throttle is equivalent to 40% power. This arrangement was implemented to improve the driver's performance "feel,"—a psychological consideration as opposed to a technical consideration.

4.6 Vehicle Brake System

In several previous gas turbine installations, conventional brake boosters were modified to operate off engine pressure since a vacuum source was unavailable, and space limitations required the use of the relatively small hydraulic brake boost. On the Baseline Engine installation, oil pressure was tapped off the flow control circuit of the power steering pump. Figure 24 describes the hydraulic system and includes use of power-steering back-pressure to actuate engine controls, such as the power-turbine-nozzle actuator and the variable-inlet-guide-vane actuator. An accumulator supplies pressure during an emergency situation. This system was tested on two vehicles and judged acceptable for future installations.

5.0 ADVANCED COMBUSTOR SYSTEMS

5.1 Emission Control

It is generally believed that the gas turbine has continuous combustion, inherently low HC and CO emission levels, and, especially with a regenerative engine, high NOx levels due to high combustion temperatures. The automotive gas turbine is far from steady-state and generally does not have continuous combustion. During the Federal Drive Cycle, the fuel flow varies abruptly between zero and 140 pph, while the engine air flow changes by only a factor of 2. See Figure 25. The high fuel spikes are necessary to overcome the gas generator inertia and provide quick response to driver demands for increased power. Additionally for good driveability, it is necessary to shut off the fuel when power is decreased to minimize gas generator coast-down time. This also minimizes fuel consumption. Though conventional combustor technology can provide very low steady-state HC and CO emissions, these contaminants are likely to be real problems during transient operation. Emission tests also included exhaust sampling of a cold start, which contributes substantially to HC and CO emissions.

The steady-state range of fuel/air ratio of the combustor for the Baseline Engine extends from 0.0018 at engine braking to 0.0113 at sustained wide-open-throttle operation. For accelerati n transients, overall fuel/air ratio increases to 0.024. The automotive combustion system is also required to be compact, quiet, durable, odor-free, low-cost, non-smoking and very reliable. It is highly desirable that it operate equally well on a range of fuels from non-leaded gasoline to Diesel 1, in any mixture, without adjustment. The high burner-inlet temperature of a regenerative engine does not make it a worse producer of NOx than a nonregenerative engine. However, it does permit leaner combustion and lower peak temperatures so that low NOx is obtained while retaining HC and CO control.

5.1.1 Ambient Effects

Figure 26 shows the typical trend of exhaust effects due to inlet-air contamination. Any addition of NOx or CO to the inlet tends to increase the exhaust concentration by an equal amount. In some cases there was less change to exhaust CO levels than would be expected from measured values of inlet levels. This indicated some ability to oxidize incoming CO, especially when operating with high burner or engine cycle temperatures. Inlet HC is partially converted to CO.

This raises the question of correcting gas turbine exhaust emissions for intake contamination. The most accepted procedure is to subtract inlet contaminant mass from the corresponding exhaust mass, thus charging the vehicle for only the net change to the atmosphere. However, it is recognized that this procedure may not yield the exact values that the vehicle would have produced with a perfectly clean inlet. It is advisable to conduct tests with minimum intake contamination.

It must be noted that the hot FID hydrocarbon analyzer is used in testing (consistent with operation in Diesel fuel) and tends to read higher HC levels than a cold unit. Experience has shown that ambient air HC levels are higher with hot analysis. However, the vehicle dynamometer test data used hot FID for the exhaust only. The inlet values based on cold FID analysis, therefore, are low by comparison, resulting in conservative correction of HC data.

The effects of ambient humidity must also be considered. Tests with droplet combustion all show a tendency for lower NOx with increasing humidity. The exact extent seems to vary with the details of the burner, but the correction to 75 grains humidity as specified in the Federal Register for gasoline piston engines is a reasonable approximation and is used by Chrysler. Limited experience with humidity effect on premixed burners indicates no effect on NOx emissions if engine temperature levels are maintained. Humidity corrections are not used when testing pre-mixed burners, although inlet humidity is maintained near 75 grains when possible.

5.1.2 Cold Starting

In order to evaluate a burner in an engine or vehicle, it must first be able to cold-start and warm-up properly. In order to meet emission standards, it must light off quickly once fuel begins flowing. Automotive goals require reliable starting down to −20°F. The conventional burner used by Chrysler in the 1960's met this requirement consistently, even on Number 1 Diesel fuel. These burners used air atomizing fuel nozzles which require an air pump at all times. Nozzle air pressure of 2-3 psid (d = differential over compressor exit pressure) is required for light-off, 3-6 psid for idle and up to 10 psid

for fuel flows at full throttle. The engine-driven air pump provided on the Baseline Engine was well developed and virtually trouble-free. However, it was costly, large, and heavy, and its use compromised the engine design to provide a suitable drive.

All single-stage, pre-mixed combustor work was conducted without the use of an air pump. Hundreds of room-temperature starts were made with gasoline fuel and hundreds of hours of operation conducted. Running and hot-engine restarting were also successful on Diesel fuel. Room-temperature starting on Diesel fuel was borderline although little effort was applied toward development. The combustor configuration ran well without an air pump, and at the worst needed a starter-driven air pump or an air storage system for starting only.

The final burner configuration used a pressure-atomizing-torch fuel nozzle, requiring 20 psid fuel pressure. When starting, fuel was supplied to the torch first so that torch light-off occured before fuel reached the pre-mixer. The main fuel nozzle was an air-blast type with good atomization when differential air pressure exceeded ten inches of water. Sufficient atomization was required during cold cranking to permit propagation of the torch flame to the droplet mixture. (Conversion to pre-mixed burning occured automatically as regenerated air reached the pre-mixer.) Most development and demonstration work used total pressure from the compressor to provide maximum nozzle air ΔP for starting. Since this air by-passed the regenerator, some penalty in fuel consumption was encountered. Testing on the Baseline Engine used only burner ΔP for this nozzle. Both commercially available and in-house-designed air-blast nozzles were used.

5.1.3 Shut-Down

It is beneficial to use a 3-way solenoid (see Figure 27) at the fuel nozzle so that engine air pressure purges the fuel back to the tank. This prevents fuel from vaporizing into the hot engine and forming deposits of soft soot. Purging therefore helped avoid plugging of the nozzle passages and prevented the discharge of soft soot on restarting. It also provided the fill-time lag so that on start-up the torch could be lit before fuel reached the pre-mixer.

5.1.4 Determination of Vehicle Exhaust Emissions-Federal Drive Cycle

The Federal CVS emission testing system which is specified for gasoline light-duty vehicles is not suitable for turbine emission testing. The turbine air flow is higher than most CVS system capacities. Large-capacity CVS systems would further dilute the already diluted turbine exhaust and make accurate emissions determination difficult. The Baseline Engine Vehicle System must average only 3.5ppm NOx to meet 0.4 gram/mile. Also, the use of Diesel fuel required hot sample lines and continuous analysis to prevent loss of sample by condensation.

The test procedure involved the use of continuous analysis of all emission species. Fast-response instruments were essential for accurate data. The vehicle was started and driven over the cycle as prescribed in the Federal Register. Emission sampling was begun a few seconds before the key was turned on and continued after keyoff until the gas generator stopped rotating. The emission levels and suitable airflow signal were continuously recorded on a multi-channel tape. See Figure 28.

The CVS Bag Sampling System was used to collect average intake air contaminant levels during a test. These contaminant levels generally were nearly constant during a test period. Efforts were made to maintain ambient humidity at a nominal value of 75 grains.

5.1.5 Calculations

The tape-recorded data was processed by computer to yield raw exhaust mass emissions. The calculations were made at one-second intervals (grams per second) and summed over the entire cycle. For 1975 test procedures, the cycle was split at the 505-second point, and the usual weighting formula was applied.

The program printed the total cycle air flow and used it with the inlet sample bag concentrations to compute intake contaminant masses. The difference between intake and raw exhaust is the net emission mass. Inputs of wet- and dry-bulb test temperatures permit computation of the inlet humidity. NOx emissions were corrected to 75 grains as specified in the Federal Test Procedure. It was believed that this correction was valid for droplet diffusion flames, but not for homogenous reactions. Complete reporting includes raw, net, and net corrected results.

The program also provided a breakdown of the emissions according to idle, acceleration, cruise and deceleration modes of operation and for specified sections of the cycle time. Total carbon computations of fuel consumption were available although, for accuracy, reliance was generally on the weighed-can method.

5.2 Combustor Development

Two basic paths of combustor development were followed. One path used droplet diffusion flames to obtain low (less than 3.0 grams/mile) NOx levels and was the combustor provided in the Baseline Engines. The second path used homogenous reaction to get very low (less than 0.4 gram/mile) NOx levels. All efforts were toward combustion control, rather than clean-up, and low emissions in all normal operations, not just on the Federal Test Cycle.

Combustor testing began on one of two "engine fixtures". These were complete Baseline Engines except that they had no power turbine. Shop air was supplied at the power turbine rotor location to provide control of regenerator inlet temperature (emission sampling was ahead of this air injection). Thus, a burner concept started out in its ultimate environment with the first test being its ability to start the engine from room temperature. The burner was tested in the quasi-steady-state conditions of an engine and its contol system. Because both variable power-turbine-nozzles and variable cooling air were used, turbine-inlet and regenerator-inlet temperatures could be set from the normal operating conditions. The one shortcoming of these fixtures was that, by omitting the power turbine and output load, the burner did not operate under true conditions during all transients, specifically engine braking.

A burner which has satisfactory start and steady-state characteristic must undergo final testing and development on a complete vehicle dynamometer. The dynamometer has driving capability to simulate engine braking, and the engine includes the automatic power-turbine-nozzle actuator. This facility was used, along with actual vehicles, to develop transient emission control.

5.2.1 Droplet-Diffusion Flames

There are two things to be done to control NOx in droplet-diffusion flames—minimize the peak temperature and minimize the time at that temperature. For CO control, (See Reference 2), the air fuel mixing must be well defined and sufficient reaction zone residence time at temperature provided. If CO is controlled HC will generally not be a problem except at flame-out and light-off conditions. Since these conditions occur up to 200 times during the Federal Cycle, precise fuel control and ignition requirements must be met. At the time of this work, the most developed burner along these lines was the burner for the Baseline Engine.

This concept first demonstrated emission levels of 0.29, 3.41, and 2.68 grams/mile net-corrected HC (Cold FID), CO and NOx, respectively, over a 1972 cold-start cycle. The Baseline Engine burner was a direct evolution of this concept, and testing on a Baseline Vehicle resulted in 0.85 HC (Hot FID), 2.58 CO and 2.10 NOx net-corrected grams/mile on the 1975 cold start cycle. On the highway fuel-economy-cycle emissions were 0.09 HC, 0.66 CO, and 1.19 NOx. Though no standard existed for this cycle, the data exhibited the proper spirit of emission control. It should be noted that driving the prescribed emission test cycle required the driver to constantly switch between accelerator and brake, thus making transient emission characteristics far more dominant than steady-state emissions. The fuel-economy cycle is more typical of the modulating-throttle plus occasional braking, characteristic of normal and prudent real-life vehicle operation.

Approximate steady state NOx and CO levels are compared with an earlier conventional burner in Figure 2[9]. Exhaust HC is typically lower than intake HC for the conditions shown. Extensive Baseline Vehicle emission tests were conducted by EPA with results reported on Pages 5-7 and Appendix A of the Ninth Quarterly Progress Report. These results show that this concept is capable of meeting relatively low NOx even in a full-sized car (4500 lbs) with relatively poor fuel economy. The same technology applied to an advanced gas turbine vehicle having twice the fuel economy should produce half the emissions.

5.2.2 Pre-Mixed Burning

It is commonly accepted that very low NOx levels (along with Low HC and CO) can only be achieved by avoiding droplet burning-i.e., by burning a homogenous, pre-vaporized and pre-mixed charge. Since the combustor must generally burn lean, it is most practical to pre-mix lean rather than rich.

The first demonstration of this combustion process was made early in 1972. A stable, lean reaction was produced with very low emissions and no visible flame. This concept was supplied with gasoline fuel, with vaporization and mixing taking place simultaneously within the burner. It would cold-start as a droplet-diffusion flame and convert automatically to pre-mixed conditions as the engine warmed up. No flame-holding device were used. However, range of operation between lean flame-out and high NOx levels was very narrow.

For the control of automotive emissions, range must be defined as the operating limits within which the emissions levels are low enough to meet the emission standards involved. Experience has shown that flammability limits are wider than emission limits. For reasonable combustor size, the lean limit, where CO becomes excessive, is the point at which reaction zone temperature is about 2000-2100°F. The upper limit (high NOx levels) is at about 3000-3200°F. These limits will vary somewhat relative to actual size of engine and vehicle, fuel type, control system, et cetera. Several concepts can be employed to provide the wide range of overall fuel/air ratios required by the gas turbine.

One of the most obvious concepts is the use of variable-geometry burners, which provide increased combustion airflow to correspond with increases in fuel flow. It was never felt that this would really be practical because of increased cost, size and weight, questionable reliability, and precise, fast-response control requirements. However, at one time there was no other apparent solution, and many attempts were conducted. These efforts produced moderate range (but never enough) and were plagued with flashback and instability problems.

A less restricted approach was taken by Solar Division, International Harvester, under EPA Funded Contract No. 68-01-0464. This approach resulted in a large, complex burner, Figure 30, capable of very low emissions over a wide range of steady-speed conditions. It was tested on one of the engine fixtures, and results are shown on Figure 31. It had poor response to transient operation and mechanical problems with the 12 variable ports. No attempt was made to provide an automatic control system for this burner since it was developed principally for fixture testing.

An alternate approach which avoided the use of variable geometry was conceived in the fall of 1973. A dual-stage combustor, as shown on Figure 32 was used with the fuel split between stages which was varied to minimize the emissions. Pressure drop was limited to 3%, although burner size and weight were somewhat greater than desired.

Considerable development effort was conducted on this concept, including dynamometer-engine and vehicle operation. A crude hydromechanical fuel splitting system enabled adjustment for the good range of steady-state emissions shown on Figure 31, which shows a comparison with the Solar burner results. With a compromise setting, it permitted street driving of the vehicle but not minimum emissions.

Further efforts were put forth to develop an electronic control system using two electronic metering valves for fuel splitting. A programmable analog computer was used for this activity. Problems of instability due to burner/control interaction during transient operation prevented the achievement of good transient cycle emission results. However, it was estimated that this combustor with a suitable-fuel-splitting control could be developed to meet a NOx level of 1.0 gram/mile in a Baseline-Engine vehicle or 0.4 gram/mile in an Upgraded Engine vehicle.

In this final concept, Figure 33, use of a torch ignitor provides the required wide range of steady-state emissions-control from a single-stage lean pre-mixer. As compared to spark ignition, the torch is continuous, provides more energy, and contacts a larger volume of pre-mixed charge. This permitted stable, low-emissions operation down to pre-mixed primary-zone fuel-air ratios of 0.015-0.020. A compact and reasonably simple combustor was demonstrated with potential for meeting the most stringent exhaust emission standards while maintaining "automotive practice". This concept showed definite potential for development to meet the 1976 standards even on the Baseline Engine vehicle.

Best emissions documented on the Baseline Engine vehicle, 4000-lb inertia weight, gasoline fuel and electronic control (which was not totally optimized) were

No.	Type	HC (Cold)	CO	NOx
68	Cold 75	2.68	8.57	0.44
71	Hot 74	1.48	7.47	0.34
76	Hot 74 (no engine braking)	1.19	3.84	0.37
69	FEC	*0	1.59	0.10

*HC emissions varied from −0.10 to 0.06 and is considered as zero HC.

HC and CO required further deceleration control development. Only the torch flame is maintained during compressor decelerations. At steady vehicle speeds on the vehicle dynamometer, exhaust HC levels were lower than intake values, and the following emissions were demonstrated:

Test No.	Car Speed	gr/mi HC (Cold)	CO	NOx
74	30 MPH	0	1.17	0.15
	40 MPH	0	0.82	0.13
	50 MPH	0	0.57	0.12
	60 MPH	0	0.46	0.17

Still another means of improving burner low-emissions-range is by raising the burner inlet temperature. Though this would increase NOx from a given burner, it permits the burner airflow to be reapportioned for leaner operation at the minimum fuel requirement (CO limit) Then the fuel flow can be increased a greater amount before reaching the NOx formation limit. Because of present material limitations, little use was made of this principle, but it is in the right direction for excellent emission control in advanced, efficient, high-cycle-temperature, regenerative gas turbines.

Another area for attention is the reaction zone. Strong recirculation and minimization of wall quenching help to obtain a good lean limit. While mixture distribution is very uniform in these reactors, wall cooling can result in high CO levels. By having the pre-mixed charge enter at a tangetial position, strong recirculation results so that a faster and more complete reaction takes place. In addition, a fence around the reaction-zone wall is used to mix in with the cooler gases flowing there.

5.3 Transient Operation

Having a burner which can operate with low emissions over a wide steady-state speed range is only part of the development effort. Making it comply with the transient emission standards is also difficult. Both the droplet-diffusion and pre-mixed burners operate lean under steady state conditions but become rich on start-up and full acceleration schedules.

5.3.1 Acceleration NOx Control

Figure 34, shows various lines that are characteristic of any fixed-geometry burner. The operating line a-d for speeds from idle to 80% speed, (which is the range required to drive the Federal emission cycle) lies between the CO and NOx limit lines indicating good emissions over this range. If the throttle is suddenly moved from idle to 80% speed, the fuel flow will follow the schedule a-b-c-d, and about 0.7 second will elapse for the speed change. NOx is controlled both by the rich combustion process and the short duration of time. If the throttle is moved slowly enough to limit the fuel schedule to bounds defined by a-e-f-d, than the NOx is controlled by the leaness of combustion, although such an acceleration will take 6-8 seconds.

The area between lines e-f and b-c is the problem. Operation just below line g-h has the hottest combustion and therefore the highest NOx formation rate. Pre-mixed burners receive a more pronounced effect because all of the mixture is at peak conditions, whereas droplet burning has rich and lean regions, each with NOx formation rates lower than the average mixture rate.

In driving the Federal Test Cycle, the actual throttle movements are dependent on many factors such as vehicle response, driver attitude and ability, throttle sensitivity and repeatability and compressor response. An effective emission control system must account for all conditions. One way to accomplish acceleration NOx control is to use a fuel control system which avoids this operating region and can jump across it. Figure 27 is a schematic of such a system as used on early vehicle demonstrations of the single-stage, lean-pre-mixed burner. For slower throttle movements, acceleration fuel is limited by orifice "A" to levels below those producing high NOx. Orifice "B" is opened only when speed demand is significantly greater than actual speed; thus A and B flow in parallel to jump to the maximum fuel schedule. For moderate rates of throttle movement, several jumps occur as speed error is alternately high and low.

This schematic also shows the power-turbine-nozzle blip arrangement used to assist in controlling acceleration NOx. Blipping is the term used for opening the nozzles during engine acceleration. By opening these nozzles slightly during the acceleration more energy can be extracted by the compressor-turbine Figure 35 shows the effect of blipping on gas generator speed and acceleration fuel flow for a stepped throttle movement from idle to 70% gas-generator-speed. Note that with blip, the speed actually overshoots demand at less than 0.6 second, and less total fuel is required Improved NOx control is primarily the result of this shorter duration of acceleration fuel flow This blip action is also triggered by a significant speed-error signal, and, in this case, the solenoid controlling orifice "B" is delayed until the blip actually takes place, thus accounting for the hydraulic lag time. The blip is accomplished by closing the nozzle actuator drain line and feeding it with oil supply to force the piston out until switch 1 is tripped. This leaves the drain closed, but stops feeding oil supply. Switch 2 prevents activation when the piston is in the extended, engine braking, position. The improvement in compressor rotor response does not necessarily mean an improvement in vehicle response, however, because the power turbine is not being fully accelerated until the blip is over and the nozzles return to the power position.

5.3.2 Deceleration HC & CO Control

The problem of controlling deceleration HC and CO is similar to controlling acceleration NOx. Again refer to Figure 34. If the throttle is suddenly closed from 80% speed, fuel flow is abruptly stopped, and the nozzle is bled back to the fuel tank, resulting in only a very narrow HC spike as the lean flame limit is passed. A second narrow HC spike occurs as fuel flow returns, and the burner relights. These narrow spikes do not prevent meeting the HC emissions standards of 0.41 gram/mile. No CO spiking is evident under these conditions. However, if the throttle is closed gradually in such a manner that the fuel-flow drops just below the CO-limit line, then CO and HC will be high throughout the deceleration, and the standards may not be met. To insure HC and CO control, the fuel control system should shut off the fuel whenever demand drops below the CO limit line established for the particular burner

An alternate approach is to maintain deceleration fuel flow at the CO-limit line and thus maintain continuous combustion. This approach showed the ability to maintain HC levels below intake values throughout the entire emission test cycle. However, driveability was impaired somewhat since gas generator decelerations were slower, and fuel consumption was increased. No significant NOx penalty was encountered.

5.4 Multi-Fuel Operation

The multi-fuel capability of several turbine combustor concepts was successfully demonstrated A broad spectrum of fuels was tested, but not necessarily optimized for emissions, on the droplet-diffusion combustor, Figure 36, and lean pre-mixed, pre-vaporized combustors, Table 7

A visual demonstration of the multi-fuel capability prepared in early '76 was comprised of 6 one-gallon containers mounted on the front bumper of a Baseline Vehicle, Figure 37 The containers were plumbed with clear plastic tubing and a valving arrangement, such that the engine could be operated on vehicle tank fuel or one of the container fuels. The alternate fuel samples were heavily doped with dye to aid in visualization. Typically, the tank fuel was diesel 1, but in many instances the fuel was a mixture of diesel 1 & 2, gasoline, and/or JP4, depending on availability Sample fuels demonstrated with a droplet diffusion combustor included diesel and gasoline, ethanol, broad-cut, coal-derived fuel, 60/40 diesel isopropanol, and 60/40 gasoline methanol

Continuing development of the pre-mixed/pre-vaporized combustor concept in a test-cell engine with alternate fuels exhibited similar results. Table 7 shows the results of steady-state idle speed and typical idle-to-70%-speed acceleration experienced during an urban-cycle test. The only adjustment made during these tests was to the torch to maintain it at stoichiometric conditions. The coal-derived fuel obtained from pyrolysis resulted in high NOx levels that were attributed to the level of chemically bonded nitrogen. Fuel containing a high content of sulfur, ash, residue and/or bonded nitrogen will require further processing to make it acceptable for turbine use.

5.5 Odor Evaluation

During the course of engine development, a major deficiency consistently identified was that of exhaust odor during cold starting, particularly when using a lower-grade diesel fuel (high sulfur content). In an effort to characterize exhaust odor on the advanced burner concepts, an engine was assembled on a portable test stand and equipped with a self-contained multi-fuel system. This would provide the flexibility to permit cold-starting the engine at various ambient temperatures down to -20°F.

After preliminary work was concluded, an advanced pre-mixed/pre-vaporized combuster was installed, and an attempt was made to associate the presence of odor with HC generated from gasoline fuel during a cold start (70°F). (Diesel fuel was not to be used with the LA's regenerator cores installed in this engine). However, odor levels were minimal and certainly not objectionable. Since the problem did not appear to be critical, the cold-start/odor evaluation was terminated to permit higher priority work to proceed.

5.6 Pressure-Drop Effects

The pressure-loss across the combustor is very important to low-pressure, automotive gas turbines, especially at low power levels. Figure 38 shows that a given engine looses power and suffers an increase of specific fuel consumption with increasing pressure-drop. As pressure-drop is reduced, SFC and engine size are reduced at a given power level. Pressure drops greater than 3% should not be considered for automotive use. The burner of the Baseline Engine has approximately 2% pressure-drop. In order to use variable-geometry burners and maintain very low pressure-drops, both primary and dilution zones may need to be varied, such as was implemented on the Solar burner.

5.7 Combustor Materials

A limited effort was made to evaluate ceramic components in combustor systems. Two silicon-nitride burner-tubes were run with the burner configuration of the Baseline Engine. One silicon-carbide-coated-graphite first-stage reactor tube was evaluated with the dual-stage concept. All test samples developed cracks after short running times. Such applications are desirable because of lower weight, thermal inertia, and potentially low cost.

6.0 CERAMIC REGENERATORS

6.1 Background

Metallic regenerators were developed and tested for several years prior to their use in the Baseline Engine. Maximum durability exceeded 3000 hours in an endurance engine. The concept of a ceramic regenerator, however, offers potential advantages in a number of areas, and, since the design of the Baseline Engine, substantial progress in the area of ceramic regenerator technology has been made. Specific areas of potential advantage are:

1. Improved engine efficiency by allowing increased engine operating temperature.
2. Lighter weight — approximately one-half that of a metal regenerator.
3. Higher effectiveness at low flow rates, due to lower axial heat conduction.
4. Simpler sealing because of low thermal distortion.
5. Potentially lower cost due to the use of non-critical materials.

Some original work was performed in this field as early as 1960. These tests were confined to a regenerator fixture, and the matrices of that time showed deficiencies of a technological and material nature. Thinner, stronger stock and finer, more uniform passages were required. These preliminary studies indicated that ceramic regenerators would satisfy the automotive gas turbine requirement if satisfactory technological progress could be made. This, of course, would involve development, not only of matrix material and shape, but also of suitable drive, suspension, and sealing systems.

During the late 1960's and early 1970's, ceramic regenerator work was deferred pending development of a reliable design by the ceramics industry. By 1973, such designs were readily available, and the task of converting the Baseline Engine was begun.

6.2 Conversion to Ceramic Regenerators

When the decision was made to convert the Baseline Engine from metallic to ceramic regenerators, several basic guidelines were established:

1. The ceramic regenerators should fit in the existing envelope with a minimum of mechanical changes.
2. Seals, drive-gear, and other related components should closely follow the established, trouble-free designs proven in the Baseline Engine.
3. The conversion should take place with a minimum of delay, necessitating the use of off-the-shelf core and seal materials.

6.2.1 Matrix Selection

Comparison of theoretical performance among several versions of available ceramic matrices and the current metal regenerator indicated that, for the same size and pressure-drop, the ceramic core should be superior to the metal core at idle and part-throttle conditions. The best overall performance should be from a ceramic matrix with rectangular passages. Results of this study are shown on Figure. 39.

On the basis of the above comparison, specifications were drawn and discussed with prospective vendors. Ceramic technology at the time was not capable of producing a rectangular matrix, but two alternate types were proposed:

- Type "A", a wound triangular or "sine wave" shape,
- Type "B", nested glass tubes forming a hexagonal shape.

Samples of currently-available matrices of both types were inspected for pressure-drop, and the final selection of each type of matrix was based on its closeness of match to the Baseline Engine's pressure-drop. Since envelope constraints required use of the same overall diameter as the metallic regenerator, matrix thickness was adjusted as necessary to correct the pressure-drop. Final matrix designs selected are shown on Table 8. Baseline metallic matrix specifications are shown for comparison.

6.2.2 Regenerator Procurement and Inspection

Several ceramic cores of each type were procured, inspected, and fixture-tested prior to installation in the engines. Inspection procedures were patterned after those developed for metal regenerators. Preliminary screening for acceptable pressure-drop was carried out with the cold-flow fixture shown in Figure 40. Metered air was introduced to a known area of the matrix and allowed to exhaust to atmosphere. Using the pressure, temperature, and flow conditions in the flow cup, the pressure-drop under engine operating conditions was calculated from Figure 41. These data were used, not only for core acceptance, but also for ensuring that each engine was fitted with a matched set of cores.

Following flow check, a leak-test fixture was used to check for porosity and internal voids. A cylindrical volume of matrix was sealed at each side of the core and pressurized. A flow-meter measured the make-up air required to maintain pressure. Each regenerator was then dimensionally checked, with particular emphasis on surface flatness. Close-up photographs of the matrix were taken for computer-aided graphical analysis of passage geometry.

Finally, each regenerator was fitted with a ring-gear and tested in the regenerator fixture This fixture was designed to match, as closely as possible, actual engine conditions. Compressed air was first heated to simulate the required compressor-discharge temperature and then passed through the high-pressure side of the matrix, where it picked up additional heat. The air was then throttled to simulate the pressure-drop across the turbines and heated to a fixture-limited inlet-temperature of 1200°F. The hot air then passed through the low-pressure side of the matrix, where it gave up much of its heat before being exhausted to atmosphere. A variable-speed external drive system was used to rotate the regenerator, and drive speed and torque were monitored to evaluate the seal coefficient of friction. Standard ASME metering orifices were used to check airflows throughout the fixture, permitting accurate measurement of seal leakage. Temperatures were recorded by means of thermocouple grids near both faces of the matrix, and effectiveness was calculated and corrected, through a computer program, for actual engine conditions of 1350°F at the inlet to the low-pressure side.

6.2.3 Drive System

Drive and suspension methods are similar to metallic regenerator practice. Optimum seal performance requires freedom of matrix movement in all directions except rotationally. To achieve this freedom, the spherical, graphite bearing of the metal core was replaced by an elliptical, graphite sleeve, which was designed to slide in a cylindrical bore in the ceramic hub. The core was rim-driven using a drive-pinion and ring-gear identical to those used with metal cores. Past experience with a variety of suspension and drive systems demonstrated the superiority of the center-support-rim-drive concept with metal cores, and this method worked equally well with ceramic cores

Two different methods of attaching the metal ring-gear to the ceramic-matrix rim were tried.

1. Mechanical mounting was used successfully with early Type "A" matrices. This method utilizes solid ceramic drive-pins cemented in the matrix rim; these pins were engaged by spring-loaded metal drive-shoes suspended from the gear and rim. This method had the best life potential at extreme temperatures, but the cost penalty was greater, and acceptable gear runouts were difficult to achieve

2. Elastomeric mounting, now the preferred method, was accomplished by fixturing the gear and its rim concentric with the matrix and injecting silicone rubber into the annular space between them This method was more economical, and accurate ring-gear runouts of less than 0 01" were typical However, careful design was required to keep the elastomer temperature below 550°F More detailed information on elastomer potential is given under "Elastomeric Drive Development," below. Figure 42 illustrates a typical elastomeric mount.

6.2.4 Seal System

In keeping with the conversion guidelines, standard diaphragm-type baseplates were used for both inner and outer seals, as shown in Figure 43. Inner rim and outer "D" rubbing seals are high-temperature graphite from the metallic regenerator assembly, and only the crossarm-seal coating was changed to achieve compatibility with the ceramic matrix The coating selected contained 85% nickel oxide and 15% calcium fluoride, this was the best available material at that time This coating has the advantages of low coefficient of friction (0.2) and extremely low wear-rate (theoretical coating life = 40,000 hours), but alleged heath hazards attributed to nickel compounds dictated the need for the eventual replacement of the nickel oxide. The program to perfect a suitable substitute is discussed under "Seal Coating Development," below

6.2.5 System Performance

Five of the Baseline Engines, fitted with ceramic regenerators of both matrix types, were endurance-tested for over 2200 hours under the severe accelerated wear and thermal shock test cycle. As shown on Fig. 13, the cycle alternately subjects the matrix to 1400°F at high-power conditions, followed by rapid cool-down to 900°F at idle. The thermal transients in this test sequence are far more extreme than any anticipated in the vehicular duty cycle and were designed to screen various matrix configurations for susceptibility to thermal fatigue cracking. A 60%-to-100%-speed acceleration was included to subject the elastomeric core/ring-gear attachment system to high-torque conditions. The engine was subsequently modified to have the regenerator cores driven directly from the power turbine reduction gearing to simulate the free-rotor concept to be used in the Upgraded Engine. This drive arrangement resulted in a more severe matrix-temperature-gradient under conditions of cold-engine start-up, followed by a rapid demand for power.

All of the regenerators performed well under the 1400°F-cycle, with 581 cycles logged on Type "A" cores and 521 on Type "B". The only difficulty experienced was with the two "Thinwall," Type "A" regenerators; both showed failure of the outer-most matrix layer under the elastomer pads after 9 cycles. Following repair and rebuild with increased flexibility in the elastomeric mount, discussed below under "Elastomeric Drive Development," each core completed 472 additional cycles without incident before the end of the Baseline Engine program.

6.2.6 Seal Coating Development

As discussed above, concern had been expressed over the use of nickel oxide as a seal-coating material because of the alleged health hazard of nickel compounds. While the amount of nickel oxide in the Baseline Engine's exhaust was extremely small (on the order of 1 $\mu g/m^3$) basic research was carried out in the area of seal coatings to seek an acceptable substitute. A number of potential materials were tested, as listed in Table 9. Fixture testing consisted of rotating a small matrix sample against a simulated seal in an electrically heated furnace. Rubbing speed, seal load, and operating temperature were set to match any anticipated engine condition, and drive torque was continuously recorded. Figure 44 shows the results of several of these tests, and illustrates the lower coefficient of friction of the Type "A" matrix as compared to the type "B", regardless of the coating used. This phenomenon was verified on a fixture test of full-sized regenerators, where typical drive torque of 70 lb-ft (Type "A" matrix) compares to 90 lb-ft for Type "B". It is believed that this discrepency results from the basic design of the matrix. The nested glass tubes are less porous than the wound ceramic, and the calcium fluoride, which acts as a dry lubricant, is less readily embedded in the glass.

Only one advanced coating (calcia-stabilized zirconia) was engine-tested. Wear-rate was considerably higher than with nickel oxide, as shown on Table 10, but the projected life of 2300 hours is still quite adequate for a development program. However, the higher required torque (110 lb-ft) produced excessive gear wear.

6.2.7 Elastomeric Drive Development

All ceramic regenerators were eventually converted to the elastomeric mounting concept. During development of this method, a number of regenerators exhibited small areas of cohesive failure of the elastomer. These tears originated at stress risers such as bubbles in the elastomer surface, and enlarged very slowly over a period of several hundred test hours, until the mount was deemed unsafe for further running and replaced. These failures are believed to be caused by a gradual shrinkage of the material over an extended period at high temperature. A comprehensive program was established to fully document changes of properties with heating.

Several alternate elastomers were evaluated, but they all showed lower properties (particularly in the area of tear strength) than the Dow-Corning Sylgard 187. Samples of Sylgard 187 showed no appreciable change in elastic or shear moduli after 300 hours at 500°F, indicating that, once initial shrinkage is allowed for, this material should function well in the Upgraded Engine environment.

To compensate for elastomer shrinkage, a flexible mount, as shown on Figure 45, was developed. This design permitted relatively free radial movement of the elastomer to allow for thermal expansion, while still retaining sufficient axial and circumferential rigidity to transmit the drive torque. As discussed above, the flexible mount was extensively tested in the endurance engine and remained trouble-free throughout the balance of the program. It should be noted at this point that the basic concept of this mount is a sound one. To verify the integrity of the design, a mount was statically tested to failure using the arrangement shown on Figure 46. Gradually increasing torque was applied to the drive pinion, and ring gear deflections were noted. The mount sustained a load of 720 lb-ft, as contrasted to a typical maximum torque of 70 lb-ft.

6.2.8 Regenerator Drive Torque Study

Much of the success of the flexible mount was undoubtedly due to the remarkably low drive-torque requirements inherent in the pressure-balanced seal design. To verify that drive torque does not increase with running time, a high-time (300 + hours) Vendor-A-core and nickel oxide crossarm were tested in the regenerator fixture. The test showed that the glaze build-up on the matrix surface reduced the drive torque by an average of 35%, with torque at 100% dropping from 81 lb-ft. to 53 lb-ft.

To further study the effect of operating conditions on regenerator torque, an in-line torquemeter was installed in the core-drive system of the endurance engine. Torque was measured over a wide range of engine conditions, with results as shown on Figure 47. It was found that the torque with the nickel oxide crossarm was unchanged over a temperature range of 1000-1400°F and was only slightly dependent on speed. As expected, the major influence on torque was compressor discharge pressure, which provides most of the force that clamps the seal elements to the matrix. Since these cores had 200+ hours at the time of the evaluation, overall torque was correspondingly low, i.e., 56 lb-ft at 100% - speed conditions. On the Baseline Engine, therefore, the maximum power requirement to drive both regenerators was less than 0.5 horsepower.

6.3 Improved-Effectiveness Matrix Development

Once the feasibility of operating the ceramic regenerators in the Baseline Engine was proven, the next step was to test matrices of increasingly higher effectiveness and to actually demonstrate the performance improvement shown possible by the theoretical studies illustrated in Figure 39. As shown on Figure 48, 1% increase in regenerator effectiveness results in a 3% reduction in idle fuel consumption. For this part of the program, it was decided to work with Type "A" matrix, in view of its proven lower torque requirements and potential for the greatest reduction in wall thickness. Several cores were tested with increasingly thinner walls and smaller hydraulic diameters, to the limit of the vendor's tooling capability. New tooling was made on the basis of the earlier test results, and the final set of cores achieved the program goals of 0.003-in. wall thickness, 0.020-in. hydraulic diameter, and 76% open area.

The fixture test results are shown on Figure 49A. The Upgraded Engine pressure-drop scaled to the Baseline Engine size, was 32 in. H_2O, — somewhat higher than the Baseline Engine design value of 24 inches and resulting in a power loss of 8 HP. It can be seen that the Upgraded Engine would have a lower airflow per unit matrix area, and the resulting pressure drop would reduce to the design value of the Baseline Engine. At these low specific airflows, the effectiveness of the ceramic matrix shows the greatest improvement over the metallic type. The gain in engine fuel economy is substantial as shown on Figure 49B. The advantage in effectiveness, combined with the benefits from higher cycle temperature made possible by the ceramic matrix, show the ceramic regenerator to be a strong contender among potential automotive turbine heat exchangers.

6.4 Ceramic Regenerator Thermal Analysis

In a free rotor engine, the regenerator matrix temperature can increase substantially within a few seconds, while the relatively massive solid hub and the matrix rim which is protected by the seal remain near their initial temperatures. This can result in significant circumferential temperature gradients as well as larger radial and axial gradients than for a regenerator which is driven by the gas generator where there is reasonably close coupling between the regenerator speed and the engine air flow. Thus, a thermal analysis for this severe condition, a cold start quickly followed by a full acceleration, was conducted in support of the mechanical design of the regenerator.

The matrix was divided into 36 pie shaped sectors and 10 thicknesses as shown in Figure 50A. The figure shown represents a grid fixed in space with the matrix rotating through it. Therefore, at any instant of time the matrix material in sector "S" will be the hottest and that in sector "A" the coolest. Figure 50B illustrates the temperature throughout the matrix after one quarter revolution from a cold start. The lettered and numbered points are consistent with the Figure 50A sector notation. At this particular instant, some of the sectors have not passed under the crossarm seal and therefore show identical temperature gradients. All of the other sectors have different gradients because they have passed under the crossarm seal and have been exposed to gas flow from both T8 and T3 for various lengths of time. When the temperature of more than one sector is identical only the higher letter or number was printed. Figure 50C shows the potential thermal deformation of the elements at this same instant for a material with the thermal expansion characteristic shown in Figure 50A. This is an LAS material developed by Vendor A.

Figures 50D, E and F are plots of calculated steady state temperatures for the same air flow, but with different speeds. They show that for a core which is rotating fast relative to the air flow, the circumferential temperature gradient would be small and a structural analysis assuming no circumferential gradient would therefore be adequate. On the other hand, for a core which is rotating slowly relative to the air flow, which would be possible with a e rotor engine, the circumferential temperature variation can be significant.

7.0 ENGINE CONTROLS

The Baseline Engine was equipped with hydromechanical controls for fuel metering and power-turbine-nozzle actuation. Additionally, a relay-type start-safety protection package was utilized which incorporated electronic over-temperature and light-off detection.

7.1 Baseline Hydromechanical Control

The fuel control provided the functions of steady-state gas-generator-speed governing, start/acceleration fuel scheduling and fuel shut-off on decelerations. As shown in Figure 51, the fuel control, driven by the gas generator, consists of a positive displacement pump, a pressure regulator, flyweight governor, an acceleration orifice and an altitude compensator. Start/acceleration fuel is scheduled as a function of compressor discharge pressure with altitude trim. Schedule changes were accomplished by orifice sizing.

The power-turbine-nozzle actuator, supplied with engine oil pressure, was a hydraulic positioner which provided modulation of the nozzles in accordance with a cam-generated schedule based on turbine exhaust temperature. This actuator also provided a fixed braking position of the power turbine nozzles for vehicle braking. Also shown in Figure 51 is the hydraulic circuit for the nozzle actuator. Transmission governor pressure is utilized (through a transfer valve) to provide a braking signal to the actuator. With vehicle speed above 15 mph and the input arm of the actuator in the idle position, full line-pressure is applied to the back of the piston to extend it to the braking position. A two-position idle is accomplished with an idle positioner to accommodate increased accessory loading, specifically the air conditioning compressor load.

In addition to the hydromechanical fuel control and power-turbine-nozzle actuator, the gas turbine engine requires a safety system. This start-safety system provides automatic start-sequencing upon initiation of the key switch. A no-start condition results if the transmission is not in the start/park position. There are four starting mode aborts as follows:

- Failure of the burner to light within 8 seconds. A lightoff constitutes a 100°F/sec. rise on turbine inlet temperature.
- Failure to reach 25 PSI oil pressure within 5 seconds.
- An overtemperature (turbine inlet temperature equal to 2000°F) for 2 seconds duration.
- Cranking time in excess of 20 seconds.

A restart can be made in the latter three cases, however, if the burner does not light, a 30-second-reset time is required to allow fuel to drain before restarting. The start safety-system logic is shown in Figure 52.

These hydromechanical controls are simple, reliable and low in cost; however, they are deficient in the following areas:

1. No allowance for ambient temperature compensation, power limiting or speed correction.

2. Turbine exhaust temperature is based on a cam-generated average-temperature schedule instead of actual temperature. This does not allow optimum economy, emissions and performance due to variations in ambient temperature, engine leakage, engine conditions, et cetera.

3. Adaptations of the hydromechanical controls for idle-speed control and nozzle opening (or "blipping") on gas generator acceleration requires complex additions such as linkage, solenoid valves, etc. and has resulted in performance less than optimum.

7.2 Electronic Control System

Additionally, the control demands of the Upgraded Engine—i.e., free-rotor gas generator, variable inlet guide vanes, water injection and low-emissions combustor-require increased control complexity. Design and development of an integrated engine control system was therefore undertaken to investigate whether and to what extent these deficiencies could be overcome and new control requirements satisfied in a cost-effective manner. This activity is reported in further detail in Reference 3 and 4.

This electronic approach was selected to provide flexibility in the development stage with final implementation dependent on the requirements. As shown in Reference 5, present electronic controllers, being of a developmental nature, are either hard-wired or printed-circuit-board with discrete components Considerations toward extending electronic control concepts and functions to high-volume production include LSI (large scale integration) technology, microprocessors and digital implementation.

A list of engine and control-system parameters is shown on Table 11, and a simplified block diagram of the electronic control system is represented by Figure 53.

The functions of the various control loops are listed below.

1. Fuel Control

   - Gas-generator-speed governing based on ambient correction.
   - Start/acceleration fuel scheduling as a function of corrected gas generator speed with the start schedule altered by power turbine exhaust temperature.
   - Fuel shut-off on decelerations.
   - Turbine-inlet-temperature limiting during starting and accelerations.
   - Maximum-speed limiting for gas generator rotor and output shaft
   - Output shaft idle-speed governing in conjunction with either the power turbine nozzles or inlet guide vanes.

2. Nozzle Control

   - Power-turbine-exhaust temperature control in power and braking modes
   - Engine braking.
   - Output shaft idle-speed governing.
   - Open nozzles for start and acceleration modes
   - Open nozzles for loss of temperature sensors at turbine inlet or exit

3. Inlet Guide Vane Control

   - Low-speed power modulation.
   - Output shaft idle-speed governing
   - Power augmentation at maximum gas generator speed

4 Water Injection

   - Power augmentation

5. Start-Stop Logic

   The same functions of the Baseline Engine package were incorporated in MOS (metal oxide semiconductor) digital logic

o Diagnostics

   The electronic control system incorporates a diagnostic connector with 55 test points to evaluate engine and control system performance Test points include conditioned and unconditioned sensor inputs, computed schedules, logic commands and control system outputs

In conjunction with the development of the electronic control systems, a computer simulation model of the Baseline Engine was constructed and utilized to assist in control concept definition and evaluation of steady-state and transient characteristics. The engine model was effective in defining loop gains and stabilizing terms; however, some schedule changes were necessary during engine and vehicle testing to improve driveability and surge-free operation

7.3 Electronic Control Implementation

The electronic controller was configured with eight wired circuit boards using analog circuitry for control functions and digital logic for starting and engine protection. Pulsed output stages were utilized for the actuators and variable-speed fuel-pump motor. Various circuit modifications were required during early operation and involved such problems as power-supply operation at low voltages, stable low-speed operation of the fuel-pump motor and noise interferences with the TTL (transistor-transistor logic) start logic. Other problems encountered were internal wiring connections as well as harness connections. Figure 54 shows the electronic controller in the test cell along with calibration equipment and instrumentation for diagnostic purposes. Figure 55 shows the controller as it was mounted in the trunk of the vehicle. The test cell installation of the programmable analog controller is shown in Figure 56. A vehicle module is contained in the rack-mounted configuration located on top of the pin-programmable read-only memory unit. This system utilizes analog sensor and output stages and performs computations sequentially in accordance with a clock-controlled digital software program.

7.4 Fuel Metering Components

The fuel metering was accomplished by a variable-speed, constant-displacement pump. Fuel flow was metered as a closed-loop function of pump speed. Fuel flows ranged from 5-180 PPH, and the pump was turned off on gas generator decelerations. Later, with the combustor torch igniter requiring continuous fuel flow, a constant-speed fuel pump was utilized with a proportional metering valve and volumetric flow sensor.

7.5 Sensors

Speed, position, temperature, flow and pressure sensors were utilized with the electronic control system. Speed signals were sensed with magnetic pick-ups, turbine inlet and exit temperatures were sensed with thermocouples and ambient temperature was sensed by a resistance sensor. Positions of the throttle-pedal, variable power turbine nozzles, and variable inlet guide vanes were sensed with linear potentiometers; ambient pressure was sensed with a LVDT (linear variable differential transformer) diaphragm transducer. Fuel flow was sensed with a paddle-wheel flow-sensor. Some test activity was performed on fluidic temperature sensors. The most successful unit tested on this program was provided by AiResearch/Phoenix. The vendor has thoroughly tested the sensor in regard to problems experienced with previous units, such as response and waveshape distortion. A description of operation of this fluidic temperature sensor as it was tested follows.

The fluidic turbine-exit gas-temperature sensor operated on the principle of detecting the change in the speed of sound as local temperature changes. The sensor consisted of a digital fluidic amplifier whose control jets were interconnected by a temperature-sensing tube. The tube transported a low-pressure pulse of air generated by the power supply and aspirated the control jets as the amplifier was supplied with air. The transport of this pulse through the tube occured at the speed of sound, which is a direct function of temperature. Upon reaching the opposite end of the tube, the pulse had sufficient energy to cause the power jet to switch from one side of the amplifier to the opposite side. This switching cycle repeated, and an output frequency was generated which was directly related to the delay time of the pulse traveling through the tube at the speed of sound. As temperature increased the frequency output increased.

This pneumatic frequency output was applied to a piezoceramic disc that transduced the signal to an electrical frequency which was directly applicable as an input to either analog or digital electronic control systems.

The fluidic sensor operated with a supply pressure of 3 psig, and had a time constant 0.9 to 1.7 seconds. The frequency output was a function of absolute gas temperature as follows:

$$f = KT^{.5}$$

where f = frequency in Hertz, K = constant, and T = temperature in °R.

A temperature-to-frequency calibration was made on the Baseline Engine by means of a three-thermocouple rake with 28-gauge chromel alumel couples in the power turbine exhaust. Figure 57 shows this calibration taken at gas generator speeds from idle to 70 percent and propshaft speeds from 900 to 2000 rpm. The sensor output waveshape contained harmonics; therefore a zero-crossing saturation amplifier

was utilized for pulse shaping. Transient data utilizing 1.5 second lead compensation is shown in Figures 58, 59, and 60 for a start, acceleration and deceleration, respectively. This sensor exhibits a frequency shift around 900°F, which produced the peaking shown in Figure 58. Control response specifications for the Upgraded Engine would require a substantial improvement in response. If the fluidic sensor were to be a viable part of the control system, the size would have to be reduced.

7.6 Actuators

The electronic control systems utilized available actuators. For power-turbine-nozzle actuation, an electrohydraulic actuator provided closed-loop trim-control in conjunction with the hydromechanical actuator. A three-way solenoid valve selected the power or braking mode on the unit. The inlet-guide-vane actuator was an extended-stroke modification of the electrohydraulic trim-actuator. The combined power-turbine-nozzle-actuator assembly is shown in Figure 61. New actuators were designed for the power turbine nozzles and inlet guide vanes on the Upgraded Engine.

7.7 Electronic Engine-Control Summary

In summation, electronic engine control was effective and was demonstrated on three vehicles. The programmable analog control with its ease of application and added flexibility proved to be a valuable development tool for control work as mentioned in Reference 4. All control requirements of the gas turbine engine were integrated into a single electronic control unit and were optimized for performance, economy and emissions control. As mentioned in Reference 3 the gas turbine engine requires greater control complexity when compared with a reciprocating engine. Further simplification of the control implementation is required along with added development of sensor interface elements. The higher acquisition cost of the electronic control package is only part of the more important total engine life cycle cost. It is in this area where cost effectiveness can be shown.

8.0 LOW-COST TURBINE ROTORS

Two manufacturing methods were investigated for the purpose of determining their potential of producing low-cost, high volume turbine rotors. One method, which was proposed by the Pratt and Whitney Aircraft Corporation, was the hot, isothermal forging process identified as Gatorizing. The other method, which was proposed by the AiResearch Casting Division of the Garret Corporation, was a casting process which is based on a reusable pattern. The compressor-turbine of the Baseline Engine was used as a model to evaluate these processes. Both companies were to provide samples of their respective processes with the blade and disc shapes of this rotor.

8.1 Gatorizing Process

This process differs from previous hot isothermal forging methods in that the temperature and forging rate are controlled either to produce a condition of superplasticity in the material being forged, or to maintain a condition of superplasticity in material previously placed in that condition by special processing techniques. This condition is essentially one wherein a material, over a specific temperature and strain rate, flows at a very low stress and exhibits extreme ductility. Exploiting the superplastic state of the material allows forging of complex, contoured shaped rotors to extremely close tolerances, which substantially reduces the input weight of the material required and also reduces machining costs. In addition, smaller, less-costly forging equipment than that required for conventional nickel base superalloy or titanium alloy forging can be used.

The forged product produced by the Gatorizing process has two distinct advantages over a cast rotor. The enhanced ductility, toughness, and cyclic capability inherent in a wrought product should contribute to the reliability and durability of the small turbine engine rotors. A forging also has greater consistency of part quality and greater freedom from internal defects than cast products.

An immediate problem for this process was the ribbing under the rim of the Baseline rotor. Ribbing is necessary in cast rotors to maintain integrity because rim cracking is encountered in low-cycle fatigue. To circumvent this, Pratt and Whitney personnel proposed that a solid disc be considered. However, measurements on material from their forging process indicated much higher levels of ductility than with casting material. They, therefore, provided complete sets of material properties of "Gatorized" IN-100 from which solid-disc designs were examined. The data included ultimate strength, yield strength, and elongation as functions of temperature. Stress rupture and low- and high-cycle fatigue data were also supplied.

To investigate the structural potential of a solid disc, a two-dimensional elasto-plastic stress-analysis calculation was coded into a computer program. The procedure followed that outlined in Reference 6. However, a problem related to the stress-strain curve approximation was discovered. The Manson procedure requires the equivalent stress and plastic strain to be adjusted to satisfy compatibility relationships. In the region close to the yield point, small inaccuracies in the stress-strain approximation curve can cause large discrepancies in the plastic strain which could prevent the program from converging on a stress-strain point. A Ramburg Osgood approximation, adjusted to intersect the yield point, was used with satisfactory results.

In support of this program, EPA contracted with Pratt and Whitney Aircraft Group, Government Products Division, to demonstrate the feasibility of low-cost production of integrally bladed automotive turbine rotors. The contract was conducted in two phases. The first phase consisted of several major task areas: a basic process demonstration, process parameter evaluation, generation of design data, definition of the manufacturing sequence, and a manufacturing cost estimate for IN-100 Chrysler-type compressor turbine rotors. In Phase II the capability of the forging process was characterized as to blade shape, and the effect of the blade shape on Baseline Engine turbine efficiency was analytically defined. Modified IN-792 and AF2-1DA were investigated to determine their ability to meet engine strength requirements. Baseline Engine turbine rotors were successfully produced in AF2-1DA. Modified IN-792 did not have consistent high temperature properties.

8.2 AiRefrac Process

To evaluate this process, which features a reusable pattern, AiResearch Casting Division was supplied with the Baseline Engine compressor-turbine-rotor wax pattern tooling. The material selected was IN-792/Hf. This was the material initially proposed for use in the Upgraded Engine design.

AiResearch personnel delivered six IN-792/Hf ribbed compressor-turbine rotors produced by the AiRefrac process. Two additional damaged rotors were also included for dimensional analysis and property evaluation. Four of the rotors were heat treated.

All eight rotors were examined by visual and zyglo techniques. In general, the overall quality of the rotors appeared to be satisfactory. Many of the defects mentioned below are minor and could be cleaned up by ordinary cosmetic grinding.

1. Grain size was very fine on hub, disc, and blade. Some grain inoculant technique appeared to have been used.

2. Surface finish appeared to be somewhat rougher than that produced by standard investment casting. However, the blades measured about 80 RMS, which is equivalent to investment cast wheels and meets print specifications

3. Most rotors had rim cracks in the notched pockets but none of the cracks extended to the base of the pocket.

4. All of the rotors contained some dirt (zyglo indications) on the cope side. This condition could reflect either the processing or the particular heat of IN-792/Hf

5. A slight under-cutting was noted at the leading edge root of many blades with numerous irregularities

6. One scrap rotor contained two notched blades (missrun or pattern defect) and two pockets with positive metal.

The heat-treated properties reported by AiResearch for three test bars machined from a rotor casting exceeded print requirements as shown below.

Rm. Temp. Tensile Props.	**Min.**	**AiResearch**
Ultimate Tensile Strength	140 kpsi	147 kpsi
Yield Strength (0.2%)	130 kpsi	135 kpsi
Elongation	4.0%	5.0%
Reduction in Area	3.0%	4.0%
Stress - Rupture		
1800°F 29,000 psi	23 Hrs	24.6 Hrs
Elongation	5.0%	9.0%
1400°F/95,000 psi	23 Hrs	49.7 Hrs
Elongation	3.0%	4.0%

Dimensional inspection of two rotors revealed the blade tip section's trailing edge to be open some 2.5 to 4 degrees. Root and mean sections were uniformly to print. Typical inspection traces are shown on Figure 62, 63, and 64. A check of the tooling showed the tooling to be to print. A review of the results with AiResearch resulted in assurance that the deviation could readily be controlled and that the rotor for the Upgraded Engine could be guaranteed to print. Their assurances were based on recent dimensional qualification of the process for similarly bladed rotors for an engine being manufactured by their Phoenix Division. Apparently, the stiffness of the re-usable pattern material can be varied within limits to match the rigidity of the airfoil section. No attempt was made to iterate on this phase of the process in casting the Baseline Engine rotors.

Efforts were made to process the rotors so that the Baseline Engine could be run at higher cycle temperatures. This required development in two areas.

1. Determining friction welding parameters for fastening the rotors to shafts made of AISI 8640 steel. Successful welding of coupons was obtained.

2. Determining suitable EDM parameters for putting arcuate slots at the bottom of the rib pockets. These are required to keep the rim/web cracks from progressing into the disc.

The inertia welding of a rotor to a shaft made of AISI 8640 material was successfully completed, as was the EDM of arcuate slots at the bottom of the rib pockets.

9.0 ENGINE CONTROL OIL SUPPLY SYSTEM

The power-turbine-driven oil pump of a free-rotor engine (accessories driven off of the power turbine) must operate over a larger speed range than when driven from the gas generator. Obtaining sufficient capacity over a broader speed-range inevitably requires a larger pump size. To minimize the size increase, a split hydraulic system was evaluated. In this system, the drain circuit of the power-steering/hydraulic-brake-boost drain system is back-pressured to create a 70-psi source for the power turbine-nozzle actuator. The system was installed in Baseline Vehicles and showed no adverse effects on the operation of either the engine or vehicle.

10. HYDRO-MECHANICAL TRANSMISSION

Performance analyses invariably indicate that use of a continuously variable transmission (CVT) would significantly improve vehicle fuel economy, but to date mechanical problems have prevented widespread use of such transmissions in automotive drive trains. However, an attractive hydromechanical CVT has been proposed by engineers from Mechanical Technology Inc. (MTI). The transmission combines variable displacement hydraulic pump and motor units with planetary gear sets in an arrangement which provides all-hydraulic power transmission for operation in the normal low-speed-ratio range and hydromechanical power transmission in direct-and overdrive-ratio ranges.

A sketch of the MTI hydromechanical CVT is presented in Figure 65, which shows the unit to be of comparable size to conventional automatic and manual transmissions of similar (100 HP) capacity. Major components of the CVT are the hydraulic units (pump and motor), the simple and reversing planetary units, and a clutch-and-band for range shifting. For breakaway and acceleration at low vehicle speeds input power is fed through the pump and motor to the sun gear of the reversing planetary and thence to the output shaft through the reversing planetary carrier. For normal vehicle road operation, input power is split between the hydraulic components and engine-driven annulus of the second planetary unit, with the major portion being transmitted through the mechanical gearing.

Since the overall efficiency of the transmission is invariably improved by minimizing the power transferred hydraulically, planetary gear ratios were selected to divide power and control speed ratios as indicated in Figure 66. A 0.4 output/input speed ratio was selected as desirable for the synchronous shift from all hydraulic to hydromechanical modes of power transmission. Between 0.4 and 0.7 speed ratios the CVT operates in a regenerative mode with hydraulic power decreasing rapidly with increasing ratio. At 0.7 ratio, power transfer is 100% mechanical, and at higher ratios the CVT operates in a split power mode. In direct drive (1:1), power transmission is 80% mechanical, but declines with increasing overdrive ratios.

Efficiency, noise, and durability were considered to be prime factors in determining the possible success of this hydromechanical CVT. Hence, an initial sub-contract was awarded MTI to design, fabricate and test the hydraulic components which are most influential in determining overall CVT efficiency. Following measurement of power-transmitting efficiencies of the hydraulic pump-motor module, overall transmission performance was to be estimated, thus permitting vehicle performance and economy calculations to be made comparing the CVT with conventional automatic transmissions. These comparisons were to be made with both gas turbine and conventional reciprocating engines. A very limited study of relative costs of the proposed CVT and conventional automatic transmissions was also included.

10.1 Summary of MTI Report

MTI has prepared a report summarizing the design and development effort expended on the hydraulic pump-module of their CVT (Ref. 6A). This report specifies basic design parameters and summarizes test information in sections devoted to pump testing, parasitic loss assessment, pump-motor module testing, and noise evaluation. However, a very limited assessment of noise and vibration characteristics could be made on available test facilities.

The CVT was designed to transmit 100 HP at input speeds in the 3600-4000 rpm range and to accept 170 lb.-ft. of input torque from 1200-2400 rpm. The ratio range of the pump-motor module was designed to be controllable from a 3:1 input/output speed range to an overdrive ratio of 1:2, thus providing a theoretical ratio-range of 6:1. Actual tests covered ratios from 2.5:1 to .516:1, a power range from .7 to 90 hp, and an input speed range from 600-3200 rpm.

Efficiency curves for typical hydraulic modules with operation in underdrive, direct drive, and overdrive ranges are presented in Figures 67, 68, and 69, respectively, (taken from the MTI report). Overall module efficiencies throughout the operating speed range lie within a 70-83% band for input torques exceeding 25% maximum. While these values represent actual CVT efficiencies for operation in the all-hydraulic power-transmitting range, substantially higher overall CVT efficiencies would be expected in the hydromechanical range where 70-100% power is transmitted mechanically. Power transmission by planetary gear sets has been shown to lie in an efficiency range of 92 to 98%. Measured hydraulic module and calculated planetary gear-set efficiencies were combined to provide overall CVT efficiencies which, in turn, were utilized to predict the EPA Urban and Highway Cycle Fuel Economy of vehicles which include the MTI hydromechanical CVT and were powered by two-shaft gas turbines and by conventional Otto-cycle powerplants.

10.2 Application of CVT to Spark-Ignition Engines

The development tests conducted on the hydraulic module of the MTI hydromechanical CVT indicated that moderate fuel economy gains are available when this type of transmission is used with a conventional powerplant. Despite the fact that continuously variable transmissions seldom transmit power as efficiently as those providing several discrete ratios, CVT's have shown better overall vehicle fuel economy by allowing the engine to operate at optimum economy over a wide range of vehicle speed and load combinations and thereby effecting fuel savings which outweigh the fuel-economy losses resulting from reduced transmission efficiencies.

For fuel economy comparisons, a specific vehicle-engine combination was selected, and the standard 3-speed automatic transmission with lock-up torque converter was compared to the MTI hydromechanical CVT and to a promising 4-speed automatic which also included torque converter with lock-up. From vehicle power requirements, engine BSFC maps, and transmission and drive-line efficiency data, EPA Urban and Highway Cycle Fuel Economy values were calculated and summarized over one-second time intervals. It was assumed that the CVT ratio would be selected to permit the engine to produce the required power with minimum fuel consumption. With this assumption fuel economy results are indicated on Table 12.

The CVT shows a 5-6% composite fuel cycle economy improvement over the current 3-speed-lockup automatic transmission with 2-2.5% additional improvement in the Urban Cycle range. However, the 4-speed-lockup automatic transmission is an anticipated improvement in current automotive transmissions, and this provides nearly as great composite cycle improvement as the CVT. Calculations show the CVT to be superior on Urban Cycle operation. However, this superiority requires verification since no complete MTI CVT has been constructed to date. Consequently its actual break-away and low-speed performance are questionable.

Since the transmission oil pump constitutes a source of significant parasitic loss which influences CVT fuel economy performance, the MTI transmission was evaluated using the conventional Chrysler A-904 pump (with suitable pressure control) and a pump of higher efficiency suggested by MTI. As may be observed, the MTI pump offers 1-1.5% improvement in overall fuel economy values. It should be noted, however, that the latter pump is not a mass-produced unit.

10.3 Application of CVT to Gas Turbine Engine

The fuel economy potential of the CVT was also evaluated for a vehicle powered with a 100 hp two-shaft, gas turbine engine. The conventional 3-speed automatic transmission with lock-up torque converter was used as the basis of comparison for this study.

The average road load fuel economy with the CVT was 4.1% better than that with the base transmission in the 20-60 mph speed range and 7% better in the 50-80 mph speed range The CVT was assumed to be operating in its most efficient mode with all of the power being transmitted mechanically Vehicle drive cycle fuel economy was simulated using various constant vehicle acceleration rates. On this basis, the CVT fuel economy advantage was about one-half that shown previously for Otto-cycle power plants, or in the 2% to 3% range.

The vehicle performance with the CVT was not evaluated for the gas turbine application However, since the modest fuel economy gains shown above were computed with vehicle rear axle ratios about 60% smaller than those used with the base transmission, the performance can be expected to be poorer. The fuel economy advantage of the CVT arrangement decreased with increasing rear axle ratios.

Thus the vehicular fuel economy with a 2-shaft gas turbine engine is relatively insenstive to the engine-to-vehicle speed-ratio optimization possible with a CVT

Additional calculations for CVT application to single-shaft gas turbine engine powered vehicles were conducted as part of the Improved Gas Turbine Study discussed in Volume 3 of this report

10.4 Transmission Cost Comparisons

A production feasibility study was made to compare to MTI hydromechanical CVT with the current 3-speed automatic transmission including lockup torque converter and with the 4-speed automatic with similar components. Based on a 500,000-unit annual production rate, the price cost of the CVT is estimated to be 35-45% higher than that of the standard 3-speed automatic. The 4-speed automatic is believed to carry a cost penalty in the 15-25% range, relative to the standard automatic Program costs, which include primarily tools and facilities, are estimated to be 2 1 2-3% higher for the 4-speed automatic than for the CVT

The preliminary nature of any cost estimates relating to the CVT cannot be overemphasized inasmuch as no complete transmission has been fabricated. Although the costs for the CVT pump-motor module and the components of the planetary set can be accurately estimated, the cost of the control gear mechanisms, as orginally suggested in the MTI proposal has been accepted, and it is unlikely that any transmission control system in its initial design stages would provide acceptable vehicle performance, economy, and emission characteristics. Although some allowance has been made for additional CVT control features which may be necessary to provide an acceptable automotive transmission, the cost of such components can only be approximated.

10.5 Summary to Date

Development work to date has indicated that the hydraulic components of the hydromechanical transmission perform efficiently and could serve as components of an automotive CVT which would be competitive with advanced 4-speed automatic transmissions in power transmitting efficiency and overall vehicle economy. However, despite the encouraging results of this inital effort, several major problems require solution to convert the hydraulic pump-motor module into a complete and acceptable automotive transmission. These would include: 1) development of the power-transmitting gearing for forward and reverse vehicle motion, 2) development of the control system required to maximize vehicle performance and economy, and 3) solution of the noise problems which are characteristic of hydraulic power-transmitting systems.

Updated performance maps depicting the economy and emission characteristics of specific engines would warrant a review of the original two-planetary-transmission gearing proposals. The review should include optimization of the ratios of the proposed plaentary gear systems, but, more importantly, studies should consider alternate gearing which might prove more efficient, especially in the overdrive range.

A major factor in determining the success of a CVT is the development of a control system which can provide the breakaway, acceleration, and shifting smoothness now provided by torque-converter automatics In additon, the CVT control must continuously relate engine operation to vehicle power requirements to assure maximum economy. While MTI has experience in this field, it is expected that the sophisticated performance demanded in automotive transmissions would require extensive development work.

Noise problems have been a serious deterrent to the acceptance of any hydrostatic or hydromechanical transmission for automotive use, and in its present state of development, the pump-motor module is excessively noisy. However, MTI has not applied conventional noise reduction techniques to the pump porting plate, nor have proposals for module isolation been included in the fabricated test unit. It is expected that rubber isolation of the hydrualic module and probably the drive-shaft couplings would be essential, as well as measures for controlling rates of hydraulic pressure change within the module. Noise suppression is considered to be a major problem which would necessitate an extensive development program

Although hydromechanical CVTs have demonstrated reasonable performance in experimental automobiles and trucks, several factors tend to discourage expanded usage of this type of transmission in the automotive field Chief among these are:

1 the extensive development work which would be required to make hydromechanical CVTs significantly superior to established 3- and 4-speed automatics in performance, economy, noise, and operating smoothness; and

2. the probability that other types of CVT may prove superior to the hydromechanical, particularly with regard to operating noise and power transmitting efficiencies

Belt and traction drive CVTs have demonstrated more quiet operation than hydromechanical transmissions, but the latter provide a much greater inherent speed ratio range None of the three competitive CVTs appears to be sufficiently well developed to:

1. justify a selection for potential automotive use, or

2. determine accurately the advantages of CVTs over conventional automatic transmissions.

In vehicles powered by single-shaft gas turbines where continuously variable transmissions are mandatory, it appears that hydromechanical and belt drive units are most promising, and that, based on current performance data, both justify continued development effort

11.0 POWER-TURBINE-DRIVEN ACCESSORIES (FREE-ROTOR)

Free-rotor is the identification given to the engine concept whereby all accessory drives (engine or vehicle) are removed from the gas generator and are driven by the power turbine. The Baseline Engine was designed with engine auxiliaries (air pump, oil pump, regenerators) driven through gearing from the gas generator, (identified as geared-rotor concept) and vehicle accessories (alternator, power steering pump, air conditioning compressor) driven from the power turbine. Schematics of the geared-rotor and free-rotor arrangements are shown in Figures 70 and 71. Potential advantages of a free-rotor system would be:

1. Reduced overall engine noise.
2. Simplified gas generator design.
3. Improved cold starting.
4. Use of gas bearings.
5. Improved idle fuel economy through reduced bearing loss.

Apparent disadvantages are:

1. The need for more sophisticated controls.
2. The need for a variable-ratio power turbine accessory drive.

11.1 Preliminary Testing

A Baseline Engine was converted to a free-rotor configuration for test cell use as shown in Figure 72. A hydromechanical fuel control system with speed limiter was improvised since a suitable electronic control system was not available. In this arrangement, engine auxiliaries were driven externally, and an equivalent value of power was applied to the power turbine via an alternator/load bank.

Test results using identical fuel schedules and selected turbine exhaust temperatures indicated response times of approximately 1.2 seconds for both the geared-rotor and free-rotor configurations. Typical free-rotor test results are shown in Figure 73. Included on the figure is a line which defines the mathematical terminus of the acceleration as used by the Contractor and which is identified as the slope-intercept method.

In subsequent tests to optimize rotor and vehicle response, it was determined that opening of the power turbine nozzles just prior to initiation of the rotor acceleration resulted in an improvement in rotor response, a reduction in the integrated transient fuel flow and a substantial reduction of emissions, specifically NOx.

11.2 Transient Operating Line

An interesting phenomenon was noted during the rotor acceleration tests. Figure 74 shows a typical steady-state surge line for the Baseline Engine compressor. Superimposed are the trans. nt and steady-state characteristics of the engine operating lines. This figure shows the compressor collector pressure during acceleration to be significantly higher than levels representative of steady-state operation. The difference in compressor pressure ratio from steady-state values has not been explained, despite analytical attempts.

11.3 Low-Speed Engine Characteristics

Theoretical analysis of the free-rotor concept showed a potential for lower idle fuel flow. However, the tests indicated that fuel-flow differences were minimal and within the limits of experimental error. Test results are presented on Table 13. Note that the power turbine output for the free rotor was increased by 1 HP to compensate for the power required to drive the engine auxiliaries at idle.

11.4 Effect of Regenerator Speed on Performance

In the free-rotor concept the regenerator cores are driven by the power turbine. This alters the ratio of gas-generator speed to regenerator-core speed, compared to the ratio for the geared rotor arrangement. Under acceleration conditions the regenerator core rotation may not be optimum to maintain best fuel economy.

Sensitivity of metal regenerators to significant speed changes was tested and is shown on Figure 75 Relatively little effect of core speed on fuel consumption of the engine is indicated. Approximately 30% speed reduction is required to increase the fuel flow by 10% at idle conditions. At higher speeds the effect of core speed change becomes even less significant. Increasing the regenerator speed considerably beyond the maximum utilization condition produced no significant changes.

11.5 Engine Conversion for Vehicle Application

Conversion to a free-rotor engine required innovative solutions in a number of critical areas

- fuel delivery
- starting
- power turbine speed governing
- oil and air pump, regenerator drive slip clutch

A complete free-rotor engine conversion was therefore undertaken to demonstrate feasibility of the system. This included:

- The auxiliaries (air pump, oil pump, and regenerators), normally driven by the gas generator, were transferred to the power turbine by relatively simple modifications as shown in Figure 76.

- An electro-magnetic face-clutch mechanism was added to rotate the accessory shaft during cranking, yet disengage at some predetermined time in the start sequence.

- A closed-loop electronic fuel-control system was incorporated replacing the hydromechanical fuel control.

- The high-speed worm-wheel and drive-bevel-gear were removed. The engine auxiliaries remained the same, being driven either from the starter or power turbine.

- A 6-to-1-ratio pulley system in tandem with the existing gas generator starter provided the correct accessory speeds during starting via polyflex belts.

- A drive member was installed on the rear face of the regenerator side worm to accept the driving jack-shaft from the power turbine. A side pocket was welded to a power turbine casting. This new addition housed the driven sprocket for the engine auxiliaries and the chain tensioner. A second sprocket was added to the existing one on the reduction gear to complete the auxiliary drive system. The driven sprocket incorporated an overrunning clutch which released the engine auxiliaries during start mode. As power turbine speed increased, eventual lock-up occured with the engine auxiliaries driven by the power turbine.

- A speed limiter installed in the above drive system prevented overspeeding the engine auxiliaries at higher power turbine speeds. This was a simple friction, slip-clutch device with a centrifugal assist.

In the initial free-rotor conversion, the power turbine would not accelerate fast enough to smoothly pick up the auxiliary shaft during starts. As a result the auxiliary shaft speed would fall off sufficiently at starter dropout to prevent a smooth increase in oil pressure. Figures 77 and 78 show these trends for both a cold and hot start condition. The lack of smooth pickup of the auxiliary shaft during starting was reduced by closing down the variable nozzles, resulting in greater torque to the power turbine.

A wide-rotor oil pump (825 in nominal) was used since the operational narrow-rotor pump (50 in. nominal) resulted in unacceptably low oil pressure at the lower speeds.

Peak power of this engine was 145 horsepower. Peak-power propshaft speeds were generally slightly lower than the geared-rotor counterpart. The basic peak-power curve is shown in Figure 79.

The overall sound quality of the free-rotor was greatly improved over that of the geared rotor. However, high-frequency air-flow noise, previously masked by gearing noise, was now dominant This noise emanated from the scroll-elbow/regenerator-cover regions.

In summation, limited experience showed that a laboratory, free-rotor gas turbine is feasible with current electronic control technology Additional experience is required to develop a reliable control system Methods of noise control must be investigated to reduce internal air flow noises A speed-limiting device showed practical us on the Baseline Engine. however, it will require further integration into the design of the auxiliary drive system

11.6 Vehicle Tests

The use of the free-rotor engine in a vehicle required some special consideration but resulted in a very acceptable system having low noise level, good starting, and good driveability.

The control system provided an output-speed limit of 3000 rpm to prevent overspeeding the auxiliary air pump. This was accomplished by throttling fuel flow to reduce output power. However, this condition was seldom in evidence since 3000 rpm represents about 60 mph in second gear or 85 mph in third gear, with the existing 2.76 rear axle-ratio.

The major item requiring vehicle development was the low-speed engine braking condition. Several items should be noted:

1. Compared to the geared-rotor arrangement, the free-rotor arrangement has an increased power turbine load ahead of the torque converter consisting of the engine oil and air pumps and the regenerator drive.

2. The engine oil pump was also used to provide actuator and trimmer power.

3. The engine oil pump had marginal capacity at 600 rpm output speed.

4. The power turbine nozzles are reversed during engine braking; thus the engine airflow applies reverse torque on the power turbine.

5. The torque converter is a poor coupling at low speeds, especially for the reversed torque of engine braking.

These conditions combine in such a manner that the power turbine could be stalled in engine braking at about 30 mph when operating with full vehicle accessory load, i.e., air conditioning, alternator and power steering. When the power turbine stops rotating, the engine oil pump is also stopped, so there is no oil pressure at the actuator or mechanical provisions to return it to the power position. The compressor-turbine is still rotating, without oil pressure or auxiliary air supply for the fuel nozzle, until the driver shuts the engine off. Since the oil pump is also driven by the starter, a restart would return the actuator to the driving position. The Upgraded-Engine power-turbine-nozzle actuator was designed for fail safe operation.

One way to avoid stalling the output is to come out of braking at higher speeds Braking would have to be deactivated below 40 mph. The goal was to provide maximum braking down to minimum vehicle speed This was accomplished as follows:

The power-turbine-nozzle actuator and trimmer were plumbed into the vehicle (power steering and brakes) oil supply, which had greater capacity for maintaining pressure at low speeds The lock-up torque converter was installed to eliminate converter slip. The controls are set to come out of engine braking at about 17 mph, before the lock-up clutch disengaged at about 12 mph Engine braking was satisfactory with these changes; problems of staying in braking and losing oil pressure were not encountered

Figure 80 illustrates the effects of torque converter lock-up during normal engine braking from 35 mph without air conditioning or wheel braking. Without lock-up the engine output speed quickly drops to 700 rpm requiring an elimination of braking, then returns to over 1,000 rpm as the nozzles return to the power position. Since braking is being demanded in response to prop-shaft speed, cycling results until the vehicle speed drops to 17 mph. The cycling could be eliminated by sacrificing engine braking in this speed range, but use of the lock-up provides the best of both. Note that, for the first 5 seconds of each figure, engine braking is 50% better with lock-up than without it A lock-up converter must be considered essential with the free-rotor concept if good engine braking is to be maintained.

Normal engine shut-downs were timed to evaluate the loss of oil pressure versus rotation of the free-rotor gas-generator shaft Some oil pressure existed until the power turbine stopped rotating, which took at least eleven seconds, even with maximum load applied (steering turned against stop) The gas generator shaft normally coasted for 18 seconds after key-off, about seven seconds without oil pressure No bearing problems were encountered, even in combination with the loss of oil pressure, during the engine braking conditions

12.0 POWER AUGMENTATION BY WATER INJECTION

One means of improving fuel economy is engine power augmentation. The use of augmentation permits the engine to be designed for a smaller size than that of an unaugmented engine. The losses associated with part-power engine operation in the steady-state driving range are consequently reduced by the smaller size, while augmentation permits attainment of the maximum power required during vehicle acceleration The types of augmentation that were investigated in this program were variable inlet guide vanes (VIGV) and water injection

It was planned to augment Upgraded Engine power by 10% through the use of water injection. Tests were conducted on the Baseline Engine to determine the required flow rate and to expose engine hardware to the mechanical and metallurgical effects of air-water ingestion. Tests were conducted with water injected in the axial direction, immediately upstream of the compressor impeller, and in the radial direction from the top of the intake housing, as shown on Figure 81. Testing began with four nozzles injecting axially. This was followed by tests using only two nozzles. Final testing employed a single nozzle at the top of the intake housing. The test results are summarized below.

12.1 Four-Nozzle Testing

The water-injection system utilized four commercially available pressure atomizing nozzles, equally spaced circumferentially and positioned slightly above mid-radius of the compressor inlet annulus. Alignment at mid-radius was not physically possible. The nozzles had a 30° -cone-angle spray and were selected to deliver a total of 111 pph water flow.

Figure 82 is a profile view looking into the inlet of the intake housing with the four nozzles spraying. The black area at the horizontal nozzle was added to visually accentuate the spray at that location. Fluid impingement on the annulus walls is essentially at the plane of the compressor inducer.

Augmentation results for 100% engine speed, constant turbine inlet temperature and varying water rate are plotted in Figures 83 and 84. Shown is a 10% increase in power at a water ratio of 1.24 times the fuel rate (111 pph water). Ambient humidity was controlled by adding steam to the cell air conditioning plenum. The test objective was to run under the most adverse conditions,i.e., at 100% relative humidity; but because of the winter season with low moisture in the outside air, only 65% relative humidity was achievable

This data is in line, however, with earlier engine data, which shows the effect of relative humidity, Figure 85. This earlier system utilized two air atomizing nozzles in the side-to-side inlet ducting two feet upstream

The compressor experienced rapid deterioration with continued water injection For the series of tests reported here 40 gallons of water were injected over a ten-hour period The steel inducer showed no distress, but the aluminum impeller was seriously eroded.

1. Along the leading edge
2. Along the pressure surface-backface corner.
3. At blade outer diameter, just behind the steel shroud
4. At the blade tips (all rounded).

12.2 Two-Nozzle Testing

Test results for two nozzles spraying directly into the compressor eye produced results essentially identical with those for four nozzles This system also was checked under transient conditions, using a solenoid and water tank pressurized by compressor discharge pressure There were no operational problems

Tests showed no appreciable change in augmentation from data previously reported. The effect of water injection on NOx is shown in Figure 86 for 100% engine condition and indicates that NOx is depressed with increased water rate This trend agreed very well with past experience. These values are for the exhaust concentration and have not been corrected for inlet concentrations.

Carbon monoxide and hydrocarbon results are not shown, since they were not appreciably affected Typical of 100% speed conditions, exhaust hydrocarbon levels were below the intake values and exhaust CO concentrations were approximately 17 ppm, 50% higher than inlet conditions

Preliminary visual examination of cast aluminum-alloy (C355) impellers revealed water-injection-related damage on the edges of impeller blades. The extent of this damage varied from mild pitting on leading edges to more severe pitting and rounding on the pressure side of the blade edges at the outside diameter. Major material breakout was observed in the areas near the shroud.

High silicon-aluminum casting alloys of this type are generally considered resistant to stress-corrosion cracking. As is the case with most aluminum alloys, whether cast or wrought, this resistance is partly due to the protection afforded by the impervious oxide film which readily forms on the surface of the alloy.

A rotor was run with water injection before sectioning for metallographic and SEM examination to determine the nature of the attack observed on the blade edges. Examination of this sample, its operating environment, and a review of the literature suggests that the most probable mechanism(s) involved in this edge deterioration is related to mechanical destruction of the protective surface oxides by erosion, turbulence and/or cavitation forces leading to rapid corrosion attack of the newly created, highly reactive unprotected aluminum-alloy surfaces. Selective corrosion combined with operating and/or assembly stresses may lead to corrosion-fatigue, which has been known to proceed at a relatively high rate. Preliminary results of these metallurgical studies showed evidence of suspected corrosion at the base of some of the more severely attacked areas. Although this investigation was conducted on a "full-shroud" rotor, visual examination of a partially shrouded rotor, Figure 87, showed that the same condition exists after running with water injection.

12.3 Single-Nozzle Testing

Combined water-injection tests and VIGV tests were conducted to determine the operational characteristics of the power augmentation systems. A single modified air atomizing fuel nozzle was used to spray the water into the top of the air intake. Water rate was controlled to 100 pph by an orifice in the nozzle. A value of approximately 11 pph of collector air was used for atomization. The fiberglass liners in the intake were coated to prevent erosion. The test results indicated that each system's contribution to augmenting power was directly additive. The results are shown in Figure 88 and show a constant 10% power increase with water above VIGV contribution

Following installation of the VIGV/water-injection equipment into a vehicle, a series of chassis-roll emissions and fuel economy test cycles were run The results are shown on Table 14. As indicated by the data, even though steady-state idle fuel consumption is lower [illegible] modulating the guide vanes, indicated cyclic fuel consumption was slightly higher This [illegible] could either be experimental error or might be indicative of a different mode of operation by the driver, when driving an engine of higher idle power.

Proving-Grounds tests were conducted to determine the effectiveness of power augmentation on vehicle performance. Maximum power accelerations were conducted for the following conditions

a. VIGV locked at zero, no water injection;
b. VIGV active (+60°@ idle to -15°@ 100%), no water injection;
c. VIGV active, water injection.

Overall vehicle weight, including two persons plus test equipment, was 4,770 pounds Some comparative acceleration times are as follows:

		Test Ambient		
Engine Condition	Time-Seconds 0-60 MPH	Temp. °F	Bar. "Hg	Humidity %
No VIGV, No WI	14.3	76 5	28.79	76
VIGV	13.5	79.5	28 79	43
VIGV + WI	12 7	81.5	28 78	53

Comparative speed and distance traces are shown on Figure 89 The improvement in performance with augmentation is reasonably consistent with the engine data of Figure 88

12.4 Final Vehicle Testing

The compressor section of an engine installed in a vehicle was inspected following a trip to Washington D C.; over 1500 miles had been accumulated with the water injection system operational. In addition, the engine had been operated with intake filters soaked by a heavy rainstorm.

Random white deposits were found on all aluminum components, as shown in Figure 90. Removal of these deposits showed superficial pitting. This deposit was not observed during dynamometer/cell water-injection tests. Blade erosion/stress-corrosion previously observed on the impeller had progressed slightly.

13.0 VIGV POWER AUGMENTATION

This section describes the experiences with Variable Inlet Guide Vane (VIGV) augmentation. The design-and-development work on the V was carried out on Baseline Engine hardware, through compressor-rig and engine testing.

13.1 Engine Operation with VIGV

In the past, the use of VIGV on the automotive gas turbine engine has been primarily for the purpose of minimizing engine acceleration time In Reference 7, a high value of idle speed was obtained by simulating the pressure ratio characteristic of a lower speed with large values of positive preswirl (in the direction of engine rotation). The study conducted in Reference 8 also employed this technique for the same reason, and, in addition, considered the use of water injection for power boost during acceleration. In Reference 9, VIGV were considered for use, not only at idle, but also at maximum speed As in References 7 and 8, positive preswirl was used at idle speed, but differing from Reference 8, negative swirl was employed near maximum speed. This simulated the pressure ratio characteristic of maximum speed at a lower speed, thus reducing the difference in engine speed between idle and maximum power.

In the Baseline Engine program, VIGV were used to improve fuel economy and emission control. This is illustrated in Figure 91, which shows the engine operating lines at 50% and 100% speeds on partial compressor maps. Differing from Reference 9, negative preswirl is employed at maximum speed, not to minimize acceleration time, but to augment engine power. Additional augmentation is provided by water injection at maximum negative VIGV travel, again, not to minimize acceleration time as in Reference 8, but to improve fuel economy in the vehicle driving range.This is accomplished by referencing the engine size to the unaugmented power at maximum g generator speed. The power losses at any given part-power condition are reduced if aerodynamic and mechanical components have been sized for a smaller reference power.

To improve fuel economy still further VIGV are used at 50% speed Similar to Reference 7 to 9, positive preswirl is used at idle speed, not, however, to achieve a high value of idle speed, but to lower the flow and pressure ratio at a low idle speed for better fuel economy, as suggested in Reference 9 Without VIGV, the Baseline Engine operation at 50% gas generator speed between peak power and idle power was achieved by reducing the turbine inlet temperature This changes the match between the compressor and turbine to a higher airflow, as shown in Figure 91 For the Upgraded Engine, the power turbine exit temperature was to be held constant for all levels at 50% speed. This reduces idle pressure ratio and airflow. It was hoped that idle fuel flow could also be reduced. Thi would depend on how well compressor and turbine efficiencies are maintained in this power range. Of particular concern, at the beginning of the program, was the uncertainty of the maintenance of good compressor efficiency over the VIGV angle range from 0° to +60°

It was also hoped that added fuel economy would come from maintaining a constant power turbine exit temperature This would avoid the cyclic heating and cooling of the regenerator and associated engine parts between peak power and idle. Lastly, it was expected that the hydrocarbon and CO emissions would be reduced by maintaining a higher value of power turbine exit temperature at idle than that of the Baseline Engine.

Hardware was designed, procured, and tested to investigate operation with VIGV on the Baseline Engine Preliminary testing was conducted on a compressor test rig with a Baseline Engine compressor These tests provided the initial experience for obtaining the best trade-off between positive preswirl at 50% speed and augmentation at 100% speed This was followed by engine testing to confirm the test rig results and provide component matching data Each of these activities is discussed in the following sections

13.2 VIGV Design

The variable inlet guide vane is an articulated design, as shown in Figure 92. This type of design provides a wider range of minimum-loss operation over a wide range of deflection angles than does and integral vane which is simply pivoted to produce the required swirl This is supported by the work reported in Reference 10 Similar approaches have been taken in Reference 11 and 12, but the forward section of the vane in these references is moveable as well as the rear The configuration in Figure 92 was selected because the data shown in Reference 10 indicated the possibility of having a stationary forward section and, thus, a low-cost VIGV configuration with a wide range of low loss deflection angle

The vane section was an NACA 0010 pro*9- modified for a trailing edge thickness/chord ratio of 016 The maximum-thickness 'chord ratio t in Reference 10 was 0 05. A value of 0 10 was used in the VIGV design in anticipation of structu. tegrity

The chord length of the vanes in Reference 10 was varied term hub to tip to give nearly constant solidity between 1 07 and 1 08 The VIGV configuration used on the Baseline Engine had a variable solidity from hub to tip This was the result of selecting a constant chord length for manufacturing simplicity To insure the attainment of the desired turning at the tip, the tip solidity was specified to be 1 0 The low hub tip ratio (0 46) of the Baseline Engine impeller resulted in mean and hub solidities of 1 45 and 2 54, respectively Flattering from Reference 10 the hub flow path was cylindrical It was hoped that the large value of hub solidity would counter the adverse effect of clearance of 60° flap angle as the edge of the flap moved away from the hub

The axial spacing from the impeller leading edge was selected to be 5 8 of the vane chord length Data presented in Reference 13 from a number of blade sections shows that wakes are dissipated at about 5/8 chord It was hoped that this would be true for the VIGV at zero degrees flap angle This would be the flap direction for most of the vehicle driving range

13.3 Compressor Rig Testing

Two compressor configurations were investigated in the compressor rig tests One configuration consisted of the Baseline Engine compressor with the rotor as shown in Figure 92 The second test configuration was identical to the first except that the separate inducer was removed

Figure 93 shows the test results obtained on the Baseline compressor configuration Data was taken with positive guide vane deflection angles of 0° and 60° at 50% 80% and 100% speeds The test results in Figure 93 show an efficiency drop from 0° to 60° vane angle change

The compressor test rig results at 100% speed are shown in Figure 94 The compressor must be augmented 8 5% in pressure ratio and flow, with little or no reduction in efficiency, in order to achieve the required 12% power augmentation Along a constant turbine inlet temperature line, the augmentation of compressor airflow and pressure ratio is 3 7% with 30° of negative guide vane angle The data shows a drop of about 2 points in maximum efficiency

Tests were also conducted without the separate inducer but the rig data showed that the separate inducer with its higher inlet blade angle configuration would be better suited to engine augmentation However a further increase in blade angle by a revision such as a blade twist might be necessary to minimize the efficiency reduction at -30° and to achieve the required increases in flow and pressure ratio For complete summary of rig testing see Reference 14

13.4 Compressor Results from Engine Testing

Engine testing began with an initial confirmation of the rig performance results with and without the separate inducer Instrumentation which duplicated that of the test rig was installed so that a direct comparison of engine and rig data could be made Tests were conducted at 100% and 50% speeds At 100% speed, data was taken at a power turbine exit temperature of 1350°F over guide vane angles from 0° to -30° At 50% speed data was taken at idle and peak power for turbine exit temperatures ranging from 1100°F to 1350°F over guide vane angles from 0° to +60°

The power augmentation results are shown in Figure 95 for tests with and without the separate inducer, respectively With the separate inducer, 3 6% power augmentation was achieved without the separate inducer, 2 0% power augmentation was achieved The augmentation is less than expected from compressor test rig results With the separate inducer there should have been 6% power augmentation and without the separate inducer there should have been 3% augmentation

It was assumed that the lack of power augmentation was due to a lack of compressor augmentation The test rig results showed that the compressor augmentation goals were not met with either inducer impeller configuration However the augmentation was better with the rotor with the separate inducer It was presumed that this was due to more favorable incidence angle matching with the larger inlet blade angle of the separate inducer Consequently it was assumed that an additional increase in inlet blade angle might yield further improvement in augmentation Accordingly a separate inducer was twisted closed approximately 2 5 degrees

Test results showed very little difference in the augmentation of compressor flow and pressure ratio with the twisted inducer. Figure 96 shows the variation of compressor flow and pressure ratio along the engine operating line, with guide vane angle, for each compressor configuration tested. The plot shows little difference in performance with the standard or twisted separate inducer. The plot also shows little difference in performance without the separate inducer.

The plots in Figure 96 show that the augmentation of compressor flow and pressure ratio is insensitive to the changes of inlet blade angle (and, hence, to incidence angle) for the rotors tested. The inability to accomplish the required compressor augmentation needed to achieve the engine augmentation goal must, therefore, be due to a deficiency in the VIGV performance or a performance coupling between VIGV and compressor. The data of Figure 96 implies that the sharp rise in VIGV loss with deflection angle occurs at a smaller value of deflection angle than indicated in Reference 10, which was used for design and performance background. Calculations were performed to deduce the VIGV loss characteristic from the engine compressor data. This was accomplished by altering the VIGV loss versus deflection angle characteristic in combination with the known zero-swirl compressor map until the compressor augmentation test data was matched. The results are shown in Figure 87 in a comparison with the data of Reference 10; the deduced loss characteristic shows the sharp rise in loss to occur at about 20° deflection angle instead of 35° as indicated by the data in Reference 10.

To obtain a quick and simple evaluation of the loss characteristic, it was decided to install a wake-rake between the guide vanes and the rotor inlet at the arithmetic mean radius (see Figure 98). The loss coefficients computed from wake-rake data are compared with the deduced characteristics in Figure 99. The results in Figure 99 show that the guide vane loss begins to rise at about -15°. The loss characteristic is much closer to the deduced estimate than to the data of Reference 10. The conclusion is that the lack of continued augmentation of compressor pressure ratio and flow beyond -20° VIGV angle is primarily due to high guide vane loss. The possibility still exists for a contribution to loss due to an interaction between the guide vane and the rotor. However, it must either be of secondary importance as a direct increment of loss, or it is the reason for the difference from the data of Reference 10. No in-depth analysis was performed.

These results suggested that the stationary forward section of the guide vane should be restaggered to impose an initial bias of -10° swirl, as shown in Figure 100. This gives an initial -10° bias, due to angle of attack, before the rear section is activated relative to the forward section. The -30° preswirl should then be achieved with aerodynamic loading shared by both the forward and rearward sections instead of completely on the rear section.

The compressor test results are shown in Figure 101. The plot shows that the -10° stators brought the compressor augmentation closer to program goals. The original 0° stator design met the augmentation goal up to about -20° VIGV angle. The -10° stator met the goal up to about -27°. It may be possible to meet the goals at higher values of negative VIGV angle with higher values of negative stator stagger angle. However, as shown in Figure 102, re-staggering the stators from 0° to -10° resulted in 50% speed compressor efficiency dropping one to three points over the range of VIGV operation. Consequently, additional negative bias on the stator could be expected to degrade compressor efficiency further at the low speeds.

The engine augmentation results are shown in Figure 103. Maximum power augmentation did not increase at VIGV angles greater than -20°. The engine results do not reflect the increase in compressor performance. At -25° VIGV angle, the pressure ratio (Figure 101) increased 1.5%, the flow increased 2.3%, and the compressor efficiency increased about one point. Collectively, this should have amounted to a 6% increase in power. The data shows only a 2.5% increase in power over the results obtained with the 0° stator at -25° VIGV angle. Consequently, the engine data was reviewed for turbine performance parameters to explain the lack of engine augmentation.

13.5 Turbine Analysis From Engine Testing

The efficiencies and pressure ratios across the gas generator and power turbines are shown in Figures 104 and 105, respectively. The gas generator turbine efficiency begins to drop at about -20° VIGV angle. To accommodate the compressor work, the pressure ratio across this turbine rises sharply. Figure 105 shows a slight drop in power turbine efficiency within the data scatter and a significant drop in power turbine pressure ratio beyond -20° VIGV angle.

These results showed that the lack of engine augmentation was due to reduction in available pressure ratio across the power turbine. This could be due to progressive reduction in gas generator turbine efficiency beyond -20° VIGV angle As efficiency drops, the pressure ratio available for the power turbine is reduced. Also, as compressor work increases with augmentation, the Mach Number increases into the interstage duct between turbines. This increases the interstage duct diffusion losses, which also reduces the available pressure ratio across the power turbine.

A study was conducted to determine the reasons for the lack of Baseline Engine power augmentation in contrast to the performance augmentation of the Baseline compressor with variable inlet guide vanes. The study consisted of computing the performances and aerodynamic states of the compressor-turbine and power turbine under augmented conditions of 0°, -15°, and -25° VIGV angles. The intent was to try to duplicate the engine results computationally and then examine the component performances and the vector diagram data for the cause.

A comparison of the computed versus the experimental power augmentation is shown in Figure 106. There is good agreement between calculated and test results. The calculated results, however, show larger reductions in power turbine efficiency with VIGV angle than indicated by the data. This is illustrated in Figure 107. The efficiency levels are different, but the trends are similar up to about -15° VIGV angle. Beyond this value, the estimated efficiency for the power turbine reduced much faster than the values computed from the data. It should be recognized that the probe sampling to obtain the component turbine data from engine tests was quite small and that a certain amount of imprecision can exist in the test results.

The sharp decrease in calculated power turbine efficiency is due to increased loss in the interstage duct due to increased Mach Number at the exit of the gas generator turbine. This is a consequence of trying to extract extra work out of a turbine which was designed for a work coefficient of 2.4 and, consequently, was designed with a high rotor exit Mach Number with significant exit swirl.

In conclusion, the development work on the VIGV and the turbine performance results from engine testing showed the aerodynamic requirements needed for engine power augmentation. In this work, a compromise was taken in compressor efficiency at part-power in order to come sufficiently close to the required increase in compressor pressure ratio and flow. Steps were taken in the Upgraded Engine compressor design to try to reduce the compromise with part-power fuel economy The Baseline Engine testing also showed the need to design the gas generator turbine with lower rotor exit Mach Number and swirl. In the Upgraded Engine, the work coefficient was reduced to enhance augmentation

14.0 HIGHER CYCLE TEMPERATURE

This task covered an investigation of the casting of a compressor turbine for the Upgraded Engine by the AiRefrac reusable pattern process with IN-792/Hf alloy. The task also covered a stress/deflection analysis of the bulkhead housing of the Baseline Engine. The purpose of these calculations was to anticipate the requirements of the housing for the Upgraded Engine, which would have a cycle temperature of 1925°F (versus 1850°F for the Baseline Engine) and an increase in maximum pressure due to augmentation.

14.1 Alloy Selection

The alloy, IN-792/Hf, was the initial material specification for the Upgraded Engine compressor-turbine rotor. This alloy combines high strength at elevated temperatures with good resistance to both oxidation and hot corrosion. Although the alloy had not been fully characterized, it had been sufficiently evaluated and tested in the Baseline Engine so that it appeared to offer the best compromise between design requirements and economic factors at the time.

Thirteen castings were received from AiResearch. All rotors were found to have numerous cracks in the pocket area between the ribs; some of these cracks extended into the disk. There were also varying amounts of subsurface microshrinkage at the hub near the disk. In spite of several changes made to the pattern and to the casting procedure, all further attempts at casting sound rotors failed. Of the thirteen castings received, three were returned to the casting vendor, three were processed for engine testing, and the balance were used for metallurgical samples and for display. The three processed rotors were used for limited service only.

Subsequently, several good rotors were cast with 713 LC and MAR-M-246. The former alloy has excellent castability but inadequate high-temperature properties. The latter alloy has mechanical properties equivalent to those of IN-792/Hf, but it has lower sulfidation and oxidation resistance. The use of a standard commercial aluminide diffusion coating was expected to provide adequate protection. MAR-M-246 was originally an alternate alloy for the Upgraded Engine compressor-turbine rotor, but, in view of the casting problems associated with IN 792/Hf, it was actually the final selection.

14.2 Bulkhead Housing Investigation

The results of a power-turbine-assembly failure indicated that axial deflection of the housing could have been a contributing factor to the failure. This prompted an investigation to evaluate the stress levels and the deflections of the bulkhead in anticipation of the strength and stiffness demands of the power-augmentation tests. These tests on the Baseline Engine involved higher pressure and temperature levels than specified in the original design. This investigation also provided an opportunity to check out the use of the NASTRAN computer program prior to use in the design of the housing for the Upgraded Engine.

The initial stress deflection analysis of the Baseline Engine bulkhead was performed at a pressure loading condition (50 psi) for which the measured bulkhead deflections were available. This was done so that the assumed constraints for the bulkhead support (which must be estimated since the bulkhead is not rigidly supported by the housing) could be verified by comparing calculated and measured deflections.

This analysis included construction of an idealized finite element model of the bulkhead and resulted in a network of grid points which define 30 elements, as shown in Figure 108. The analysis was made considering the bulkhead-housing flange joint as rigid (no rotation or displacements) and as a guided cantilever (no rotation but displacement allowed in vertical direction only). As shown in Figure 109, the results for the guided cantilever support condition agree favorably with the measured deflections, indicating that some vertical deflection of the upper flange occurs. Vertical deflections were also measured during the experimental pressure tests. The maximum calculated principal stress is equal to 25.5 ksi, as shown in Figure 108.

15.0 LINERLESS INSULATION

15.1 Background

Linerless insulation was evaluated on the Baseline Engine as a cost-reduction concept. The original configuration used a sheet-metal form that provided a cavity into which the insulating material was injected. The linerless insulation eliminates the need for a sheet-metal form to encapsulate the injected insulation. The linerless insulation is molded to the flowpath contour and secured in place with high-temperature adhesive.

Chrysler recognized the high cost of sheet metal in combination with production assembly problems and began a limited in-house investigation of linerless insulation during the mid-1960's. As part of the government contract, dual test and development programs were carried out on materials supplied by the Foseco Company and by Chrysler Corporation.

15.2 Test Results

A summary of the test results, with comments, is given on Table 15. An engine cross-sectional view identifying the affected areas within the engine is shown in Figure 110. Aside from rare unexplained occurence of erosion or material break-out, both insulations show comparable life.

Linerless insulated sub-assemblies yield heat losses similar to those of the sheet-metal/insulation system of the Baseline Engine. A gas generator, instrumented with skin thermocouples, and a power turbine section were fitted with linerless insulation as shown in Figures 111 and 112. After test results were obtained standard sheet metal was placed over the linerless insulation. Material removal was minimal to fit the sheet metal. This approach allowed considerable flexibility and practicality to the test since removal of the insulation required the form to be destroyed, along with possible loss of instrumentation. Simultaneous performance and oil heat-rejection tests for both sub-assemblies showed no significant change in heat rejection or BSFC for the two types of insulation techniques. Additional supporting data were provided by the gas-generator-support skin-thermocouples in which temperatures repeated very well. The BSFC results are given in Figure 113. A complete linerless insulated engine housing is shown in Figure 114.

16.0 CONCLUSION

This volume of the Final Report for the Baseline Gas Turbine Development Program has presented the results of Baseline Engine documentation and the results of tests conducted to investigate concepts for component improvements. The Baseline Engine documentation consisted of defining the performance characteristics of the engine and of a vehicle powered by this engine. The component improvement program evaluated the following concepts:

1. Advanced combustor systems
2. Ceramic regenerator
3. Integrated control system
4. Low-cost turbine rotors
5. Engine/control oil supply system
6. Hydromechanical transmission
7. Power-turbine-driven accessories
8. Power augmentation
   - Water injection
   - Variable inlet guide vanes
9. Higher cycle temperature
10. Linerless insulation

On a standard automotive day (85°F Temp., 29.92" Hg. Press.) the Baseline Engine delivered a nominal value 150 HP at design speed and at a design-speed turbine-inlet-temperature of 1850°F. This was the typical performance achieved and is based on the performance characteristics of ten engines. The pressure ratio at design speed was 4.1:1 at a mass flow rate of 2.3 lbs/sec and a rotational speed of 44,610 rpm. Design-speed SFC is 0.54 lb/hp-hr; idle-power SFC is 1.90. Vehicle testing showed a combined cycle fuel economy of 8.0 mpg (gasoline) and 8.8 mpg (diesel) with a zero-60 mph acceleration time of 11 seconds in a 4500-lb vehicle.

The following summarizes the testing carried out on the different advanced concepts.

- A variety of combustor configurations were investigated: pre-mixed/pre-vaporized, droplet-diffusion, dual-stage, torch ignitor, and variable geometry. The configuration with pre-mixed/pre-vaporized combustion combined with a torch ignitor yielded the lowest emission values (0.41 gram/mile HC, 3.4 grams/mile CO, and 3.1 grams/mile NOx), and was best suited to vehicle driveability.

- Three ceramic core configurations were investigated for the regenerator. Within the range of specific flow required for the Upgraded Engine, a configuration with a triangular shape yielded values of effectiveness as much as 4 points higher than values for the metallic core used as reference.

- Testing showed that engine controls must be more sophisiticated than the original controls used on the Baseline Engine. A closed-loop control on turbine exit temperature was successfully applied to the Baseline Engine.

- Two new manufacturing processes were explored for potential for low- cost production of turbine rotors. Both the reusable pattern process by the AiResearch Casting Division of the Garret Corporation (AiRefrac) and the superplastic forging technique (Gatorizing) by the Pratt & Whitney Aircraft group showed some promise.

- Tests conducted on the hydromechanical continuously variable transmission (CVT) revealed little gain in fuel economy with this type of CVT. Other types, such as belt-drive, were recommended for investigation.

- The arrangement of driving engine accessories from the power turbine instead of the gas generator was shown to be more practical and of lower cost.

- Power augmentation with water injection was successfully demonstrated, but the results showed a strong need for erosion protection for the compressor. Augmentation of compressor performance with variable inlet guide vanes (VIGV) was demonstrated, although the increase in design-speed pressure ratio was 5.4% versus the goal of 7.8%. Power augmentation with VIGV was 4% versus the goal of 12%. For the amount of compressor augmentation achieved, the engine power augmentation should have been 8%. The miss in achievable augmentation was caused by deteriorated turbine efficiency at maximum compressor augmentation. Aerodynamic design parameters would have to be revised to employ augmentation on the Upgraded Engine.

- Two high-temperature alloys were investigated for the Upgraded Engine compressor-turbine rotor: IN-792/Hf and MAR-M-246. Rotors made of MAR-M-246 were cast successfully in the AiRefrac process. No sound castings were made of IN-792/Hf with this process.

- The use of linerless insulation was successfully demonstrated.

All the advanced concepts, except for items 5 and 6 above were applied to the design of the Upgraded Engine. The development effort carried out on the Baseline Engine and the test results are described in this volume.

References

1. Barth, A.: Chrysler Baseline Gas Turbine Vehicle Tests-January 1974-October 1974, Emission Control Technology Division, Office of Air and Waste Programs, Environmental Protection Agency.

2. Heywood, J. B. et al.: Jet Aircraft Pollutant Production and Dispersion, AIAA Journal, May 1971.

3. LeFevre, H. P., Lewis, L. D., and McKinley, L.E.: An Automotive Gas Turbine Control System. ASME Paper 76-GT-123.

4. Dent, J. R., LeFevre, H.P.: Advancements and Applications of Programmable Analog Control Technology, ASME Paper 76-GT-122.

5. Integrated Control System Sub-Contract, Electronics System Group, AiResearch Manufacturing Company of California, Division of Garrett Corporation.

6. Manson, S. S. and Millenson, M.B.: Determination of Stresses in Gas Turbine Disks Subjected to Plastic Flow and Creep. NACA Report No. 906, March 1948.

6A. Jones, Henry F., Jr.: Continuously Variable Hydromechanical Transmission Hydraulic Module Performance. Mechanical Technology Inc. Technical Report No. MTI 78TR12, prepared for Chrysler Corporation under Contract No. E (11-1)-2749,5.7b, February 1979.

7. Penny, Noel: Rover Case History of Small Gas Turbines. SAE Paper 634A, January 1963.

8. Castor, J. D, Davis, R.C. and Riddle, B.C.: Automobile Gas Turbine Optimization Study. Prepared for the Environmental Protection Agency by AiResearch Manufacturing Company of Arizona, July 1972.

9. Sheridan, David C., Nordenson, Gary E. and Amman, Charles A.: Variable Compressor Geometry in the Single-Shaft Automotive Turbine Engine. SAE Paper 740166, February 1974.

10. Serovy, G.K. et al.: Experimental Performance in Annular Cascade of Variable Trailing-Edge Flap, Axial-Flow Compressor Inlet Guide Vanes. ASME Paper 70-GT-106.

11. Jones, B.A., Single Stage Experimental Evaluation of Variable Geometry Inlet Guide Vanes and Stator Blading. (Part VI, Final Report) NASA CR-54559, March 15, 1970.

12. Bilwakesh, K. R.: Evaluation of Range and Distortion Tolerance for High Mach Number Transonic Fan Stages, Volume I. NASA CR-72787, January 1971.

13. Lieblein, Seymour and Roudebush, William H.: Theoretical Loss Relations For Low-Speed Two-Dimensional-Cascade Flow. NACA TN 3662, March 1956.

14. Pampreen, R. C.: The Use of Variable Inlet Guide Vanes for Automotive Gas Turbine Engine Augmentation and Load Control. SAE Paper 760285, February 1976.

TABLE 1

Baseline Engine

Descriptive Data

Power	150 HP @ 3500 rpm
Pressure Ratio	4.1
Air Flow	2.29 lb/sec
Compressor Speed	44,610 rpm
Turbine Inlet Temperature	
Steady State	1850°F
Acceleration	2000°F
Power Turbine	
Maximum Speed	45,500 rpm
Reduction Gear Ratio	9.6875
Regenerator	
Speed	21 rpm
Matrix Diameter	15.5 in.
Matrix Height	3.5 in.
Stock Thickness	0.002 in.
Overall Dimensions	
Length to Transmission Mounting Flange	35.5 in.
Width	27.6 in.
Height	29.9 in.
Weight, Complete Engine—Dry	600 lb.
Gas Generator Acceleration, Idle-to-Maximum Speed	1.2 sec.

TABLE 2

Engine Characterization

RPM Comp	22,877	27,452	32,028	36,603	41,178	43,466	44,610
Press. Ratio Comp., P2/P1	1.545	1.865	2 290	2.825	3 500	3.865	4.080
Eff. Comp. (1-2, Total)	.765	.776	.792	.797	.784	.769	.766
Eff. C.T. (5-6, Total)	.76	.78	.80	.82	.84	.85	.86
Eff. P.T. (6-8, Total)	.67	.67	.68	.685	.69	.695	.70
Eff. Burner	.984	.986	.989	.993	.997	.998	.998
Effectiveness Reg	.901	.898	.892	.885	.877	.874	.873
ΔH Comp., BTU/LB	22.64	32 87	44.12	56.70	71.79	80.17	84.40
ΔH C.T., BTU/LB	24.57	35.05	46.59	59.53	75.02	83.68	88.01
ΔH P.T., BTU/LB	8.70	15.42	23.77	32.11	40.02	42.84	48.34
HP, Acc. & Loss, C.T	1.85	2.47	3.33	4.46	5.86	6.70	7.12
HP, Acc. & Loss, P.T	1.80	2.40	3.50	4.90	5.40	5 90	5.90
HP Net Output, P.T	9.5	21.4	42.1	71.3	109.9	128.2	150.9
Fuel Flow, LB/HR	12.5	19.2	29.7	44.1	63.1	73.4	81.5
BSFC, LB/HP-HR	1.32	.90	.71	.62	.57	.57	.54
Gas Flow, LB/SEC							
W1	.790	1.010	1.293	1.620	2.001	2.181	2.274
W3	.750	.957	1.224	1.532	1.889	2.059	2.146
W4	.772	.986	1.259	1.575	1.942	2.114	2 204
W5	.781	.997	1.275	1.596	1.970	2.146	2.238
W6	.769	.979	1 253	1.570	1.941	2 116	2.207
W8	.787	1.006	1.288	1.613	1.993	2.172	2.266
W9	.791	1.012	1.296	1.626	2.010	2 192	2.287
Pressures (Total), PSIA							
P1	14.67	14.65	14.63	14.58	14.53	14.49	14 48
P2 (= P3)	22.66	27.33	33.49	41.20	50.84	56.02	59.06
P4	22.48	27.12	33.27	40.97	50.60	55.78	58.81
P5	22.08	26.52	32.49	39.98	49.42	54.42	57.42
P6	17.07	18.69	20.88	23 38	25.98	27.01	28 42
P8	15.03	15.15	15 32	15.55	15.87	16 04	16.16
P9	14.74	14.77	14.82	14.90	15.03	15.10	15.15
Temperatures (Total), °F							
T1	85.	85.	85	85.	85.	85	85.
T2	178.0	220.3	266.8	318.6	380.6	414.8	432.0
T4	1145.5	1148.4	1150.0	1152.1	1155.1	1158.0	1198.0
T5	1431.4	1494.6	1568.3	1647 7	1730 8	1772.3	1850.0
T6	1338.0	1362.9	1394.4	1425.6	1453.5	1463 7	1527.5
T8	1290 6	1291.1	1292.2	1293.4	1294.4	1294.6	1339.5
T9	343.3	383.2	429.5	480.6	540.1	571.2	594.9
Flow Leaks							
LB/LB Into Station							
20	.00204	.00214	00218	.00224	.00230	.00235	.00238
25	.00689	00636	.00585	.00539	00507	.00498	.00496
34	.035						.035
38	.00235	.00290	.00340	.00385	00425	.00450	.00460
39	00470	.00580	.00680	.00770	.00850	.00900	0092
46	.00384	.00408	.00432	.00460	00493	00517	.00522
48	.00235	00290	.00340	.00385	.00425	.00450	.00460
68	.0196	.0214	0213	.0209	0197	0188	0185
80	.00151	.00156	.00164	.00167	00173	.00178	.00186
Heat Leaks BTU/LB							
Flow into Station							
20	.354	393	416	423	.435	.444	445
40	1 870	1.762	1.553	1.336	1.138	1 055	1.069
50	631	.980	1 742	2 480	3.085	3.311	3 441
60	768	899	1.119	1.663	1.734	1 900	1 882
80	1.989	1.855	1 626	1 394	1 185	1 098	1.110

TABLE 3

Baseline Engine

Endurance-Testing Tear-Down Results

	Final Teardown Component		Earlier Components	
	Hours	**Condition**	**Hours**	**Reason for Removal**
Engine Housing	4653.7	Good		Not Removed
Engine Insulation (Linerless)	820.7	Good	3828.0	Update
Burner Cap Insulation (Linerless)	1218.4	Good	2256.0	Update
Impeller	4654.1	Good		Not Removed
First-Stage Turbine Nozzle	4277.0	Good		Not Removed
First-Stage Turbine Rotor	3970.1	Good		Not Removed
Second-Stage Turbine Rotor	573.5	Good	3831.8	Disc Cracks
Total No. of Starts	40861			

Table 4

TABLE 4

Baseline Turbine Car Summary at End of Program

Car Number	618 (C-2)	624 (B-1)	667 (B-2)	671 (B-3)
Engine Number	101-408 AM	Engine	404-413 T	403-422A
Delivered HP	150	Removed	N/A	N/A
Curb Weight, Lbs.	4396	4560	4436	4441
Power Throttle	No	No	Yes	Yes
Braking Stroke	Extended	Extended	Normal	Normal
HC Control	Bleed	Nozzle Bleed	Nozzle Bleed	Nozzle Bleed
Accel Orifice, In.	—	—	0.041	.039
Open Noz on Accel.	Yes	Yes	No	No
T C Stall Speed	1700	1700	1700	1700
Axle Ratio	2.76	3 55 Sure-Grip	2.76	2.76
Tires	GR-78-15 Poly	HR 78-14	HR 78-14	GR 78-15 Poly
Oil Temp Control	170-175°F	Maximum Cooling	Maximum Cooling	Maximum Cooling
Battery Size	85 amp-hr., 500 amp @ 0 F	95 amp-hr , 580 amp @ 0°F	85 amp-hr., 500 amp @ 0°F	95 amp-hr., 580 amp @ 0°F
Blow-By System	Std Can	Pall Demister	Std. Can	Std Can
Inlet Filters	Std. Paper	Std. Paper	Std. Paper	Std. Paper
Fuel	Gasoline	Gasoline	Diesel	Diesel
Burner	Droplet-Diffusion Burner	Lean Pre-mixed, Pre-vaporized	Droplet Diffusion Burner	Droplet-Diffusion Burner
Special Parts	Ultra Control PAC-250 Modine Oil Cooler	Garrett Control, Water Injection Equipment	P/S Oil to Power Throttle Cloth Interior	Nexdamp Intake Duct P/S Oil to Power Throttle
Status at End of Program	Demonstration vehicle	Out of Service	Out of Service	Support to DOE @ Washington D.C.
Odometer Reading, Miles.	11378	13566.3	17636	18081
Total Hrs	701	620	723	812
Total Starts		5392	3816	4419

T/C = Torque Converter
P/S = Power Steering

TABLE 5

Comparative Vehicle Noise Levels—dBA

	Baseline Turbine (1973) (Vehicle)	Baseline Turbine (1966) (Vehicle)	1974 Production V-8
Idle—At Front of Car	71	70	66
Idle—At Rear of Car	62.5	64	68
30 MPH—Driver's Ear	60	61	59
60 MPH—Driver's Ear	70	68	72

TABLE 6

Sound Test Results

	Vehicle's Left Side Decibels	Vehicle's Right Side Decibels
SAE J986a Drive-By Test		
Run 1	74	71
Run 2	72	71
Average	73	71
SAE J986a Drive-By Test, Discrete Frequencies		
Frequency (Hertz)		
125 Hz	78	76
	80	75
250 Hz	71	72
	71	71
500 Hz	72	71
	73	71
1000 Hz	74	70
	72	68
2000 Hz	64	62
	61	61
SAE J986a Drive-By Test, Discrete Frequencies*		
125	82	76
	76	77
	78	
250	73	74
	75	74
500	72	72
	73	72
1000	68	68
	68	67
2000	60	60
	62	60

*Procedure modified: Vehicle accelerated wide open throttle from stop instead of wide open throttle from 30 mph.

TABLE 7

Alternate Fuels

Emission effects of several fuels with advanced, premixed combustor on the Baseline Engine, under idle power at 704°C Power Turbine exit temperature.

	Steady-State			Transient*
Fuel	HC_6 (Net) ppm	CO ppm	NOx ppm	NOx ppm
Unleaded Gasoline	0	97	3.8	18
No. 1 Diesel	0	50	4.6	32
Ethyl Alcohol	0	53	1.7	11
Isopropyl Alcohol	0	64	3.0	14
Methyl Alcohol	1.5	330	0.8	11
Coal Derived	0.4	180	32.0	70

*Peak observed NOx during gas generator acceleration from idle to 70% engine speed.

ppm - Parts Per Million

TABLE 8

Baseline Metallic and Ceramic Matrix Specifications

Matrix Configuration	Hydraulic Diameter	Stock Thickness	Passage Length	% Open Area
Metallic (rectangular)	0.028 in	0.0020 in.	3.50 in.	85
Type "A" (triangular)	0.025 in.	0.0045 in.	2.58 in	67
Type "B" (Hexagonal)	0.027 in	0.0045 in.	3.00 in.	67

TABLE 9

Potential Seal Coating Materials

Seal Composition	Mode of Application
NiO-CaF_2	Plasma Spray
$ZrO_2(CaO)$-CaF_2	Plasma Spray
CoO-BaO-B_2O_3-CaF_2	Glass Glaze
$NiCr$-CaF_2	Plasma Spray
CoO-CaF_2	Plasma Spray
$ZrO_2(Y_2O_3)$-CaF_2	Plasma Spray
$Li_2O(ZnO)SiO_2$	Glass/Ceramic

TABLE 10

Crossarm Seal Wear Rates Engine Endurance Test

Test Conditions	Wear Rate (μm/hr)	Seal Life (Hrs.)*
Type "A" Matrix NiO-CaF_2 Seal 250 hours	0.022	40,000
Type "B" Matrix NiO-CaF_2 Seal 250 hours	0.056	16,000
Type "A" Matrix ZrO_2 (CaO)-CaF_2 170 hours	0.380	2,300

*Based on nominal coating thickness of 0.035 in. (890 μm)

TABLE 11

Engine and Control System Parameters

T_3	Gas Generator Turbine Inlet Temperature
T_5	Turbine Exhaust Temperature
T_1	Ambient Temperature
P_1	Ambient Pressure
Ngg	Gas Generator Shaft Speed
$\frac{Ngg}{\sqrt{\theta}}$	Corrected Gas Generator Speed
δ	Ambient Pressure Correction = $\frac{P_1\ PSIA}{14.7\ PSIA}$
θ	Ambient Temperature Correction = $\frac{T_1\ °R}{545°R}$
N_{os}	Output Shaft Speed
α	Throttle Pedal Position
β	Power Turbine Nozzle Angle Position
γ	Inlet Guide Vane Angle Position
W_f	Fuel Flow, in Pounds Per Hour
V_s	Vehicle Velocity

TABLE 12

Fuel Economy Improvement of Reciprocating Engine with CVT Versus Standard Automatic Transmission with Torque Converter Lock-Up

Transmission	% Economy Improvement Over 3-spd. Trans. With Torque Conv. Lock-Up				
	EPA Cycle			Avg. Economy	
	Urban	Highway	Composite	20-60 MPH	50-80 MPH
4-Speed Auto. Trans. With Torque Conv. Lock-Up	4.5	5.5	4.9	10.2	7.0
MTI Hydromechanical (Chrysler A-904 Oil Pump)	7.7	1.4	5.2	6.5	0.3
MTI Hydromechanical (MTI Oil Pump)	9.2	2.5	6.1	7.5	1.4

TABLE 13

Free Versus Geared Rotor Fuel Flow at 50 Percent Speed Road Load Points for Baseline Vehicle

RPM	MPH		Minimum Accessories		Full Accessories (Including A/C)	
			Power Turbine Horsepower	Fuel Flow, Lb/Hr	Power Turbine Horsepower	Fuel Flow, Lb/Hr
600	10	Geared Rotor	2.4	10.4	5.2	11.1
		Free Rotor	3.4**	10.4	6.2**	11.4
900	20	Geared Rotor	5.2	11.0	*	*
		Free Rotor	6.2**	10.9	*	*

*Requires higher gas generator speed.

**Includes 1 HP compensation for externally-driven engine auxiliary drive (regenerator, lube pump, fuel control, air pump).

TABLE 14

Car B-1 Chassis Rolls Emissions and Fuel Economy Tests

Variable Inlet Guide Vanes, Water Injection, Preprototype Integrated Control System

No. 1 Diesel Fuel

Test No.	Test Cycle	Net Grams Per Mile (1) HC	CO	NOx (2)	MPG Weighed
	VIGVs modulated ' + 60° at idle (5.5 HP power turbine output at 10.6 lb/hr fuel flow)				
	Power turbine modulated to maintain corrected exit temperature = 1300°F (85° Standard Day)				
29	Emissions, hot '72	.94	2.99	2.28	*
30	Emissions, hot '72	.88	1.44	2.52	8.17
31	Emissions, cold '75	.86	*	1.94	7.77
31	Emissions, hot '72	1.04	2.15	1.94	—
32	Emissions, hot '72	.67	*	2.15	8.29
33	Highway Fuel Economy (3)	—	—	—	14.38
	VIGVs locked at 0° (8.0 HP (idle) power turbine output at 11.9 lb/hr fuel flow)				
	Power turbine modulated to maintain corrected exit temperature = 1300°F (85°F Standard Day)				
34	Highway Fuel Economy (3)	—	—	—	14.52
35	Emissions, cold '75	.41	2.58	2.10	7.90
35	Emissions, hot '72	.34	2.12	2.03	—
36	Emissions, hot '72	*	2.21	2.13	8.24
37	Highway Fuel Economy (3)	—	—	—	14.83
38	Highway Fuel Economy (4)	—	—	—	15.51

(1) Integrated trace data, net = exhaust - inlet
(2) Corrected for humidity
(3) Cycle begins from engine start after 10-minute soak; Turbine exit temperature ≃ 875°F
(4) Standard test procedure- fully warm engine, start from engine idle, turbine exit temperature - 1300°F

— Data not taken
* Data Voided

Table 15

TABLE 15

Linerless Insulation Evaluation Summary

Description	Chrysler Power Plant*	Hours	Condition	Foseco Power Plant*	Hours	Condition
Burner Cap S/N 111A***	102	1,662	Minor spalling/repair	102***	53	Minor cement repair
S/N 118	102/106	2,908	Cement repair			
S/N 403	102/429	1,825	Minor repair			
High Pressure Housing	102	1,129	Minor cracks	427	15	
	406**			429	767	Minor cracks
	428	224	Minor cracks			
Gas Generator Support S/N 108	425	20	Good condition			
Front Bulkhead	102	1,129	Cracks and separation	427	15	
	406**			429	767	Serious cracks/repair
	428	224	Cracks/repair			
Low Pressure Housing	102	1,129	Minor cracks; erosion/repair	427	15	
	406**			429	767	Minor cracks and erosion
	428	224	Severe erosion/repair			
Power Turbine Support						
P.T. 110***	102	246	Minor cracks	100 (P.T. 109)	759	Good
P.T. 403	425	10	Good condition			
P.T. 406	429	767	Hairline cracks/repair			
P.T. 409	428	164	Good			

*Power Plant 102-4000-Hour Endurance Engine (Loaner)
Power Plant 106-General Performance Engine (Loaner)
Power Plant 406-Reinforced Bulkhead
Power Plant 427-Scaled Down Burner Fixture
Power Plant 428-Program Free Rotor Engine
Power Plant 429-Program Endurance Engine

**Parts Not Yet on Test
***Insulation Out of Service

Baseline Engine
Cross-Section

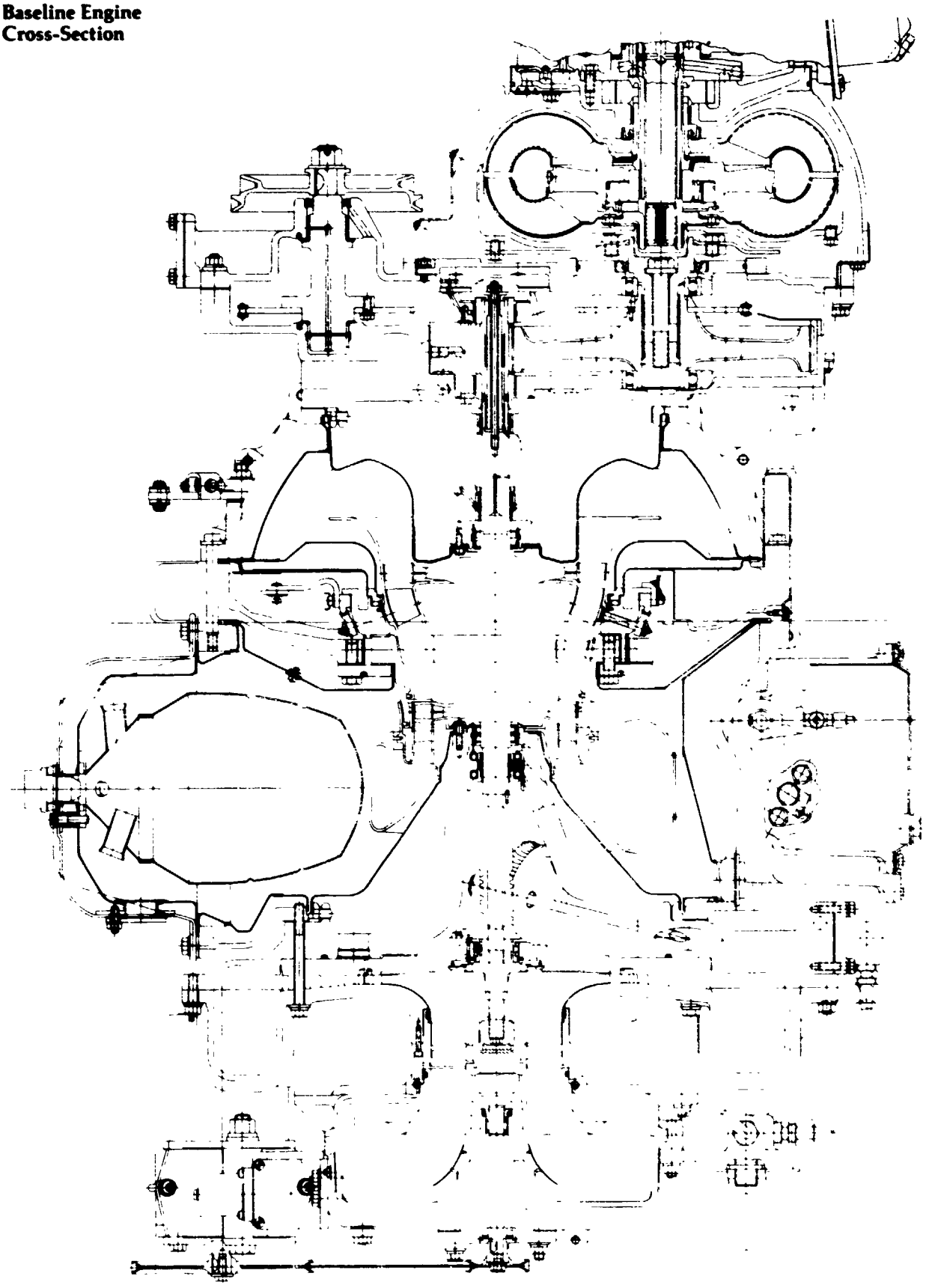

Figure 1

Baseline Engine

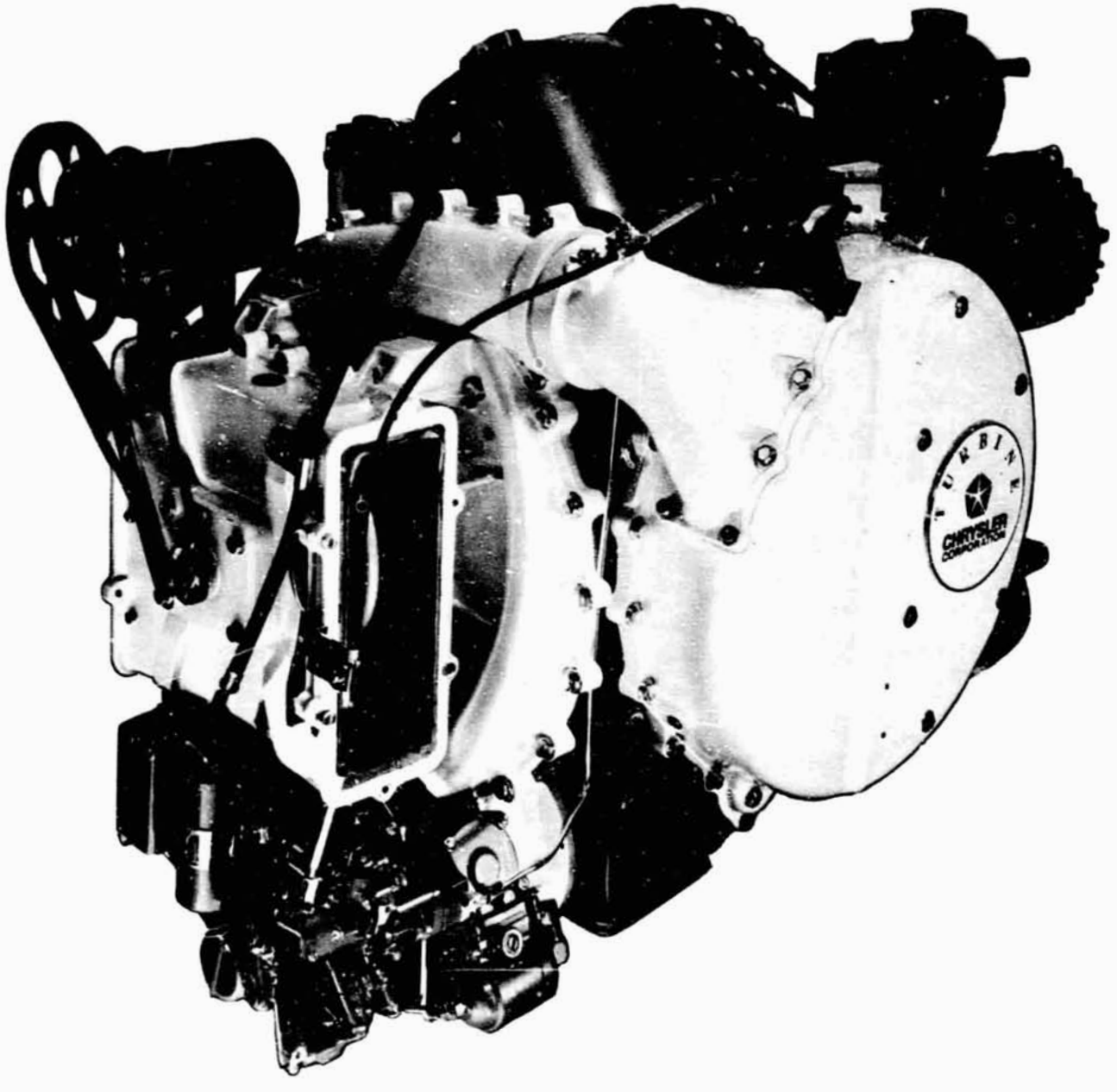

Figure 2

Engine Characterization Schematic

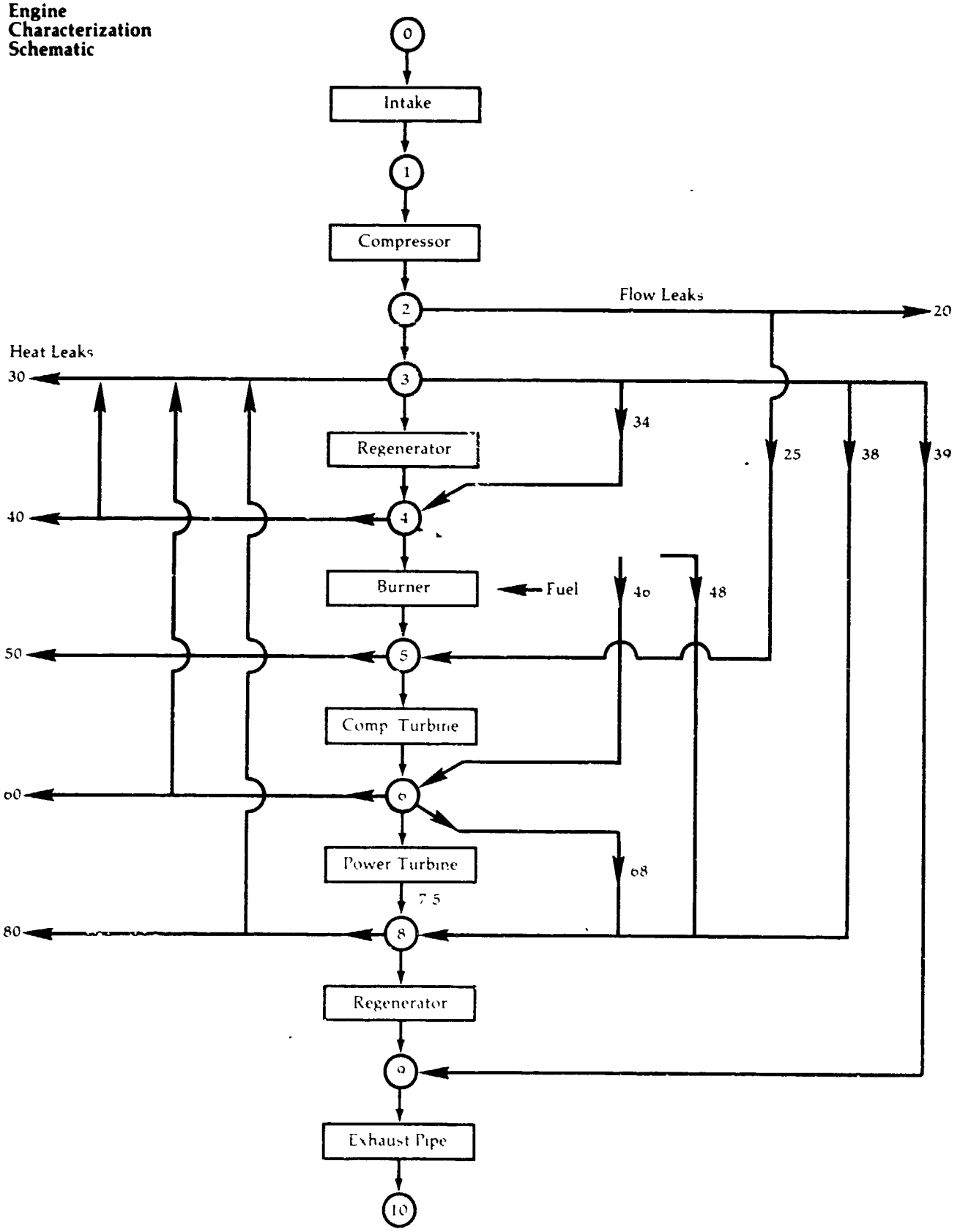

Figure 3

Baseline Engine Station Notation

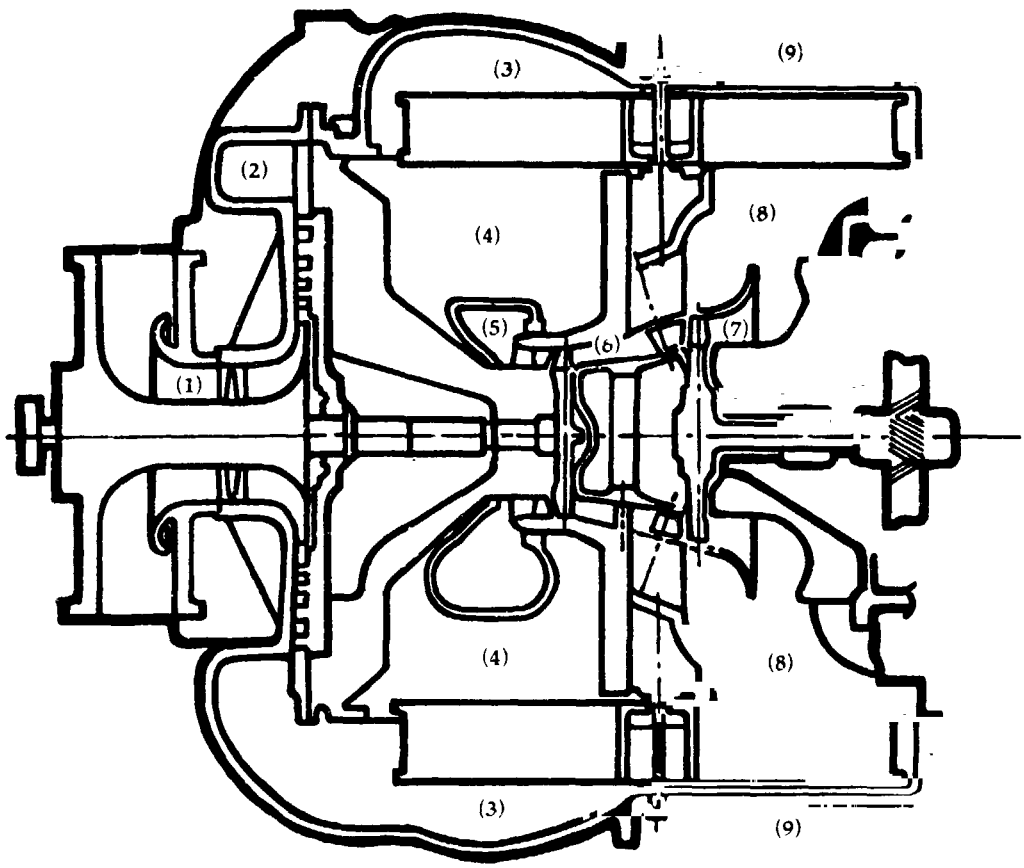

(0) Ambient
(1) Compressor Inlet
(2) Compressor Outlet
(3) Regenerator Inlet (Cold Side)
(4) Burner Inlet
(5) Compressor Turbine Inlet
(6) Power Turbine Inlet
(7) Power Turbine Outlet
(8) Regenerator Inlet (Hot Side)
(9) Regenerator Outlet

Figure 4

Engine Output Power

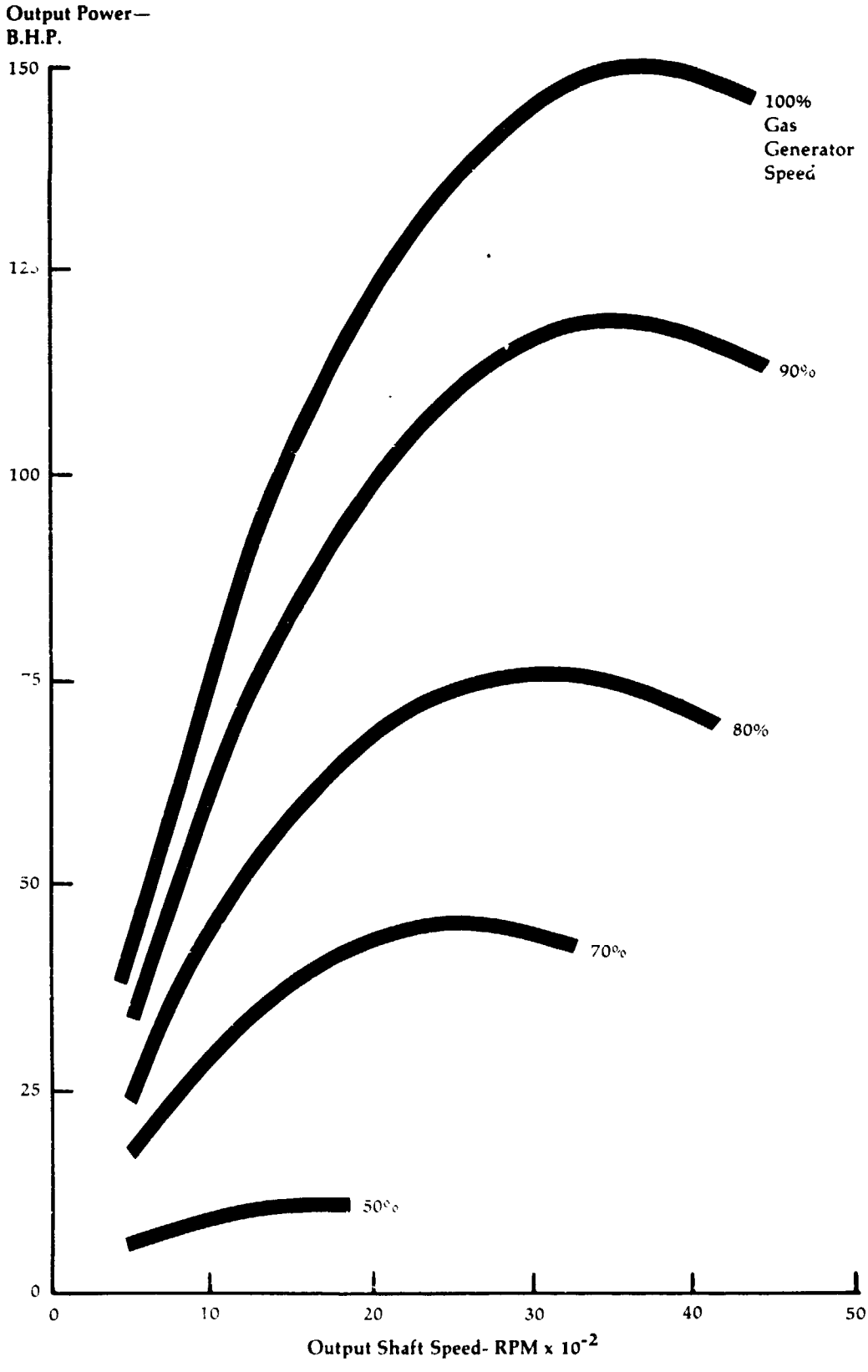

Figure 5

Engine Output Torque

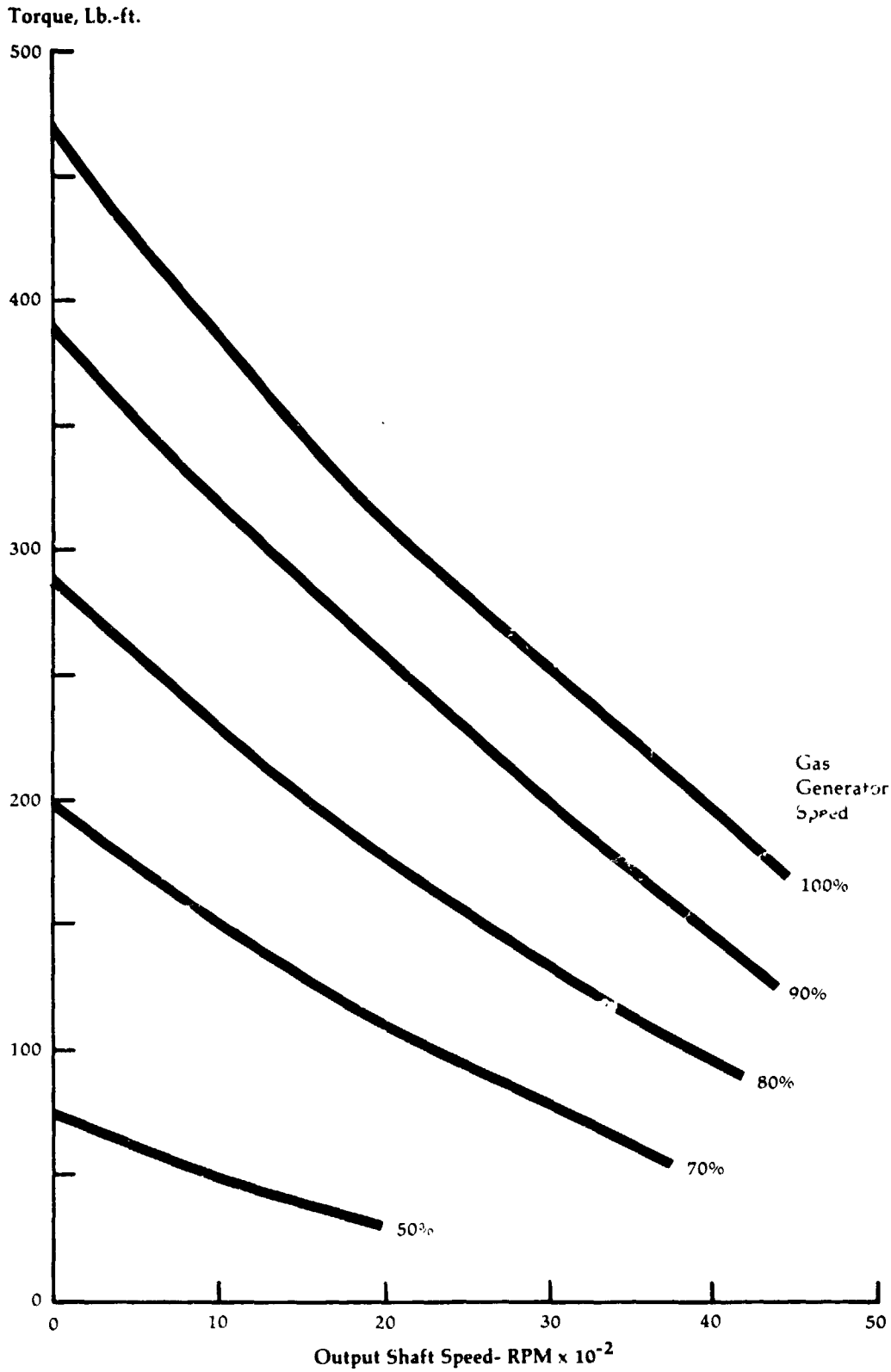

Figure 6

Engine Starting—Ambient Effects

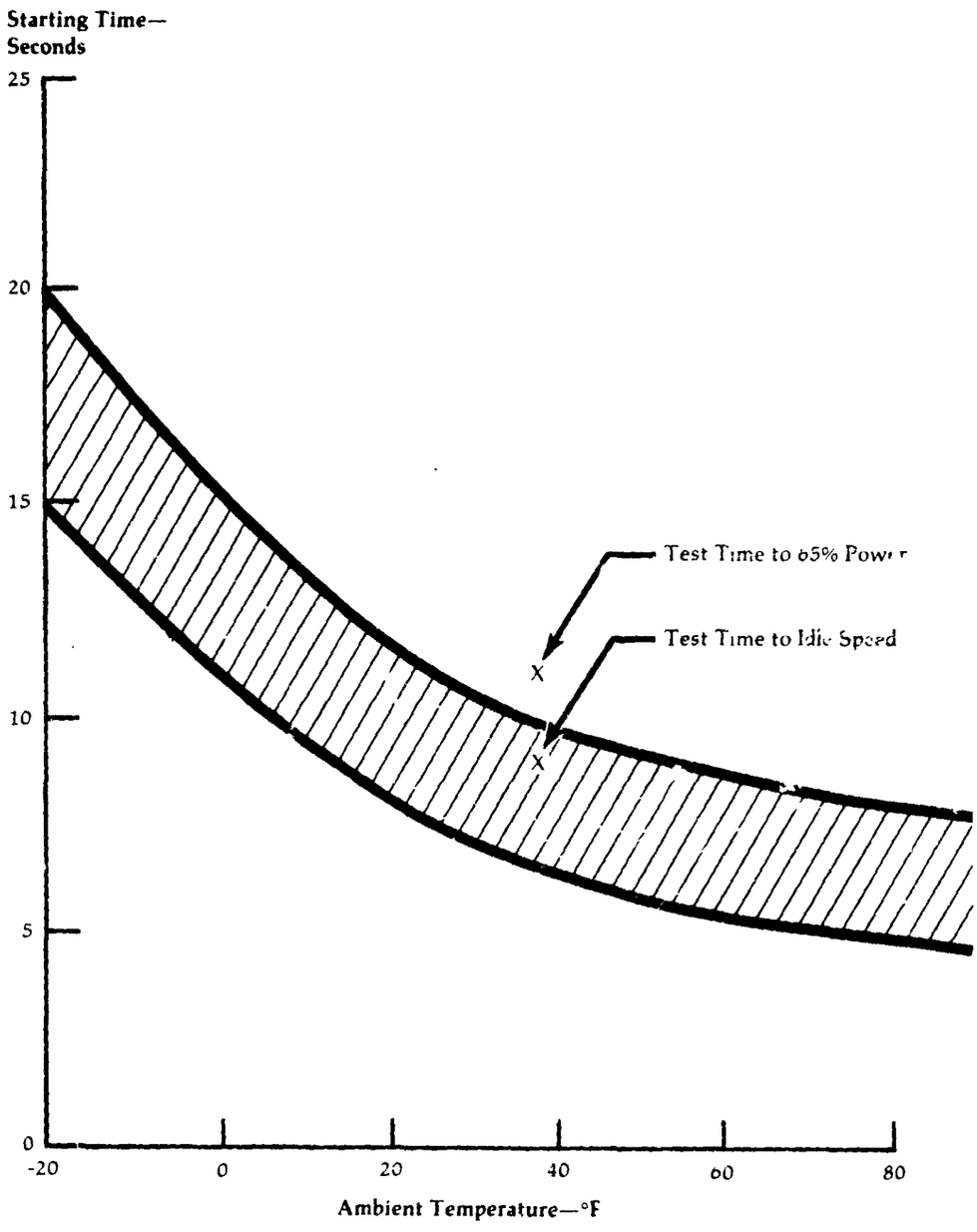

Figure 7

Brake Specific Fuel Consumption

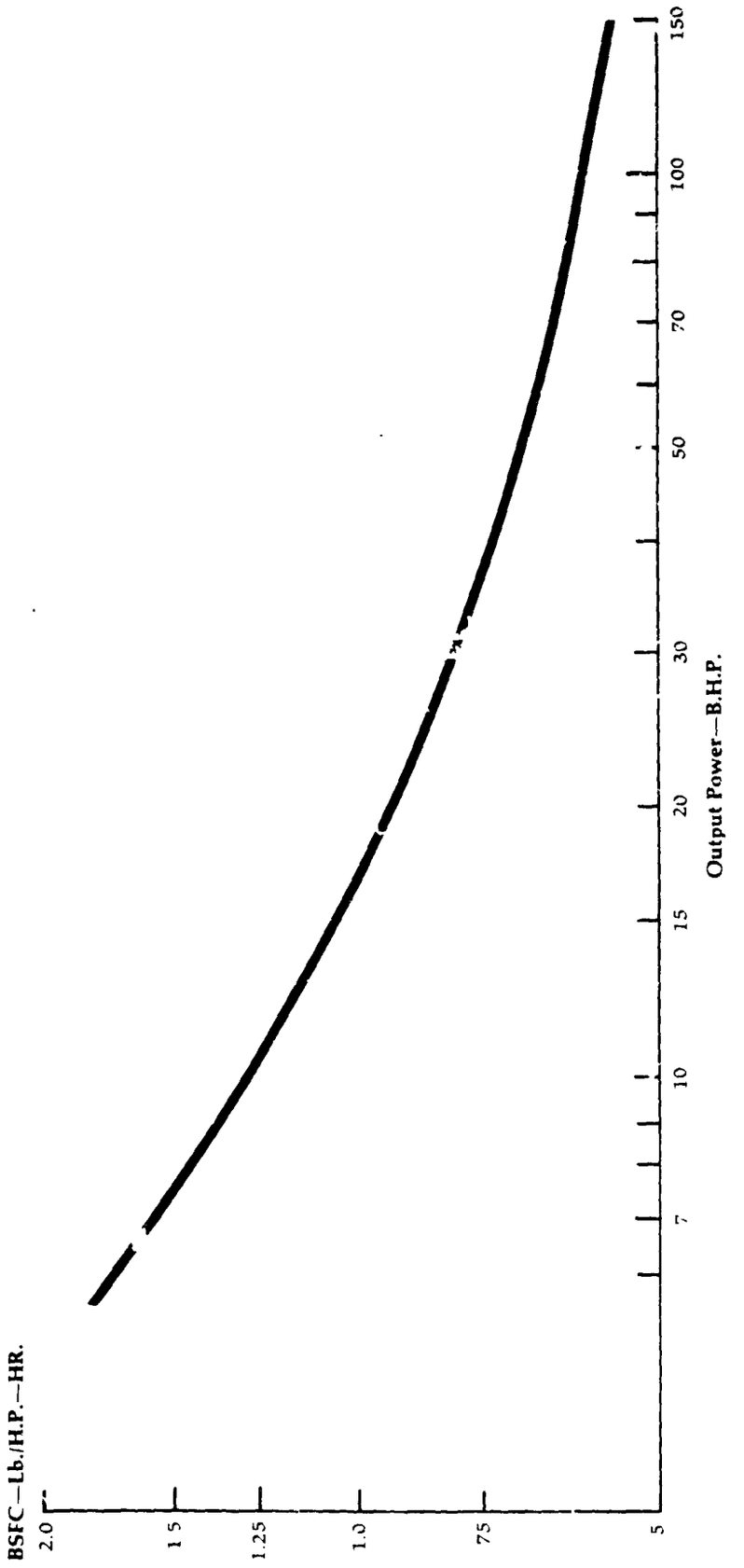

Figure 8

Typical Emissions
Steady State

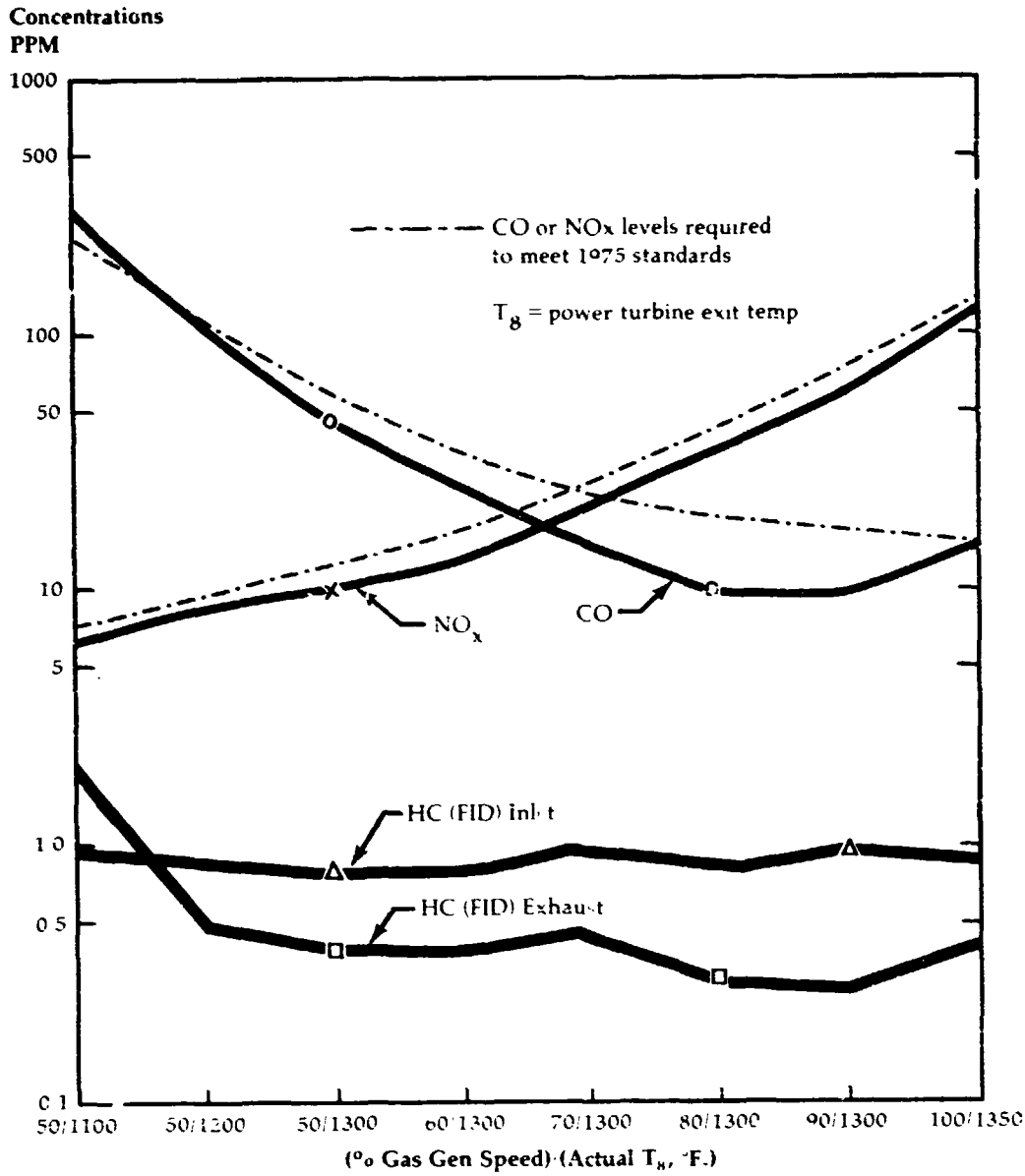

Figure 9

Gas Turbine Endurance Cycle Record

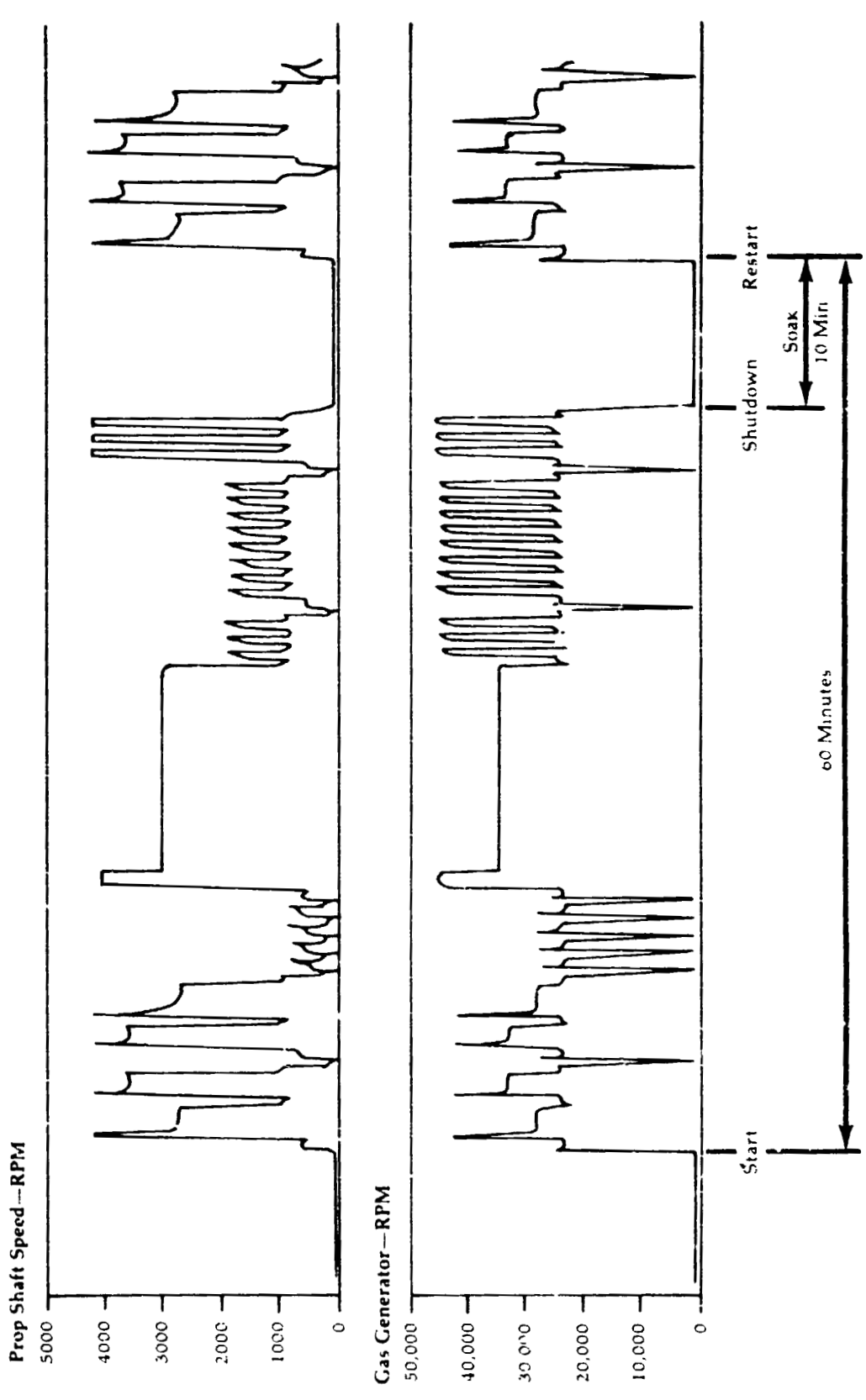

Figure 10

Baseline
First Stage
Turbine Rotor

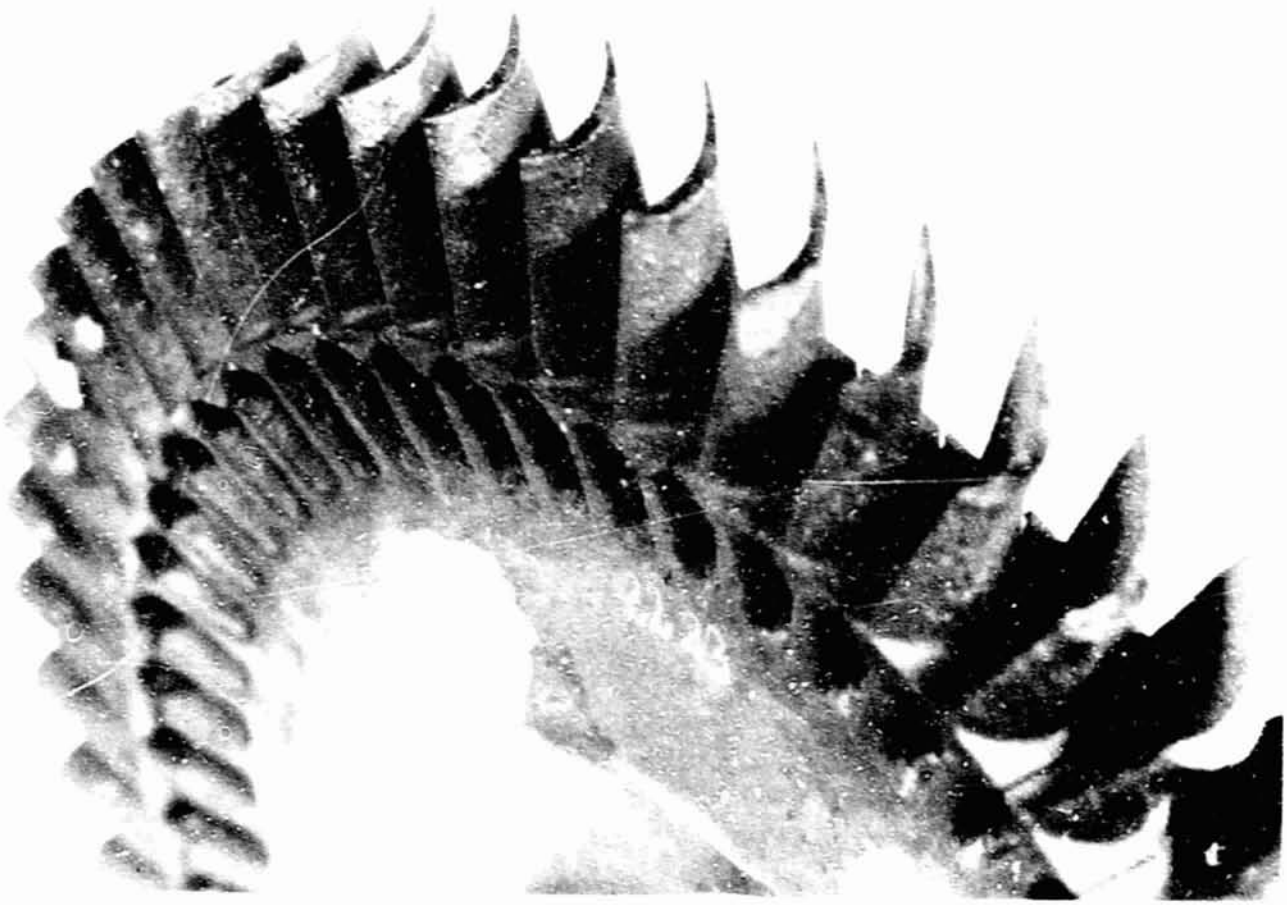

Figure 11

Baseline
First Stage
Turbine Nozzle

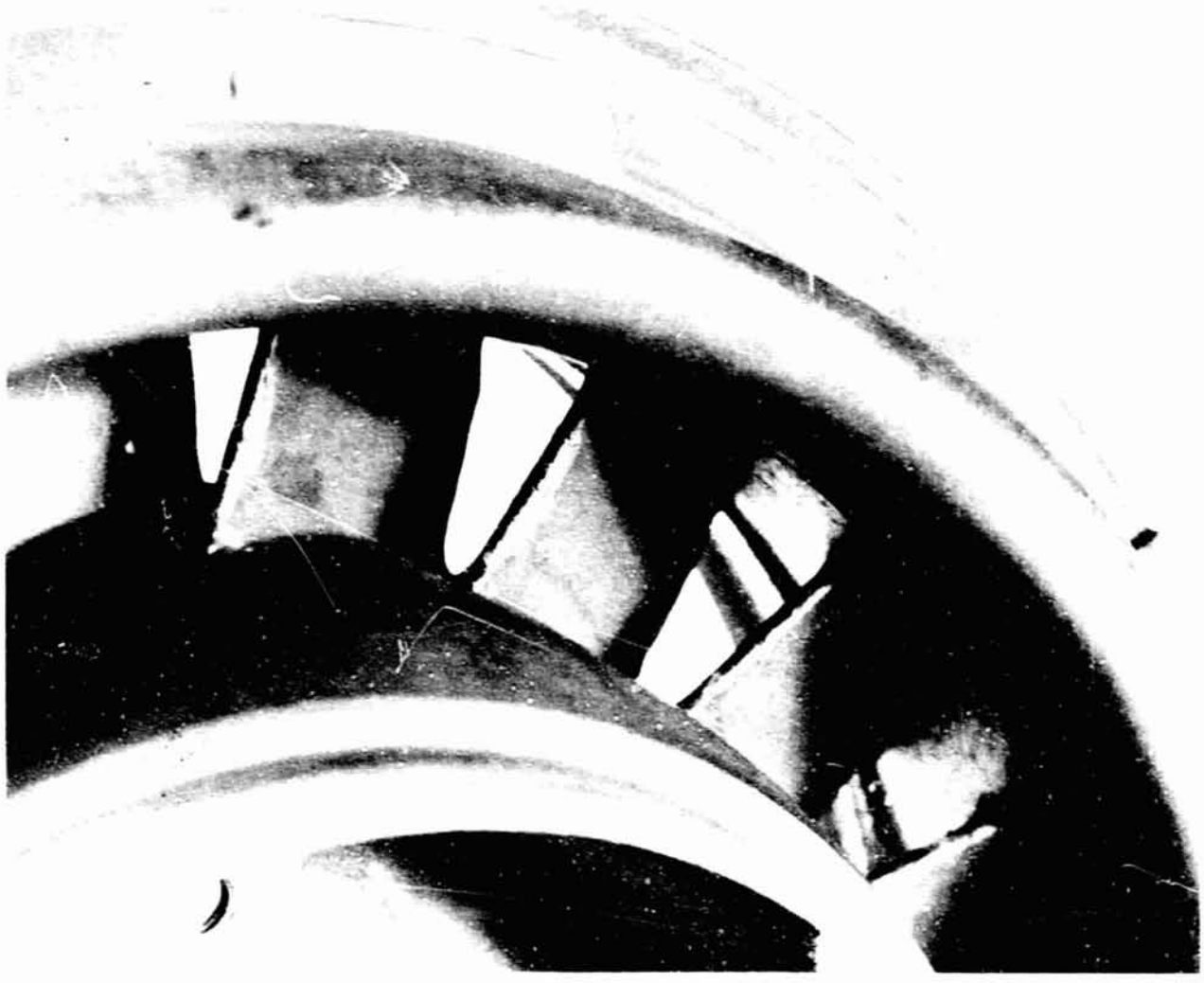

Figure 12

Modified
Endurance Cycle
For Ceramic Cores

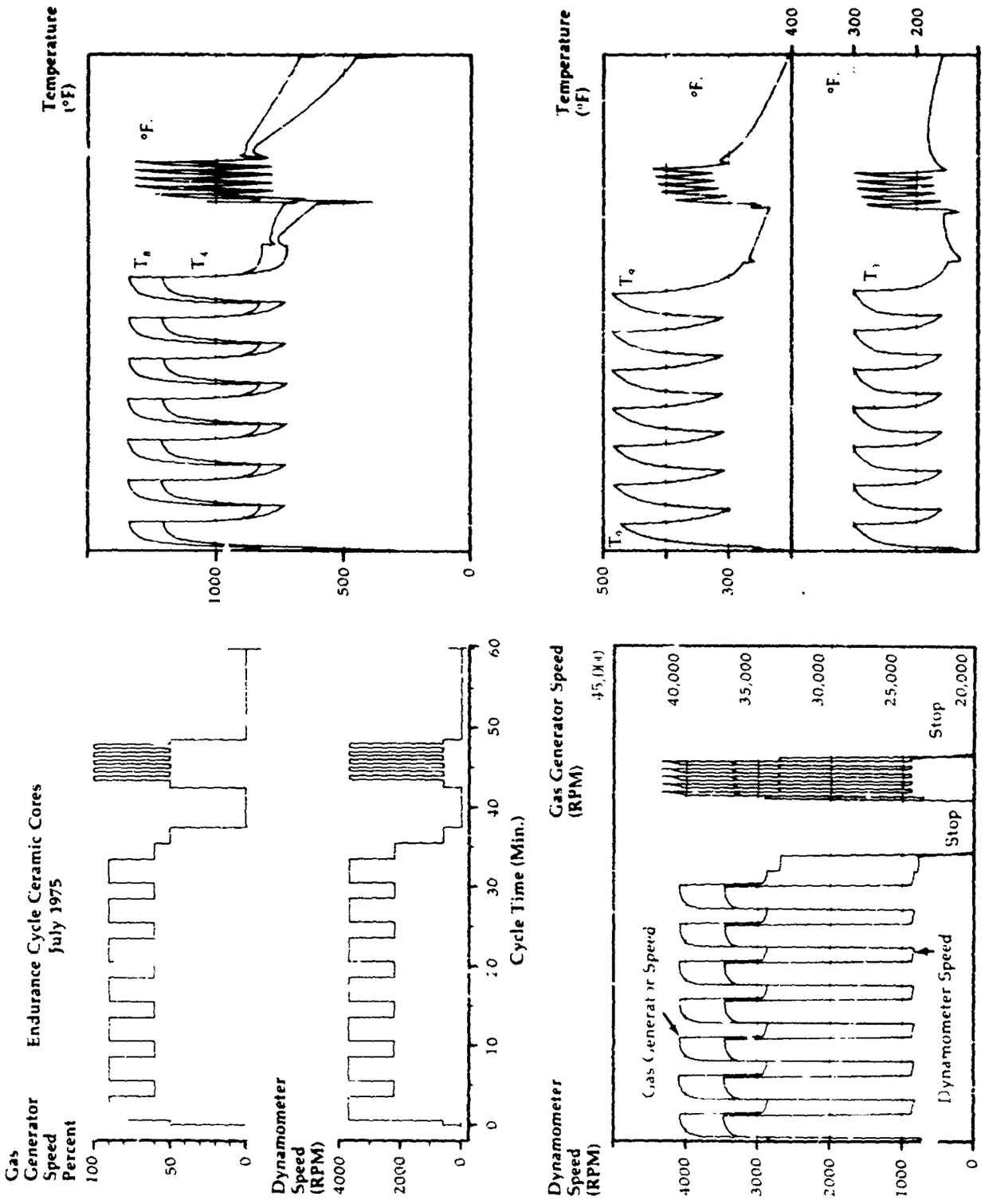

Figure 13

Coefficient of Thermal Expansion Type "A" Ceramic Core

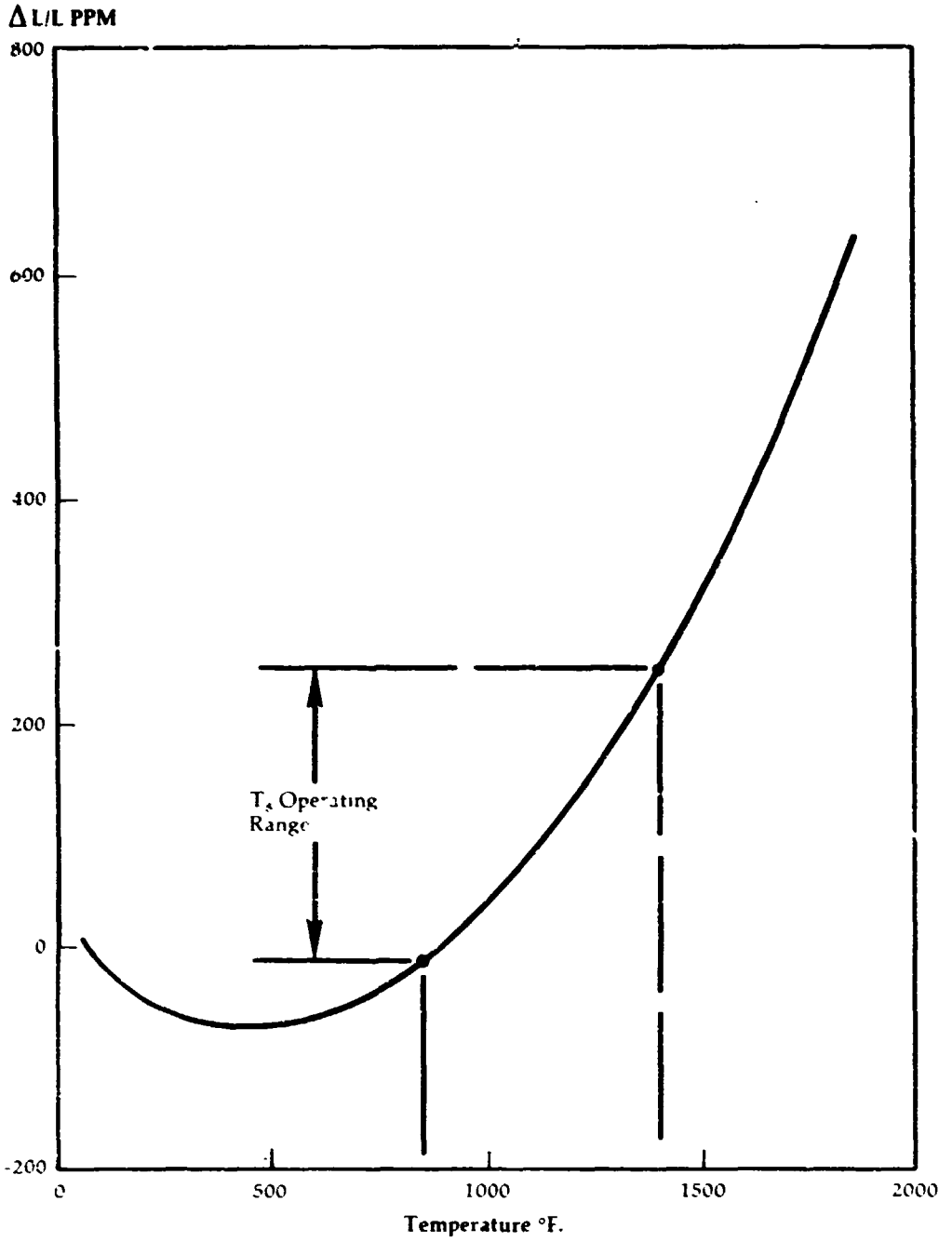

Figure 14

Baseline Turbine Powered Vehicle (Cross Sections)

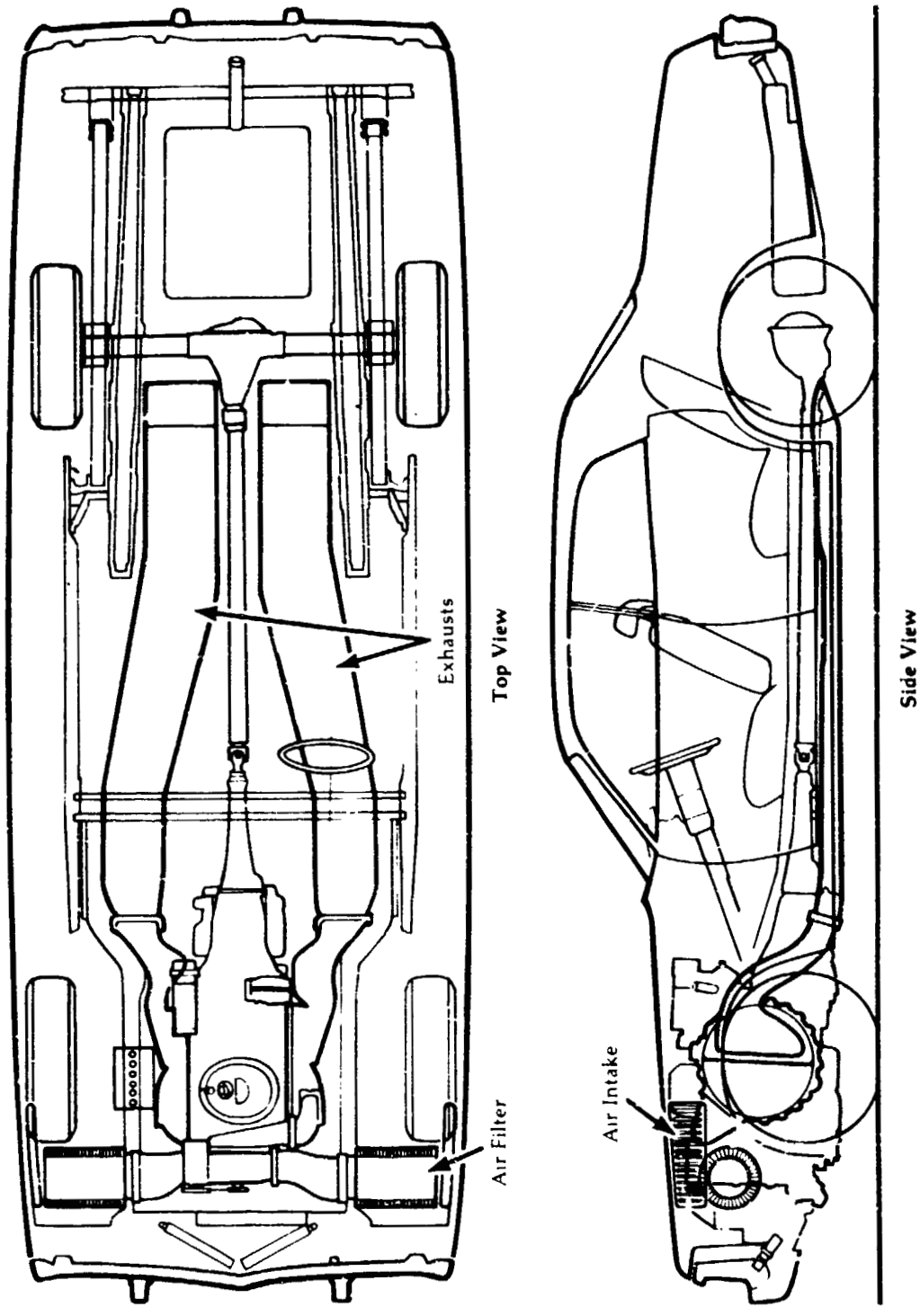

Figure 15

Baseline Vehicle

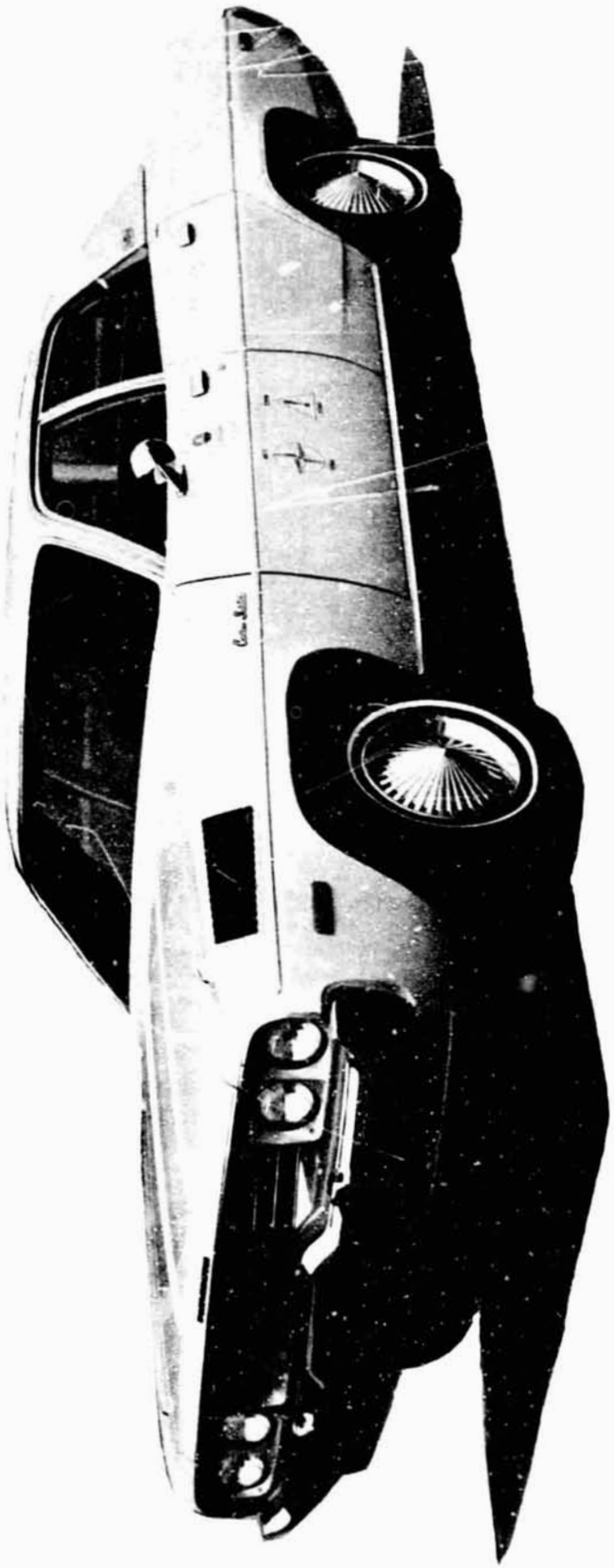

Figure 16

Baseline Vehicle Performance Speed and Distance vs. Time

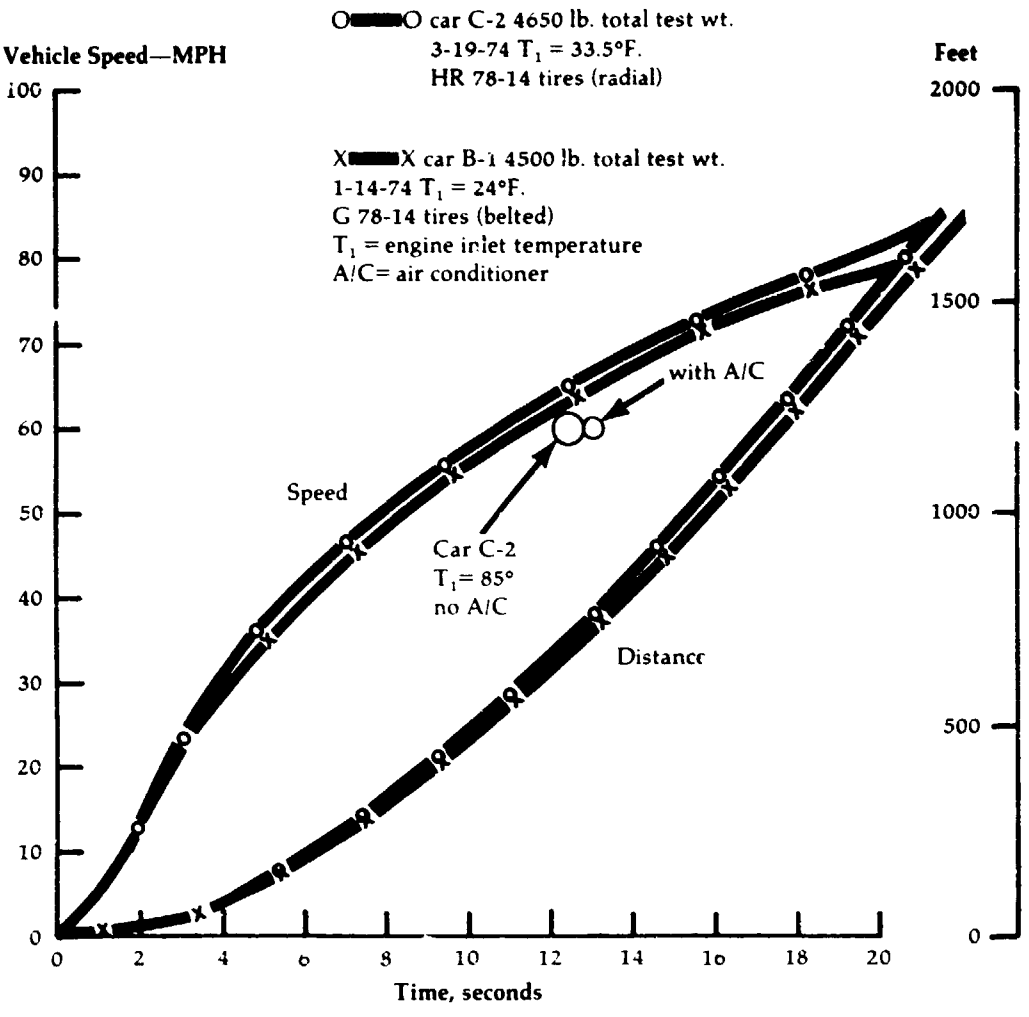

Figure 17

Baseline Vehicle Performance Vehicle Deceleration Rate with Engine Braking

Car C-2
3-11-74

HR 78-14 tires
T_1 = 37°F.
max. T_8 = 1140°F. in decel
T_1 = engine inlet temperature
T_8 = power turbine exit temp.

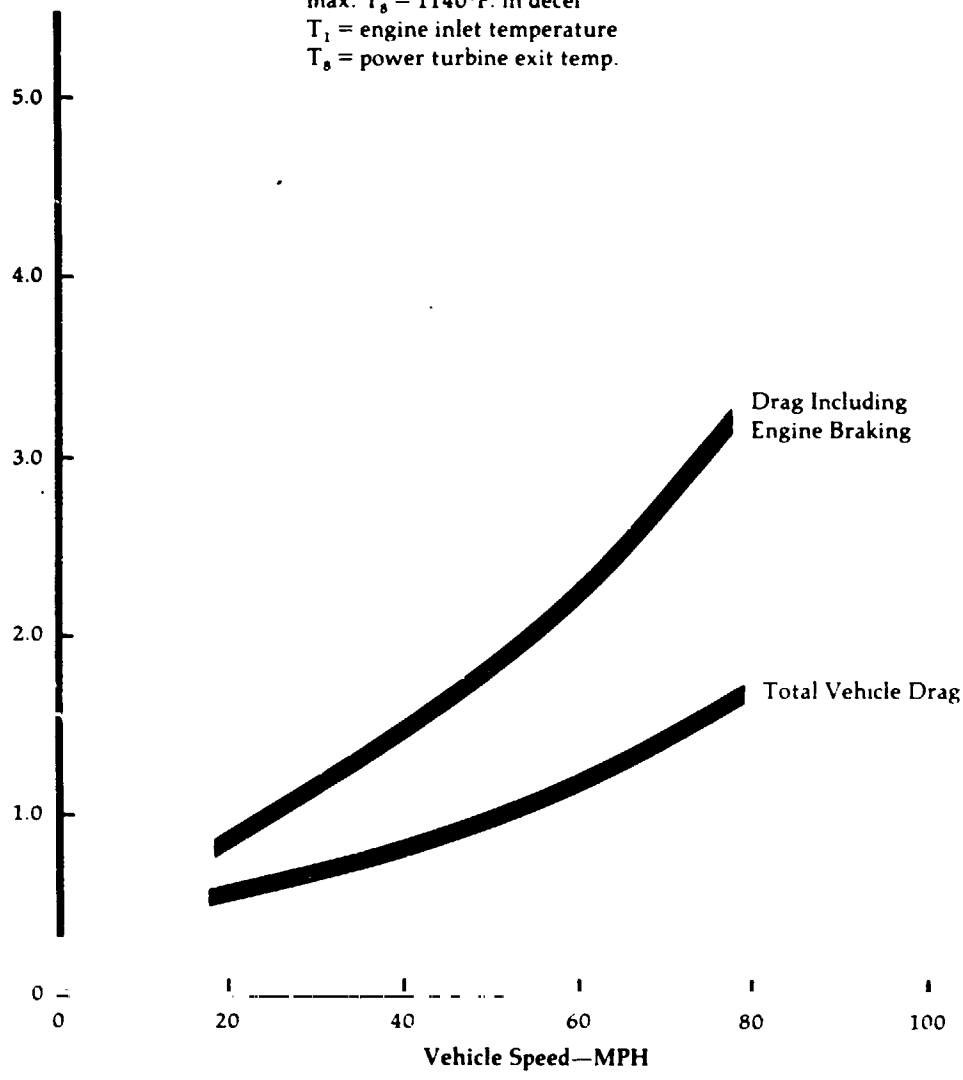

Figure 18

Baseline Vehicle Fuel Consumption Effect of Cycle Temperature

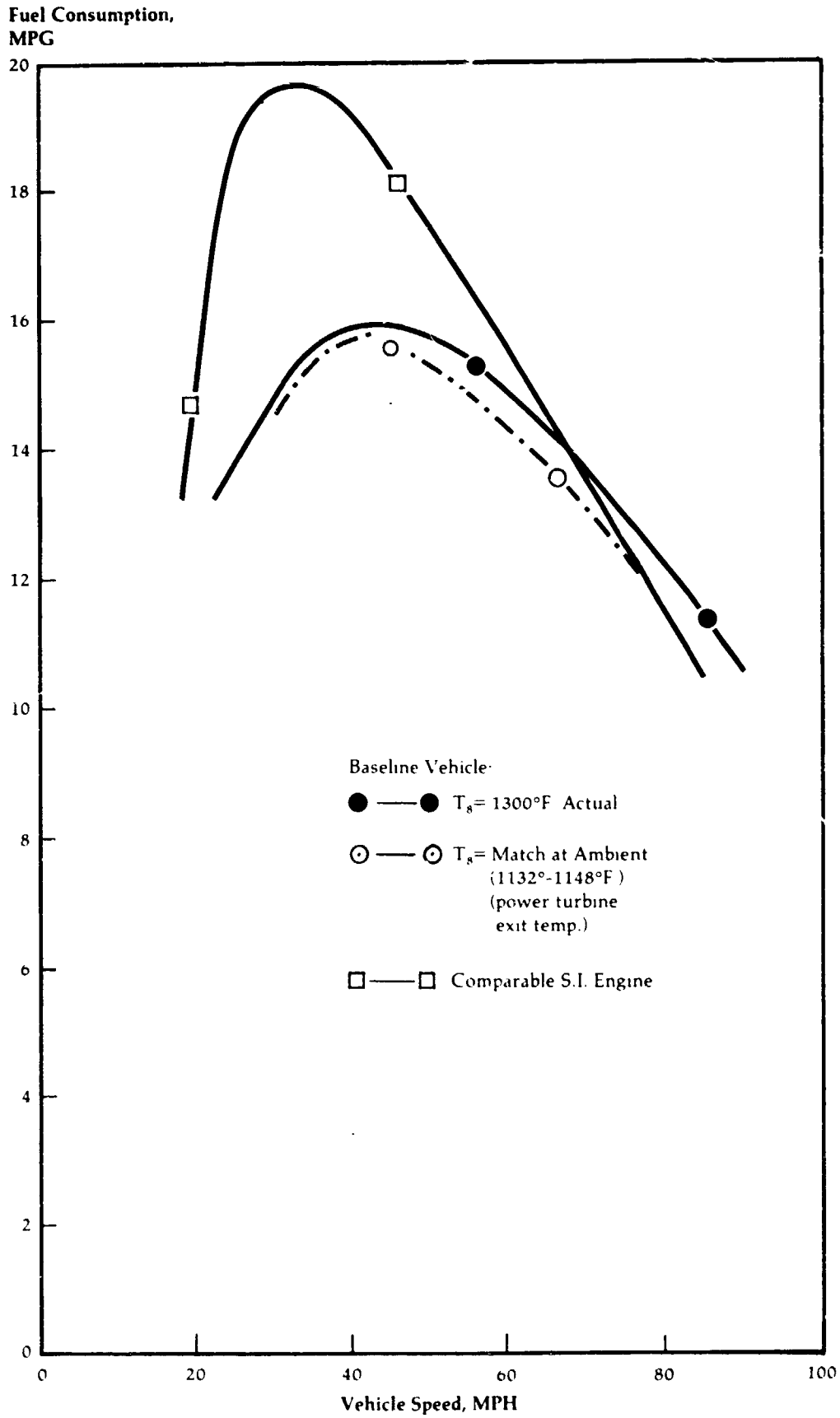

Figure 19

Effect of Exhaust Pressure On Engine Performance

Design Engine Speed

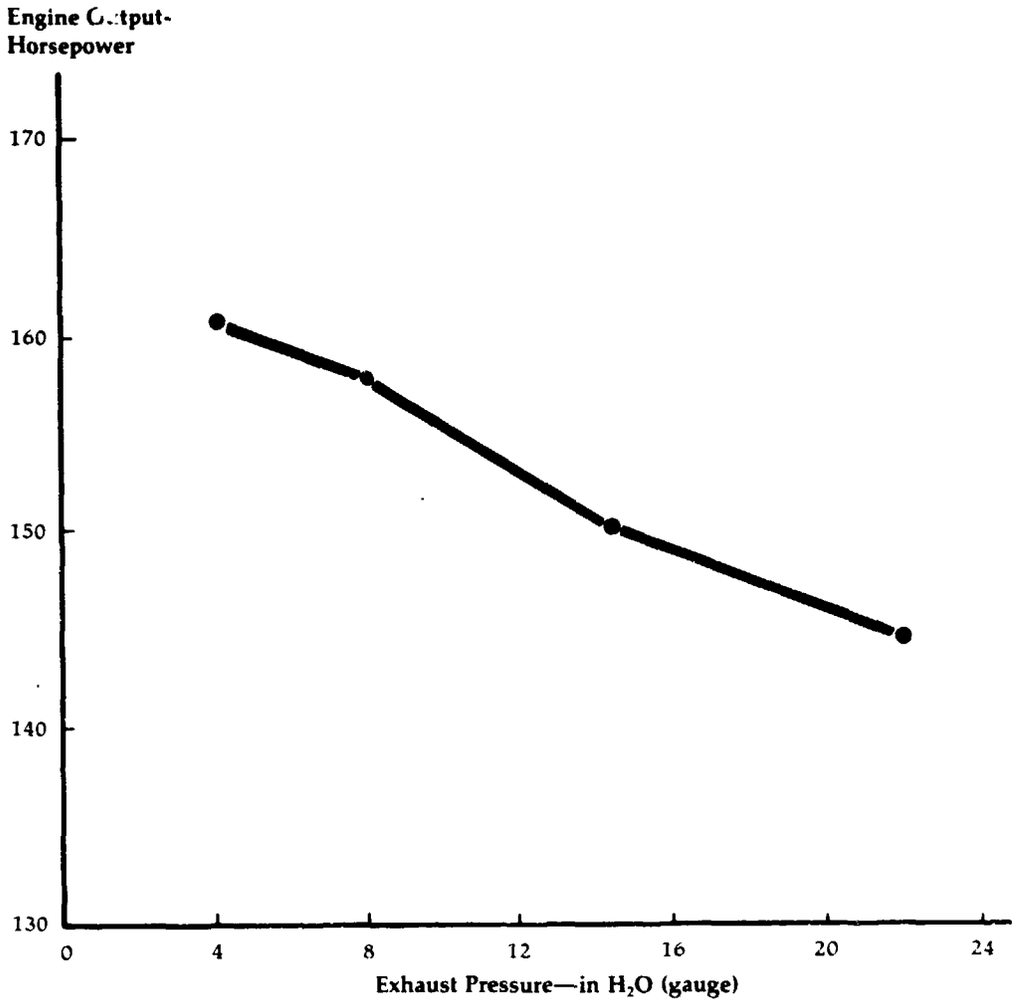

Figure 20

Car Comfort System

(Schematic)

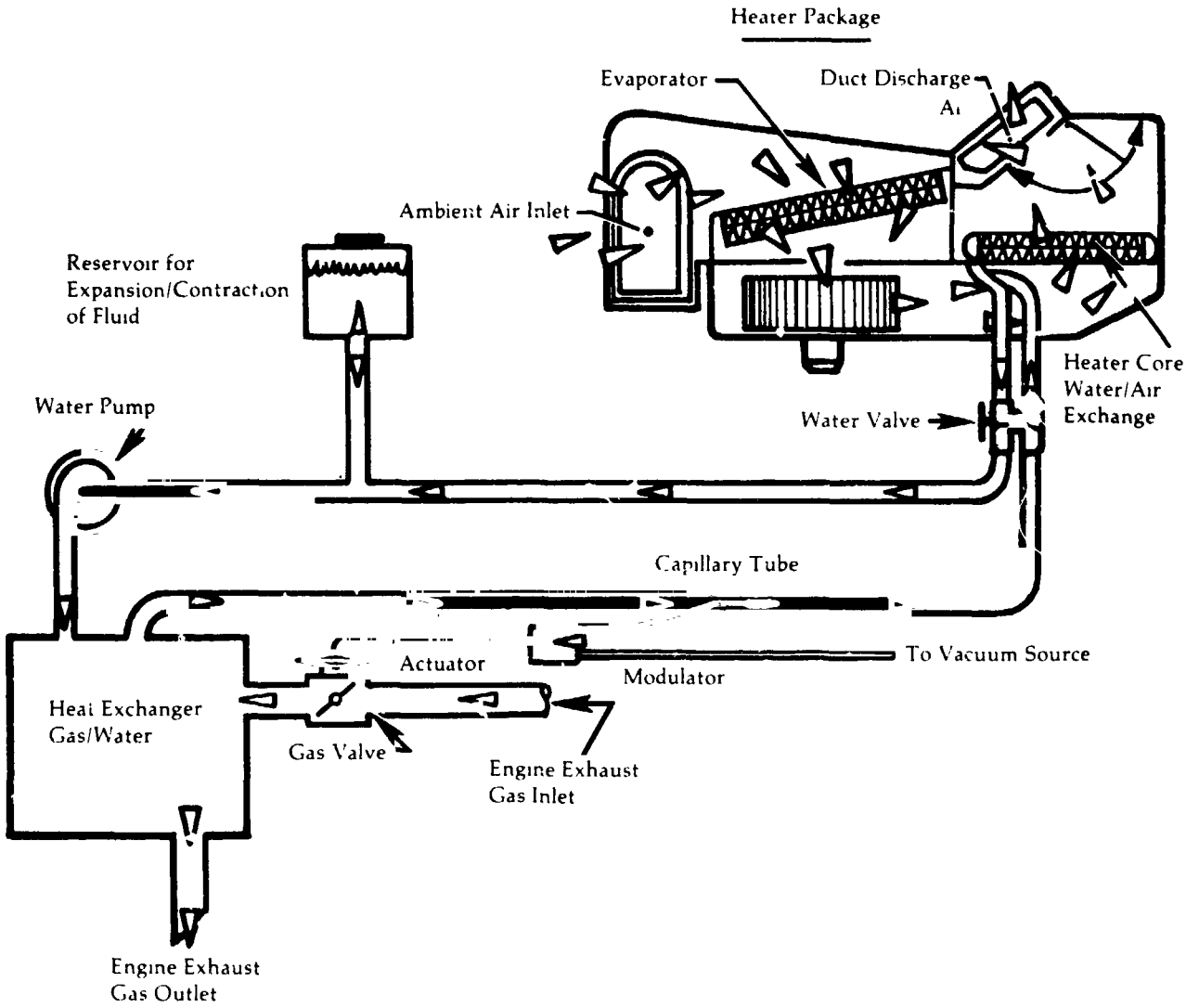

Figure 21

Engine Speed Timers in Vehicle Trunk

Figure 22

Baseline Vehicle-Use Cycle

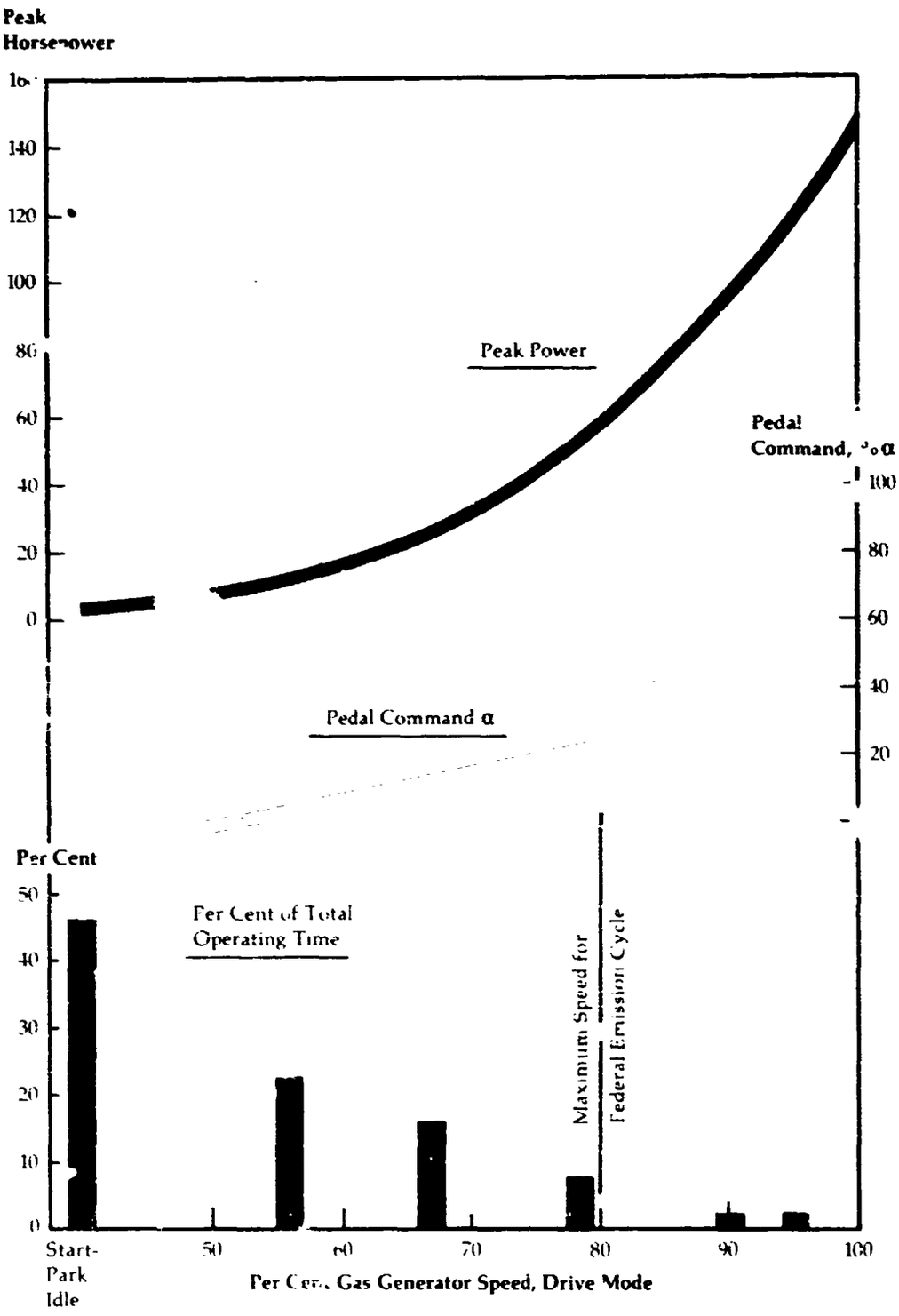

Figure 23

Vehicle Hydraulic System

(Schematic)

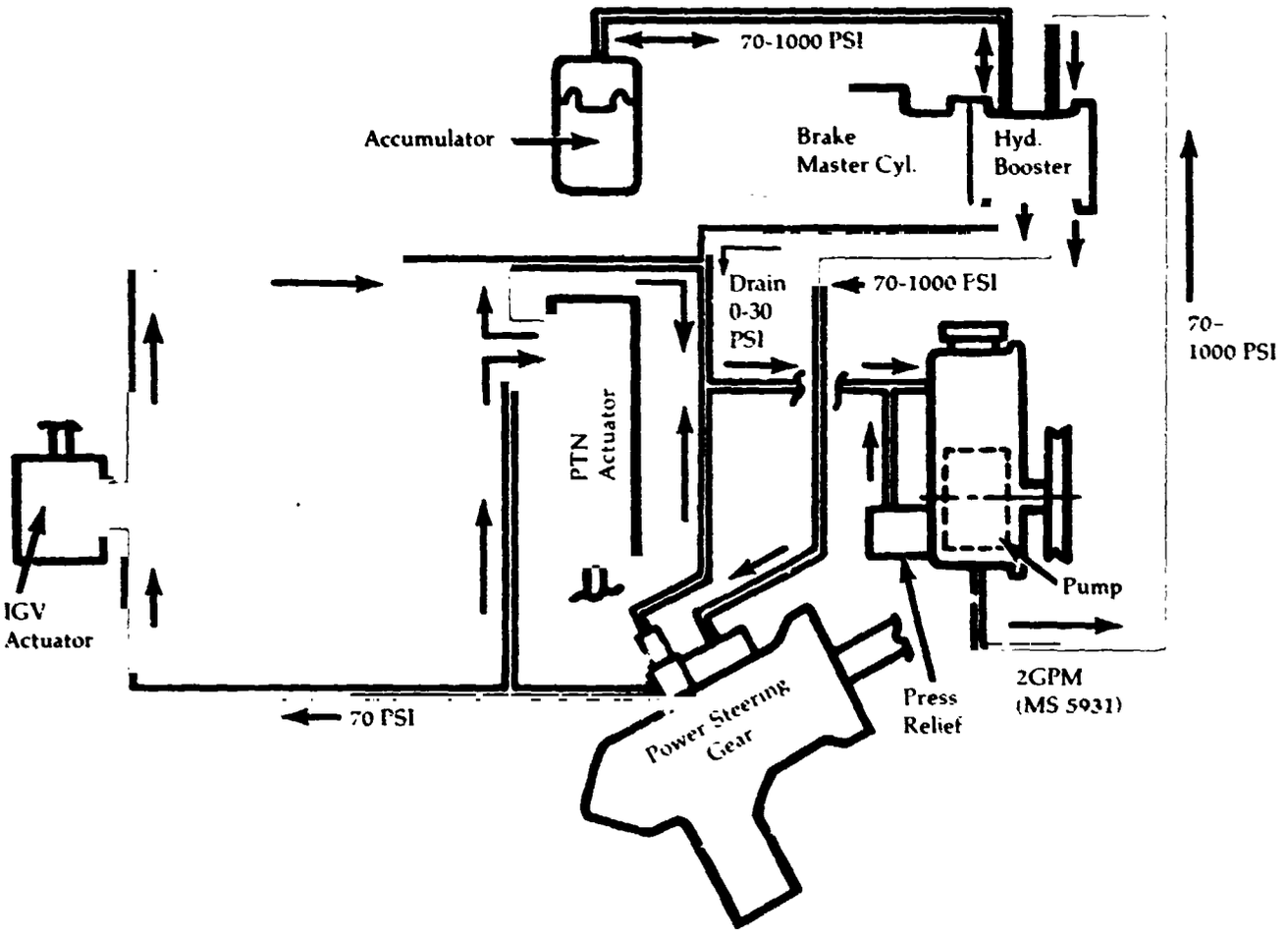

Figure 24

Variations of Air and Fuel Flow

Federal Drive Cycle

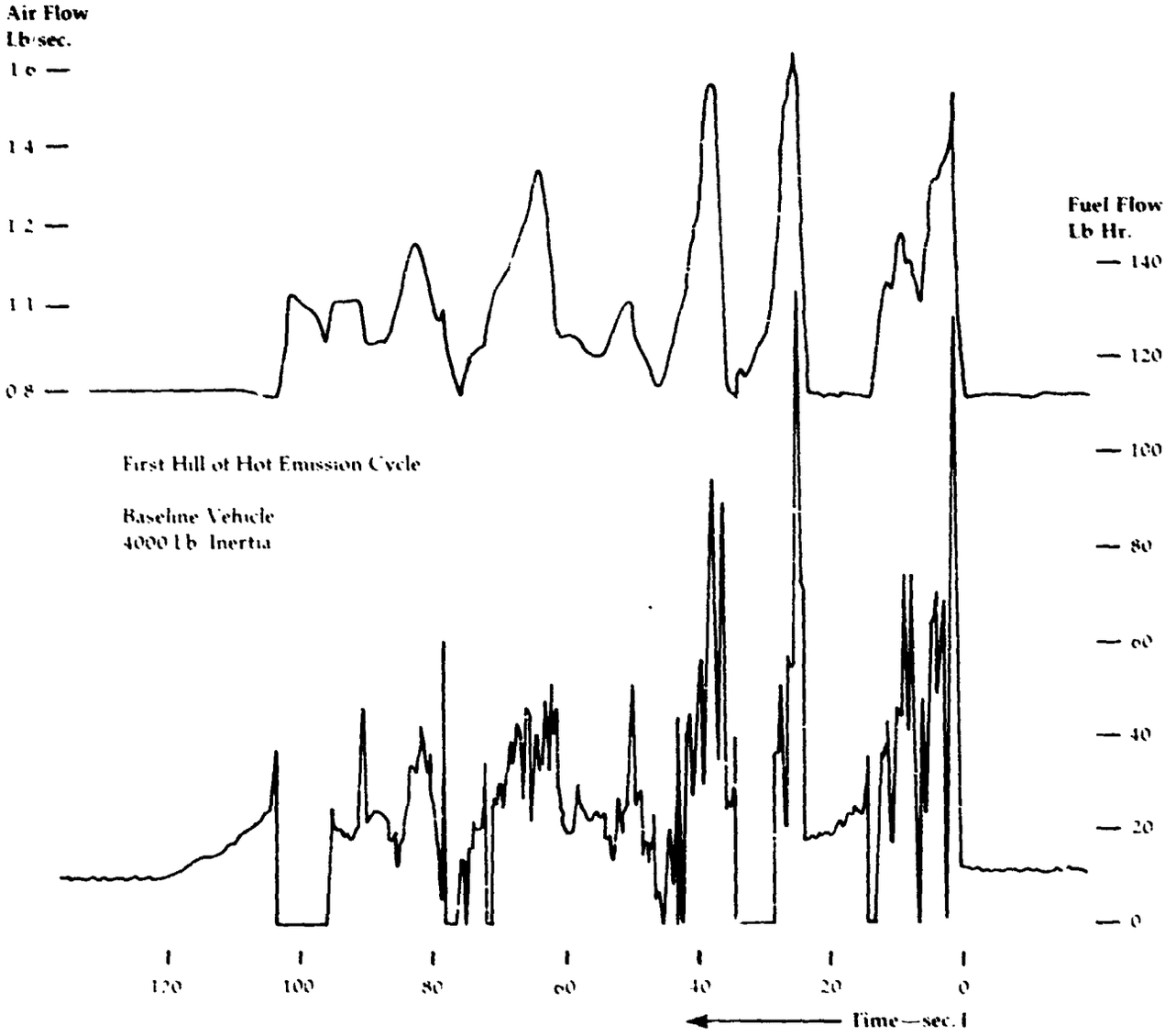

Figure 25

Effects of Inlet Contamination on Exhaust Levels

Normal Operating Temperatures at Various Speeds

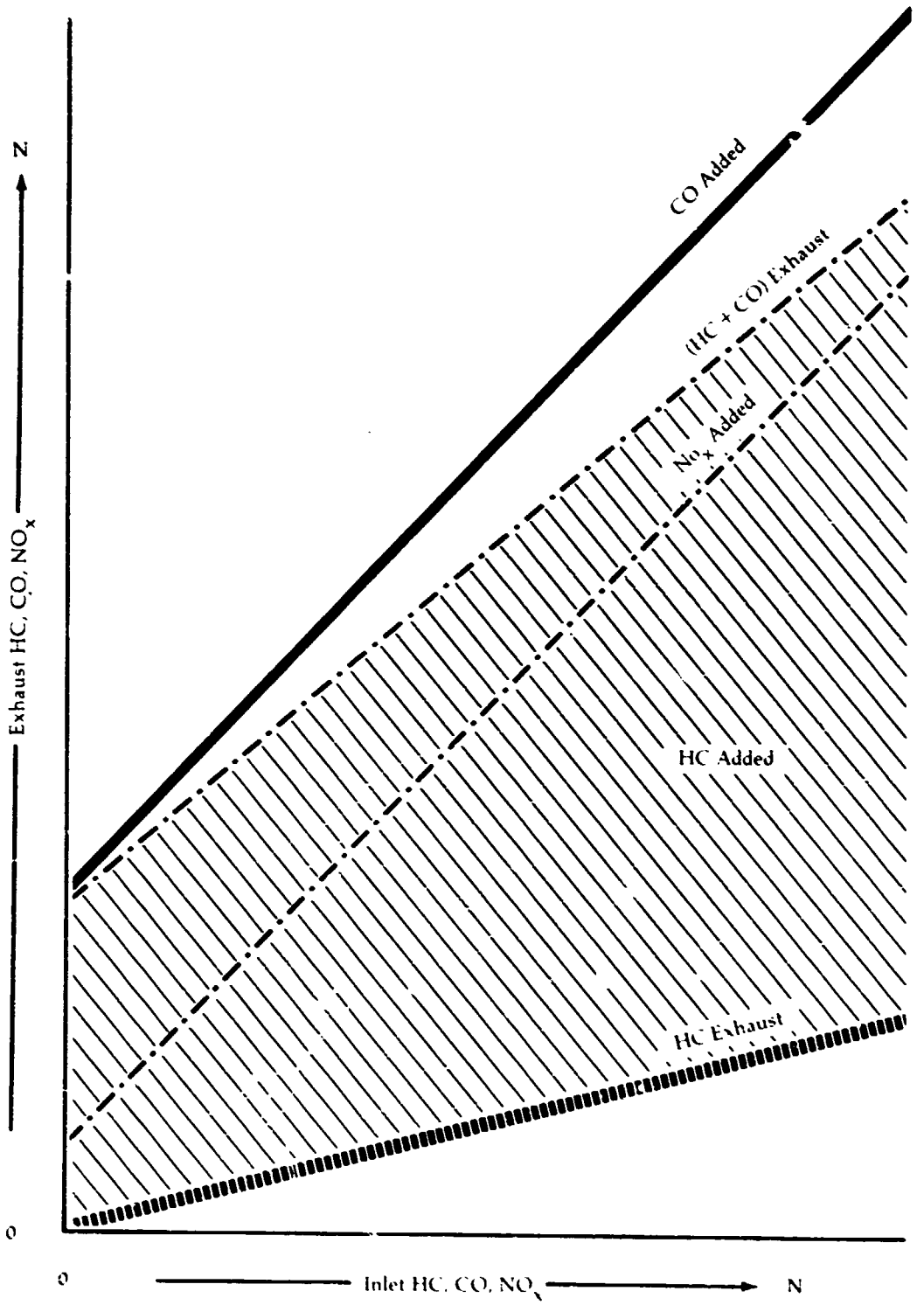

Figure 26

Hybrid Engine Control System

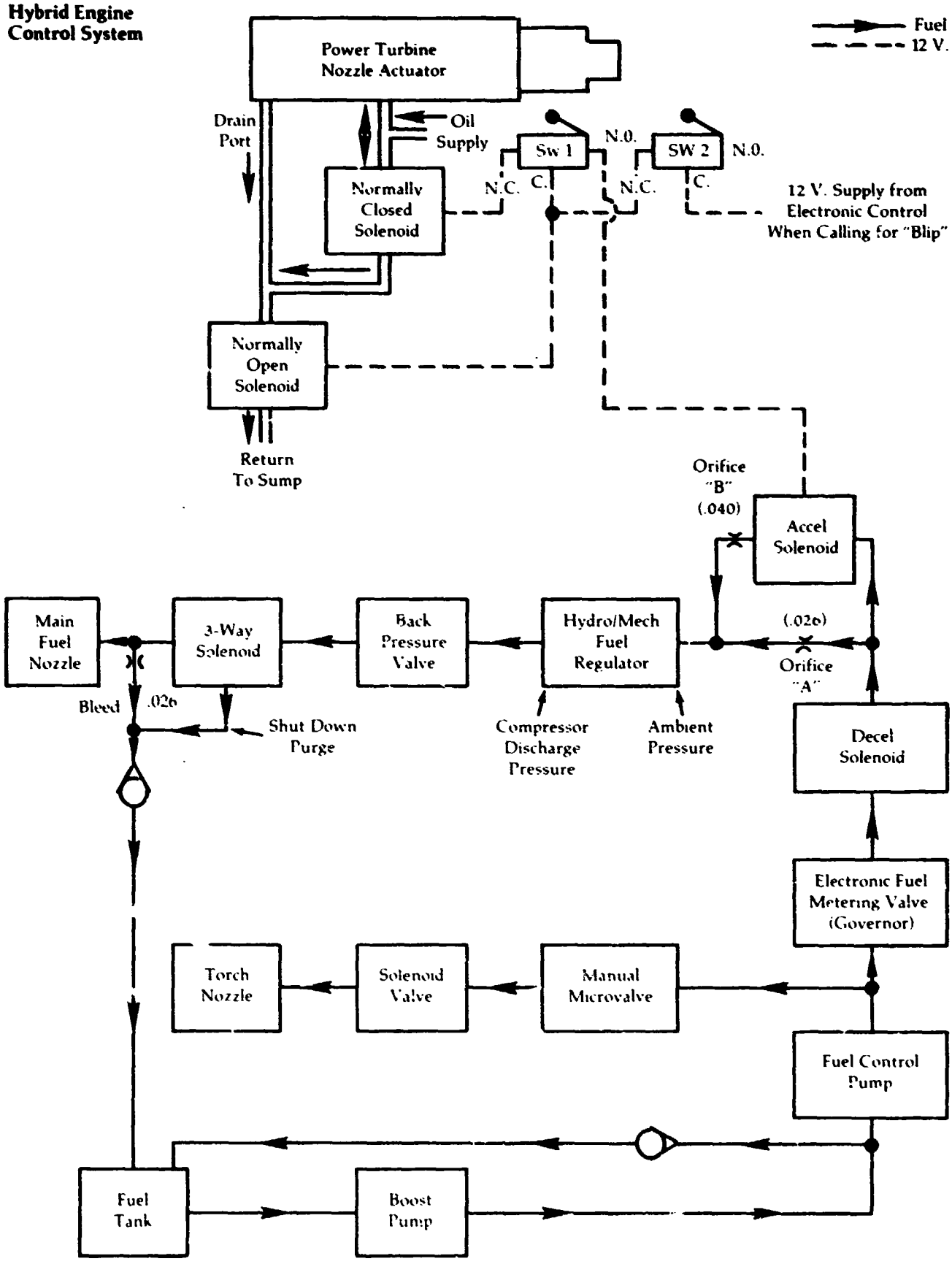

Figure 27

Automotive Gas Turbine Emission Test System

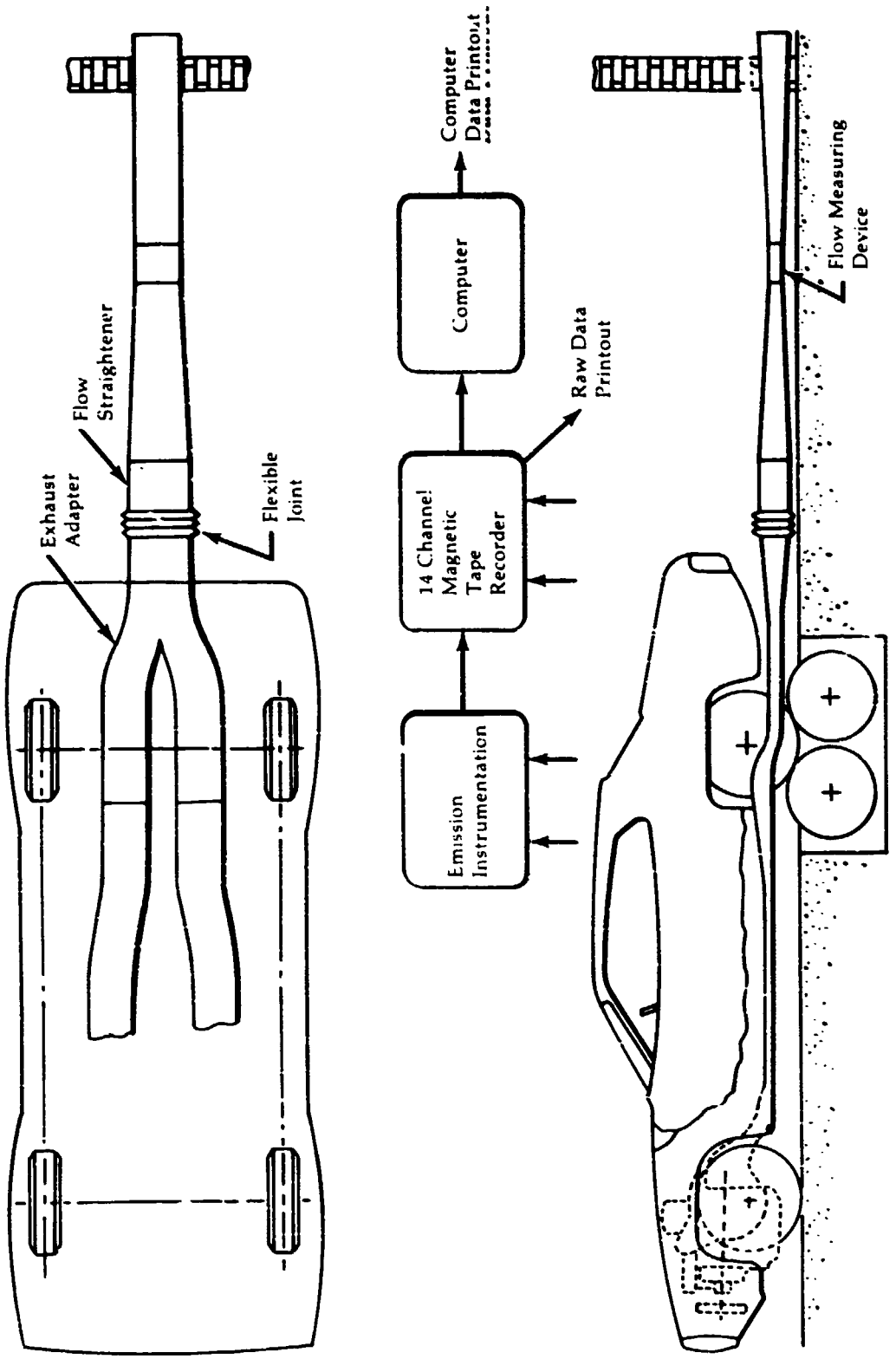

Figure 28

Exhaust Emissions

Steady State Vehicle Speeds

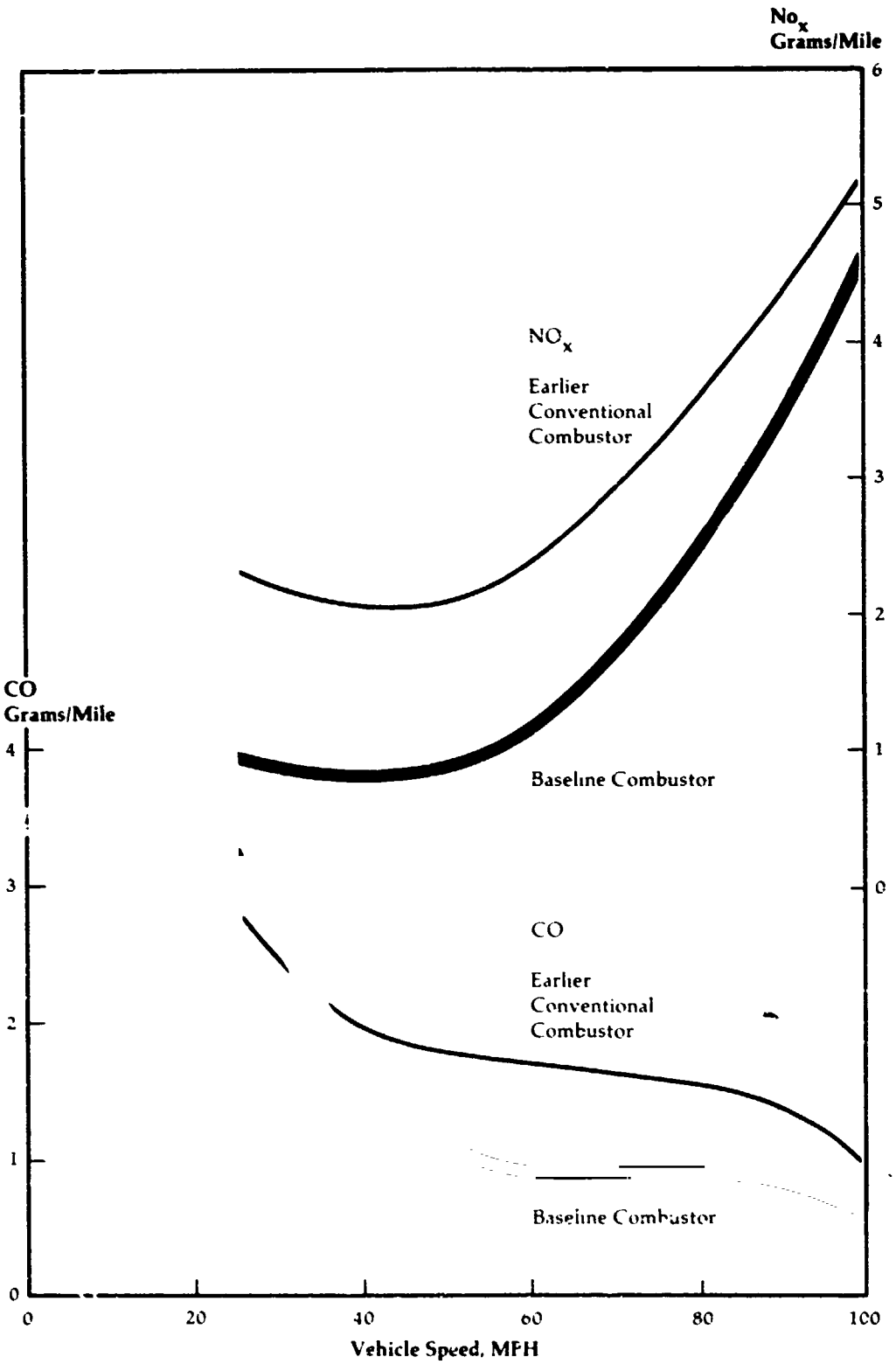

Figure 29

Solar Combustor
Variable Geometry

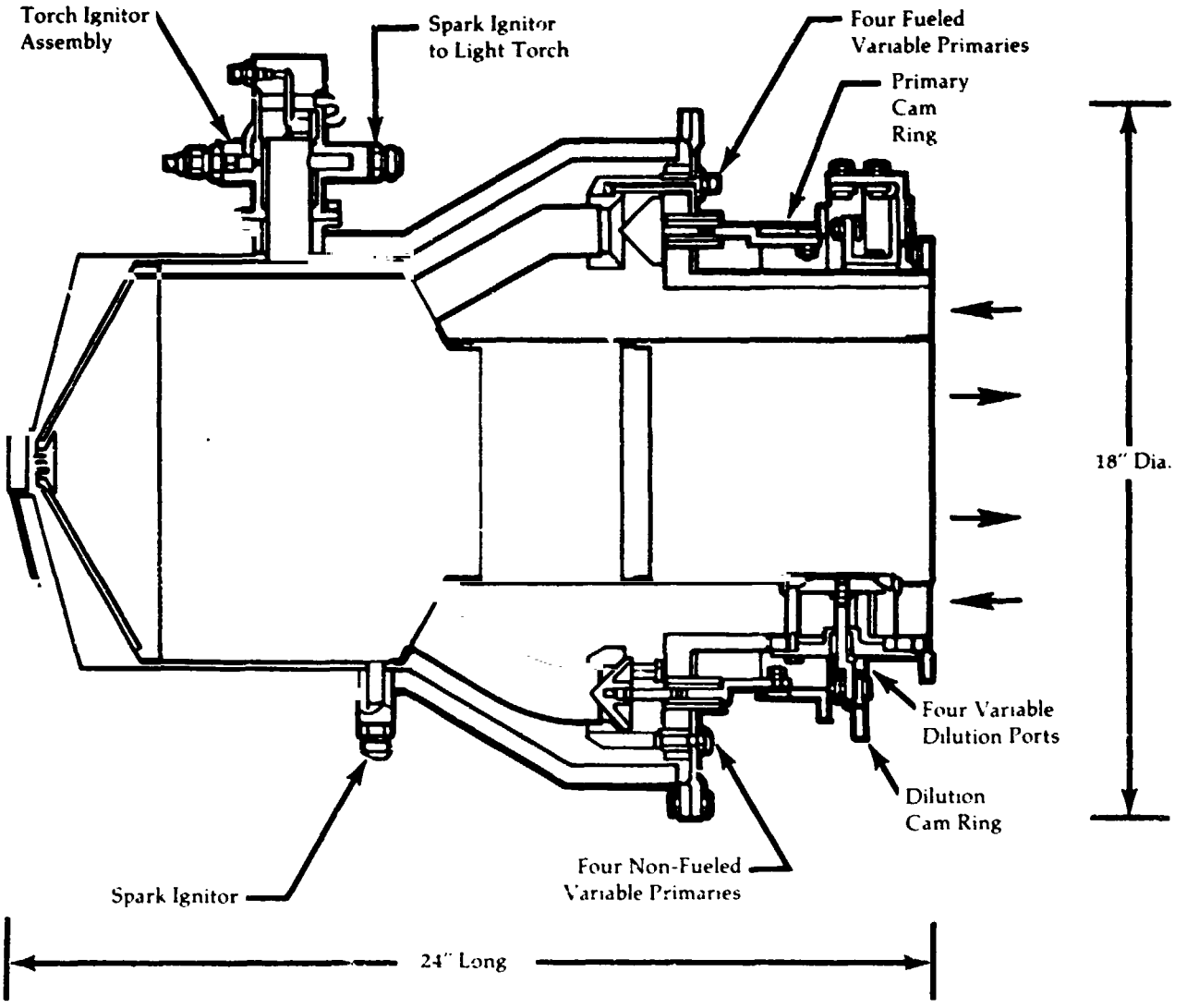

Figure 30

Comparison of Steady State Emissions

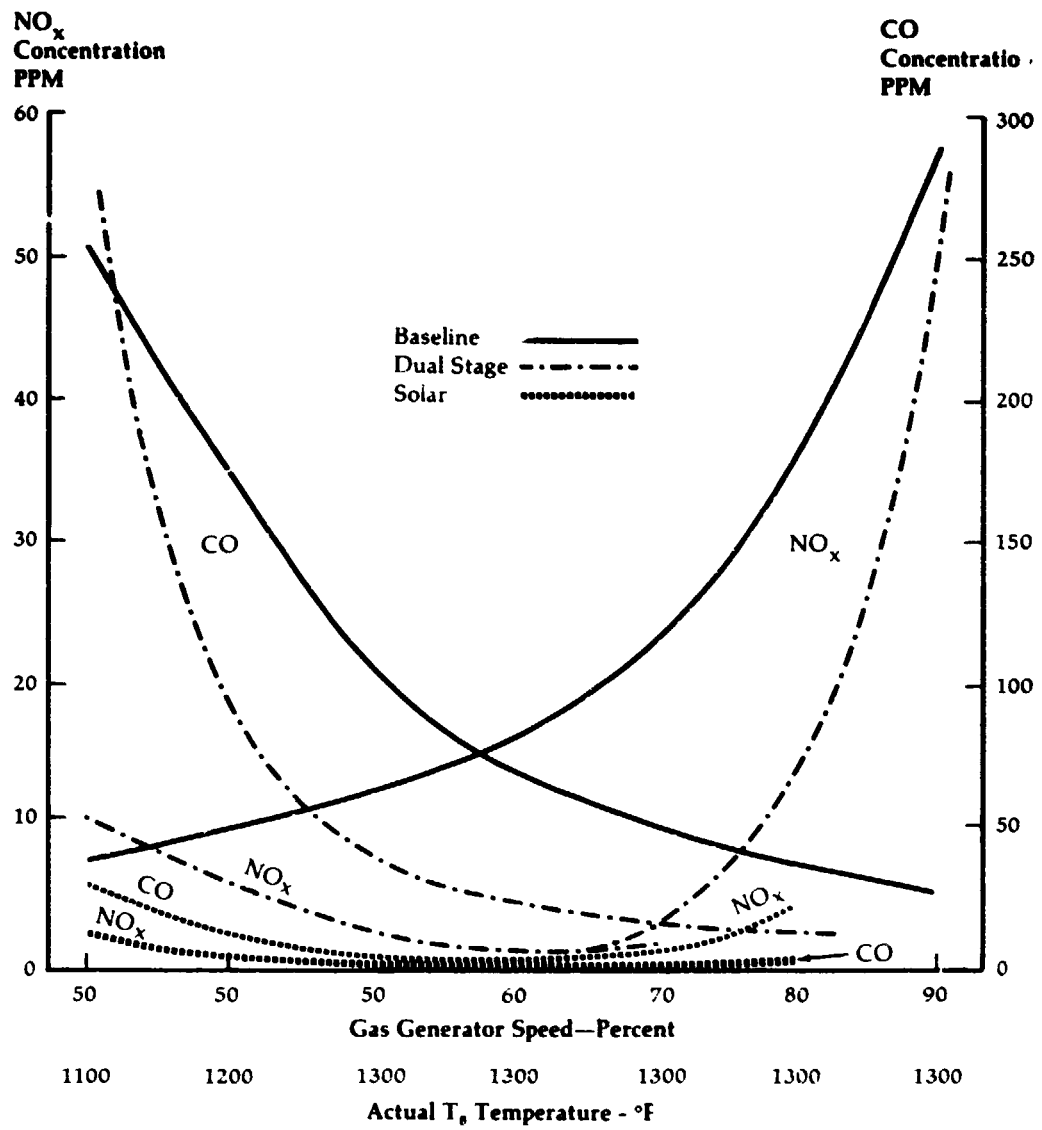

Figure 31

Dual Stage Combustor

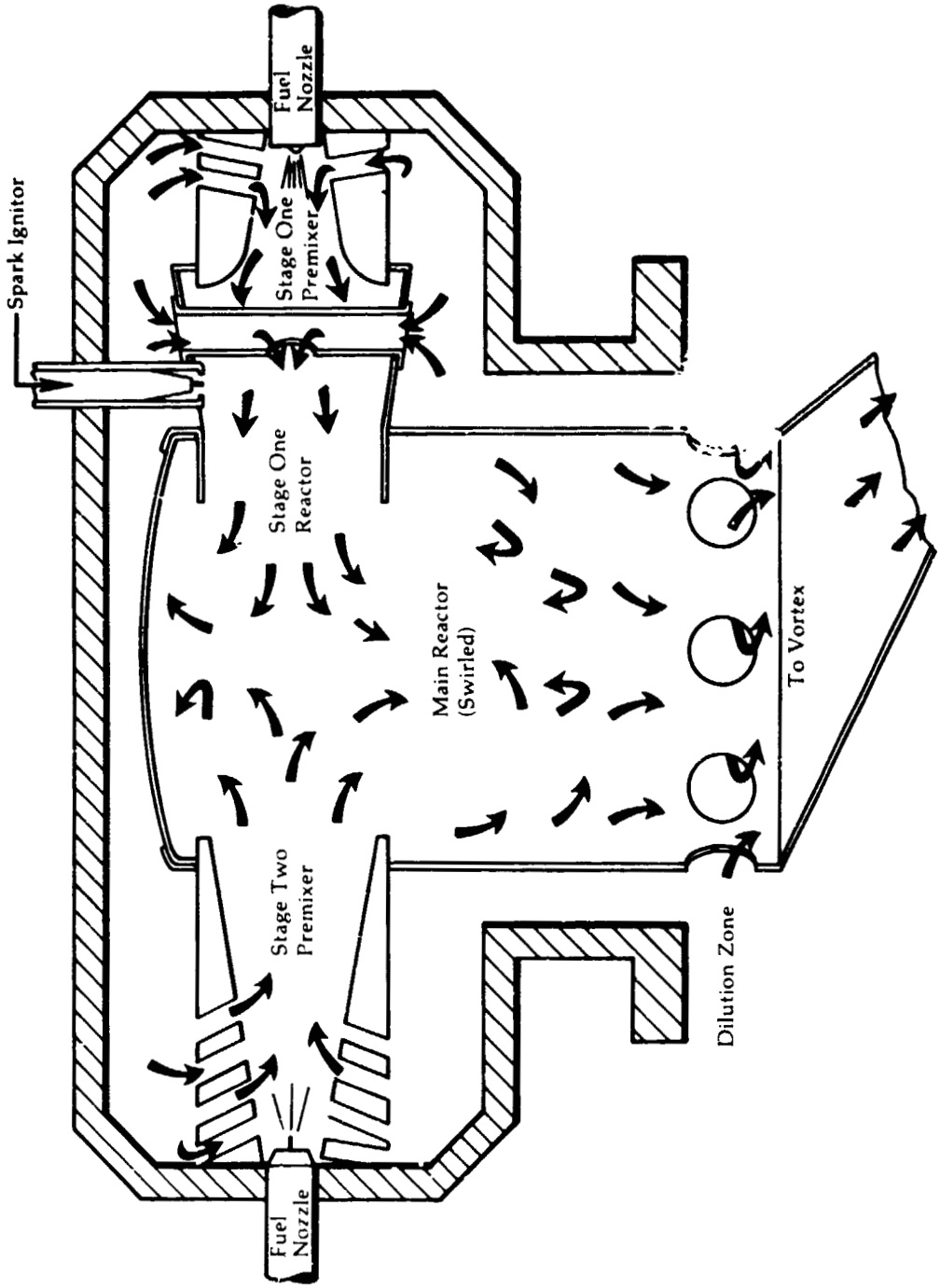

Figure 32

Pre-Mixed Combustor With Torch Ignitor

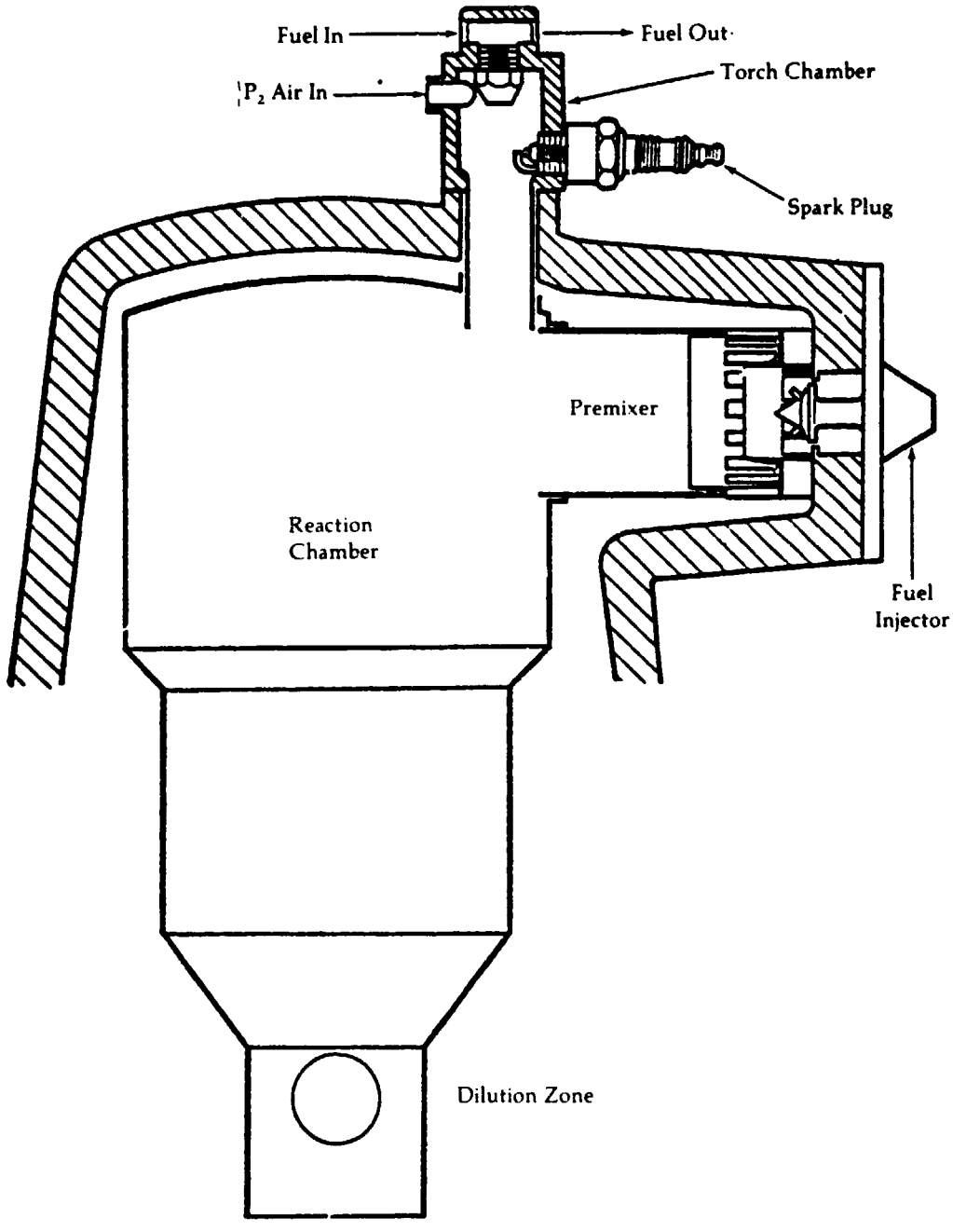

Figure 33

Engine Fuel Requirements And Constraints For NOx Control

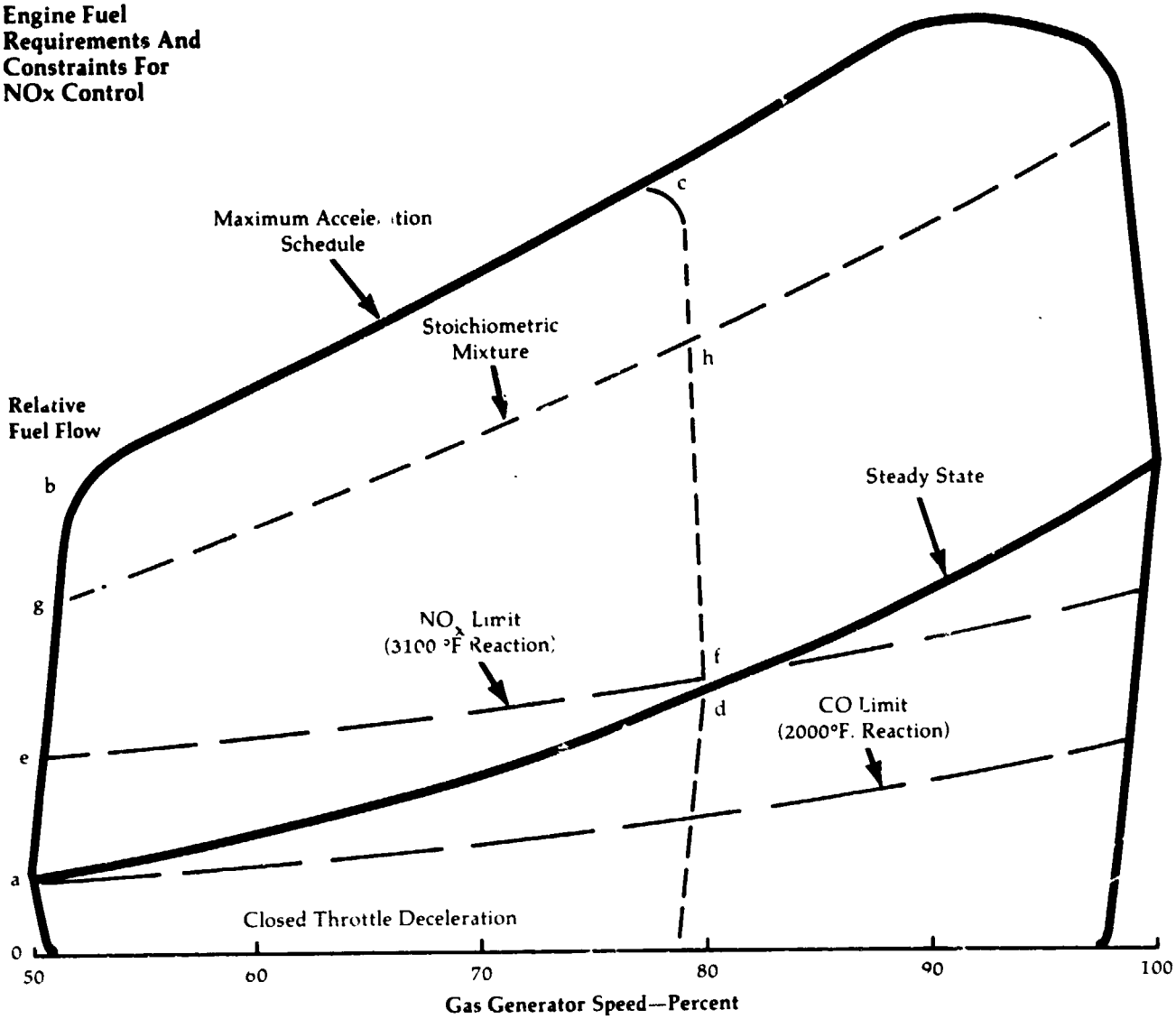

Figure 34

Effect of Turbine Nozzle Control on Fuel Flow and Rotor Response

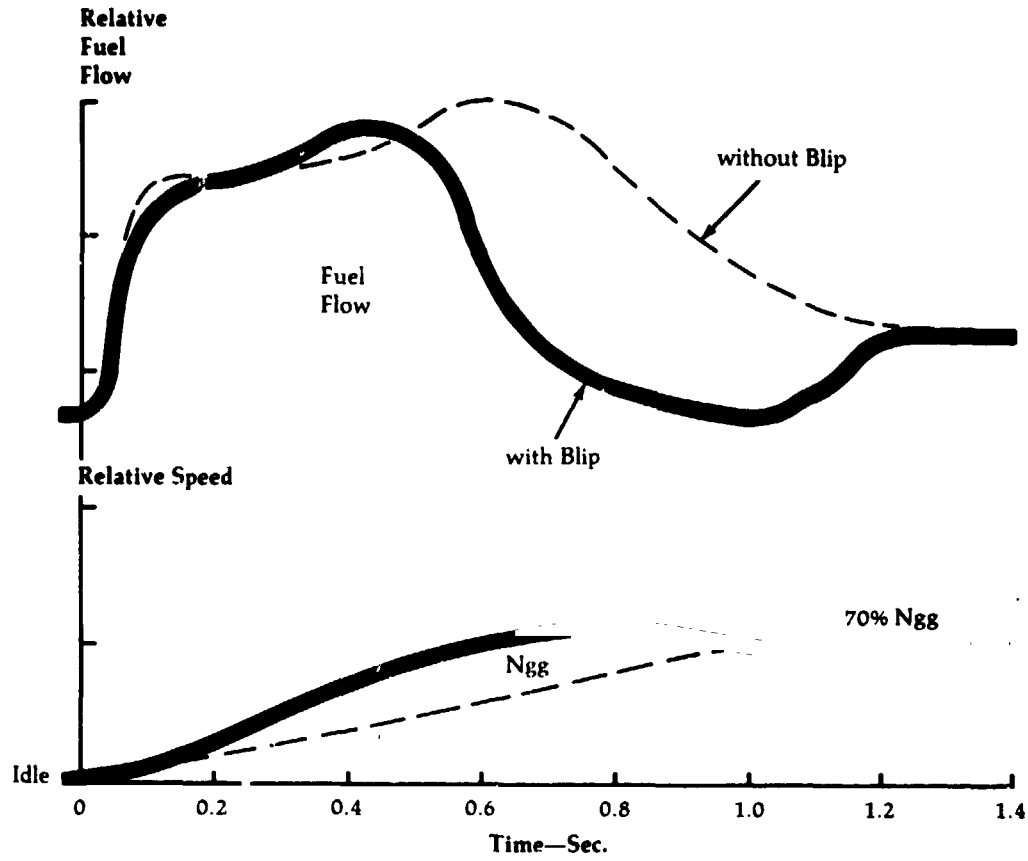

Blip= nozzle angle change from operating line match point setting

Ngg= gas generator rotational speed

Figure 35

Effect of Fuel Types on NO_x Formation

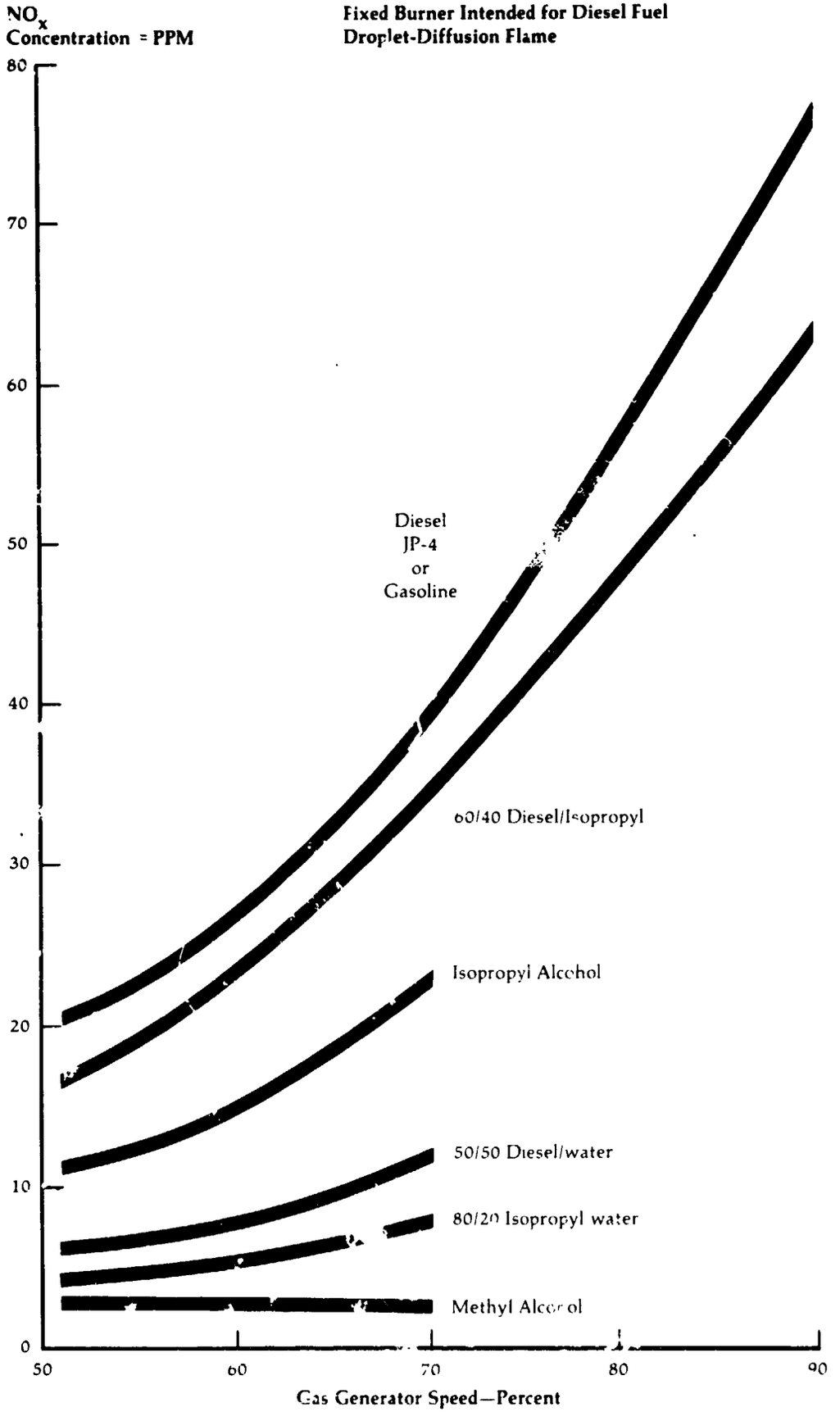

Figure 36

Vehicle with Multi-Fuel P mbing Arrangement

C-2

Figure 37

Effect of Burner Pressure Drop on Engine Performance

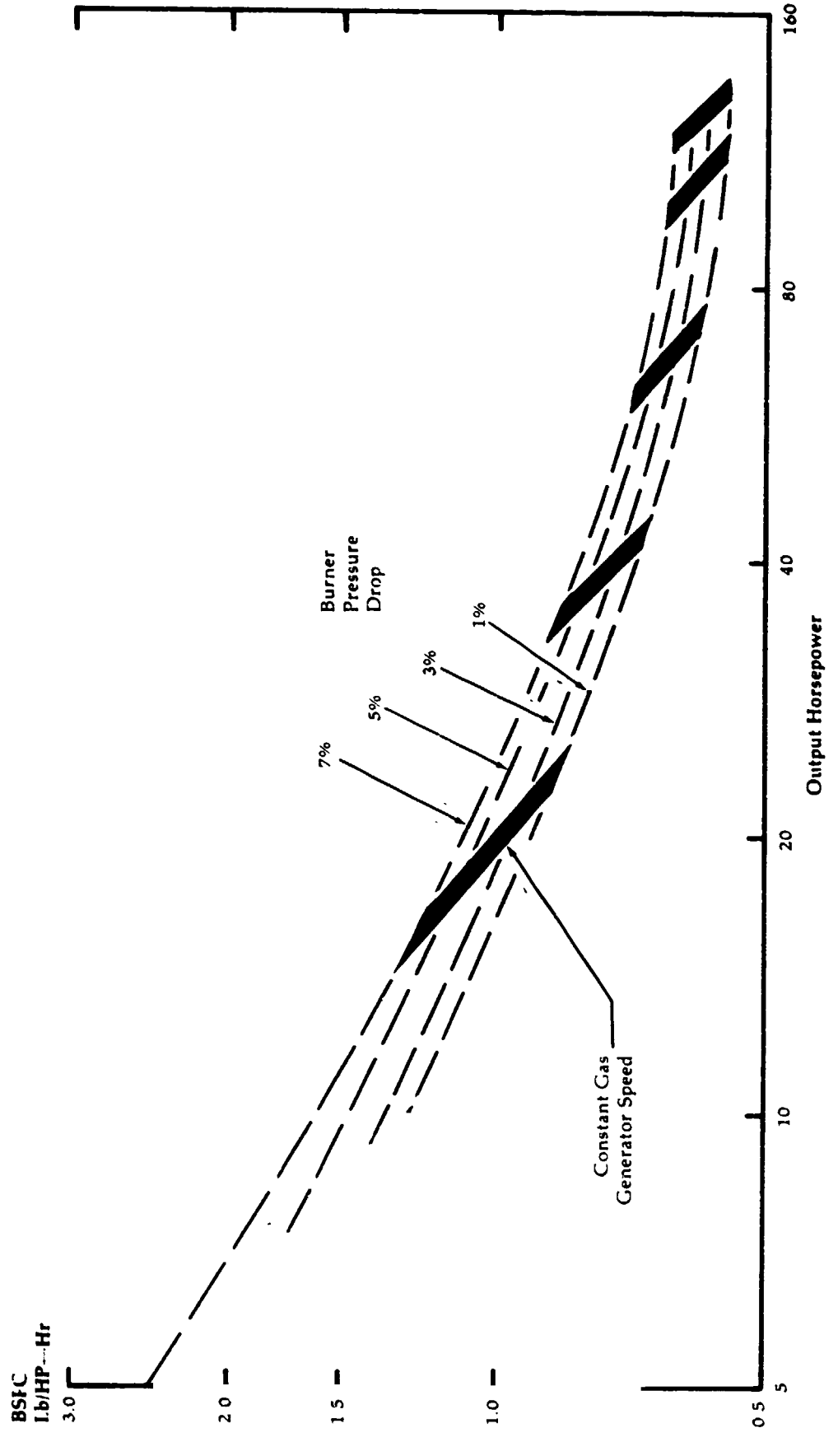

Figure 38

Ceramic Matrix Configurations

Effectiveness Comparison

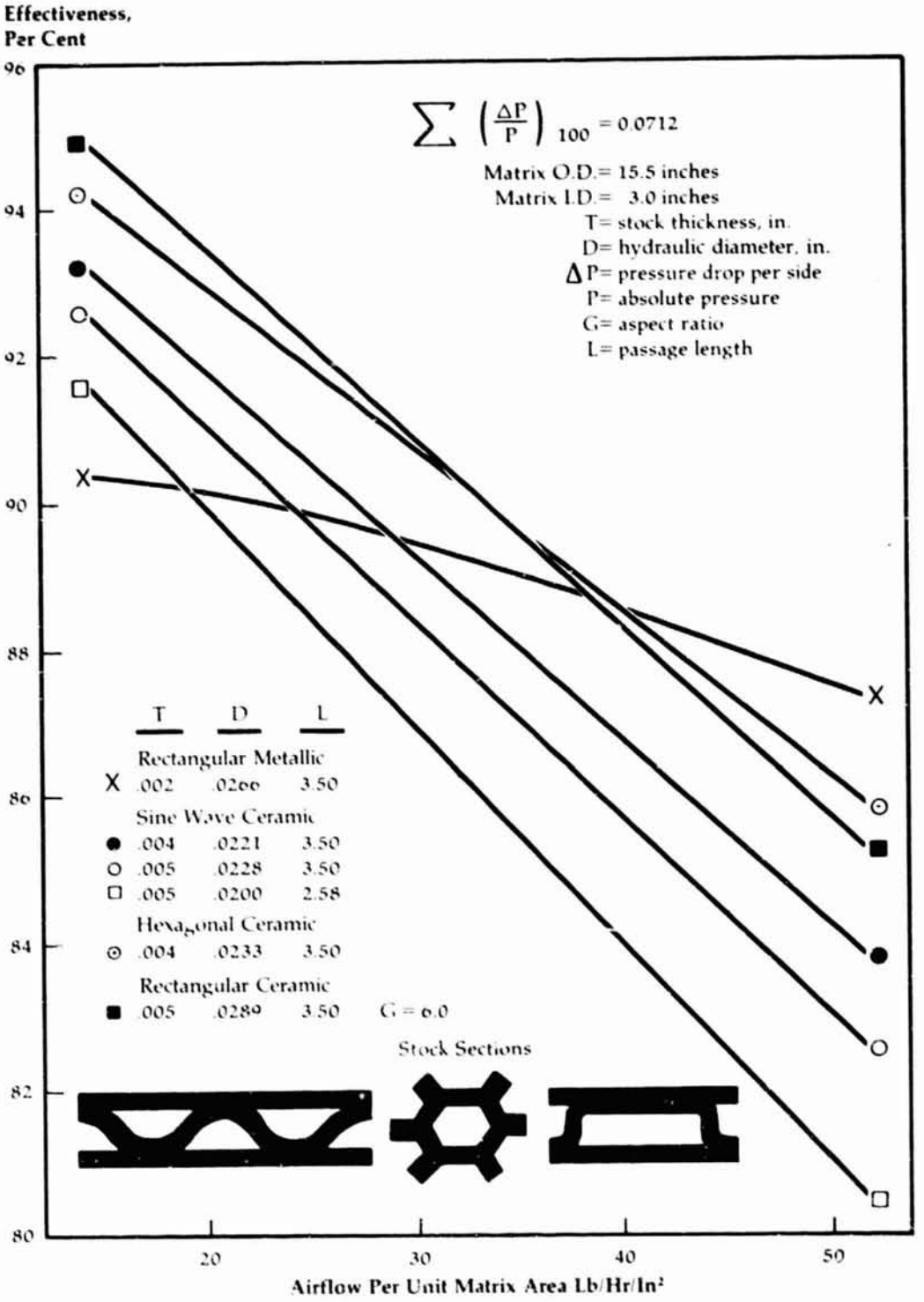

Figure 39

Regenerator Matrix Pressure Drop Test Schematic

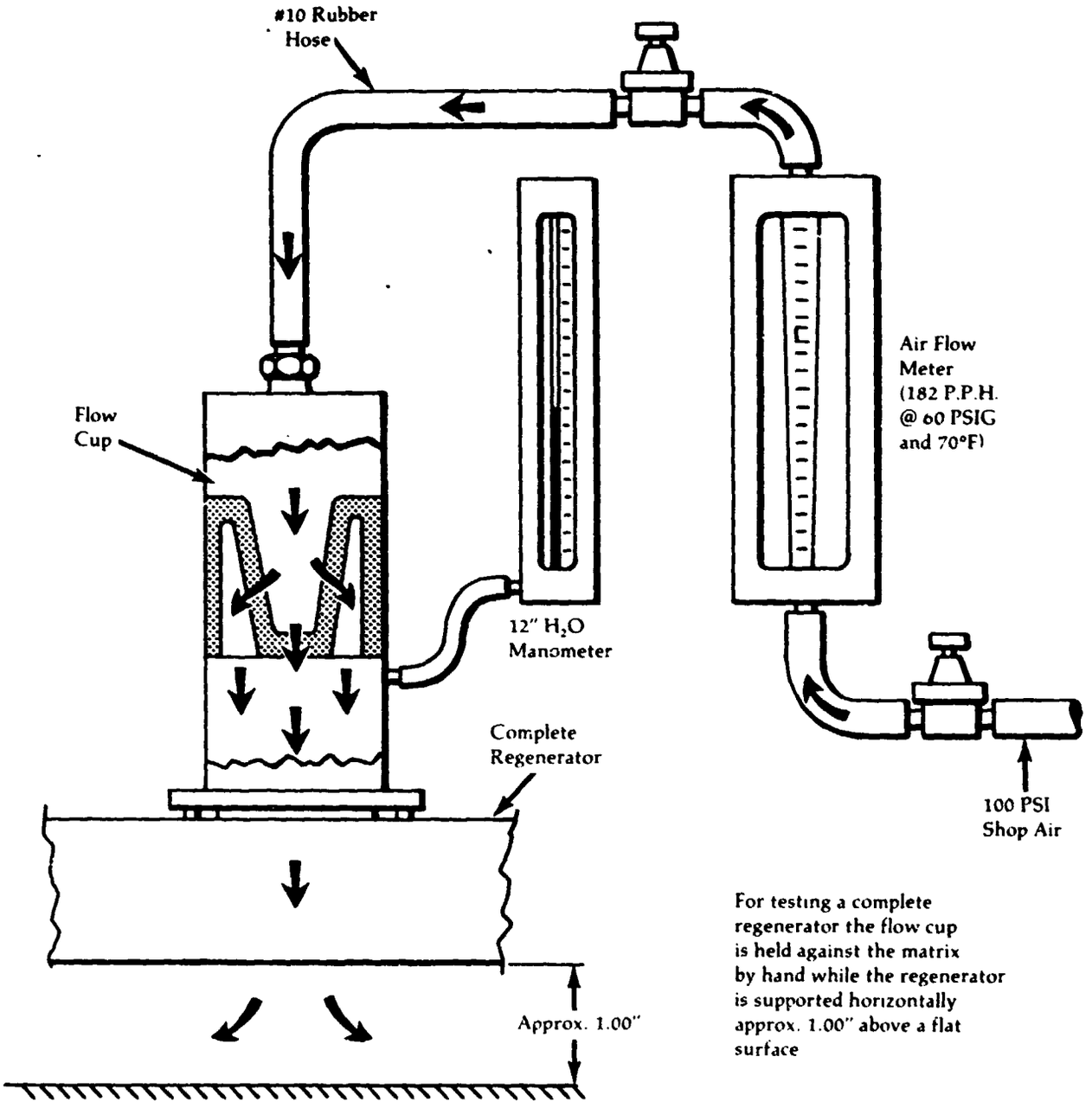

Figure 40

Regenerator Pressure Drop— Engine Simulation

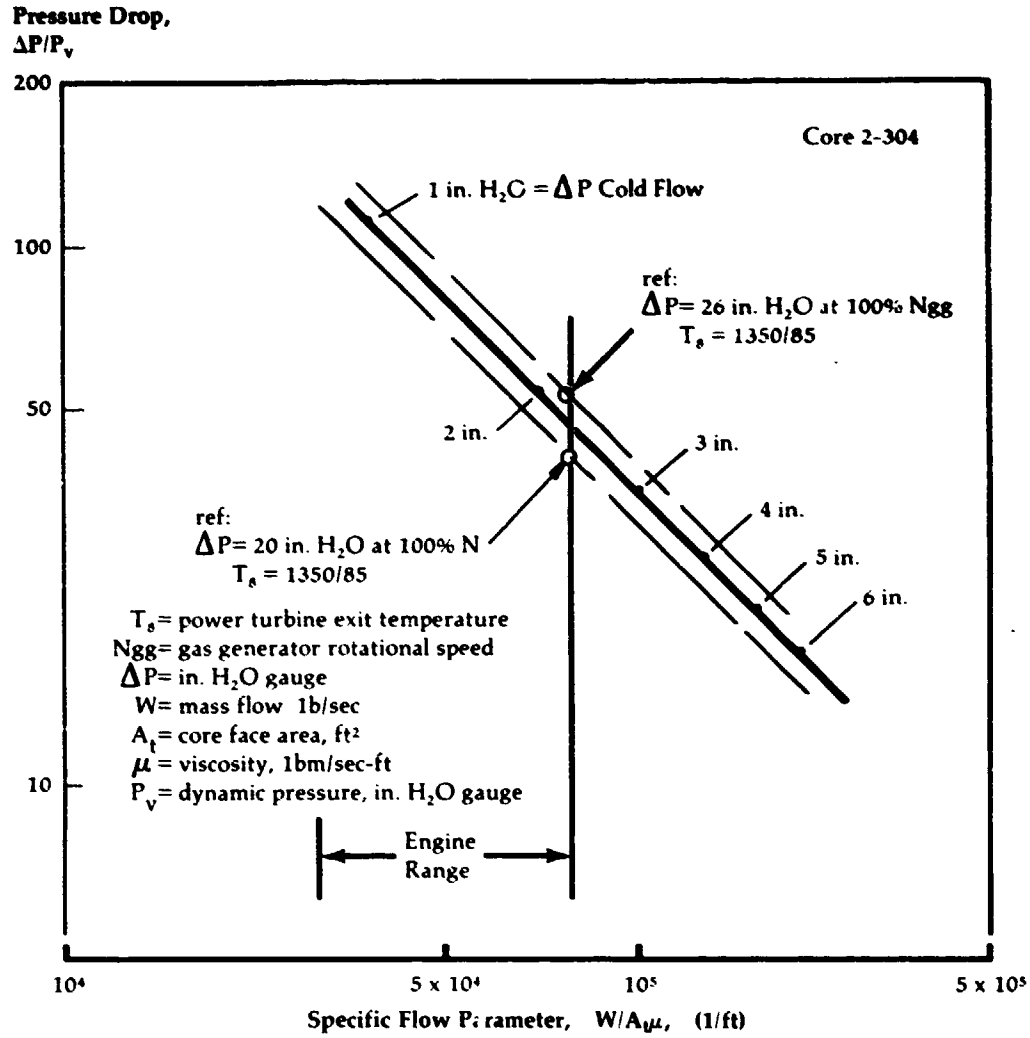

Figure 41

Elastomer Gear Mounting

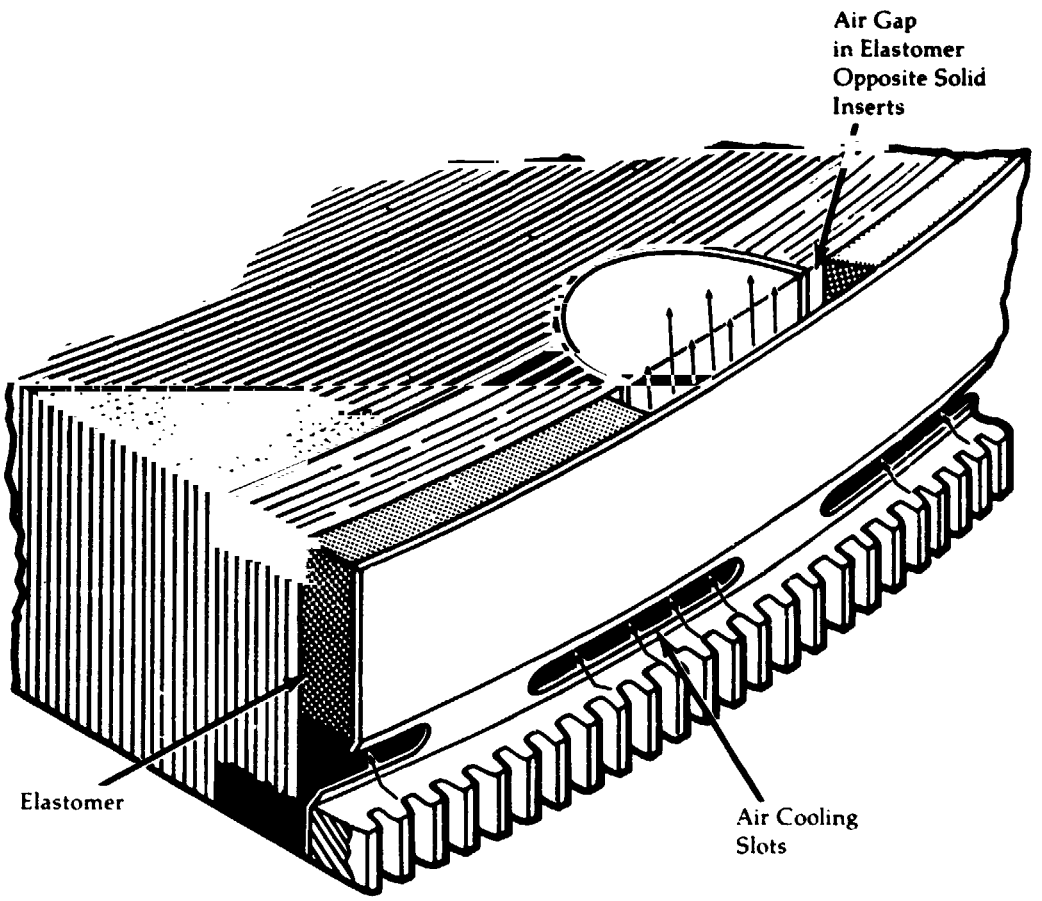

Figure 42

Regenerator Seal Configurations

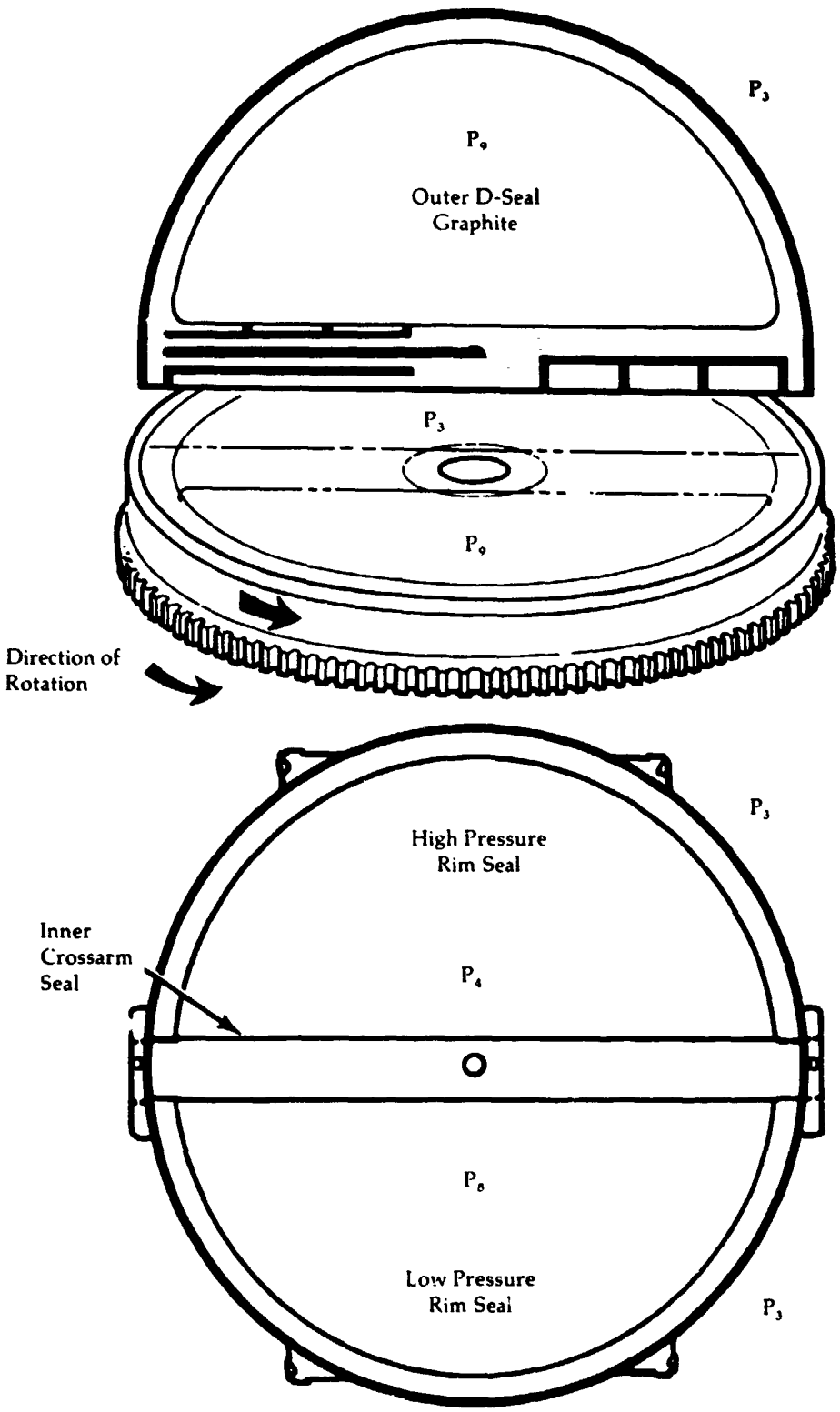

P_3 = regenerator inlet, high pressure side
P_4 = regenerator exit, high pressure side
P_8 = regenerator inlet, low pressure side
P_9 = regenerator exit, low pressure side

Figure 43

Coefficient of Friction for Two Ceramic Matrices and Various Seal Materials

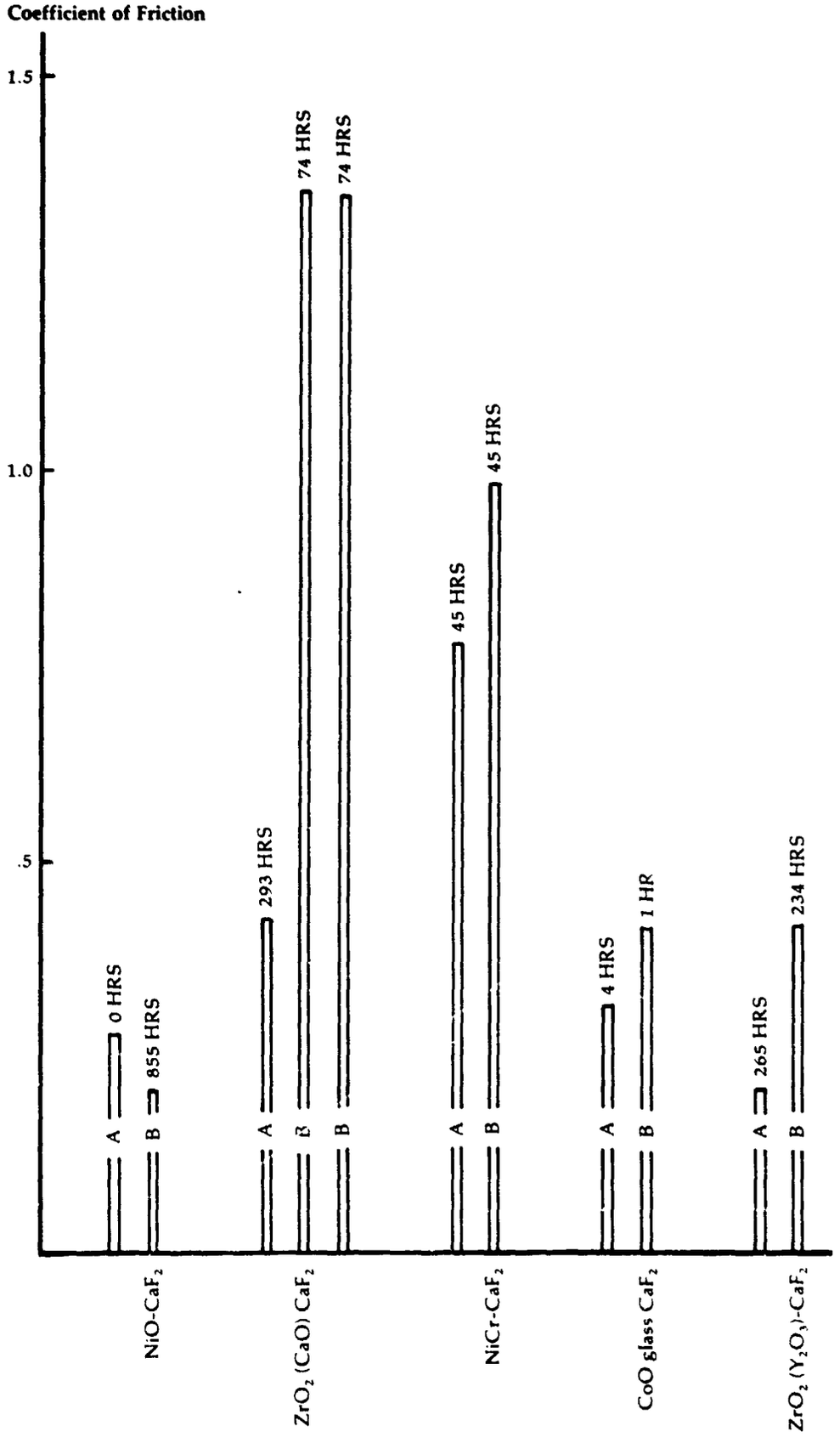

Figure 44

Flexible Elastomeric Regenerator Mount

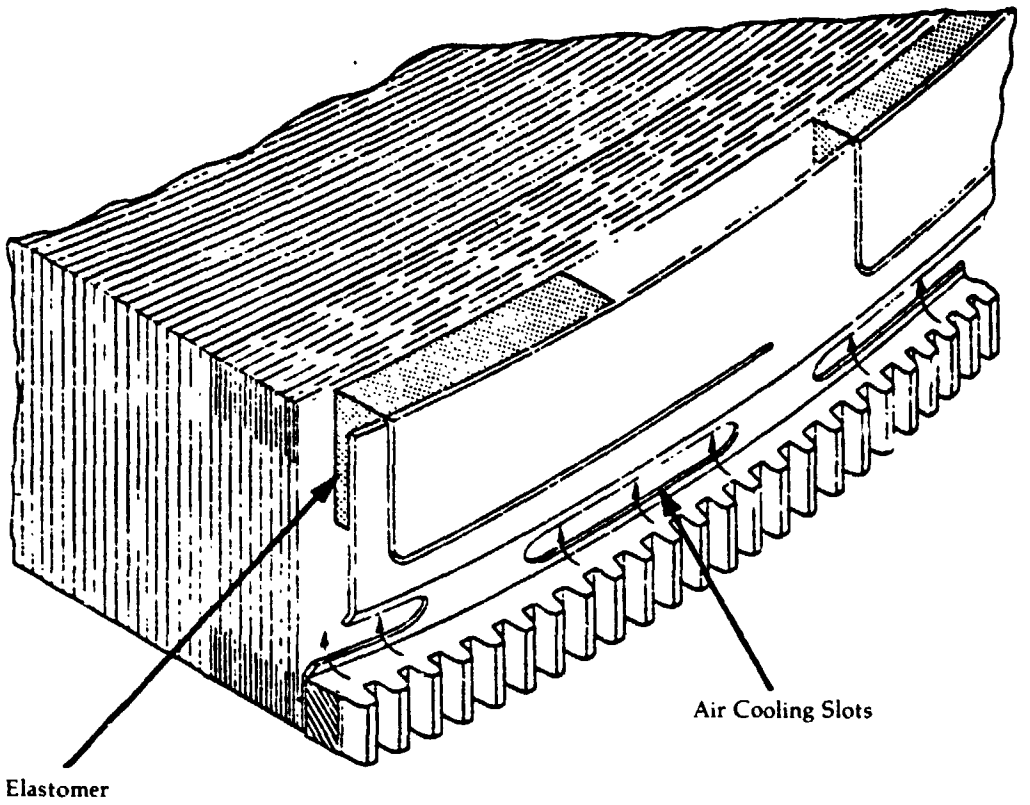

Figure 45

Deflection Test Elastomeric Mounting

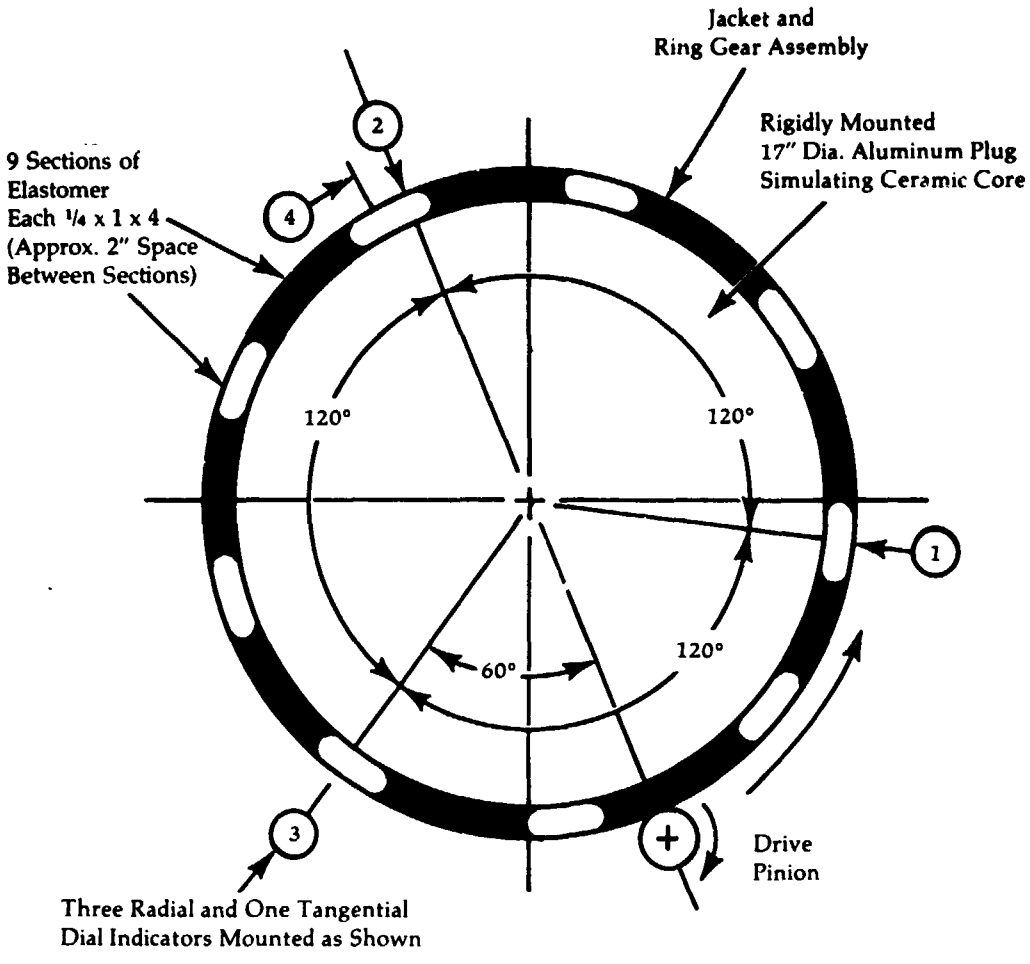

Torque lb-ft		Deflection at each indicator, In.			
At Pinion	At Core	1 Radial	2 Radial	3 Radial	4 Tangential
5	90	+.005	+.001	—.006	+.012
10	180	+.009	+.001	—.011	+.047
15	270	+.016	+.001	—.017	+.074
40	720	(Bond to Metal Failed)			+.175

Figure 46

Regenerator Core Torque Characteristics

Nickel Oxide Crossarms Against Thin-Wall "A" Matrix

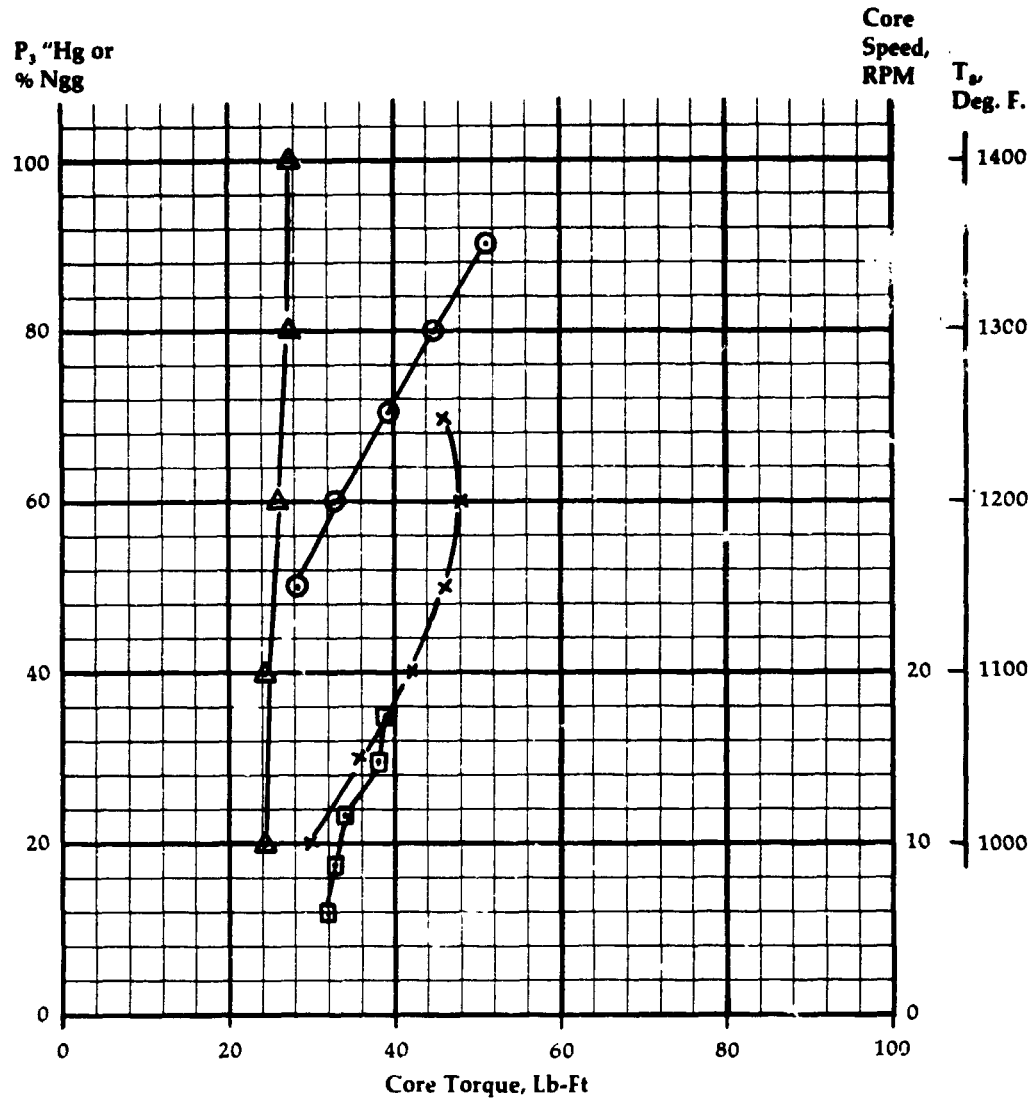

Variable	Steady Condition		
	T_8 °F.	P_3 "Hg	Core Speed RPM
△ T_8		20.5	5.9
X P_3	1400		11.8
□ Core RPM	1400	30.0	
O Ngg	1230/1245 (Engine Match Power)		

T_8 = power turbine exit temperature
P_3 = regenerator inlet pressure, high pressure side, "Hg gauge

Figure 47

Relative Fuel Flow Change with Regenerator Effectiveness

50% Engine Speed

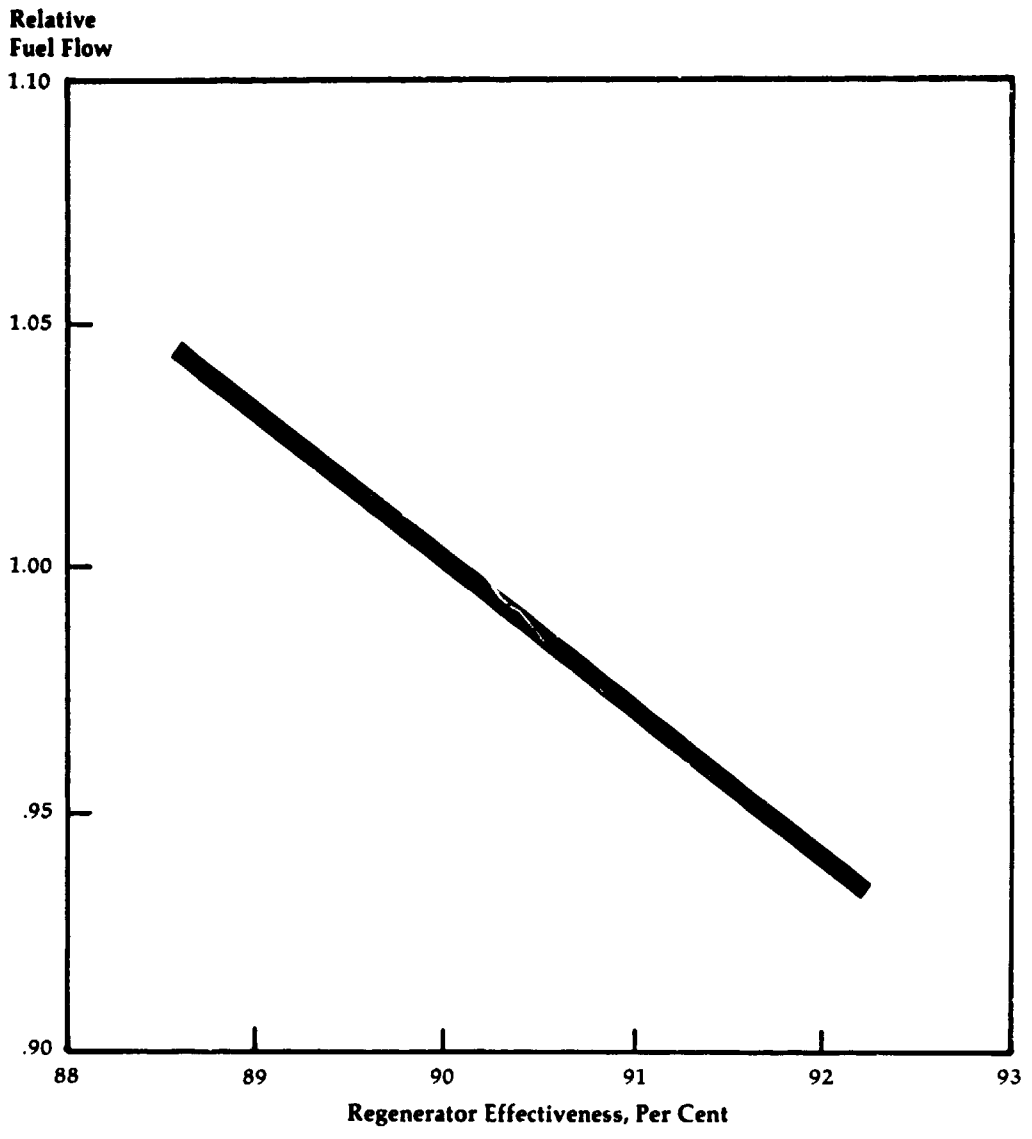

Figure 48

Effectiveness vs. Specific Airflow For Type "A", Type "B", and Baseline Metallic Matrices

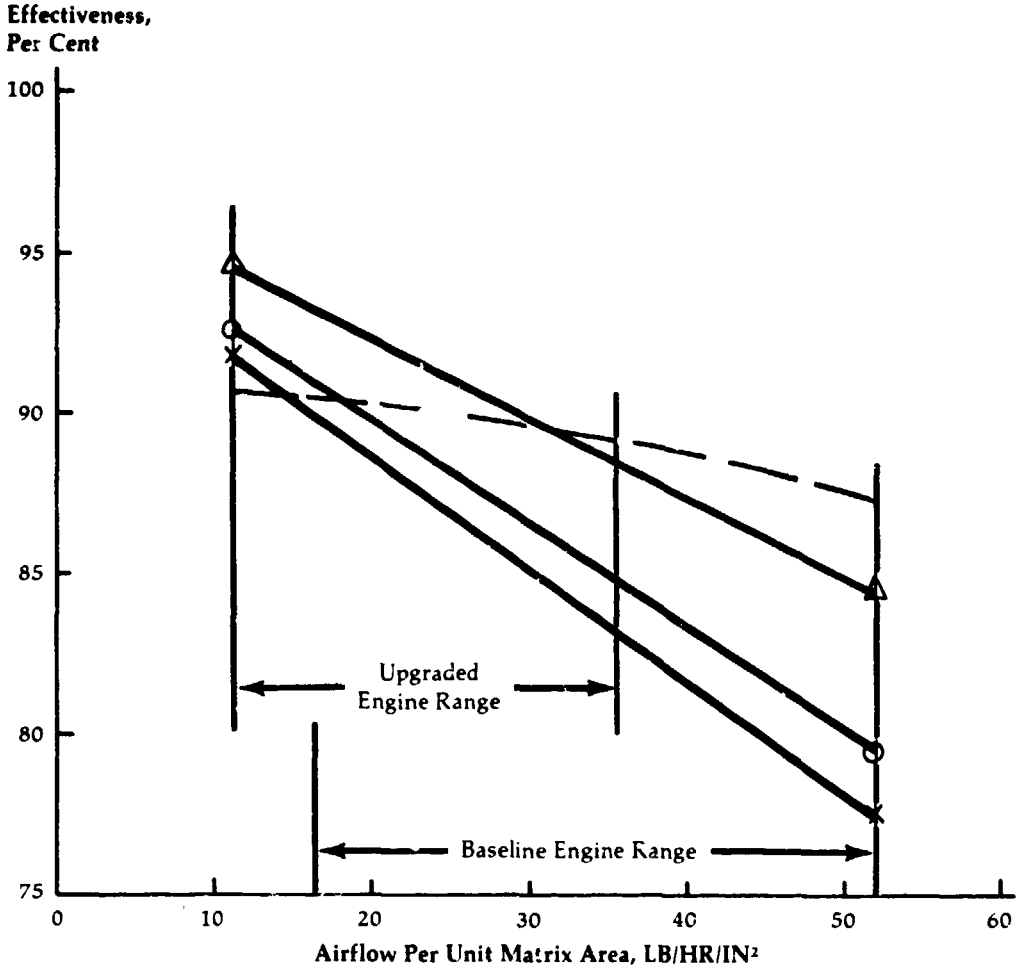

	Hydraulic Diameter In.	Stock Thickness In.	Passage Length In.	% Open Area	ΔP "H_2O
X—X Baseline Type "A" Wound Triangular (Sine Wave)	0.025	0.0045	2.58	67	24
⊙—⊙ Baseline Type "B" Nested Tubes (Hexagonal)	0.027	0.0045	3.00	67	24
△—△ Thinwall Type "A" Wound Triangular (Sine Wave)	0.020	0.0030	3.00	76	32
– – – – Baseline Metallic	0.027	0.0020	3.50	85	24

ΔP = core pressure drop, low pressure side, in. H_2O gauge

Figure 49A

Effect of Ceramic Cores on Engine Fuel Consumption

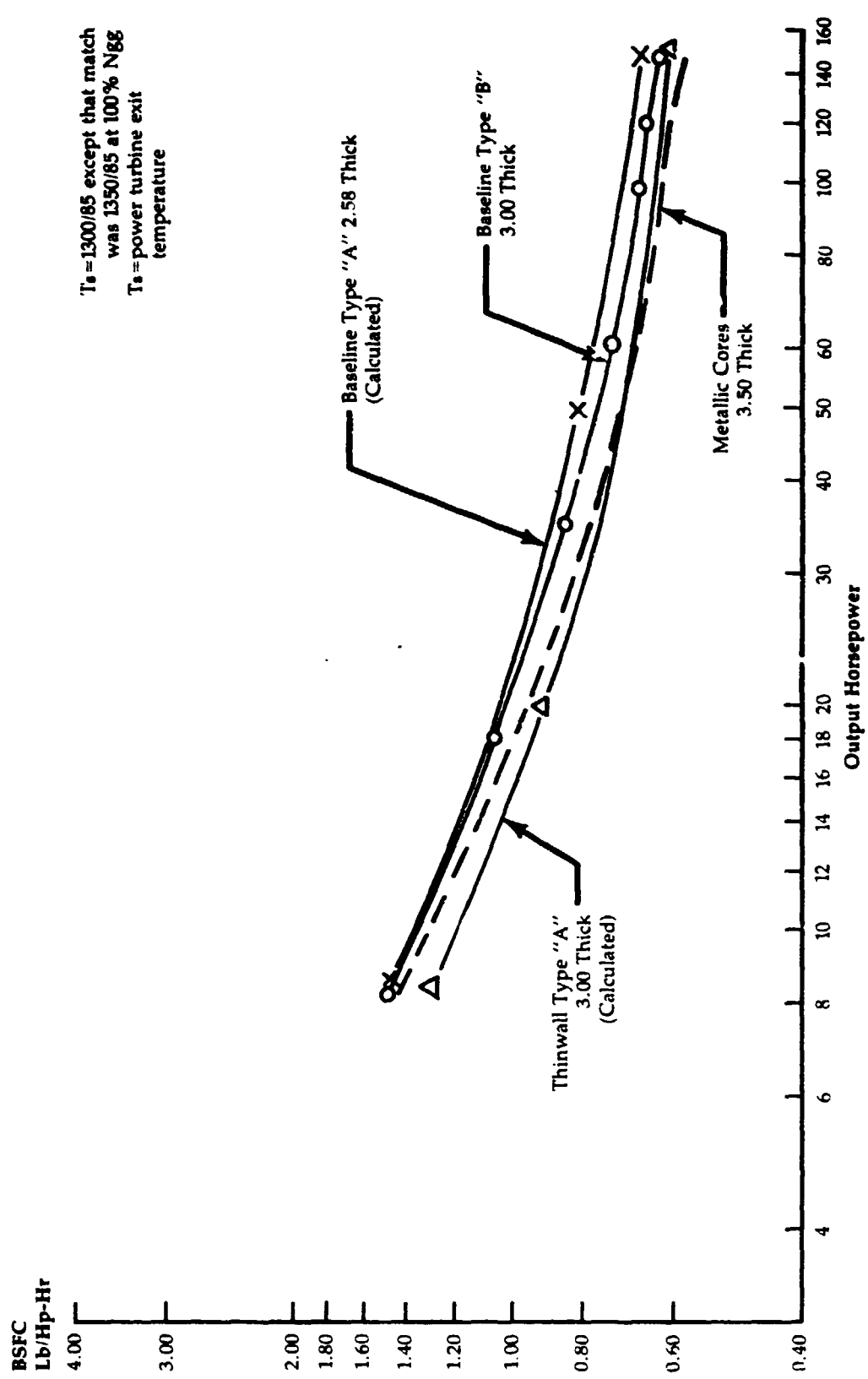

Figure 49B

Regenerator Matrix Model

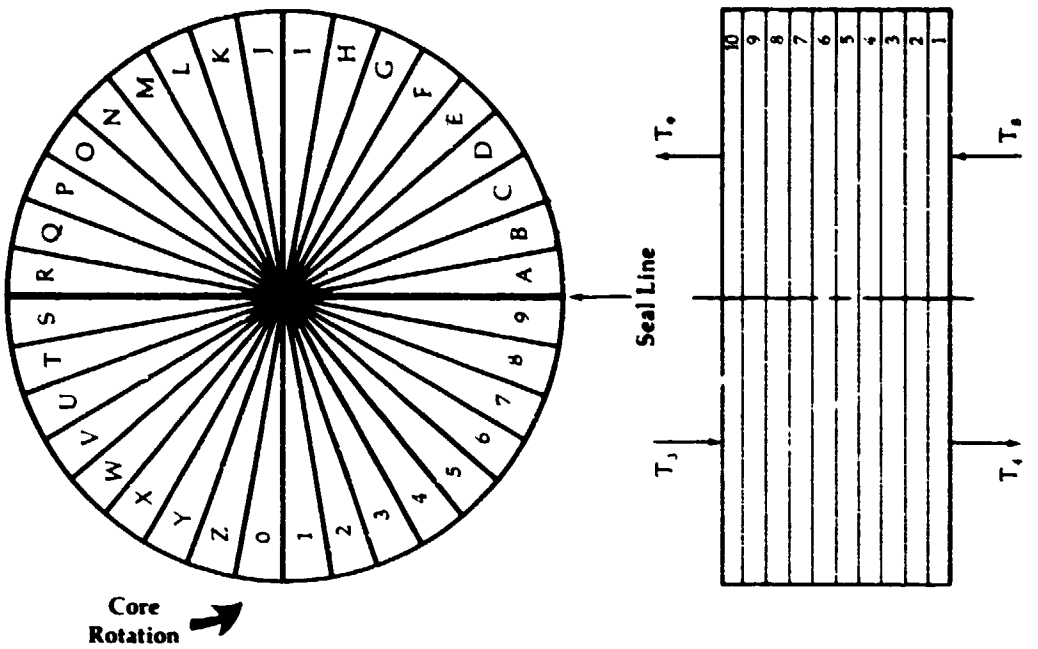

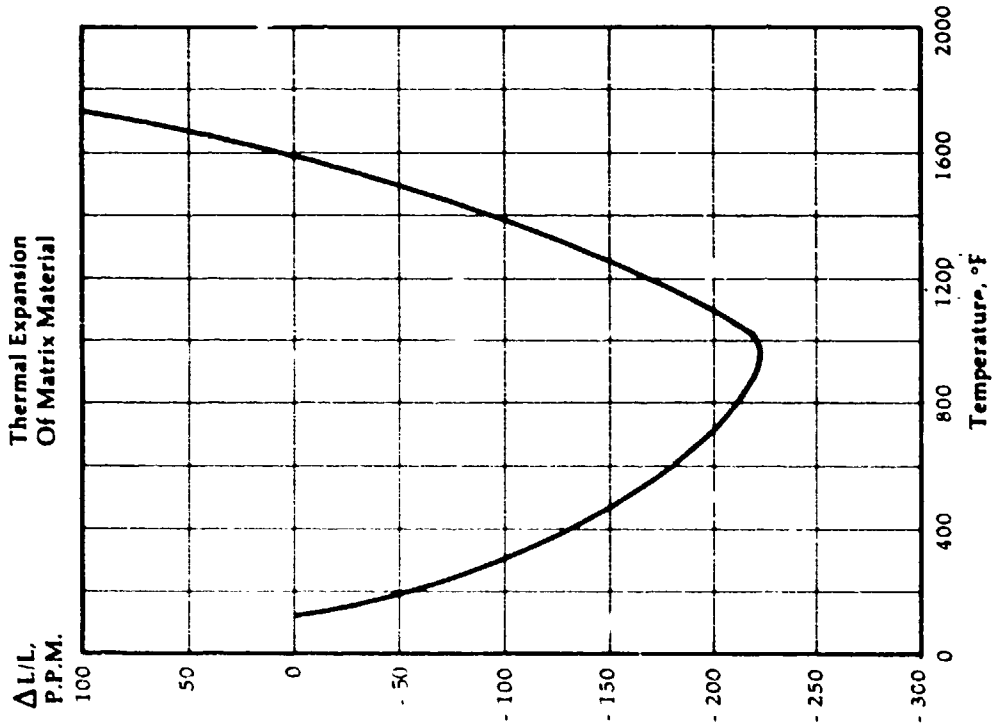

Figure 50A

Regenerator Core Temperature vs Axial and Circumferential Location

1/4 Core Revolution After Cold Start

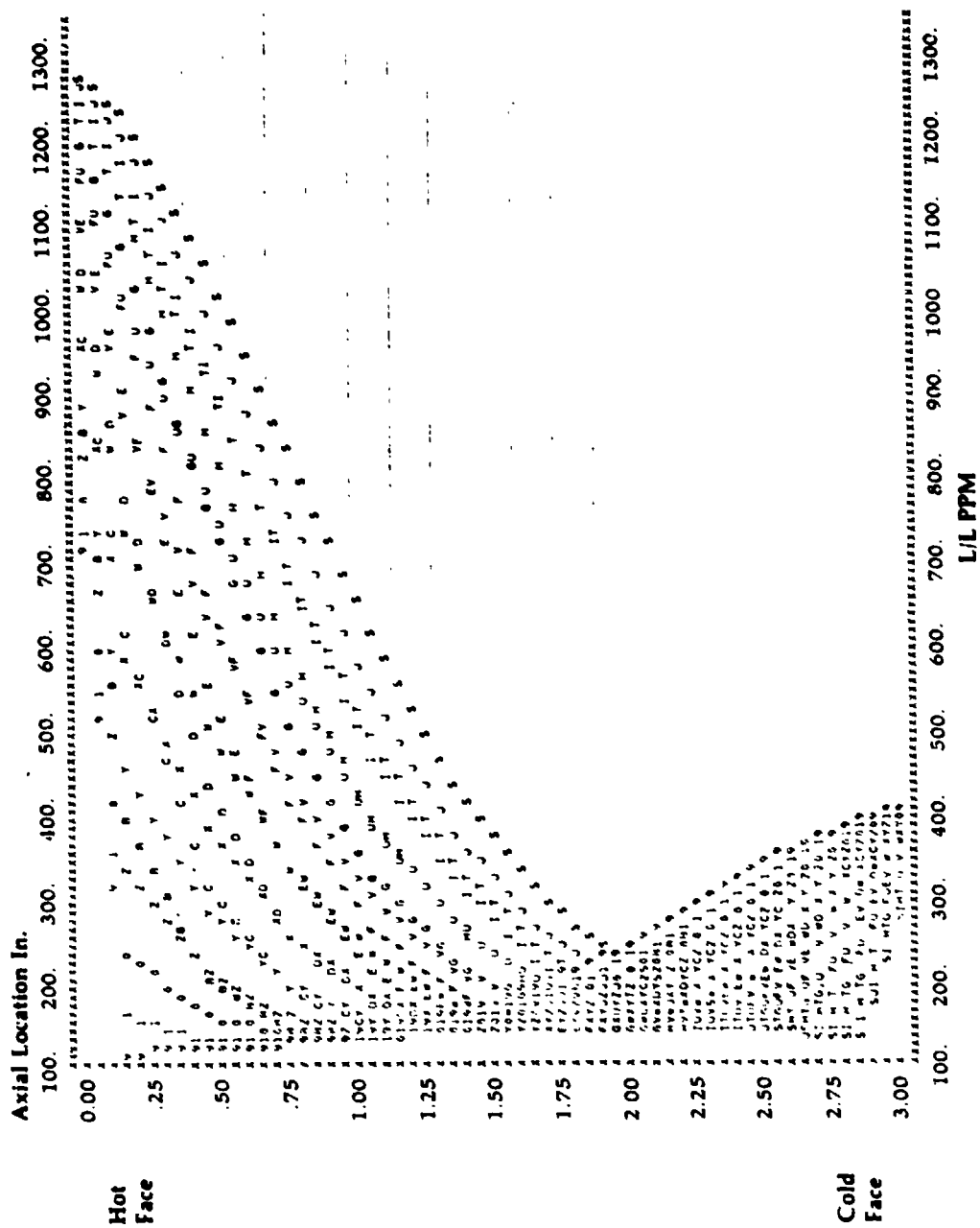

Figure 50B

Regenerator Core Deformation ΔL/L PPM Vs Axial and Circumferential Location

1/4 Core Revolution After Cold Start

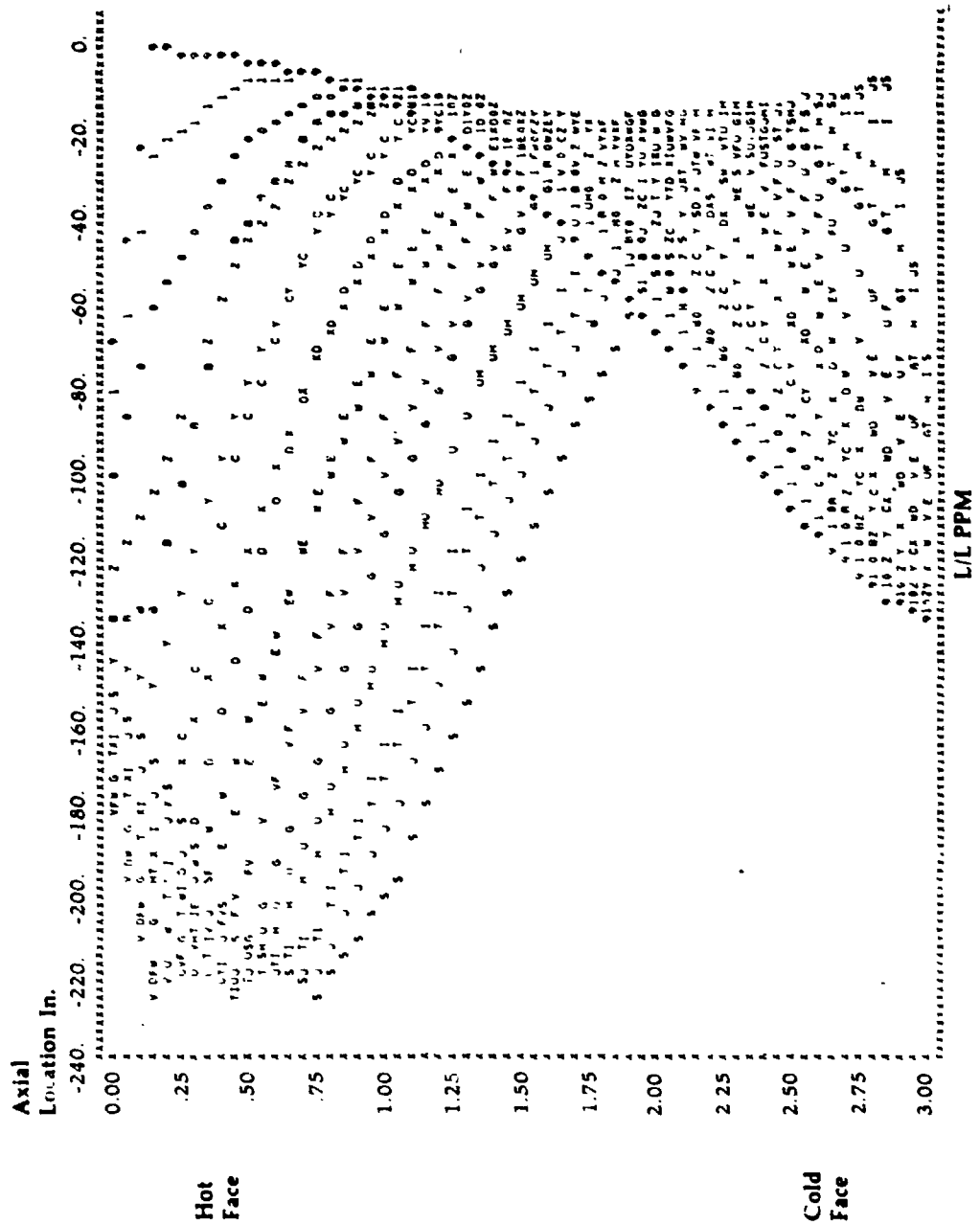

Figure 50C

Steady State Regenerator Core Temperature vs Axial and Circumferential Location

At 6 RPM Thermal Equilibrium was Reached after 9 Core Revolutions with a Circumferential Temperature Gradient of 540°F.

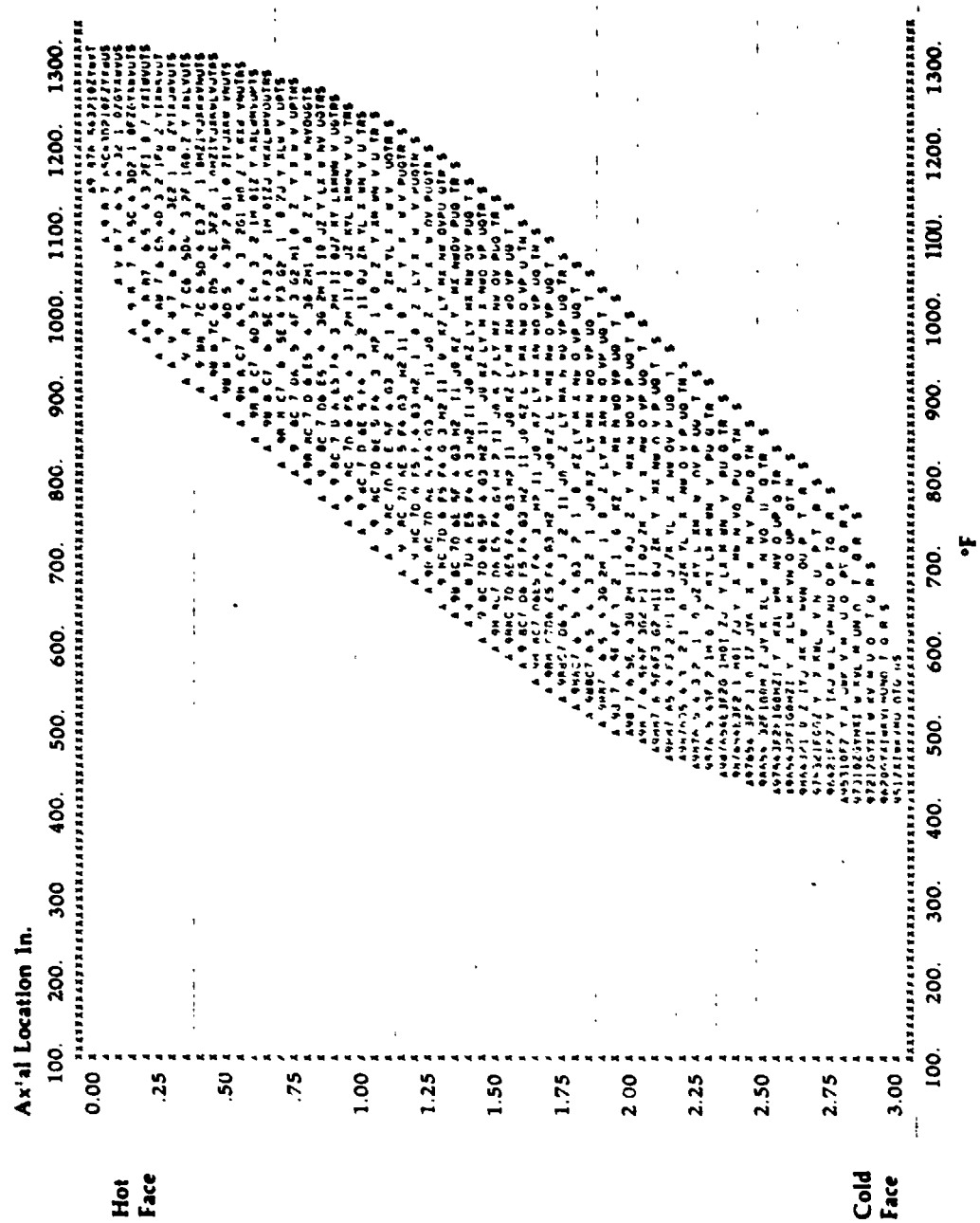

ORIGINAL PAGE IS
OF POOR QUALITY

Figure 50D

Steady State Regenerator Core Temperature vs. Axial and Circumferential Location

At 12 RPM Thermal Equilibrium was Reached after 19 Core Revolutions with a Circumferential Temperature Gradient of 250°F.

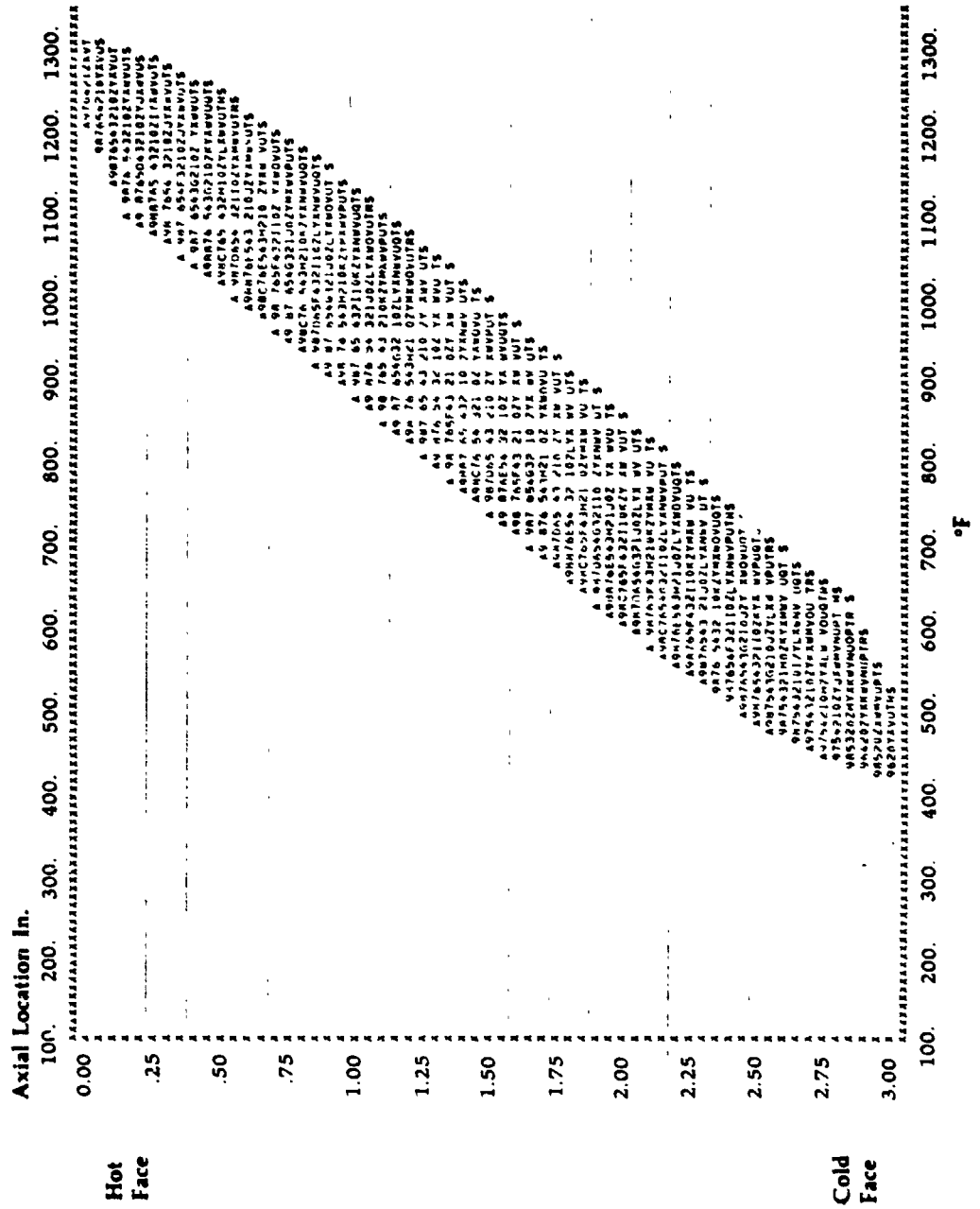

Figure 50E

Steady State Regenerator Core Temperature vs Axial and Circumferential Location

At 24 RPM Thermal Equilibrium was Reached after 42 Core Revolutions with a Circumferential Temperature Gradient of 125 °F.

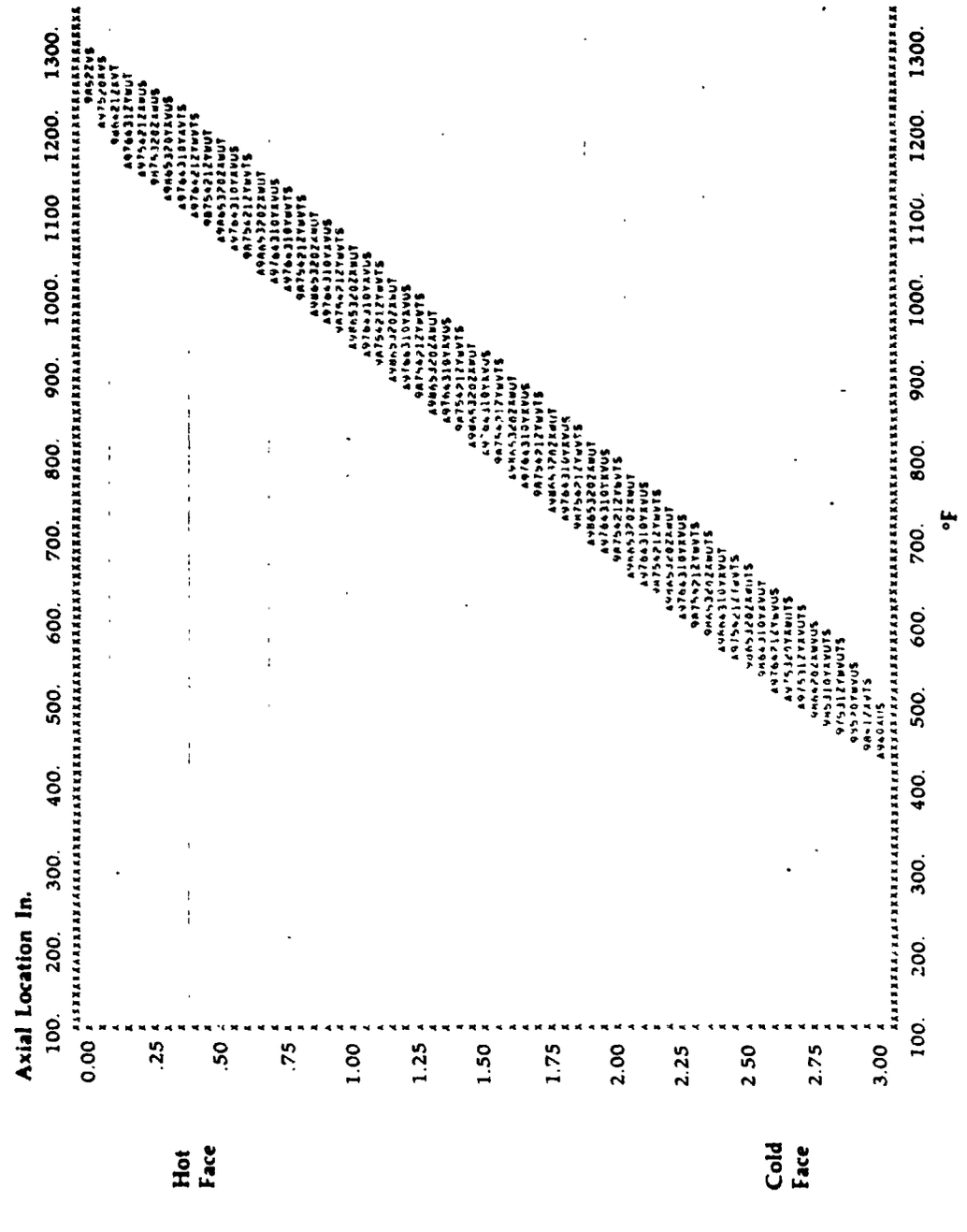

Figure 50F

Baseline Engine Control System

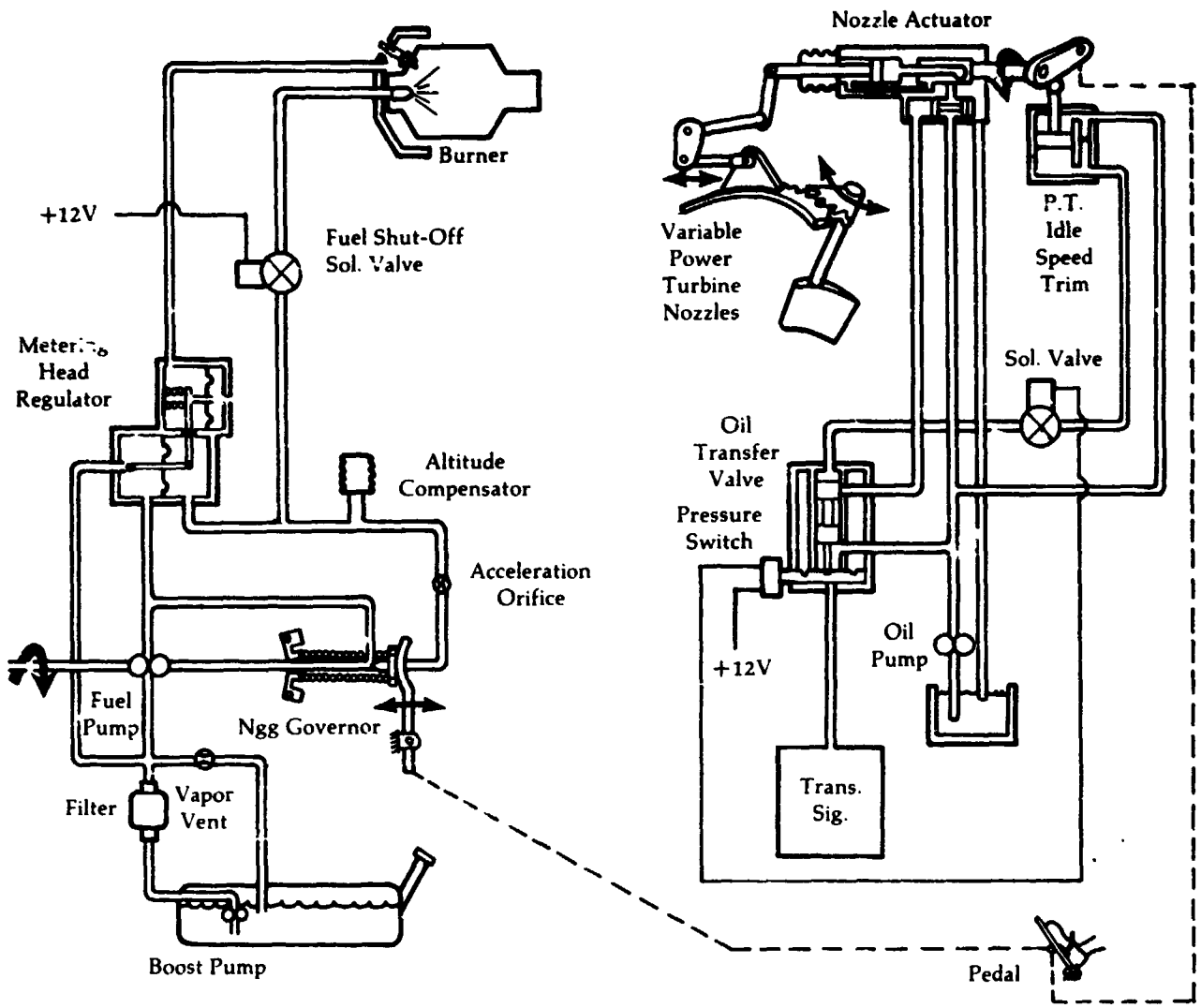

Figure 51

Start System Logic

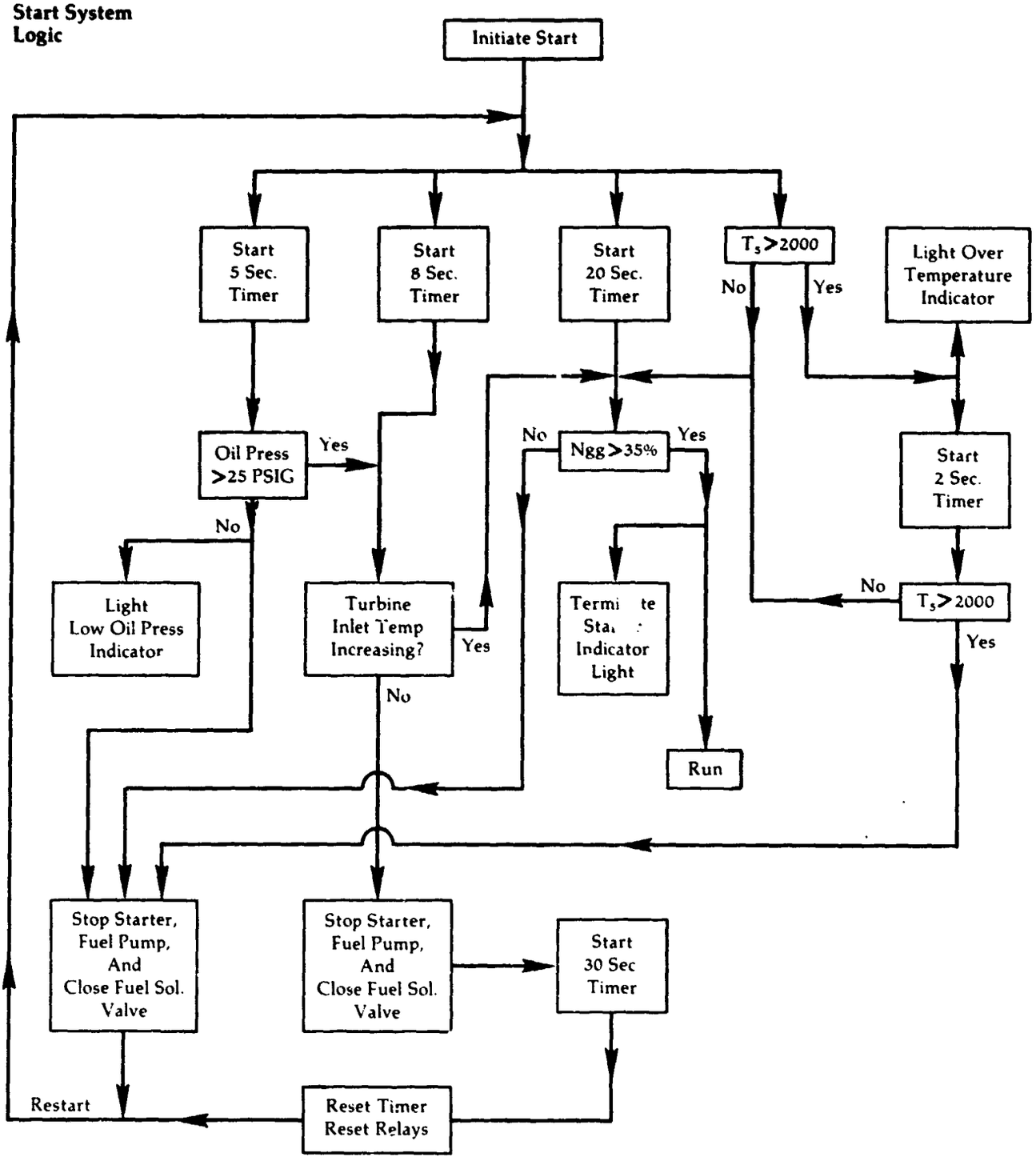

Figure 52

Simplified Functional Diagram Preprototype Integrated Control System

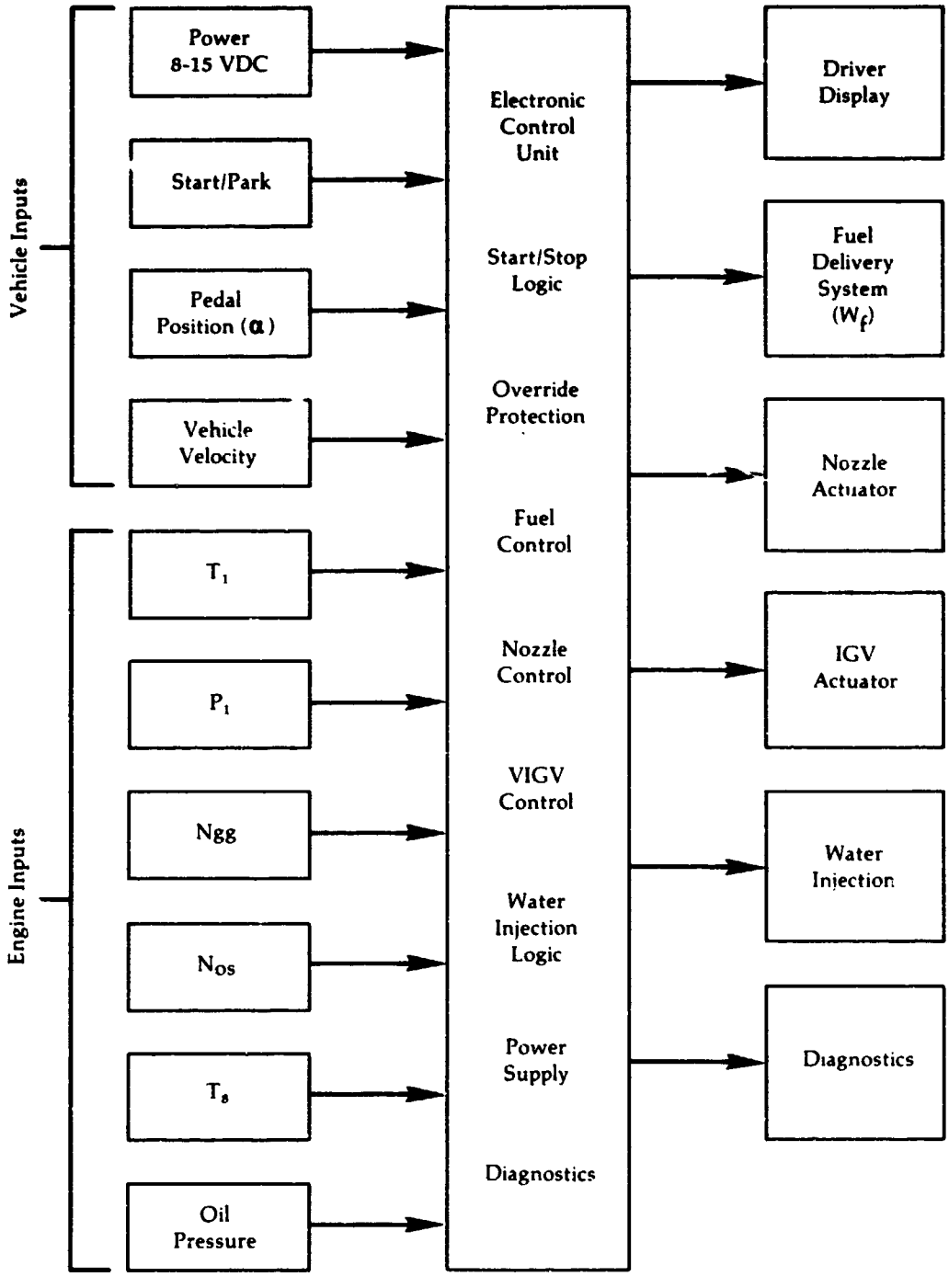

Figure 53

Electronic Engine Control in Test Cell

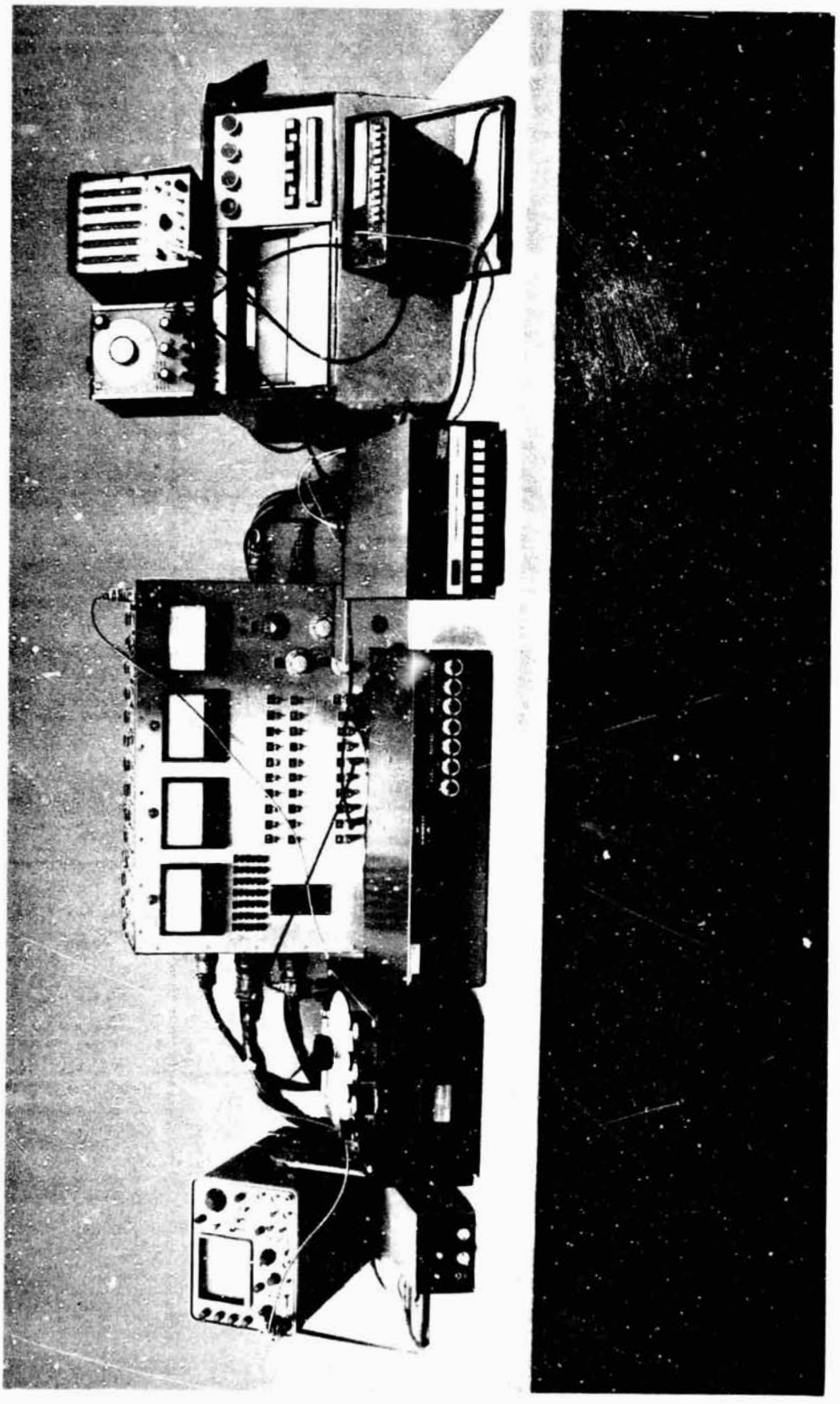

Figure 54

Electronic Engine Controller in Vehicle

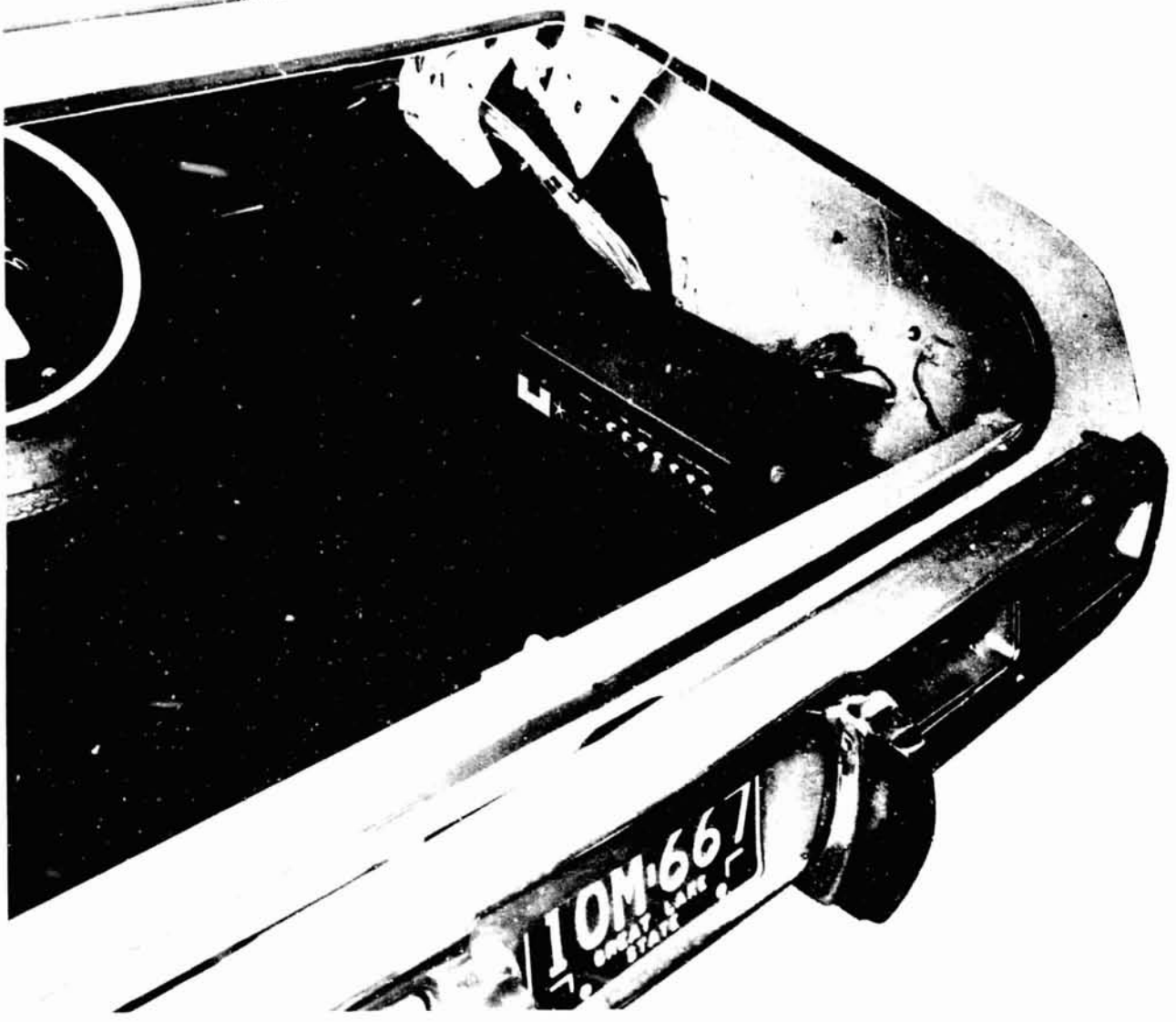

Figure 55

Test Cell
Installation of
Programmable
Analog Controller

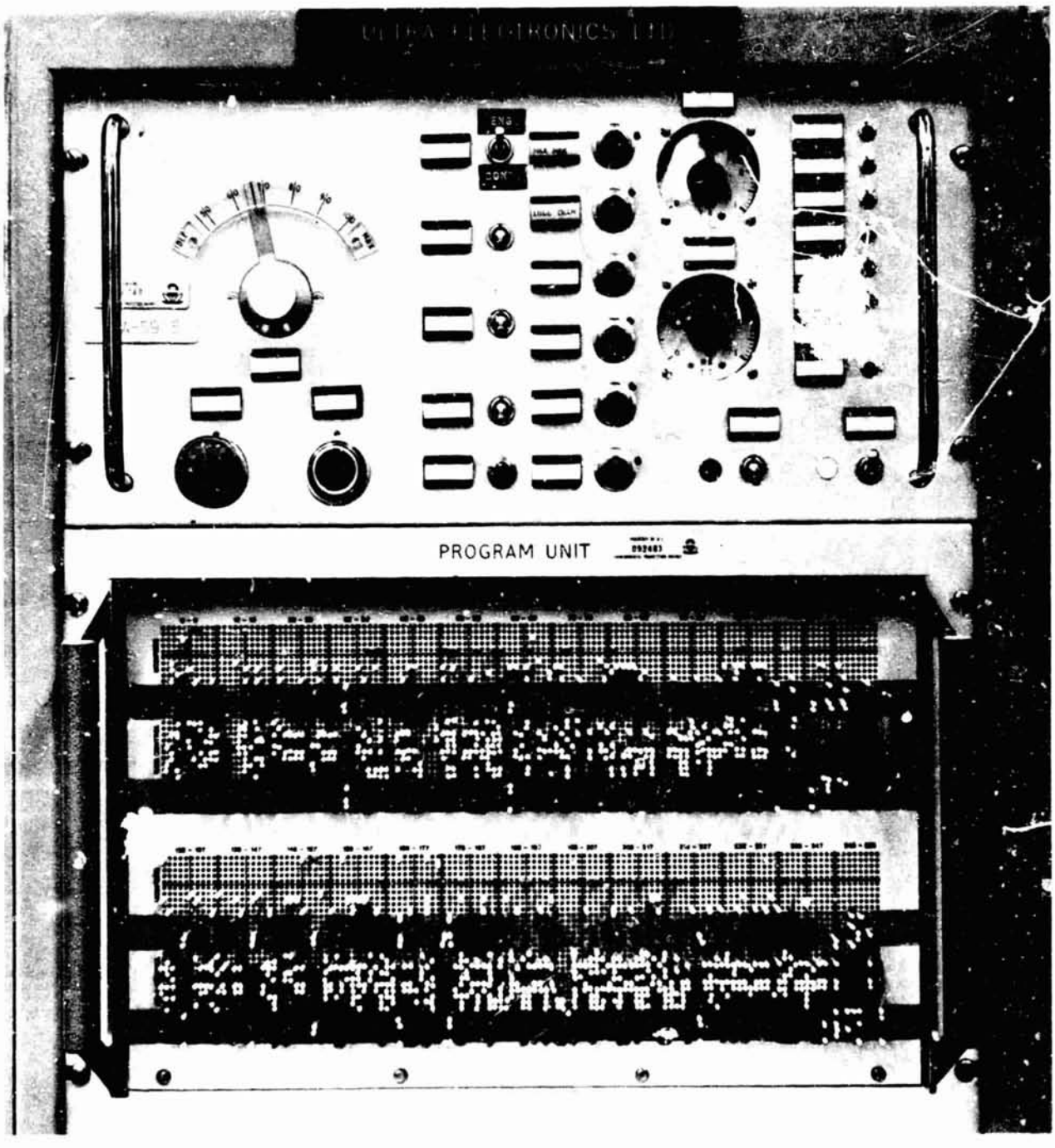

Figure 56

AiResearch Fluidic Temperature Sensor Tests

Output Frequency vs. Temperature

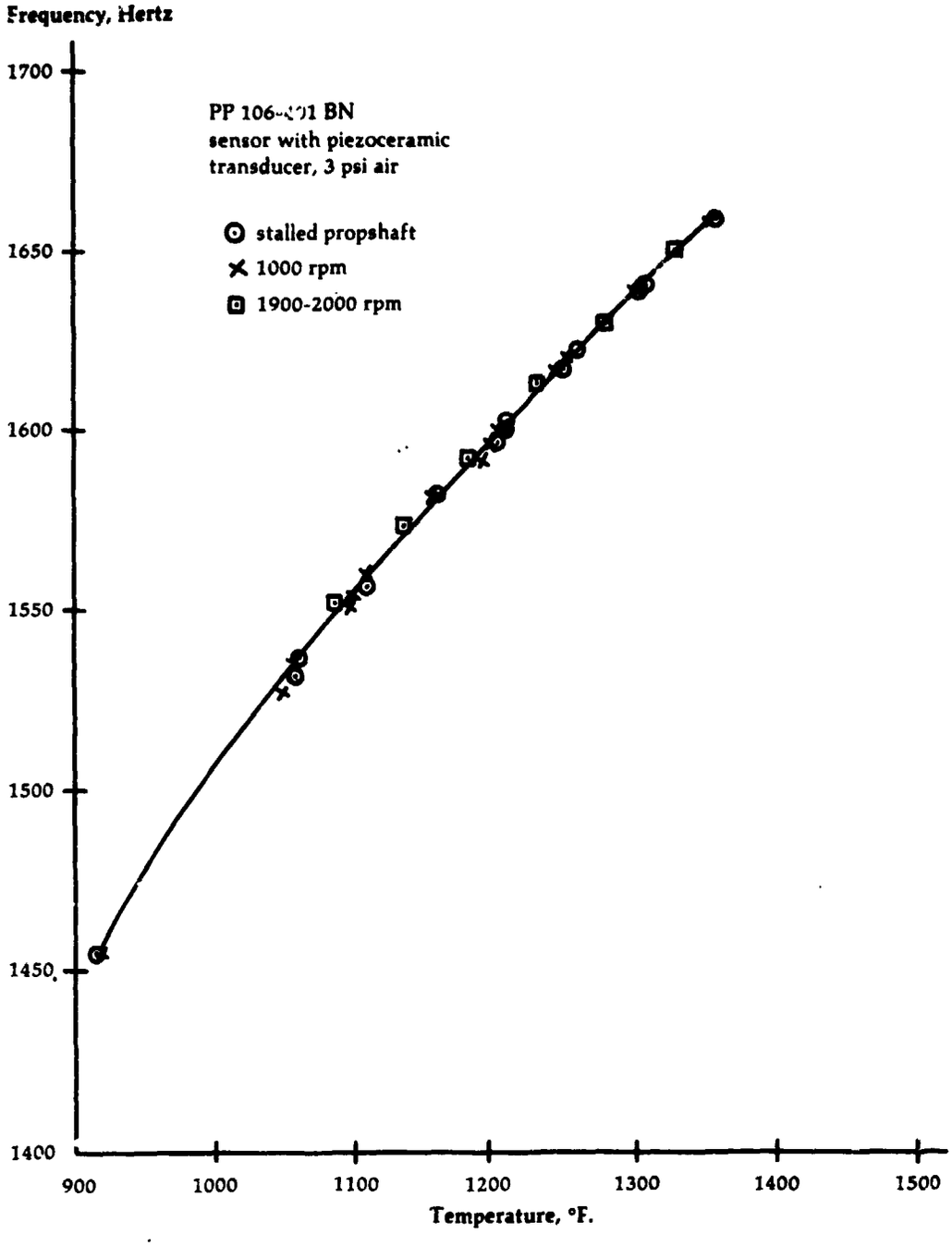

Figure 57

AiResearch Fluidic T_8 Sensor Hot Start— Transient Data

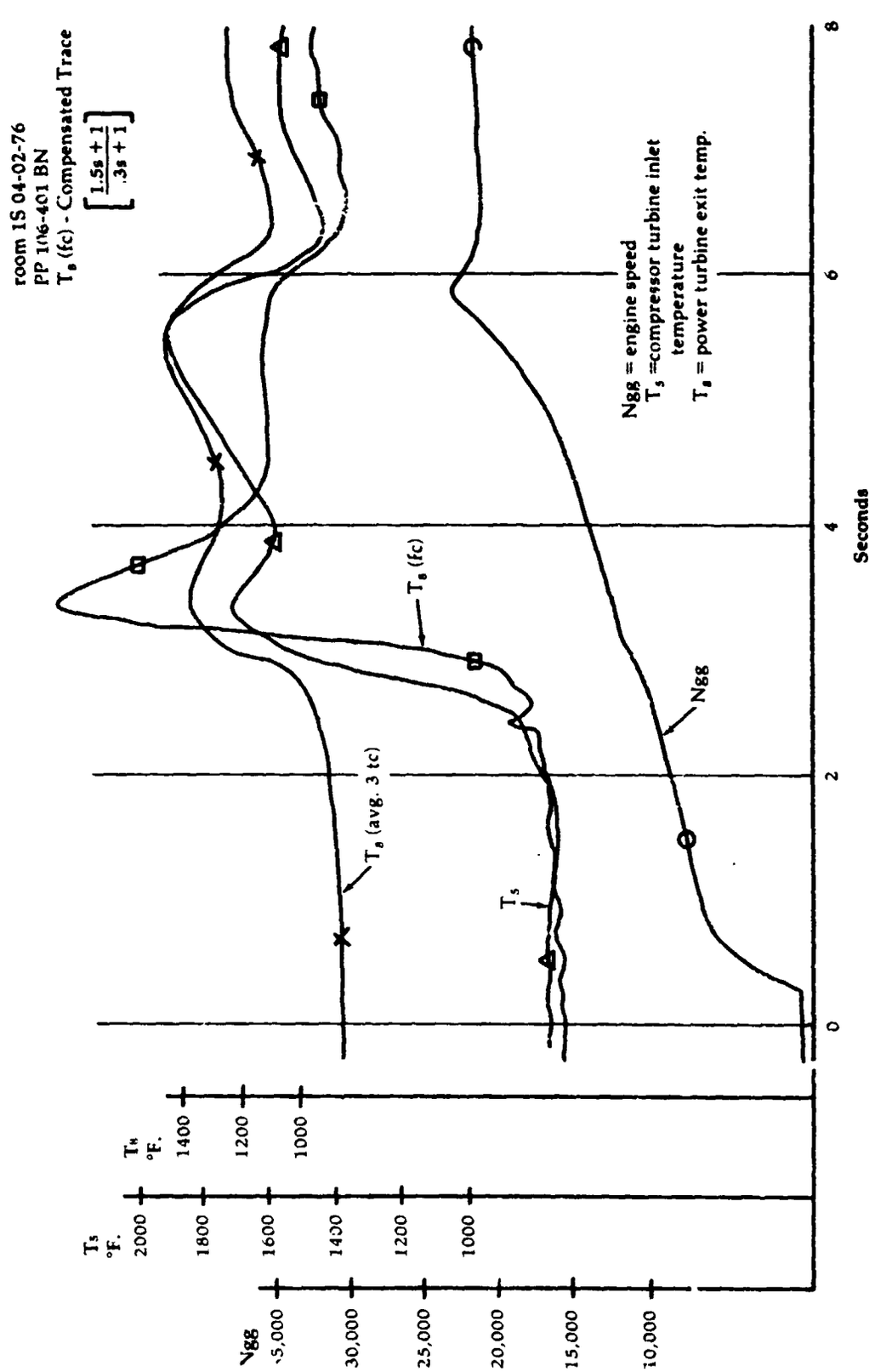

Figure 58

AiResearch
Fluidic T_8 Sensor
Aceel-Transient
Data

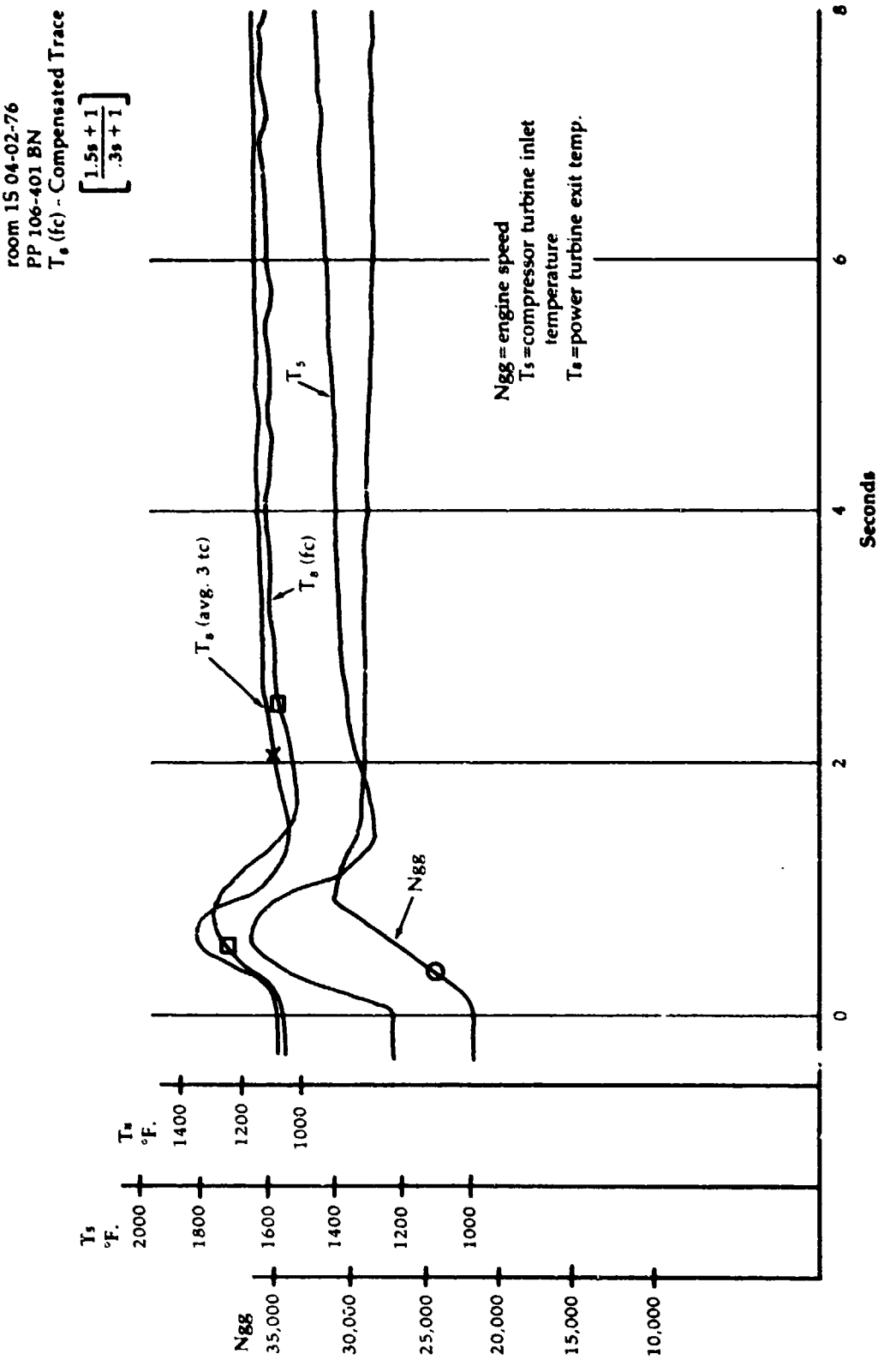

Figure 59

AiResearch
Fluidic T_8 Sensor
Decel-Transient
Data

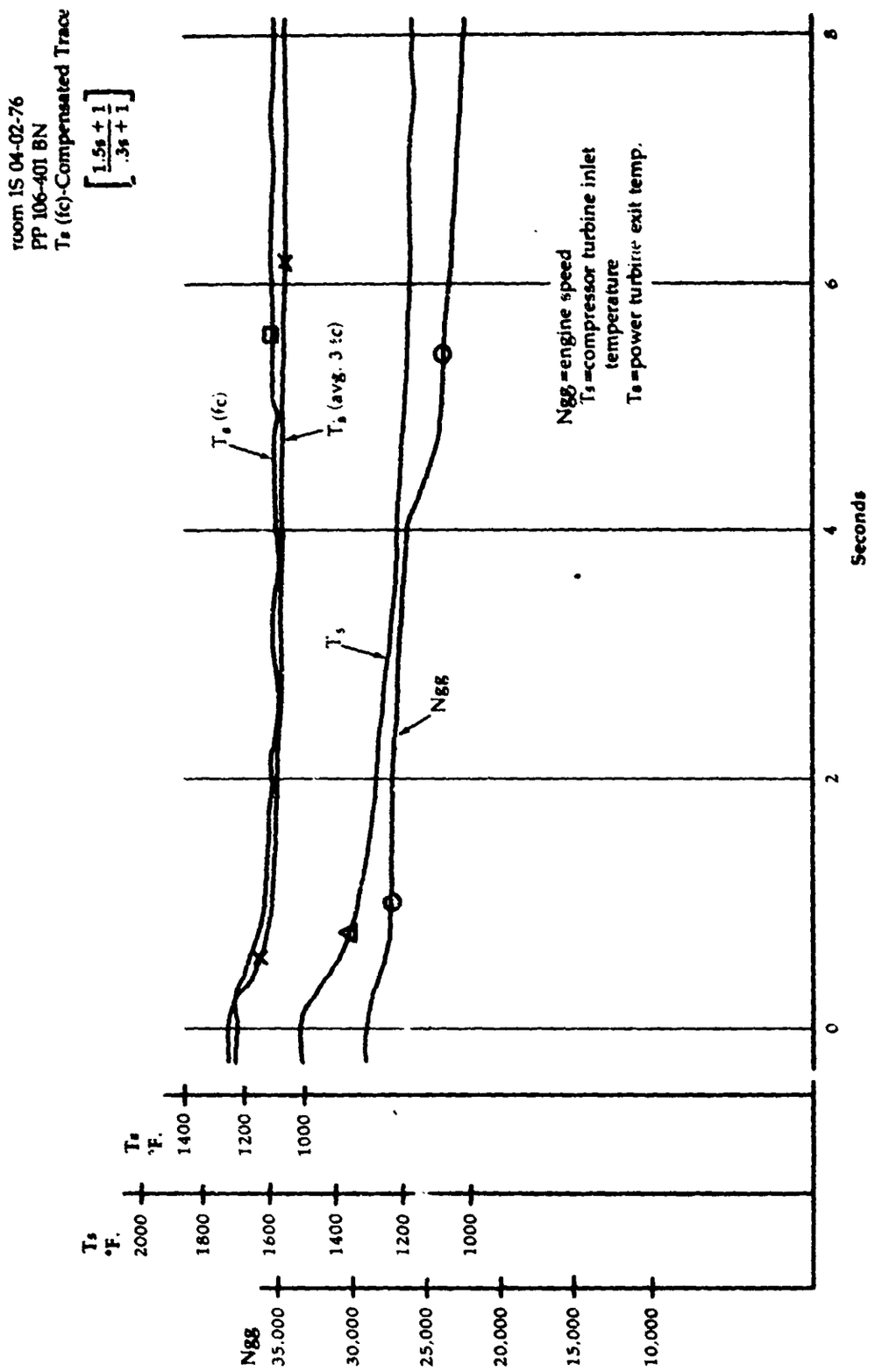

Figure 60

Power Turbine Nozzle Actuator Assembly

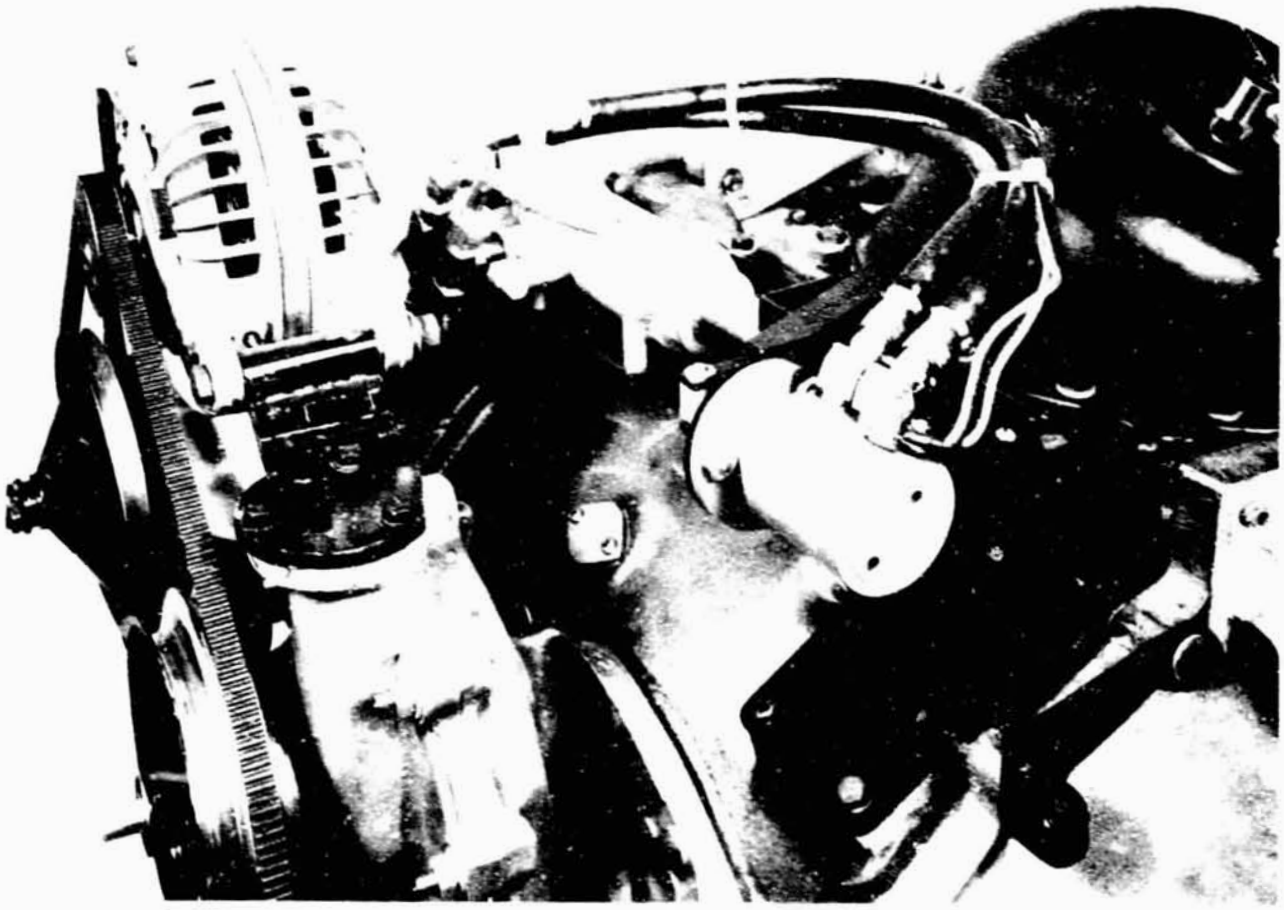

Figure 61

Inspection Results for Baseline Engine Compressor Turbine Blades Cast from AiRefrac Process- Tip Section

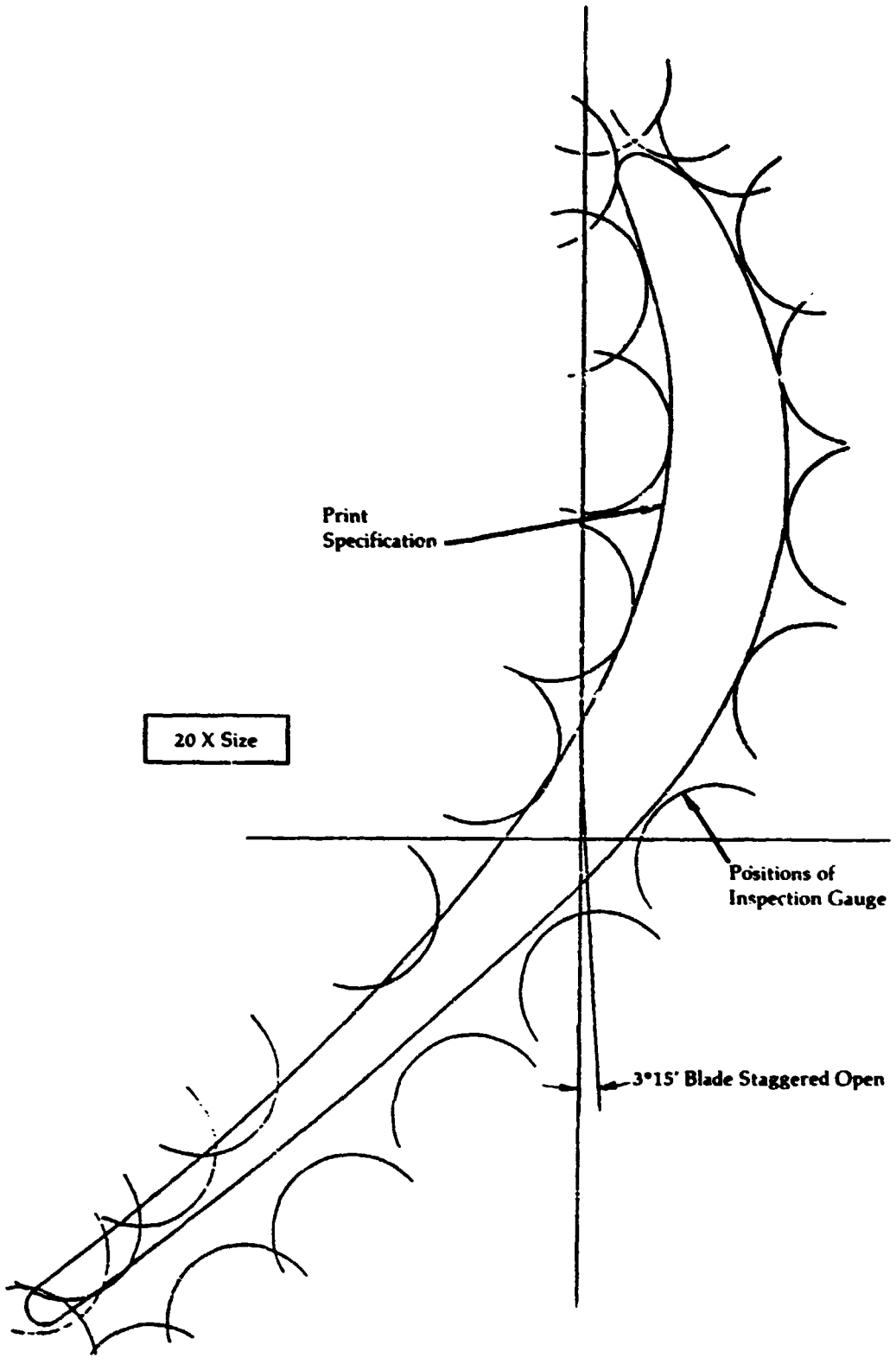

Figure 62

Inspection Results for Baseline Engine Compressor Turbine Blades Cast from AiRefrac Process- Root Section

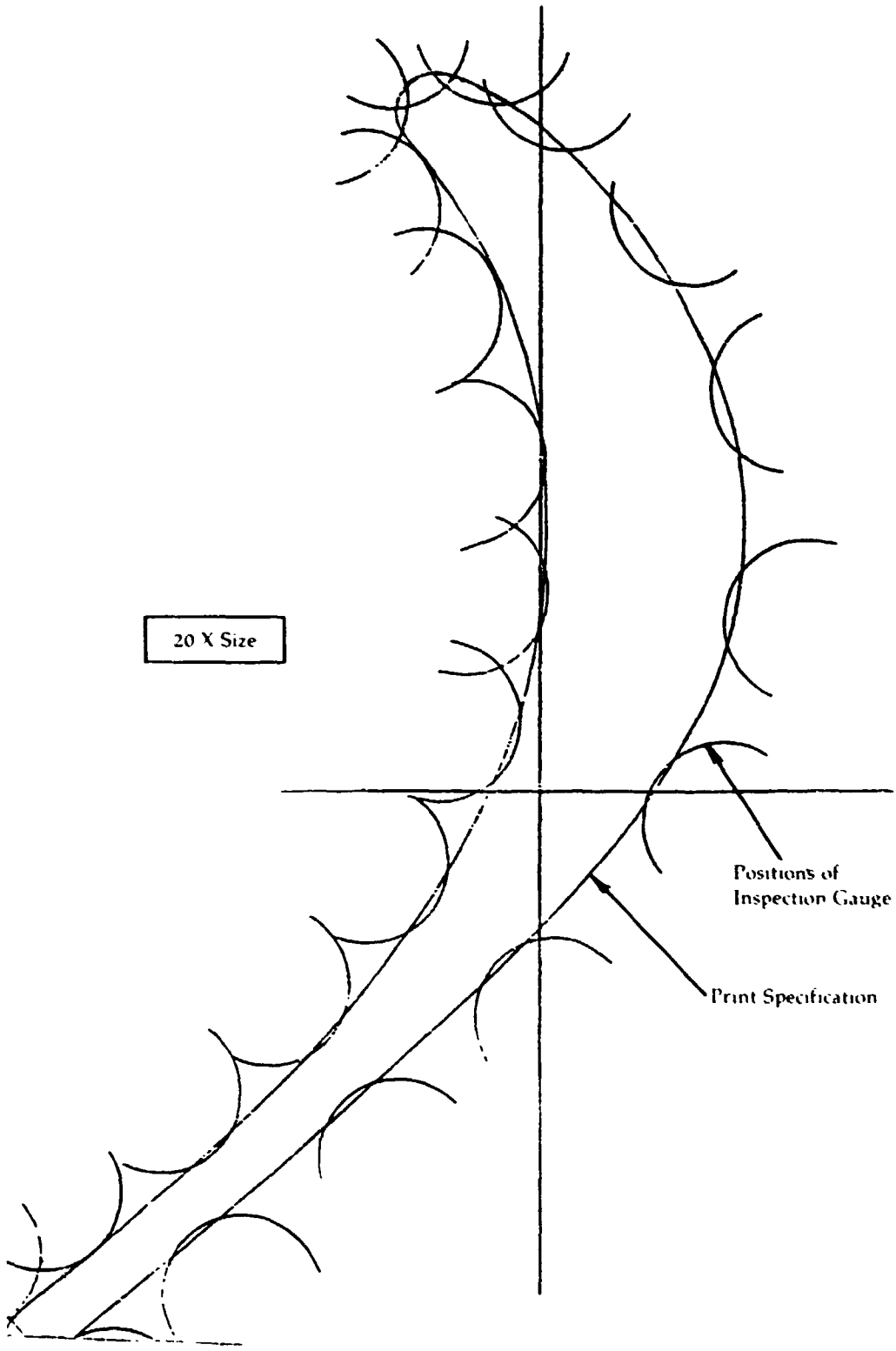

Figure 63

Inspection Results for Baseline Engine Compressor Turbine Blades Cast From AiRefrac Process-Mean Section

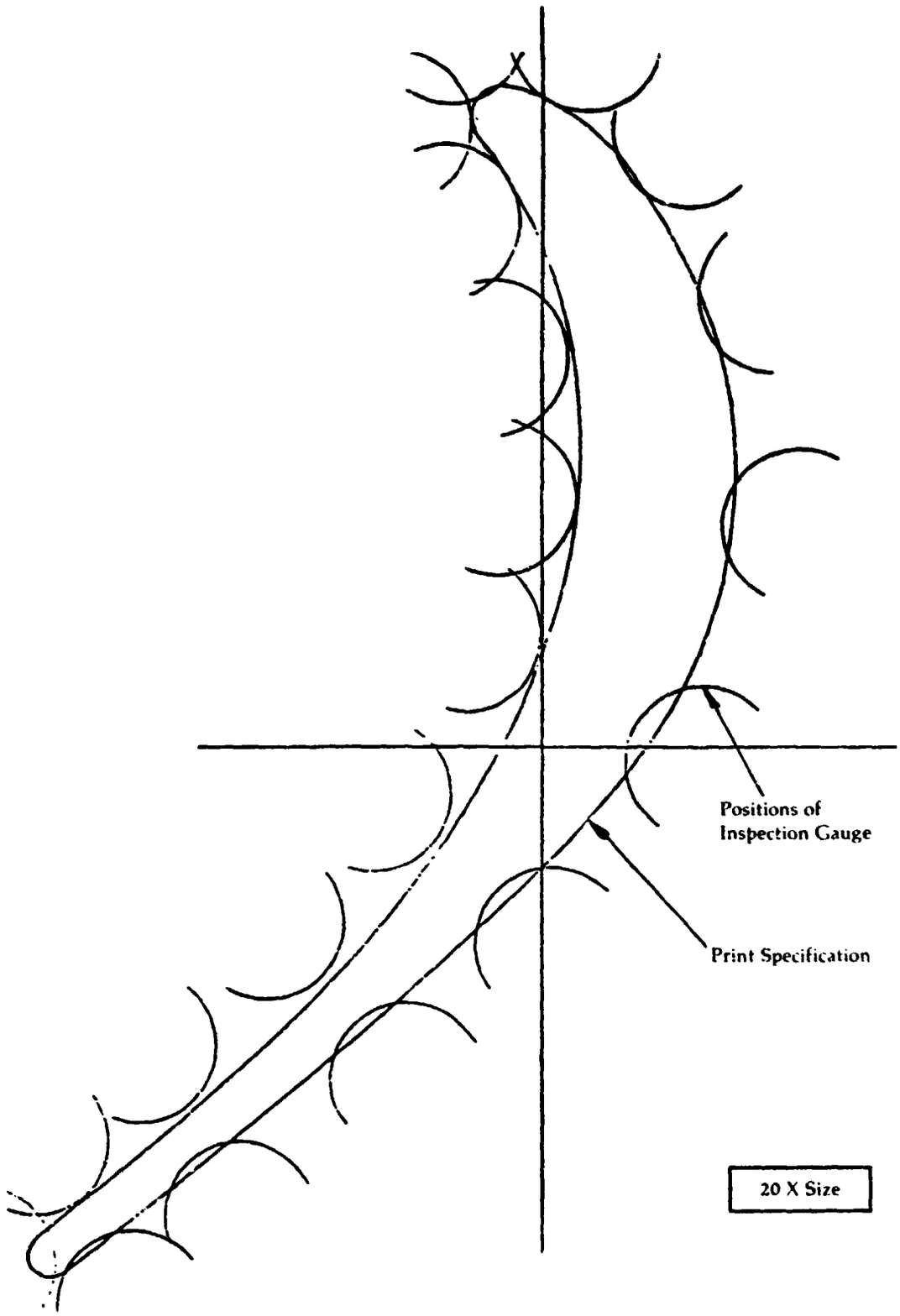

Figure 64

Continuously Variable Transmission-Hydromechanical Type Designed By Mechanical Technology Inc.

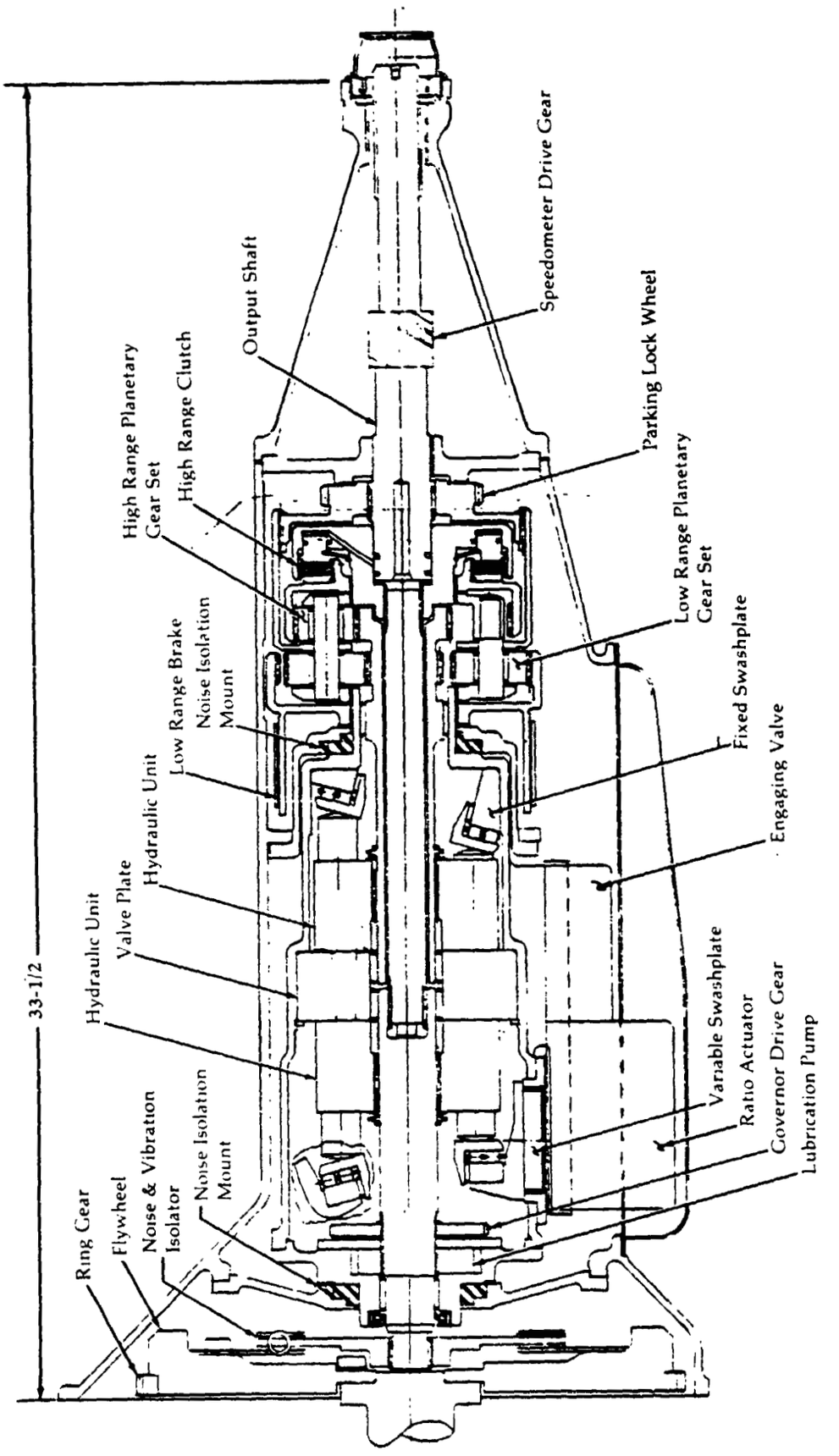

Figure 65

MTI Hydromechanical Transmission

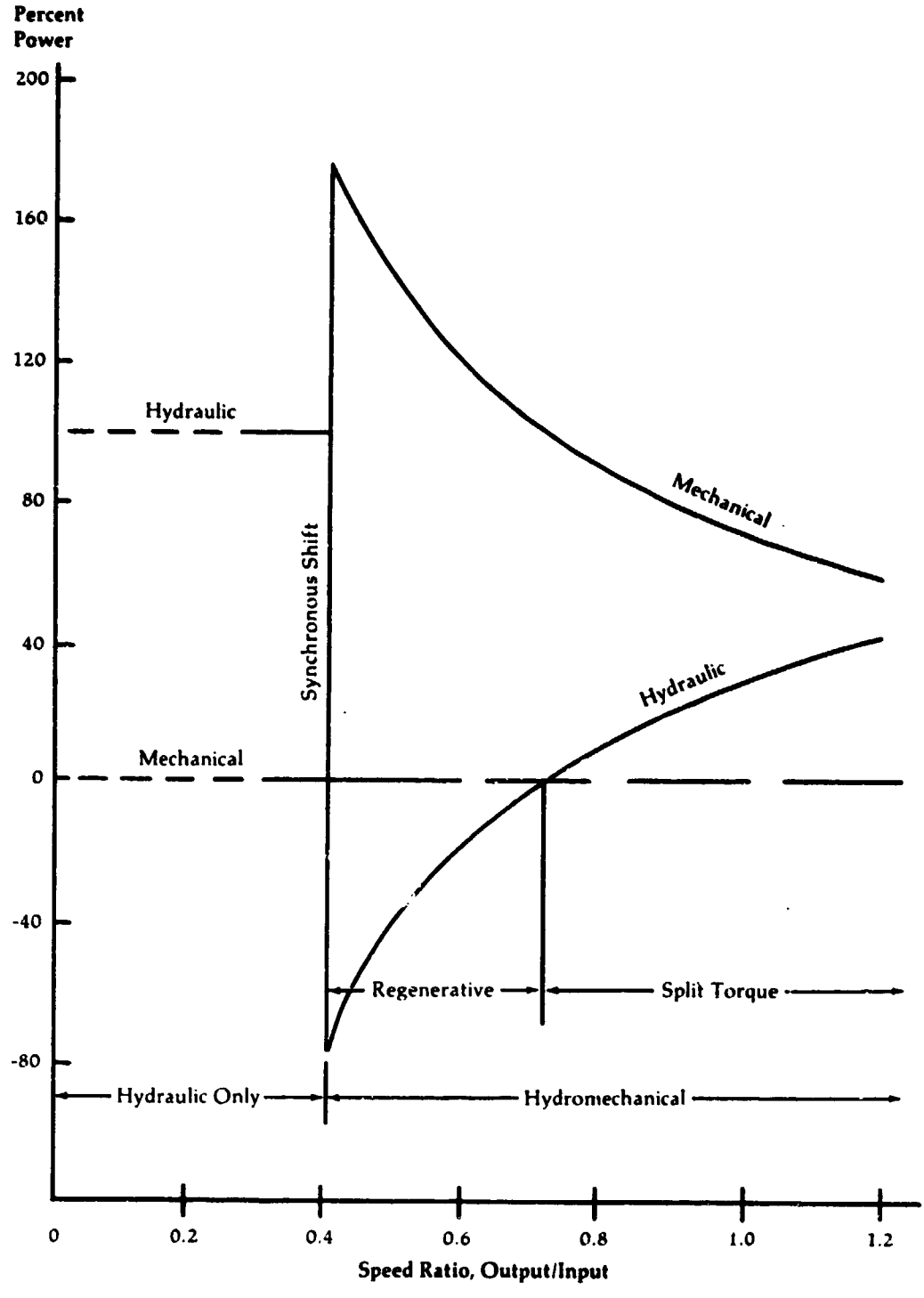

Figure 66

MTI Variable Displacement Pump-Motor Module

Efficiency versus Torque

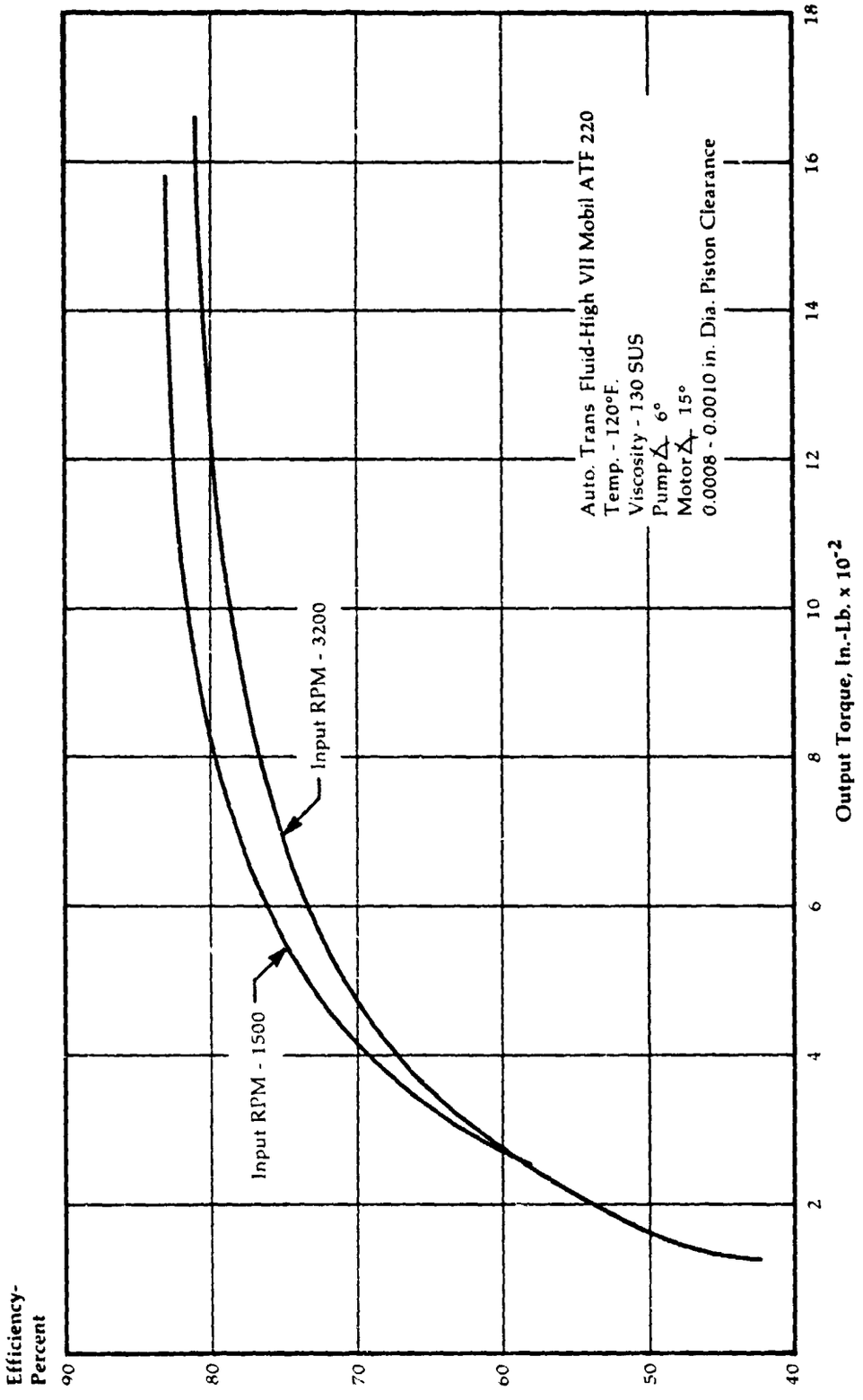

Figure 67

MTI Variable Displacement Pump-Motor Module

Efficiency versus Torque

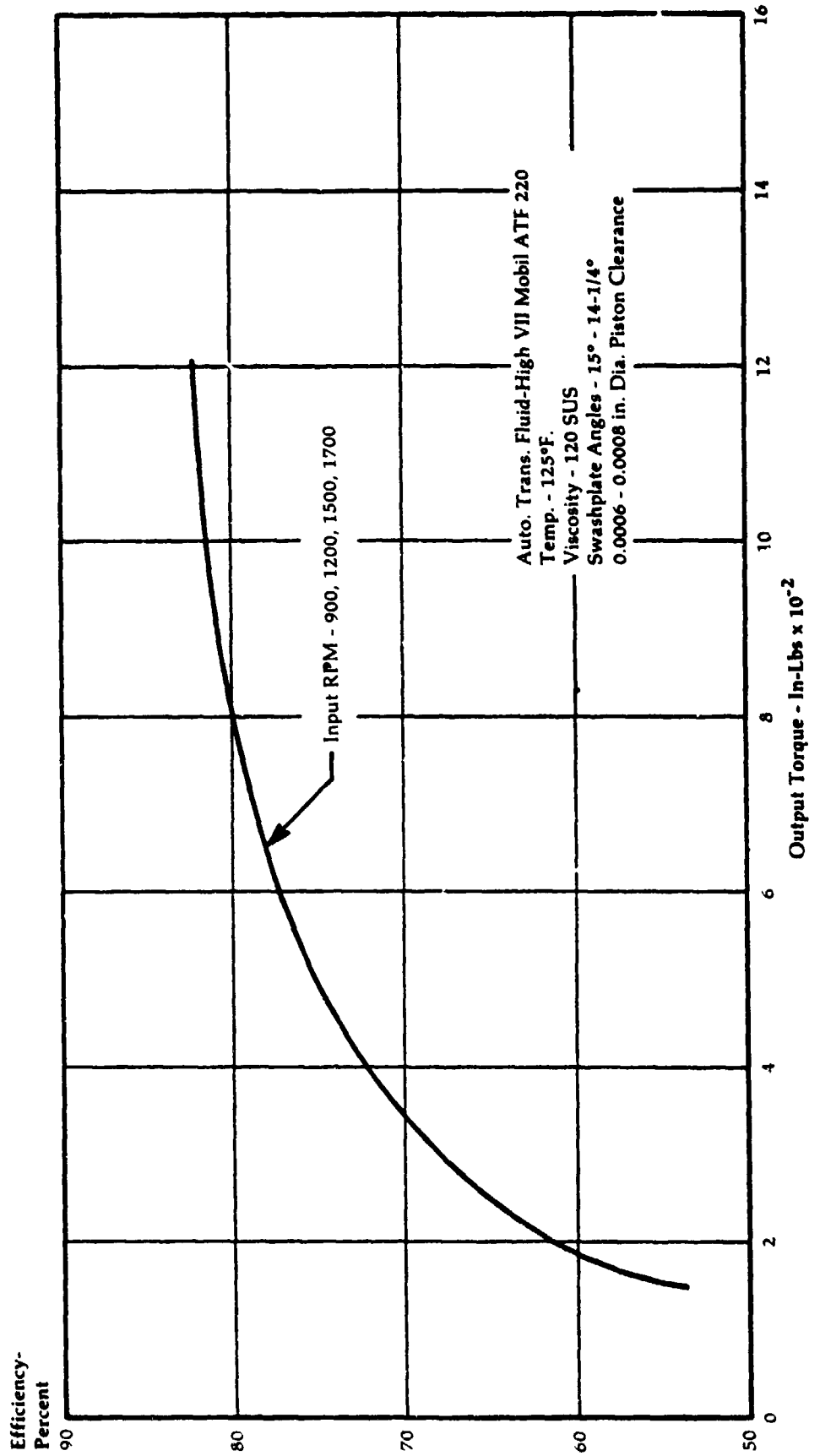

Figure 68

MTI Variable Displacement Pump-Motor Module

Efficiency versus Torque

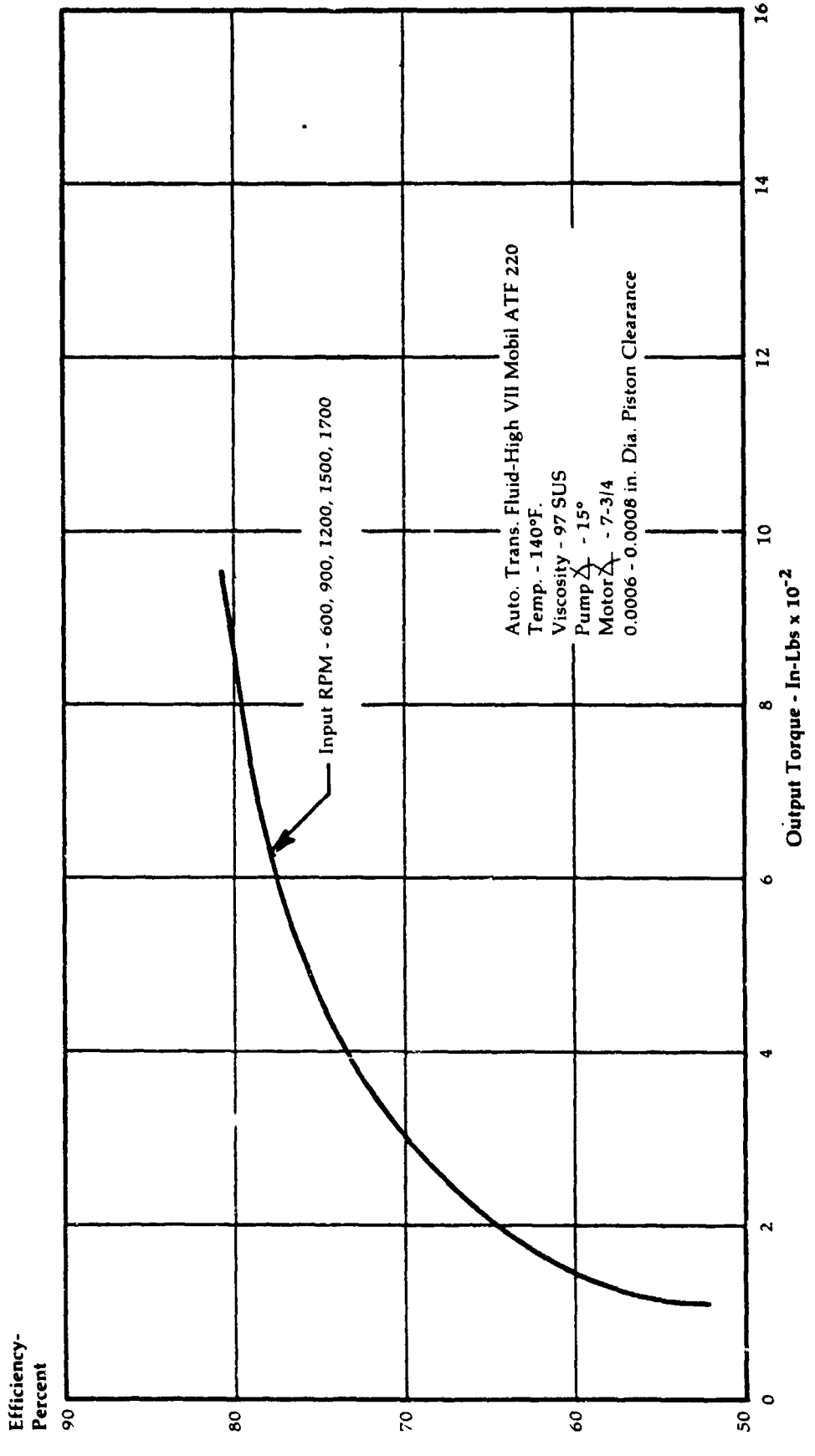

Figure 69

Geared Rotor Concept

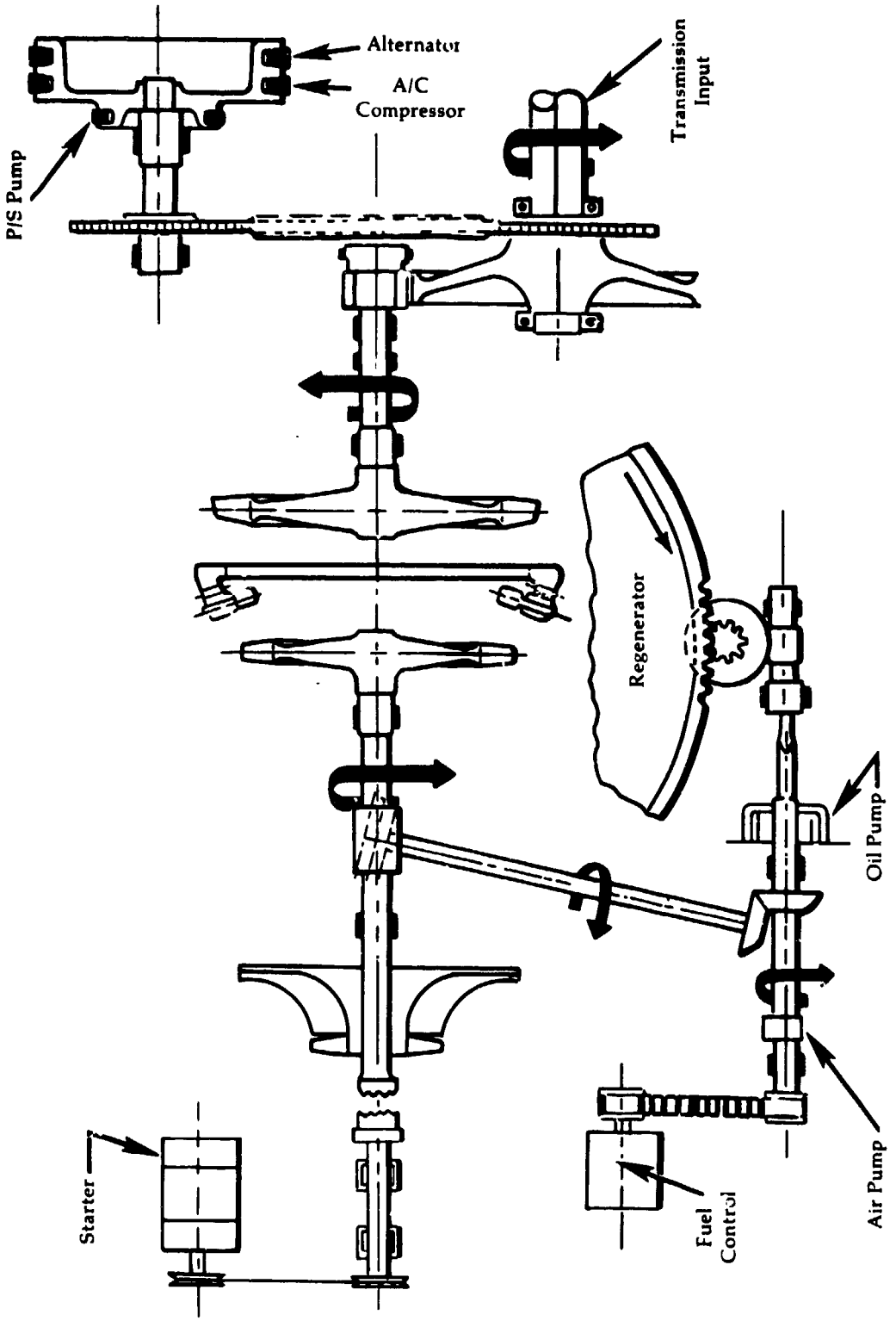

Figure 70

Free Rotor Concept

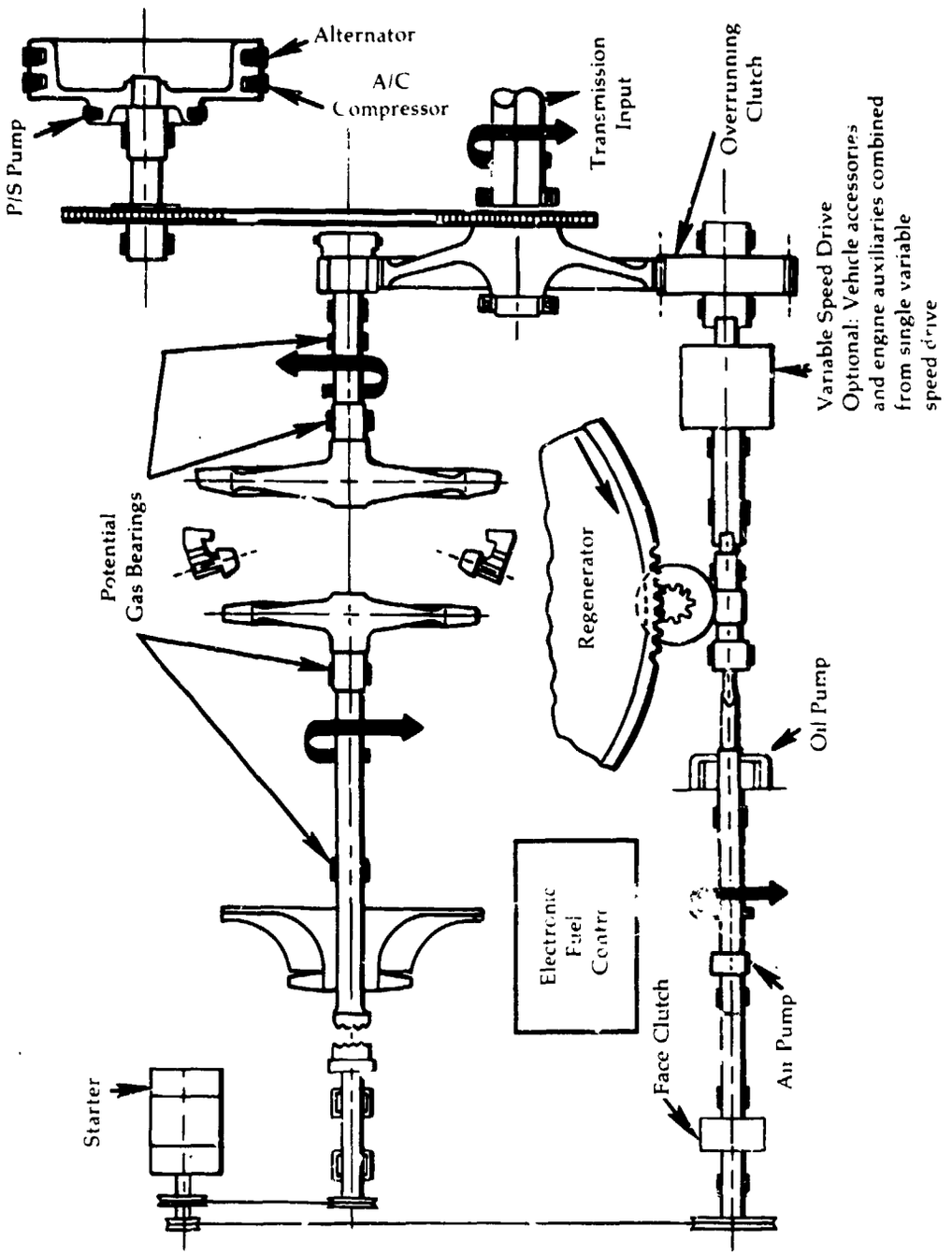

Figure 71

Schematic for Free Rotor Simulation Test

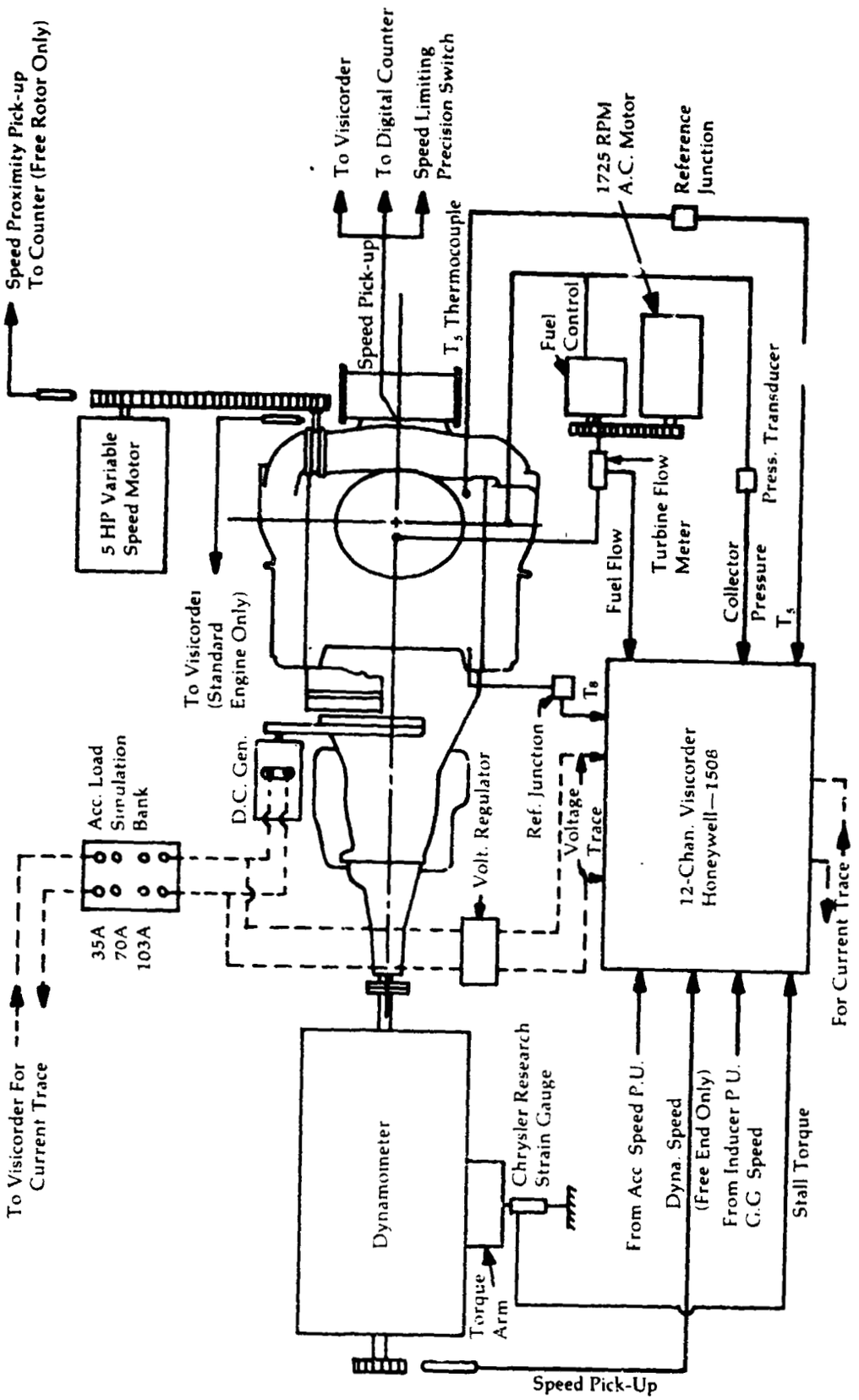

Figure 72

Gas Generator Acceleration - Free Rotor Configuration

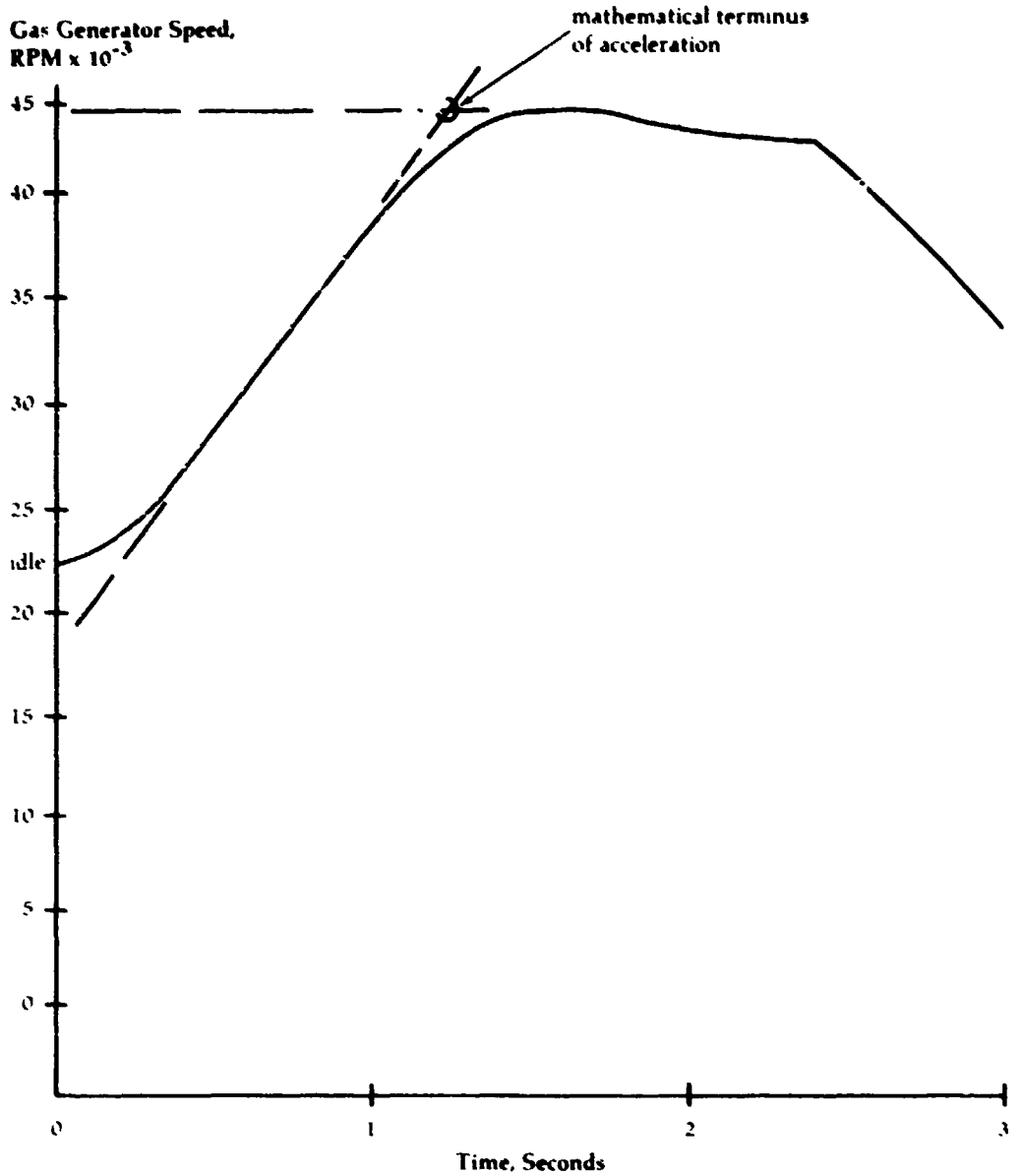

Idle - 22 300 RPM
T_5 - .225° F

Power into Converter	1.7 hp
Ancillary Load	2.8 hp
Total Power Developed	4.5 hp

Fuel Schedule No. 4
Torque Converter "B"

T_5 - power turbine exit temperature

Figure 73

Variation of Engine Operating Line with Acceleration Time

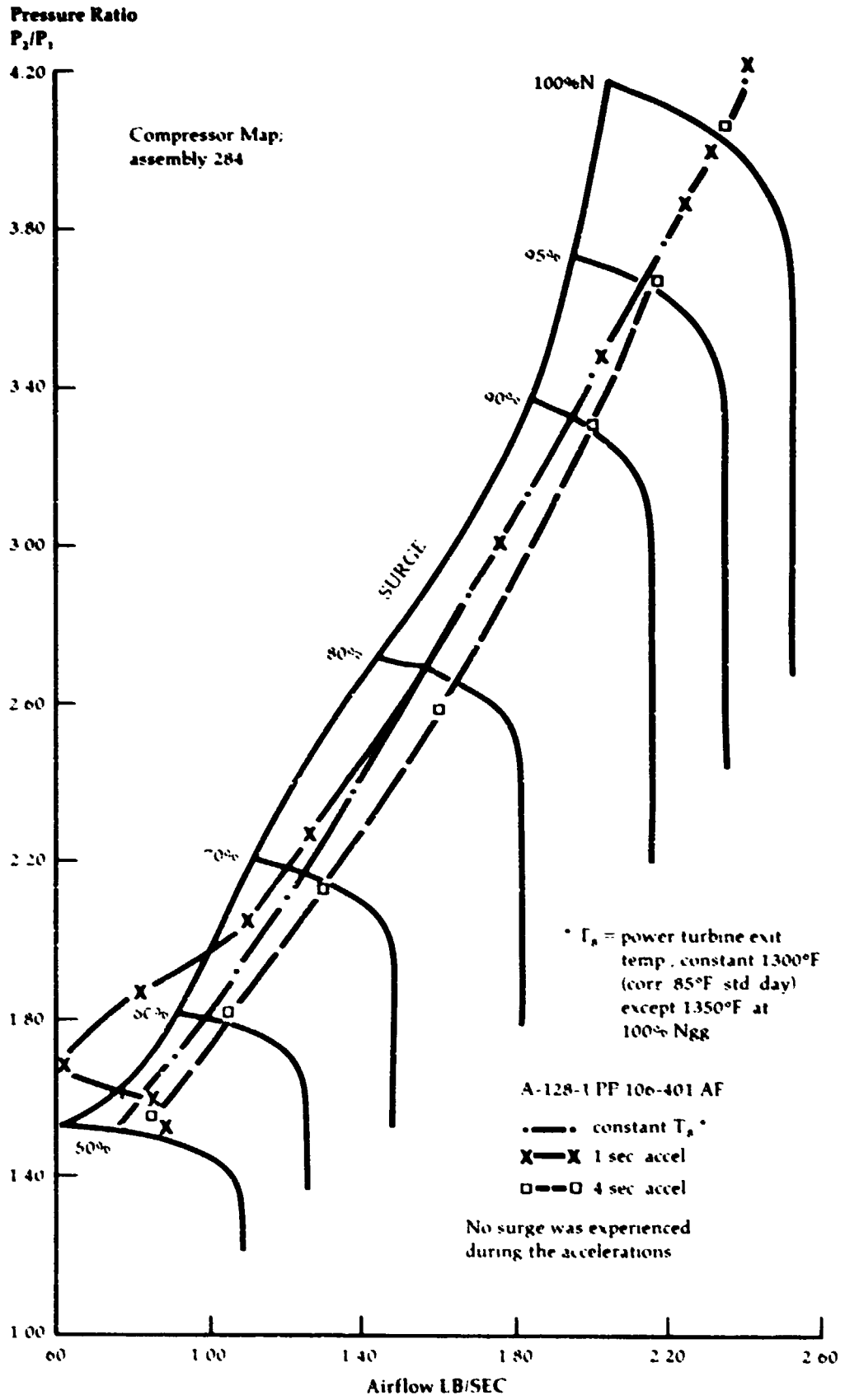

Figure 74

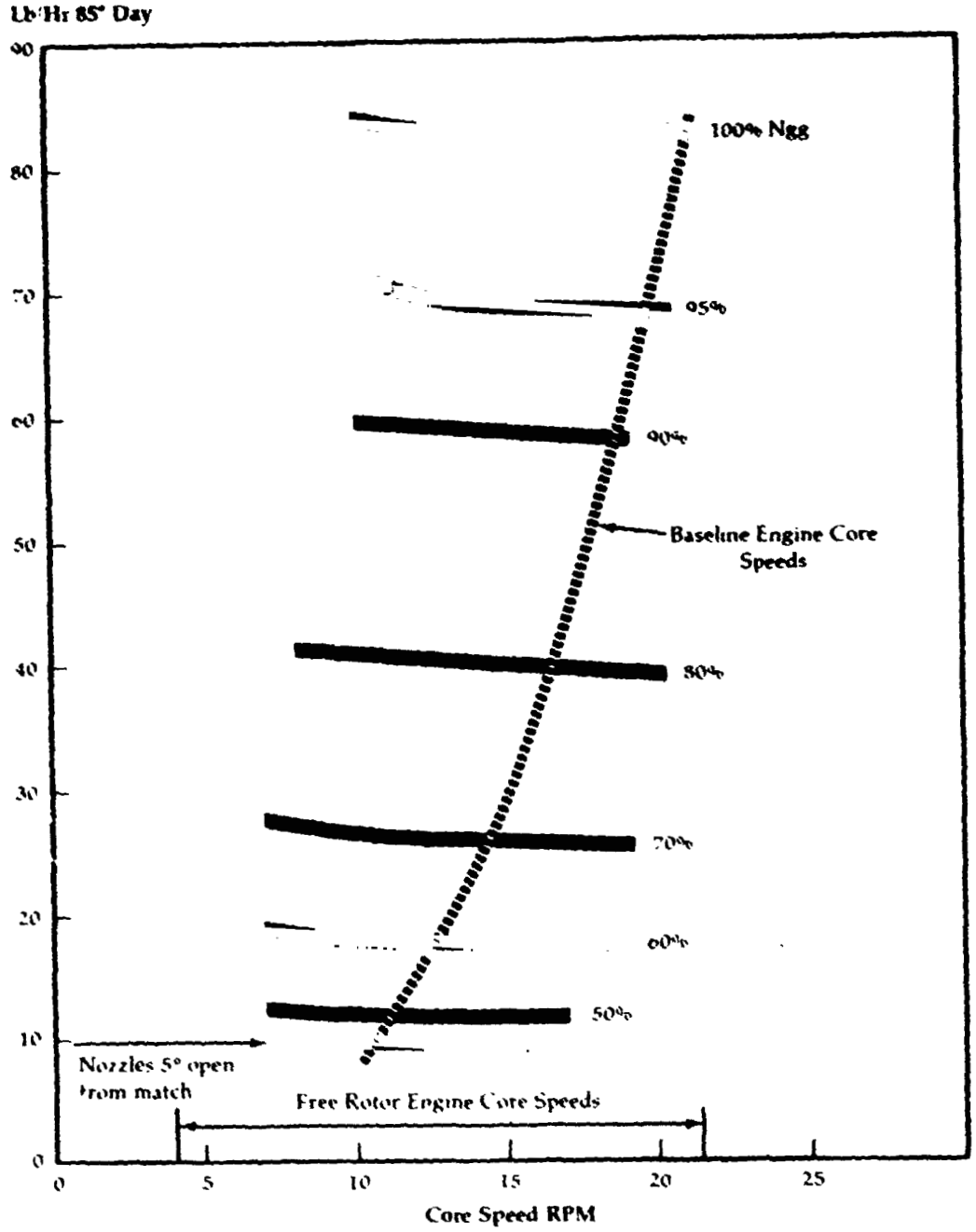

T_5 = 1300°F. (corrected 85°F std day) power turbine exit temperature except for open power turbine nozzle condition as noted

Ngg = gas generator rotational speed

Figure 75

Free Rotor Conversion of Baseline Engine

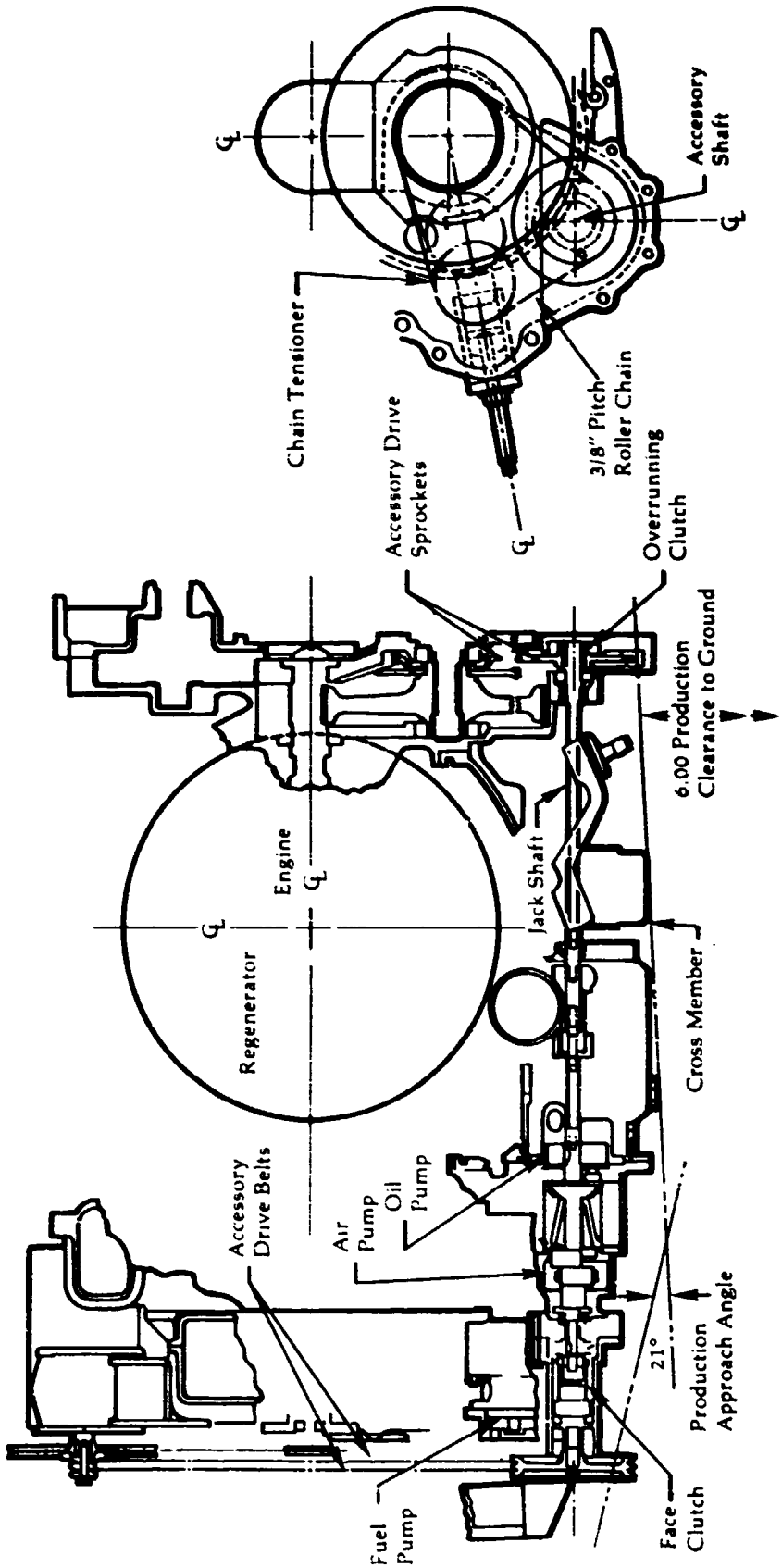

Figure 76

Cold Start—Free Rotor Engine

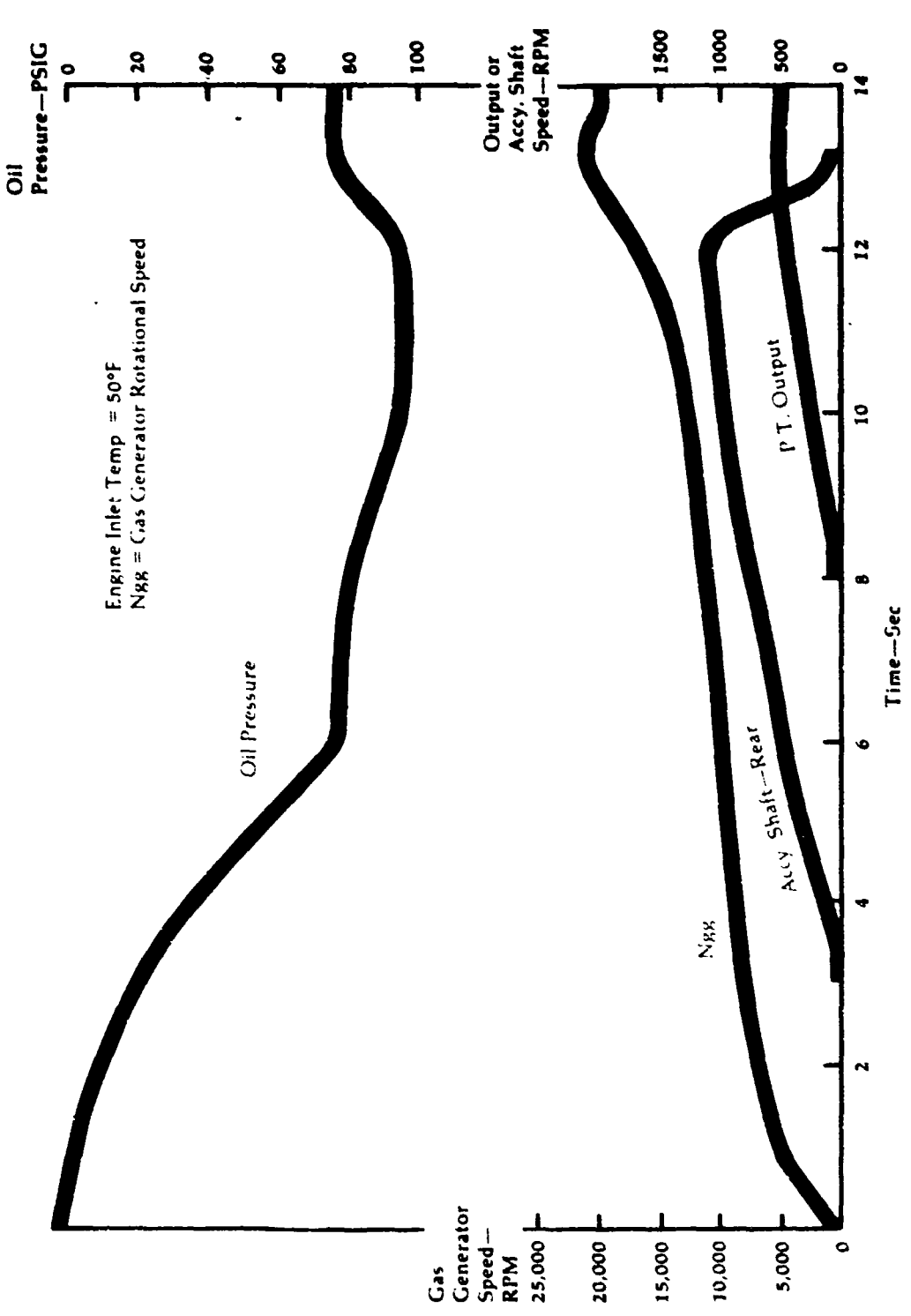

Figure 77

Figure 78

Hot Start—
Free Rotor
Engine

Turbine Inlet Temp. = 900°F.
(1850°F Peak During Accel)

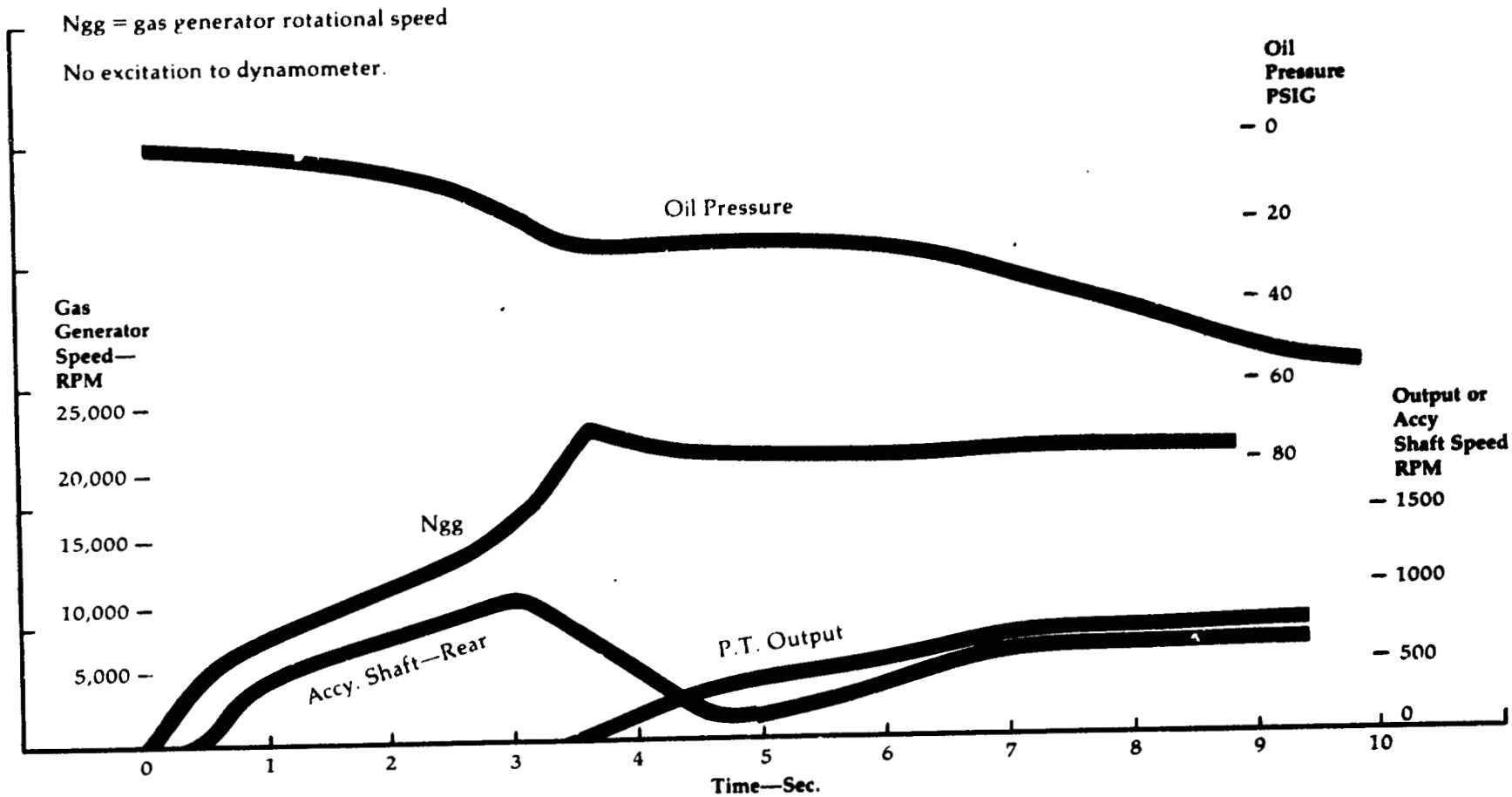

Engine Performance Map

Free Rotor Configuration

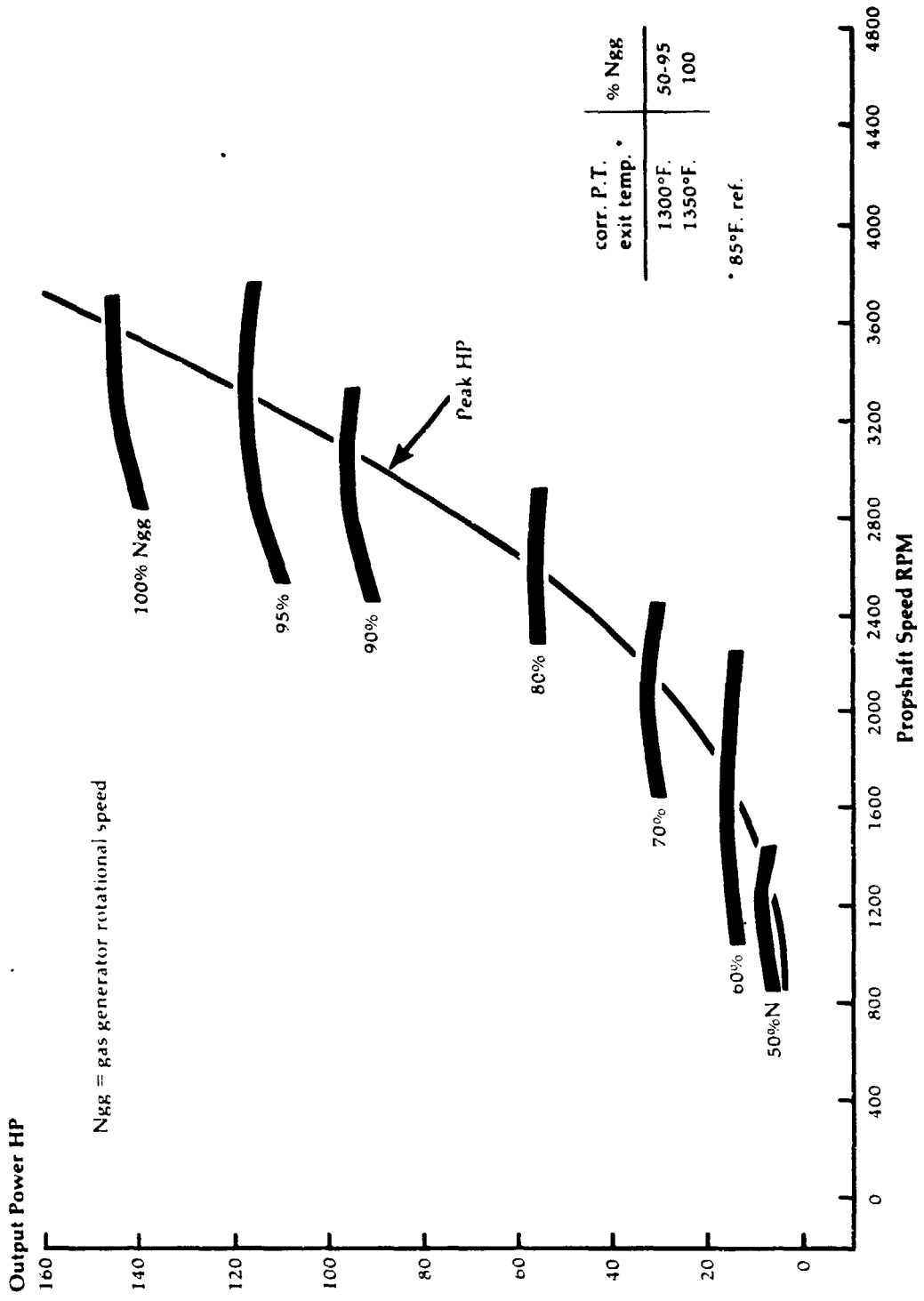

Figure 79

Vehicle Coastdown

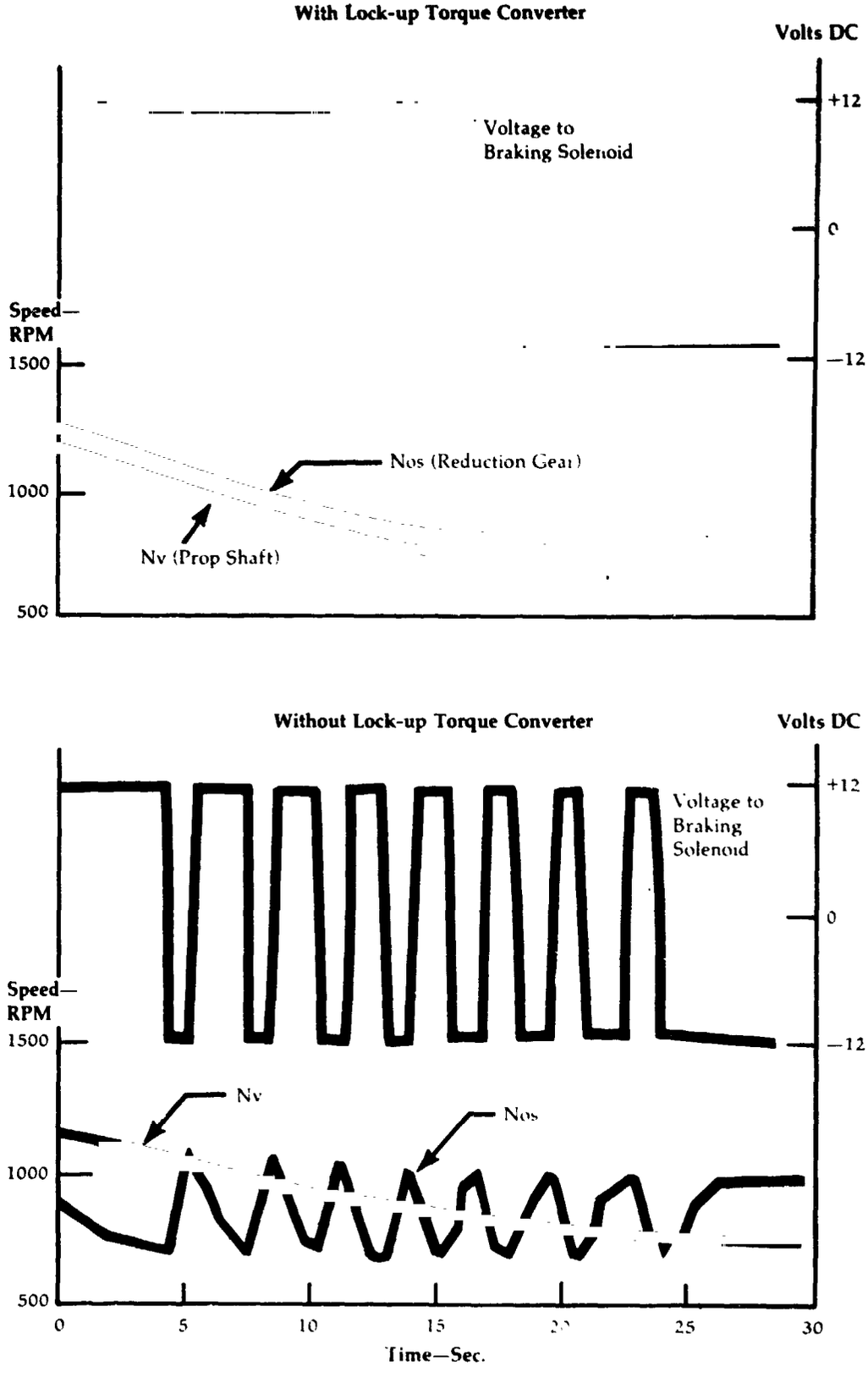

Figure 80

Water Injector Locations Used in Engine Tests

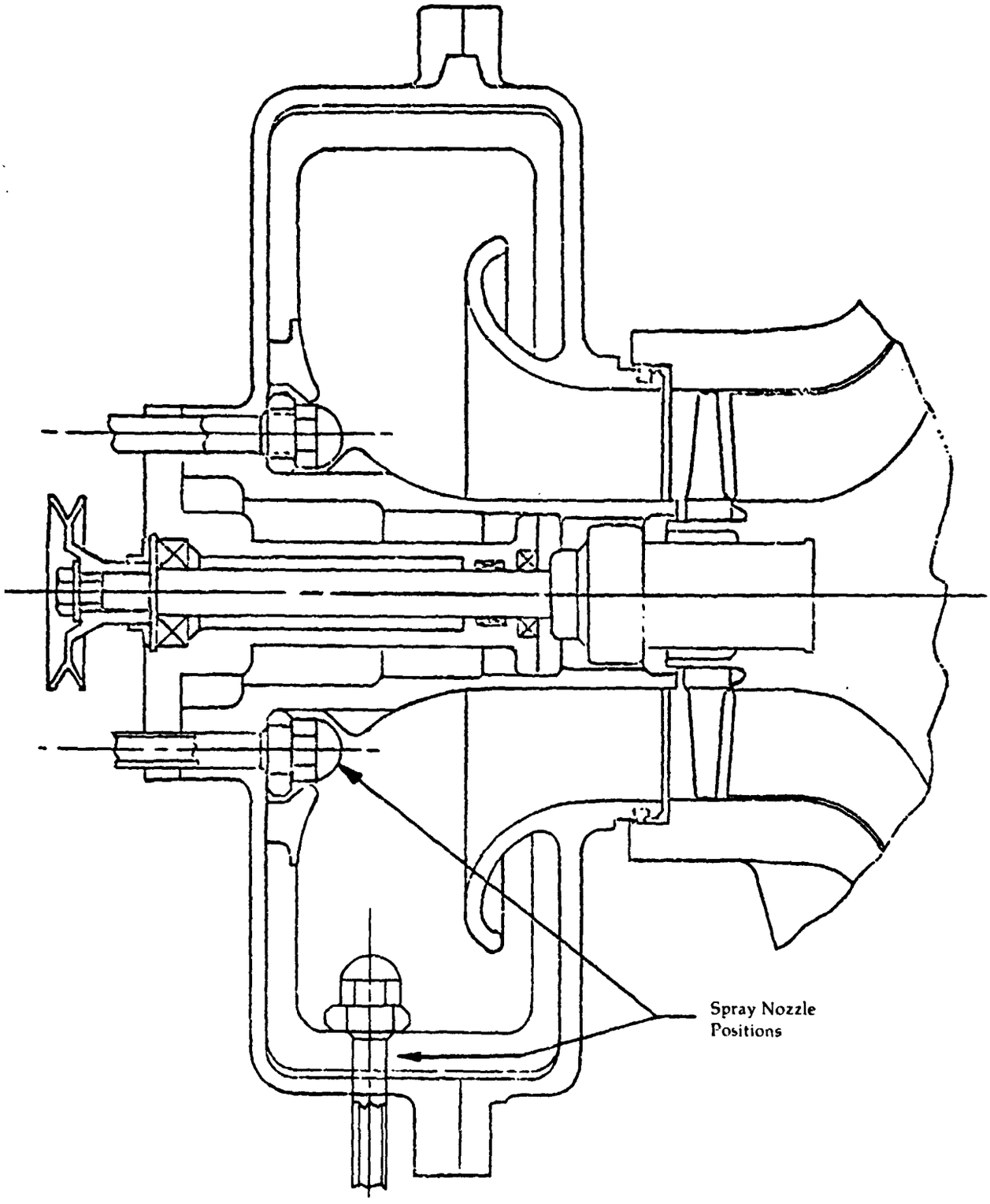

Figure 81

Water Injection
Spray Pattern of
Axially-Directed
Nozzles

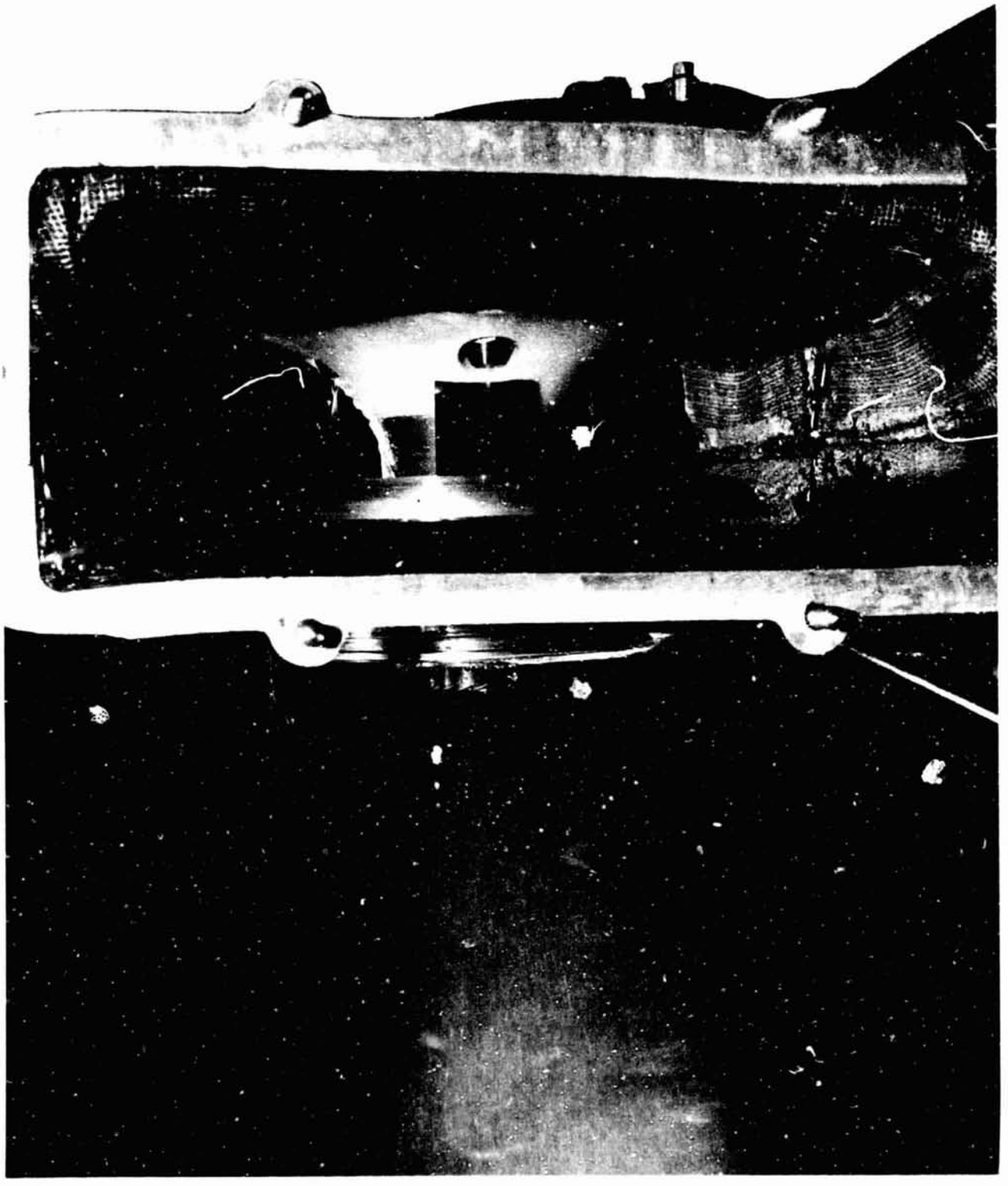

Figure 82

Engine Characteristics for Power Augmentation

Constant T_5 at Peak Power Prop Speeds

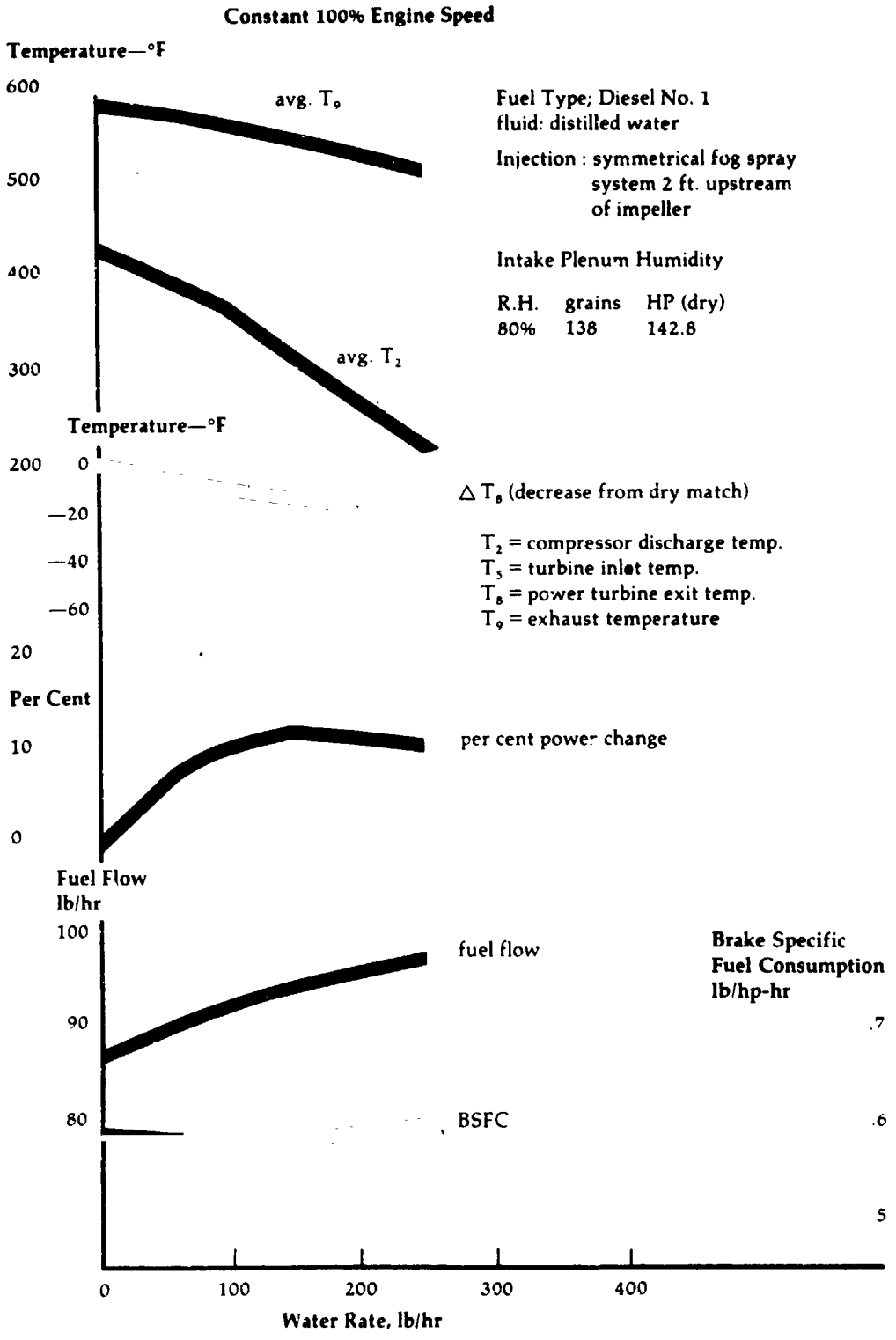

Figure 83

Engine Characteristics for Power Augmentation

Constant T_5 at Peak Power Prop Speeds

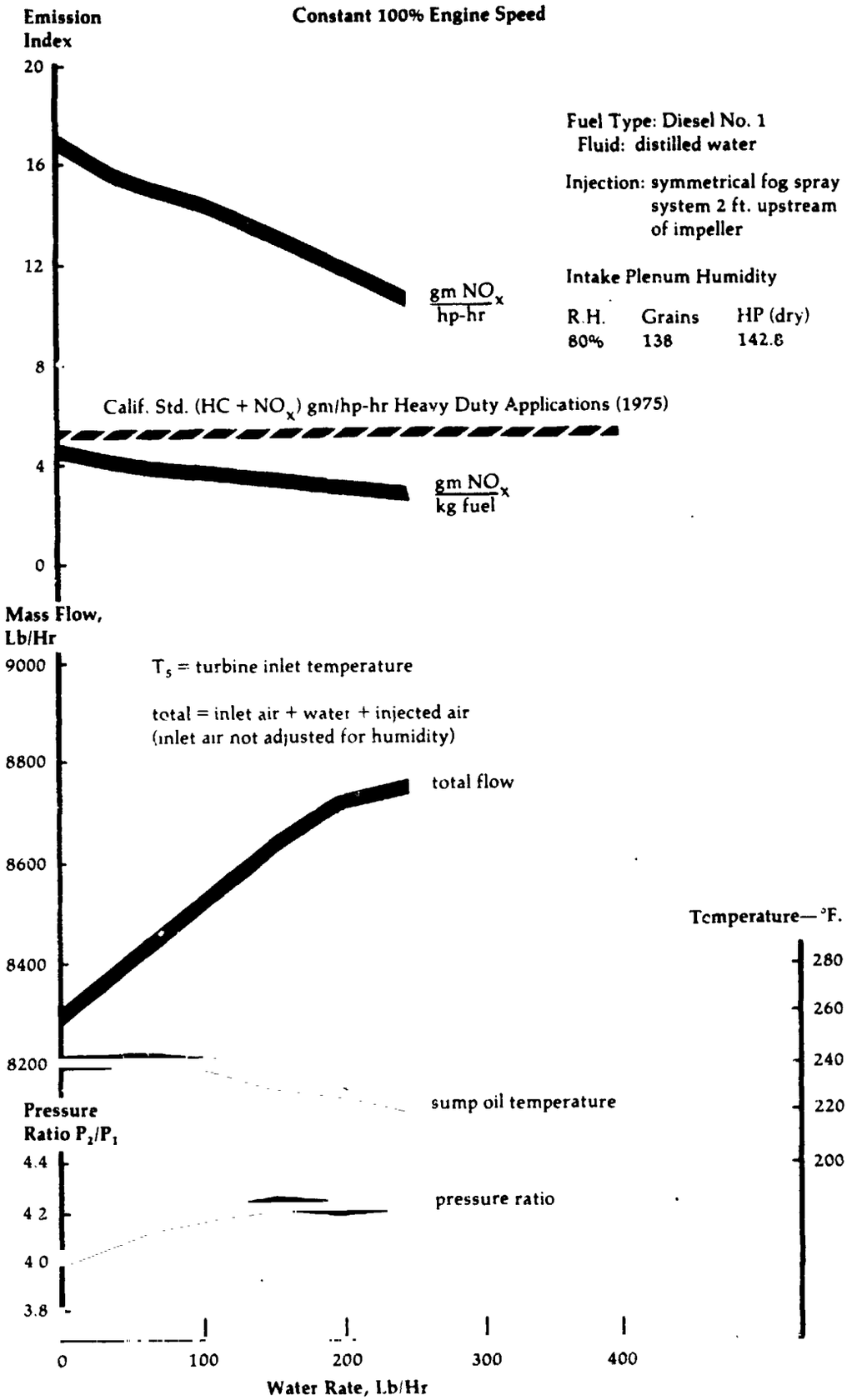

Figure 84

Effect of Ambient Relative Humidity on Power Augmentation

100% Engine Speed

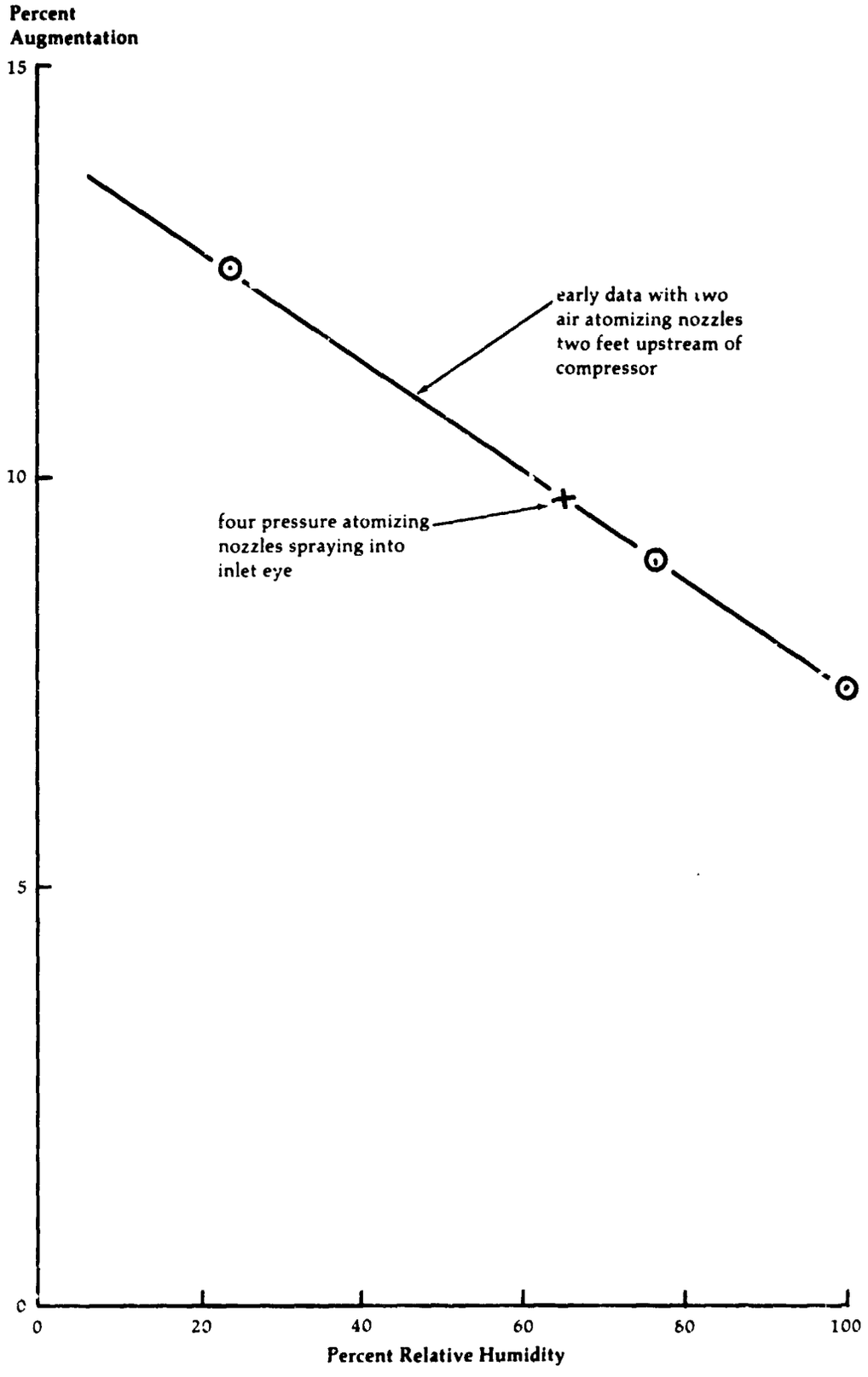

Figure 85

NO_x Emission Rates in Power Augmentation Tests

Constant T_5 at Peak Power Prop Speeds

Constant 100% Engine Speed

A-128-1 PP 425-409 AT with droplet-diffusion burner

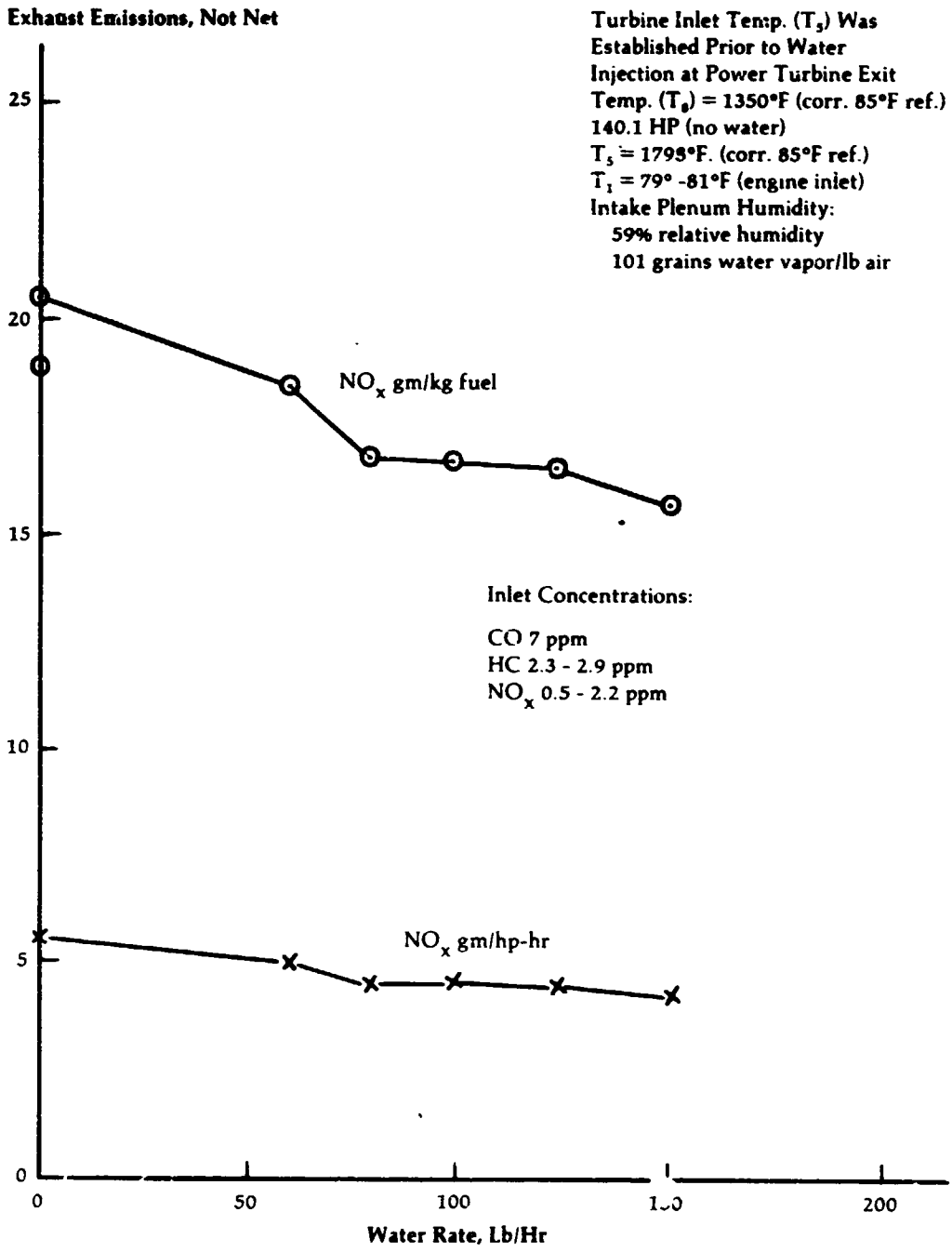

Figure 86

Impeller Damage Due to Water Injection Testing

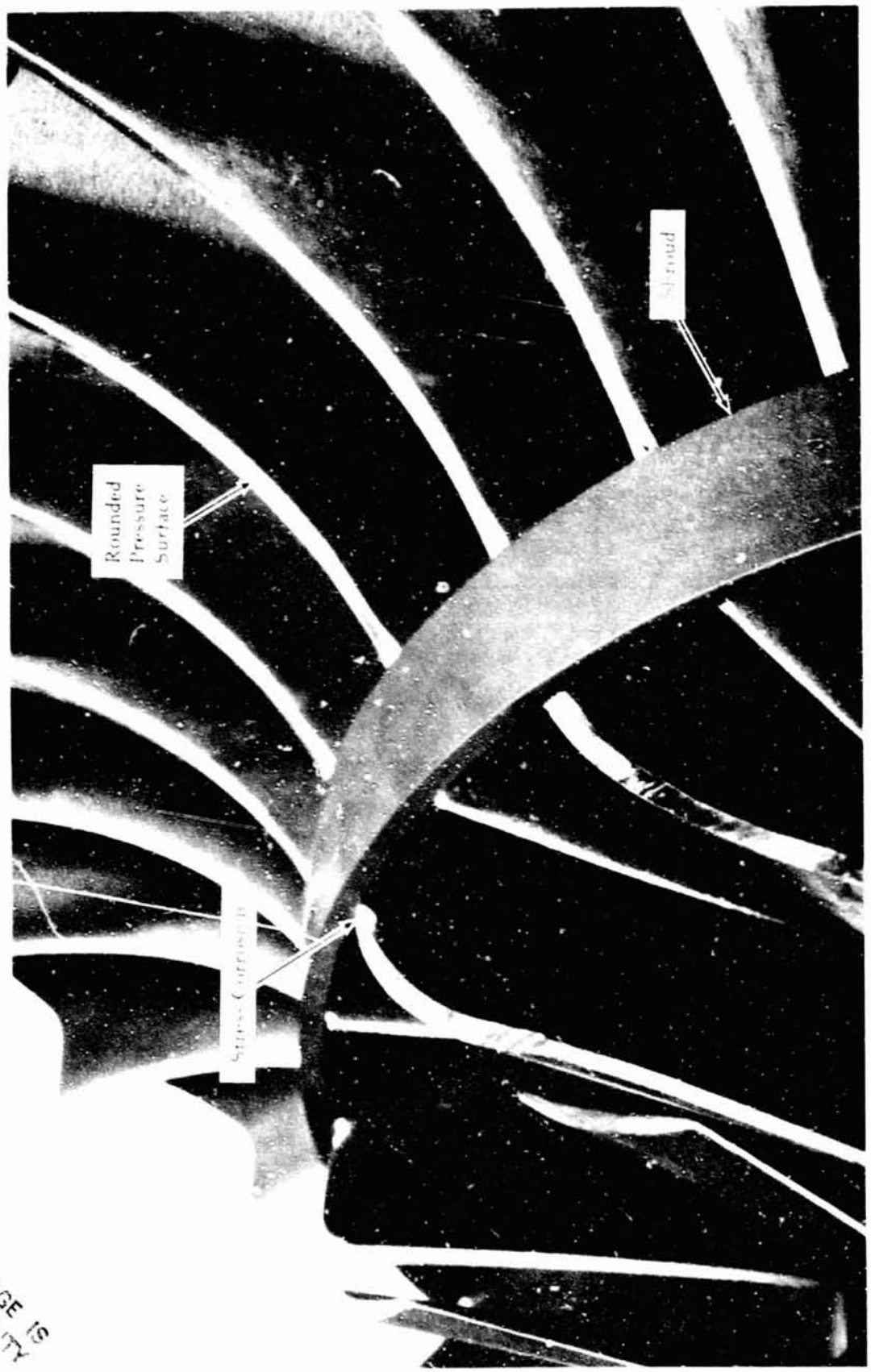

Figure 87

Power Augmentation with VIGV and Water Injection

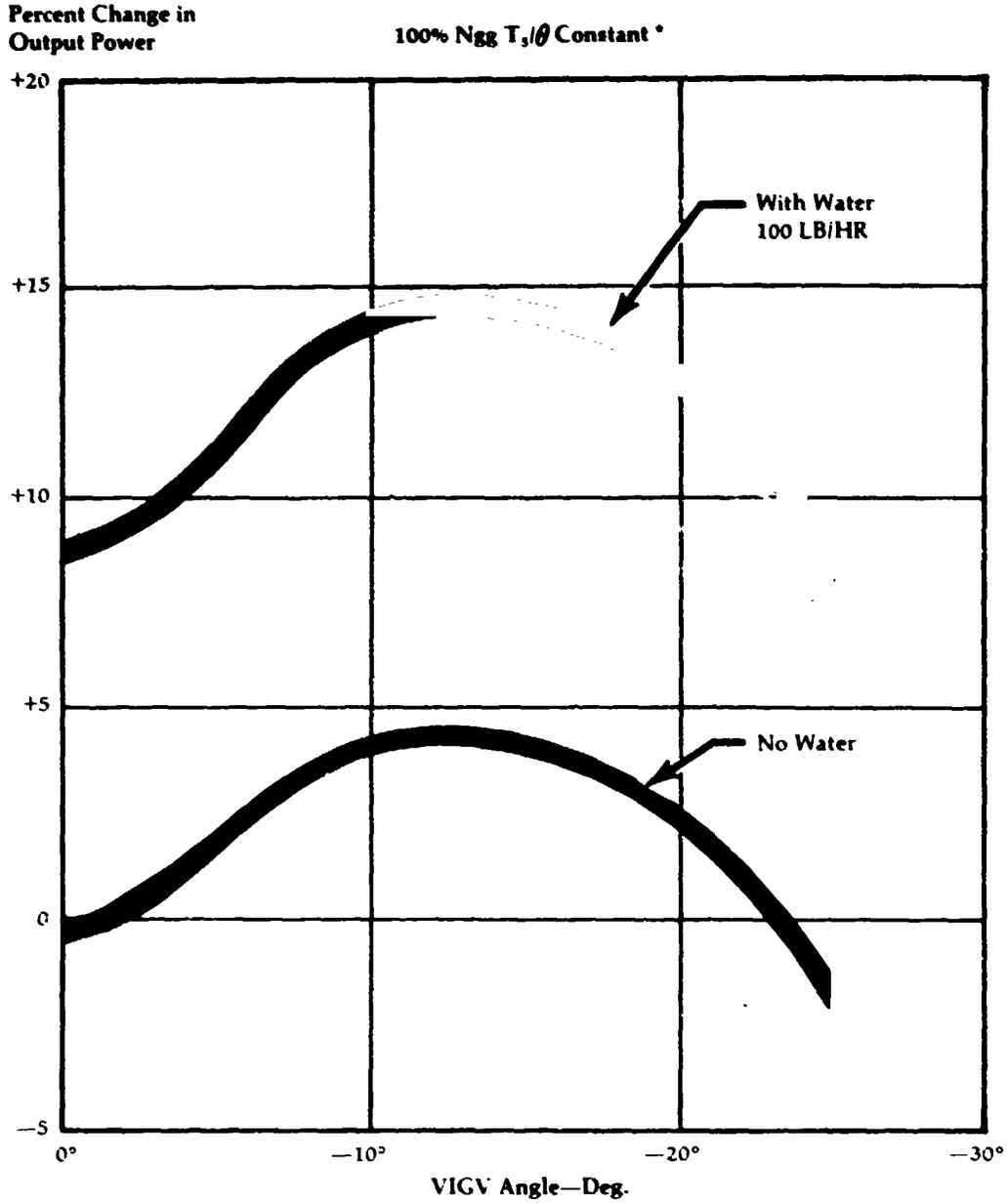

*T_5 = turbine inlet temperature
Ngg = gas generator rotational speed

Figure 88

Vehicle Performance with Power Augmentation

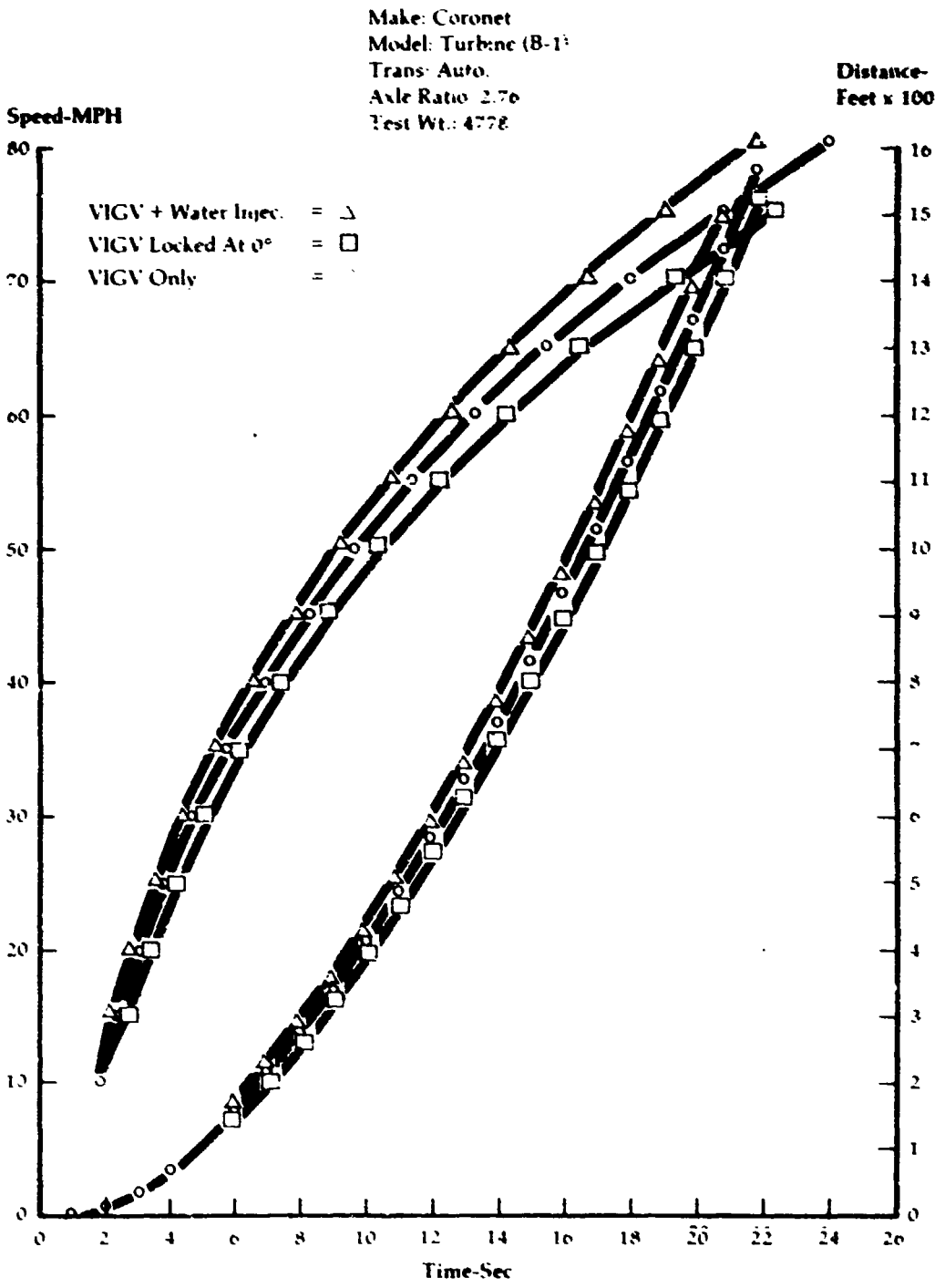

Figure 89

Water Injection
Gas Generator
Vehicle B 1

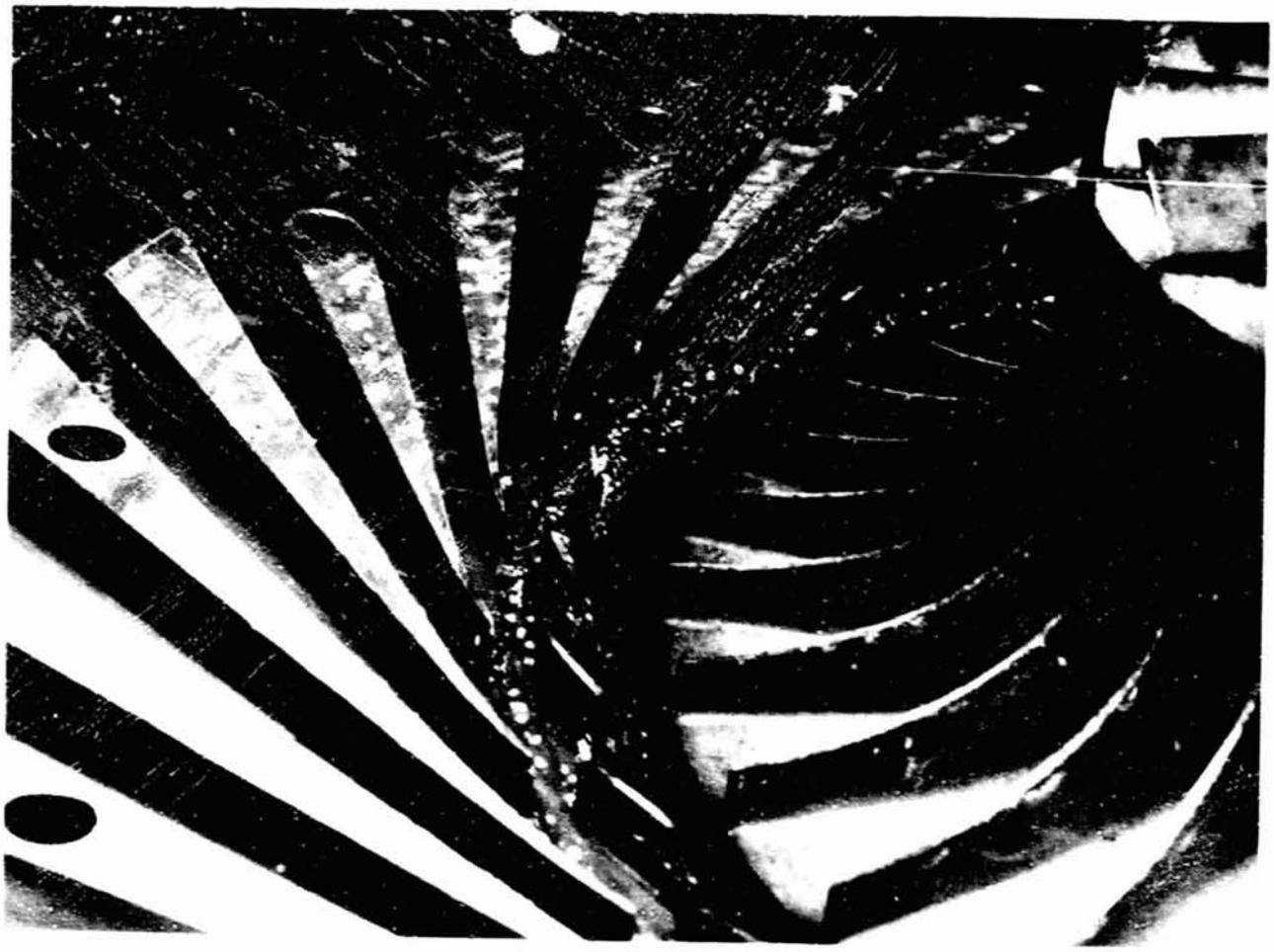

Figure 90

Changes in Engine Operating Line on Compressor Map with VIGV Application

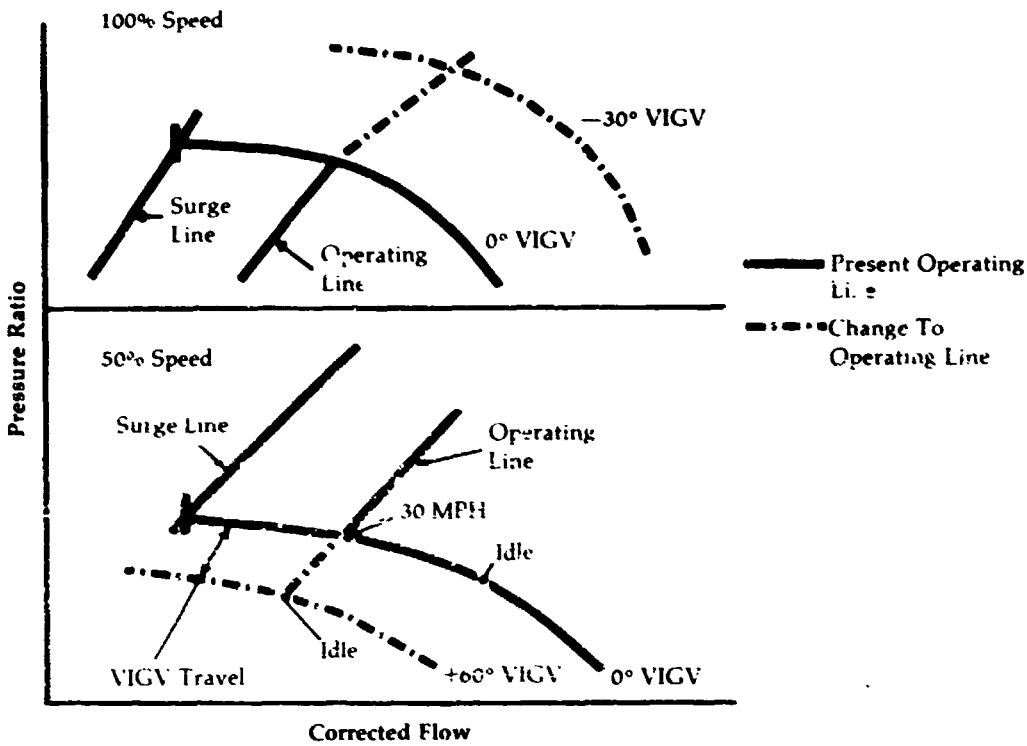

Variable Inlet Guide Vanes on Compressor Assembly

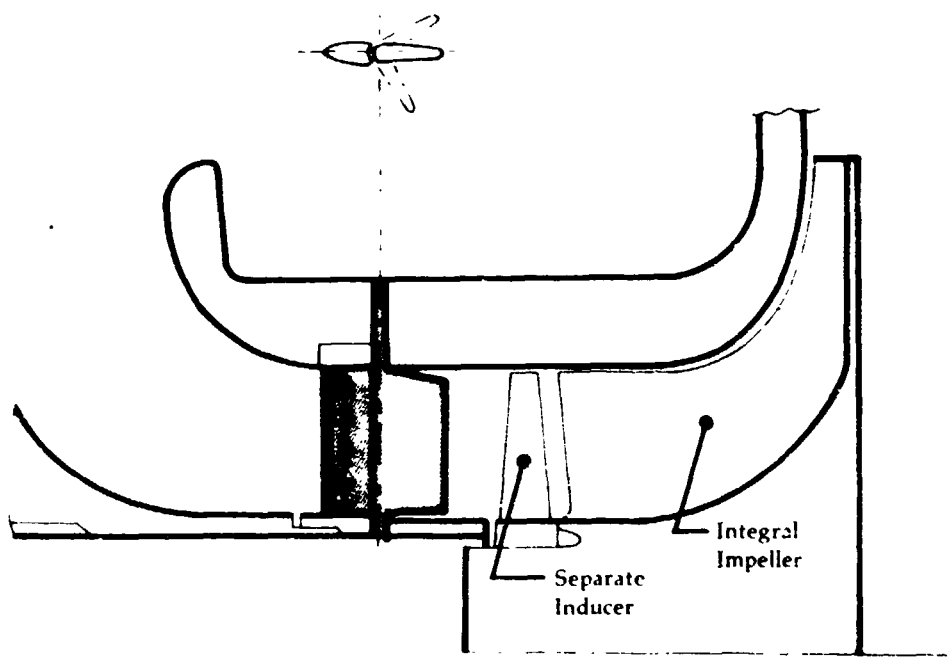

B-52 Compressor Performance with Variable Inlet Guide Vanes

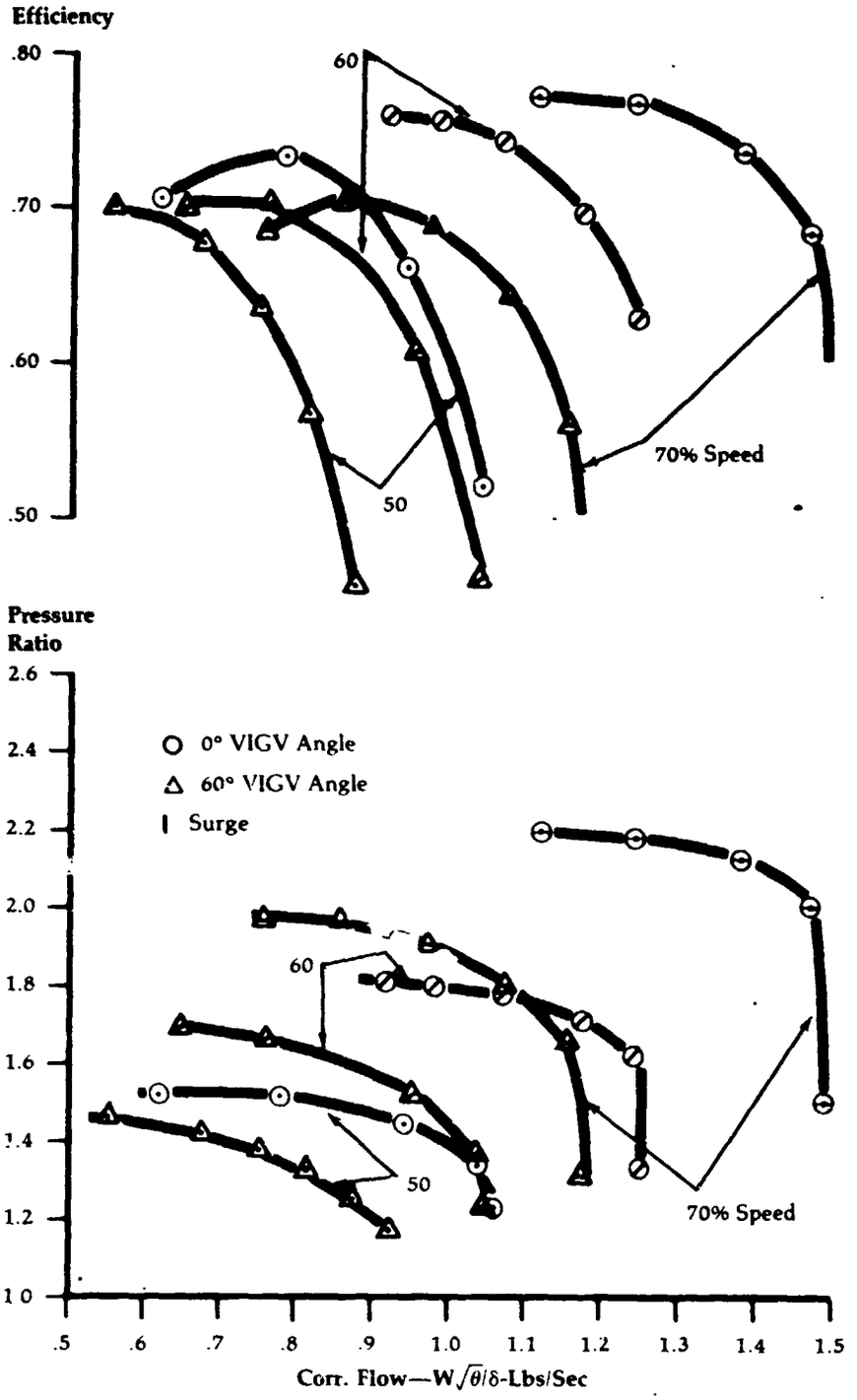

Figure 93

B-52 Compressor Characteristics at 100% Corrected Speed with Variable Inlet Guide Vanes

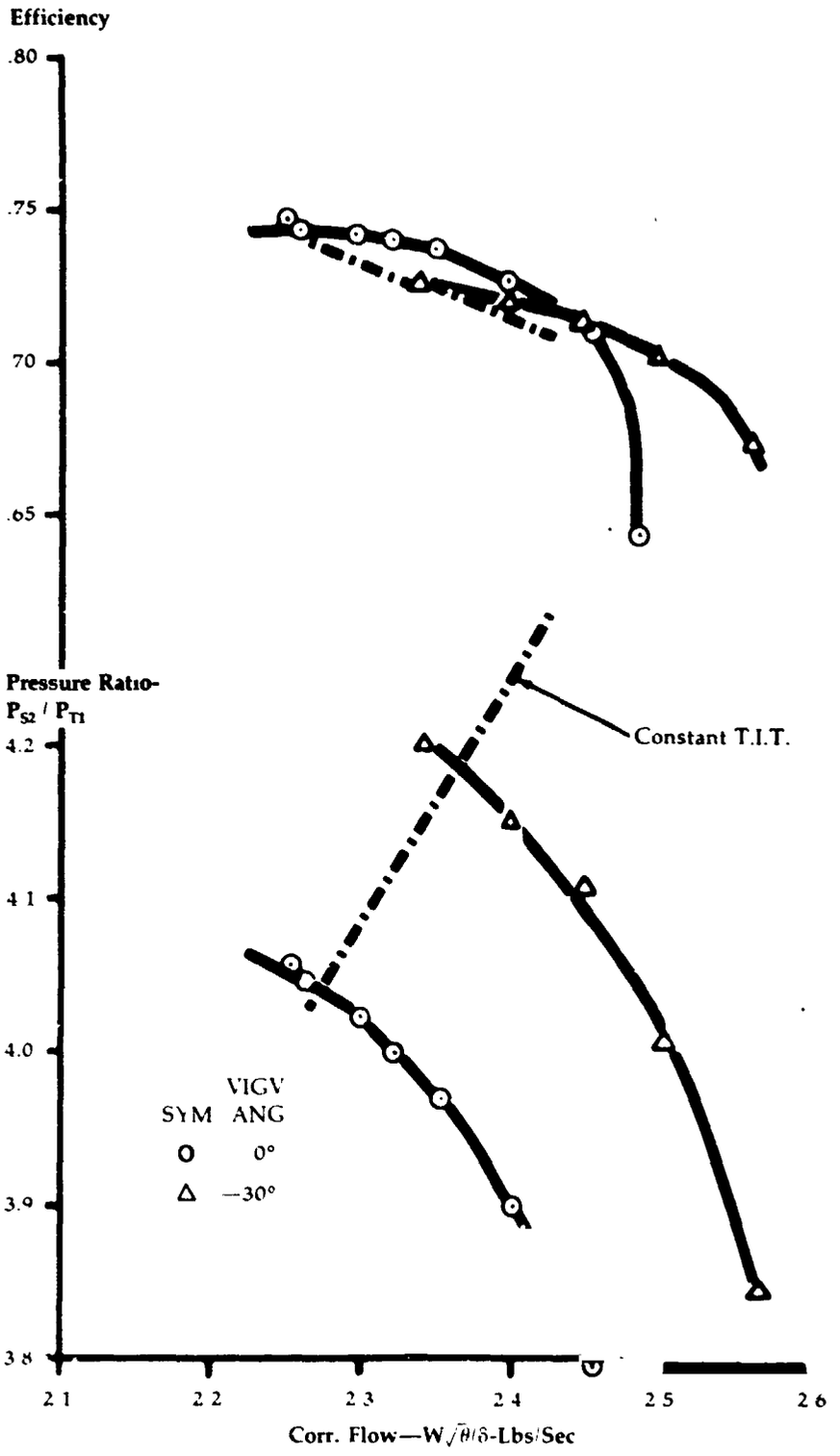

Figure 94

Effect of VIGV Angle on Peak Power at 100% Corrected Speed

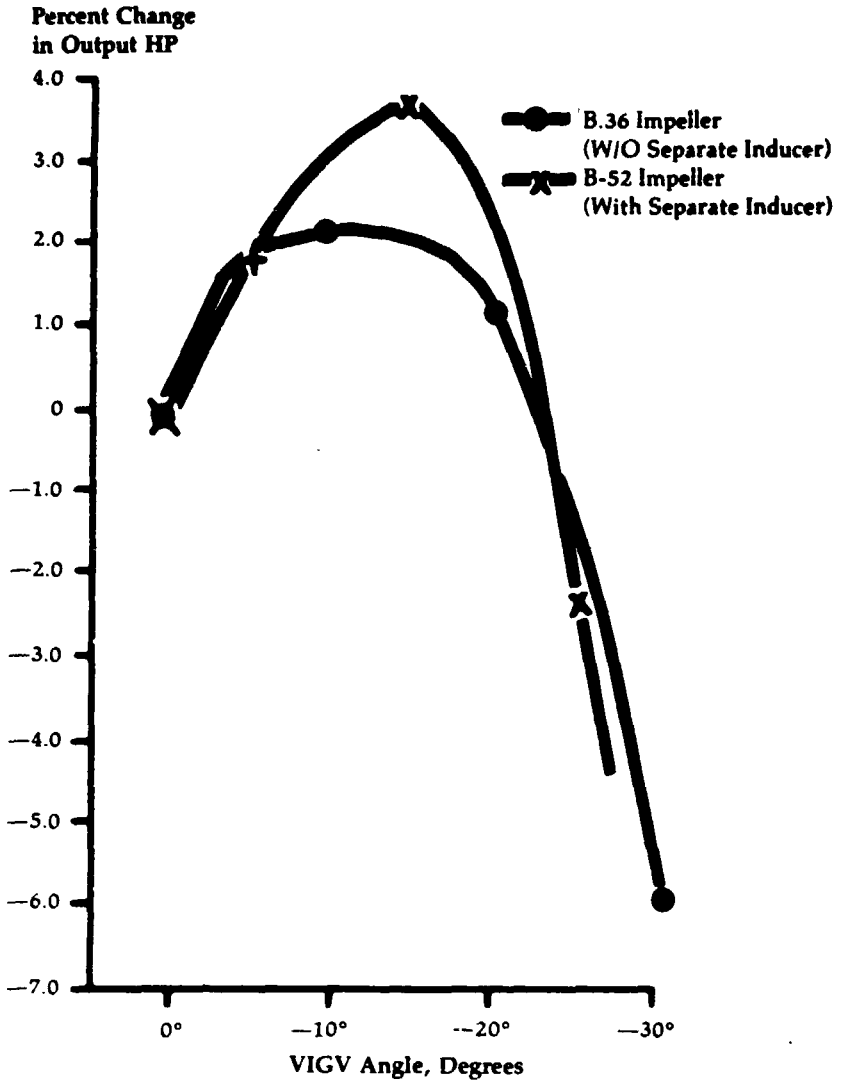

Figure 95

Variable Inlet Guide Vane Tests Power Augmentation at 100% Corr. Speed Compressor Test Results

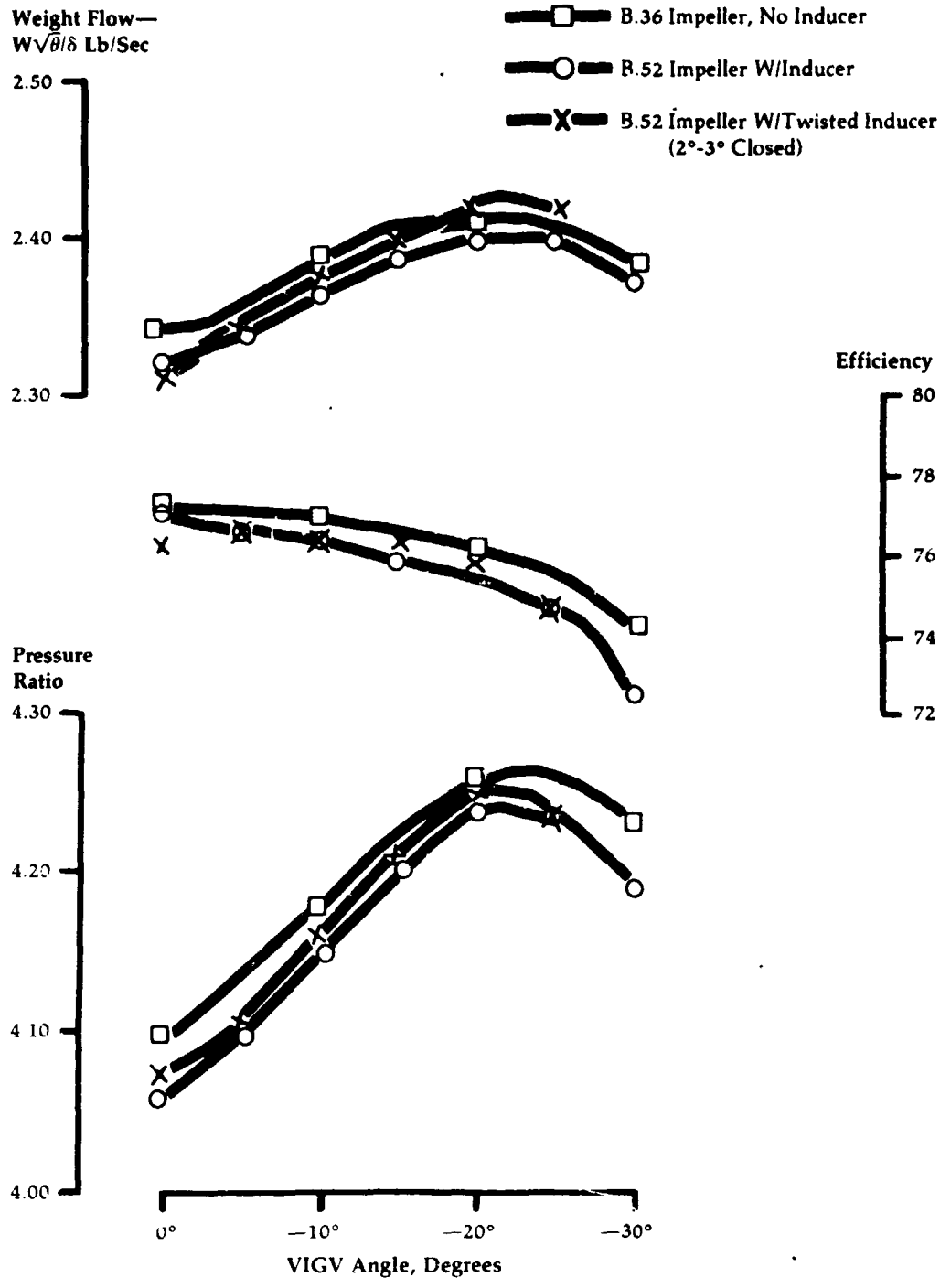

Figure 96

VIGV Loss Characteristics

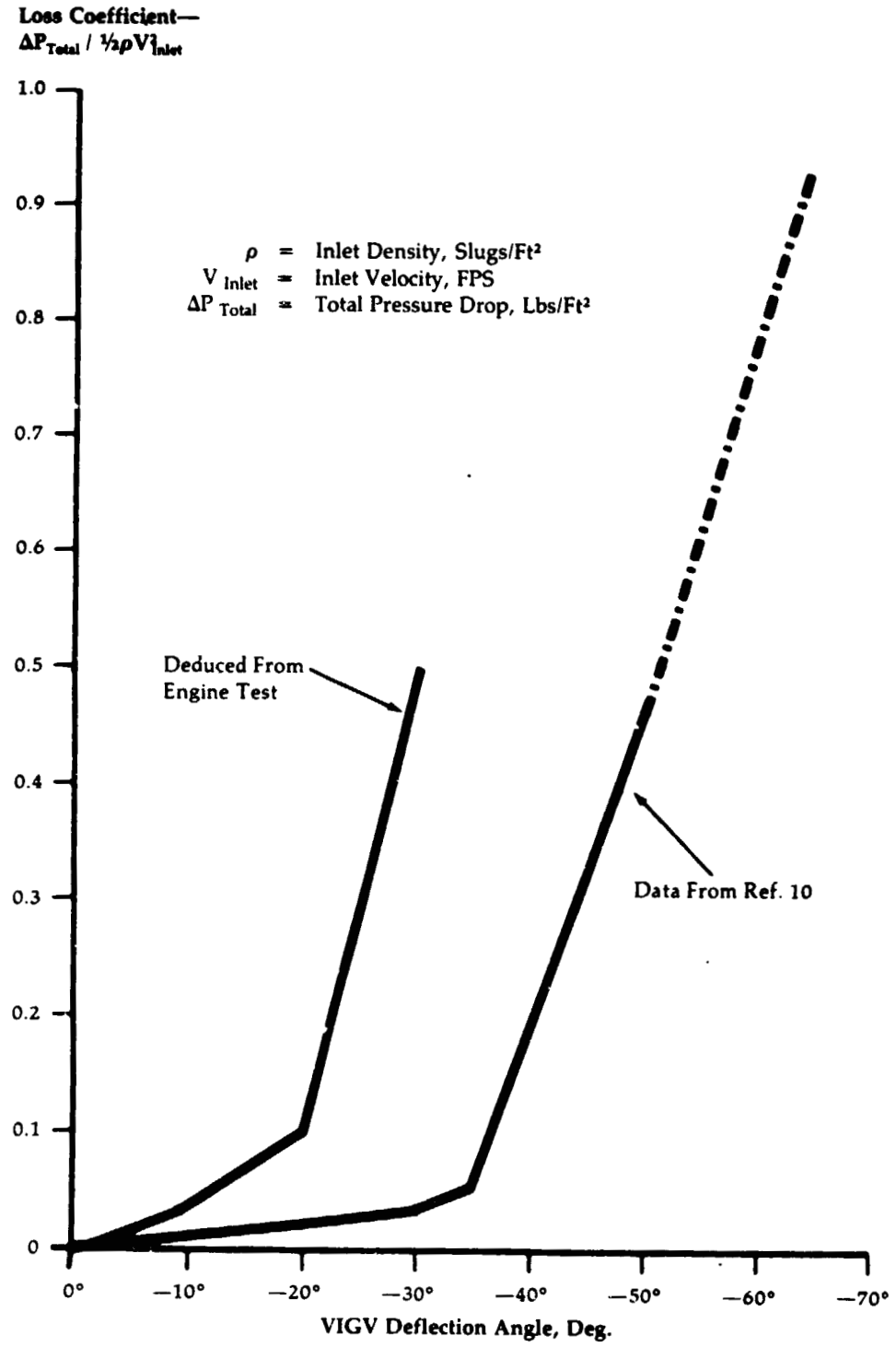

Figure 97

Instrumentation Behind Variable Inlet Guide Vanes on Baseline Engine

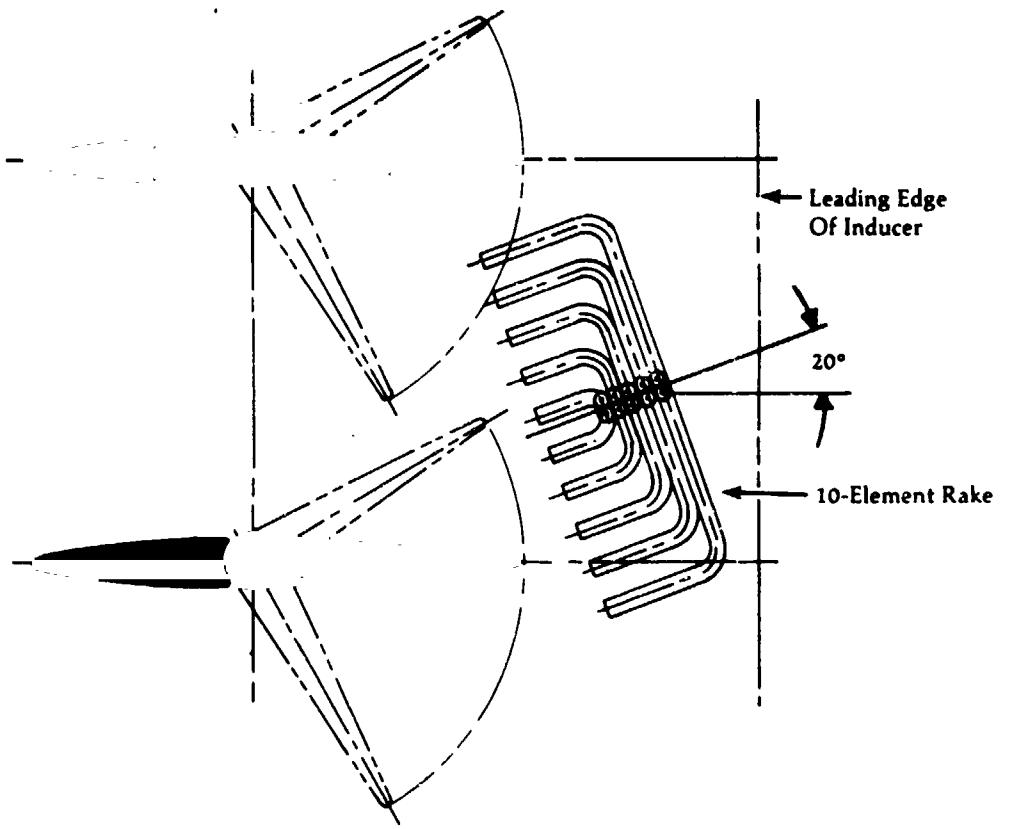

Figure 98

Variable Inlet Guide Vane Loss Characteristics

Comparison of Experimental Pitch-Line Loss Coefficients with Cascade Data and Deduced Values from Baseline Engine Compression Test Data

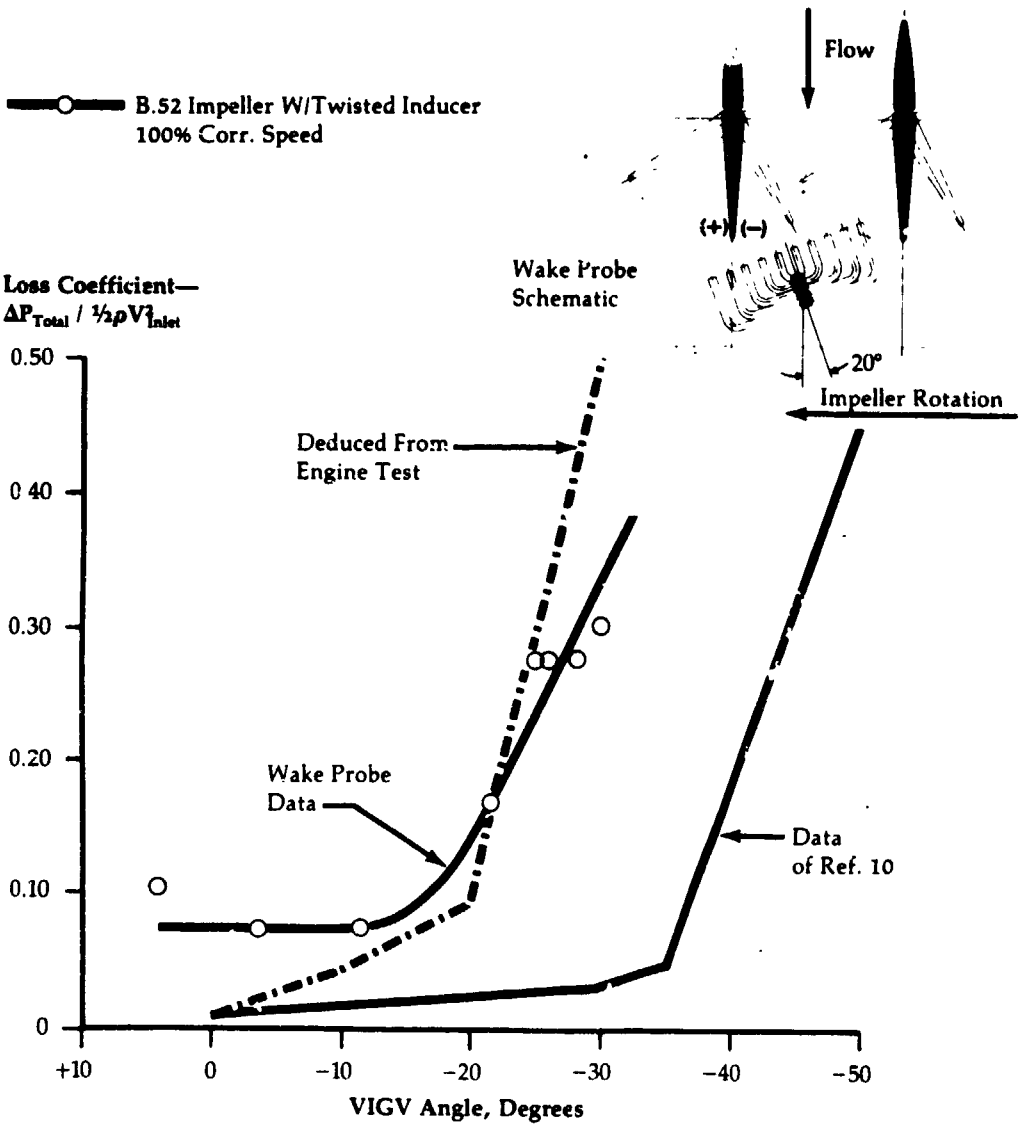

Figure 99

Comparison of Original vs. Revised VIGV Forward Section on Baseline Engine

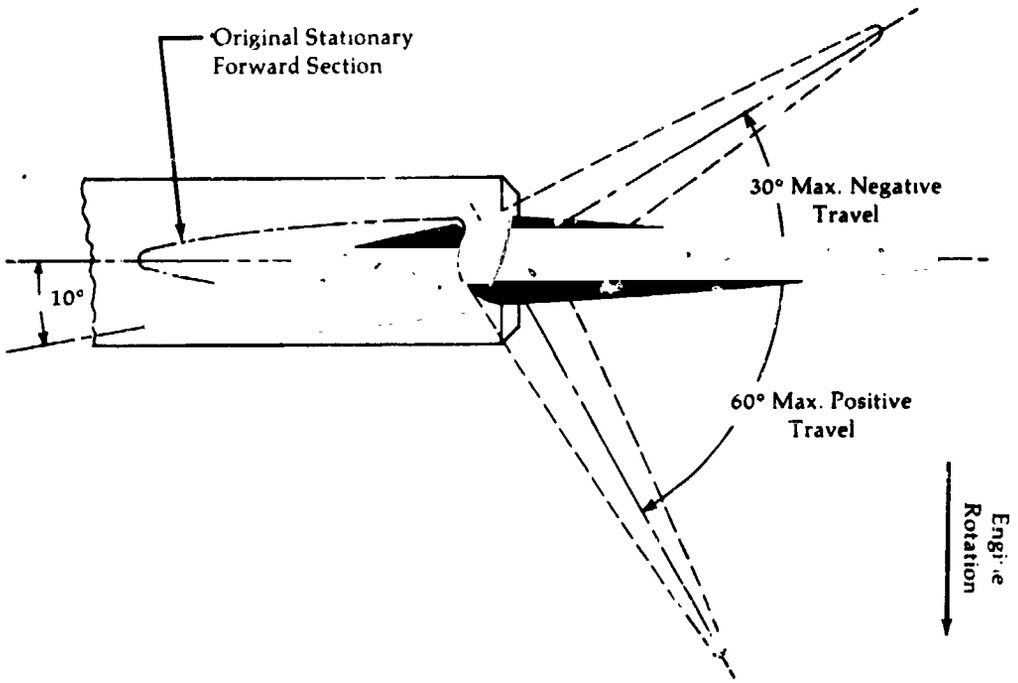

Figure 100

Engine Parameter Characteristics With VIGV Augmentation at 100% Corrected Speed

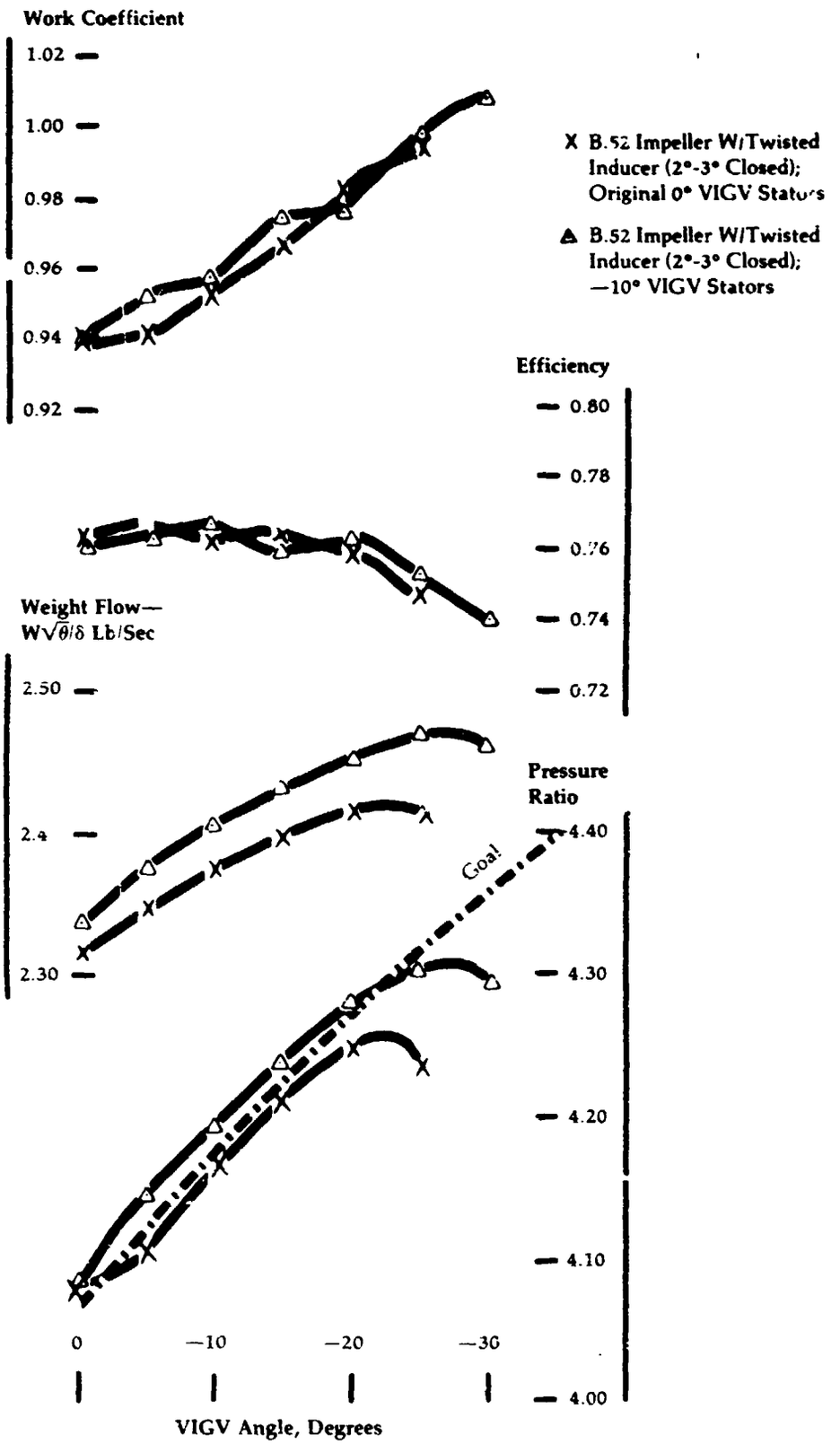

Figure 101

Variable Inlet Guide Vane Tests Compressor Efficiency and Pressure Ratio at 50% Corr. Speed Peak Power Points

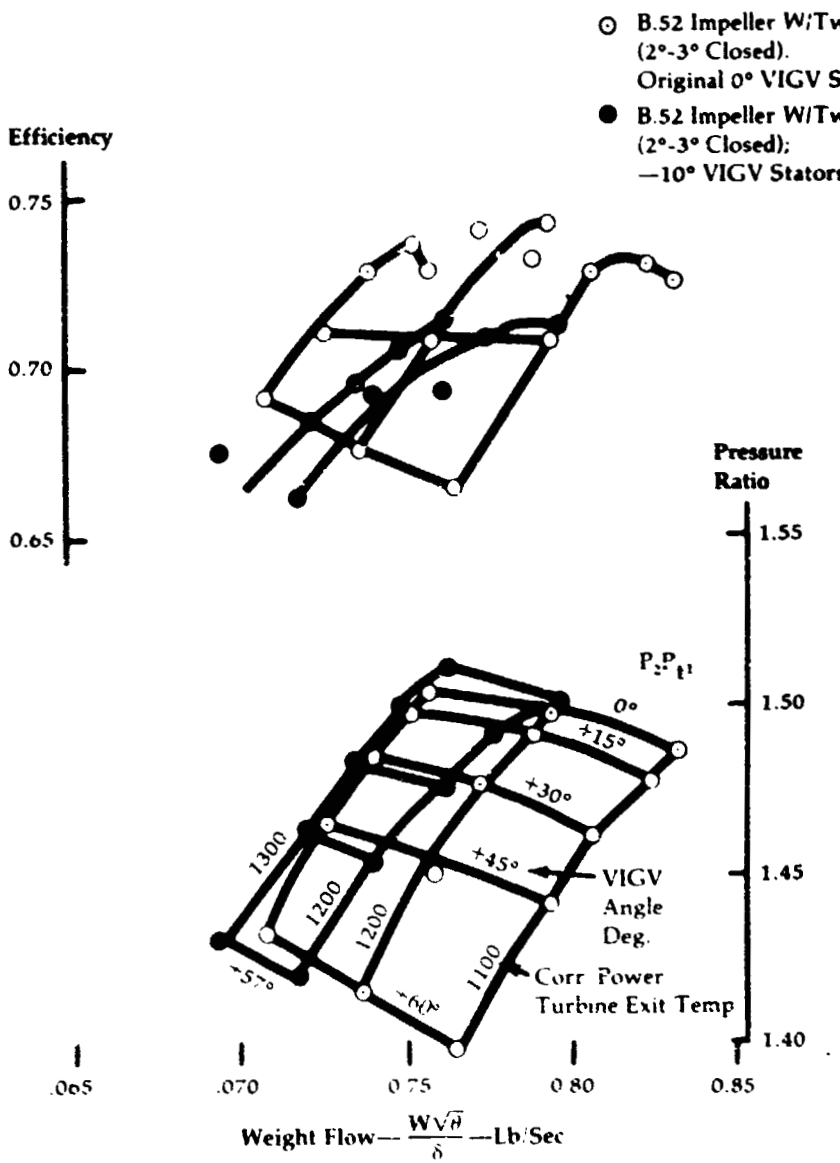

Figure 102

Effect of VIGV Angle on Peak Power at 100% Corrected Speed

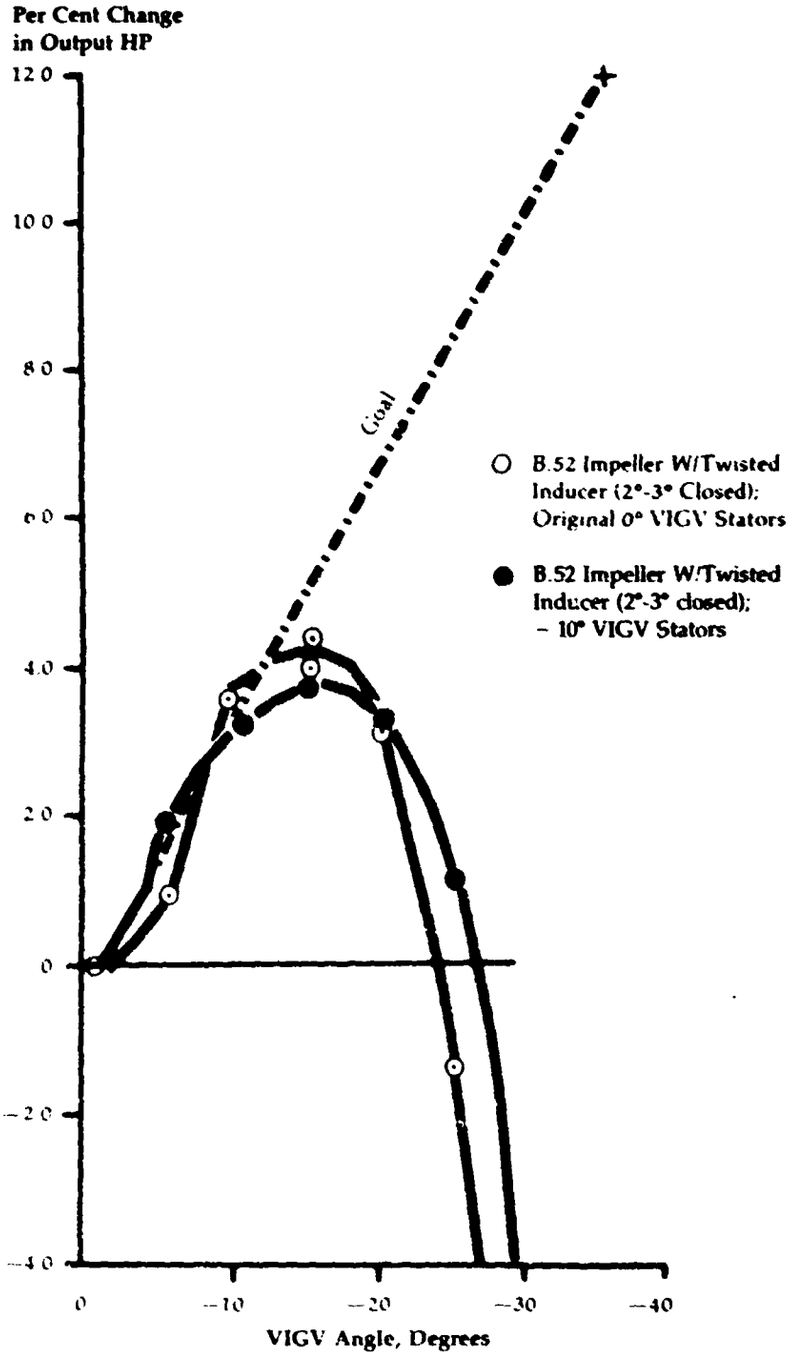

Figure 103

Gas Gen. Turbine Characteristics with VIGV Augmentation at 100% Corr. Speed

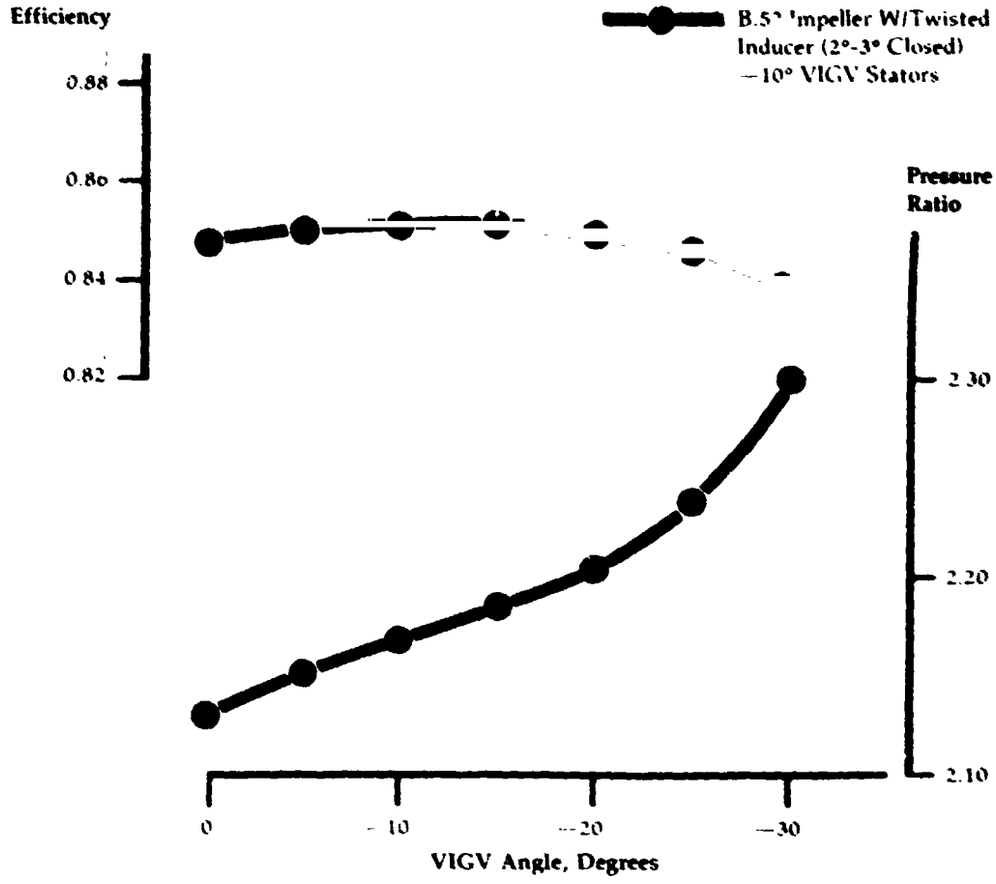

Figure 104

Power Turbine Characteristics with VIGV Augmentation at 100% Gas Generator Speed

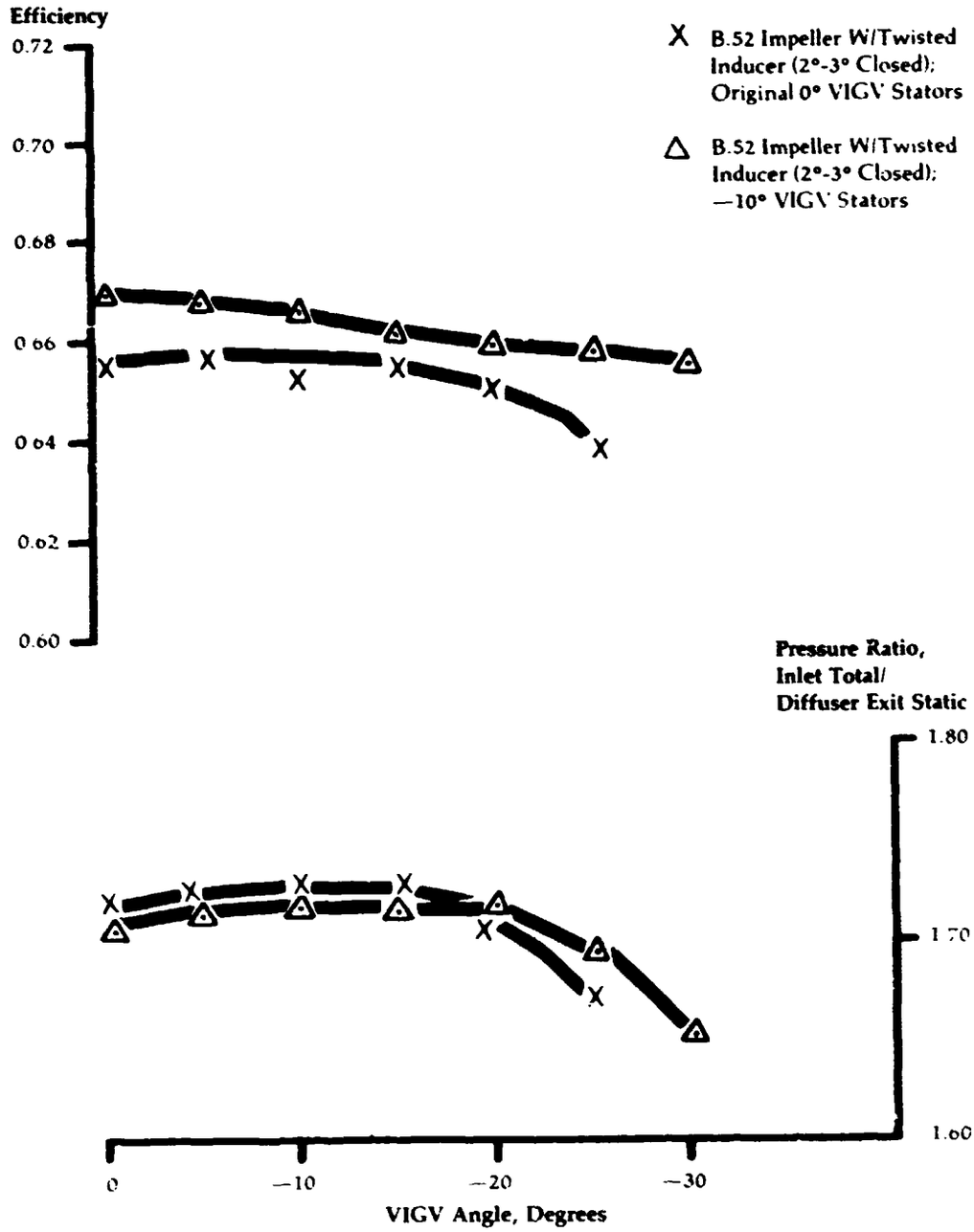

Figure 105

Effect of VIGV Angle on Peak Power at 100% Speed

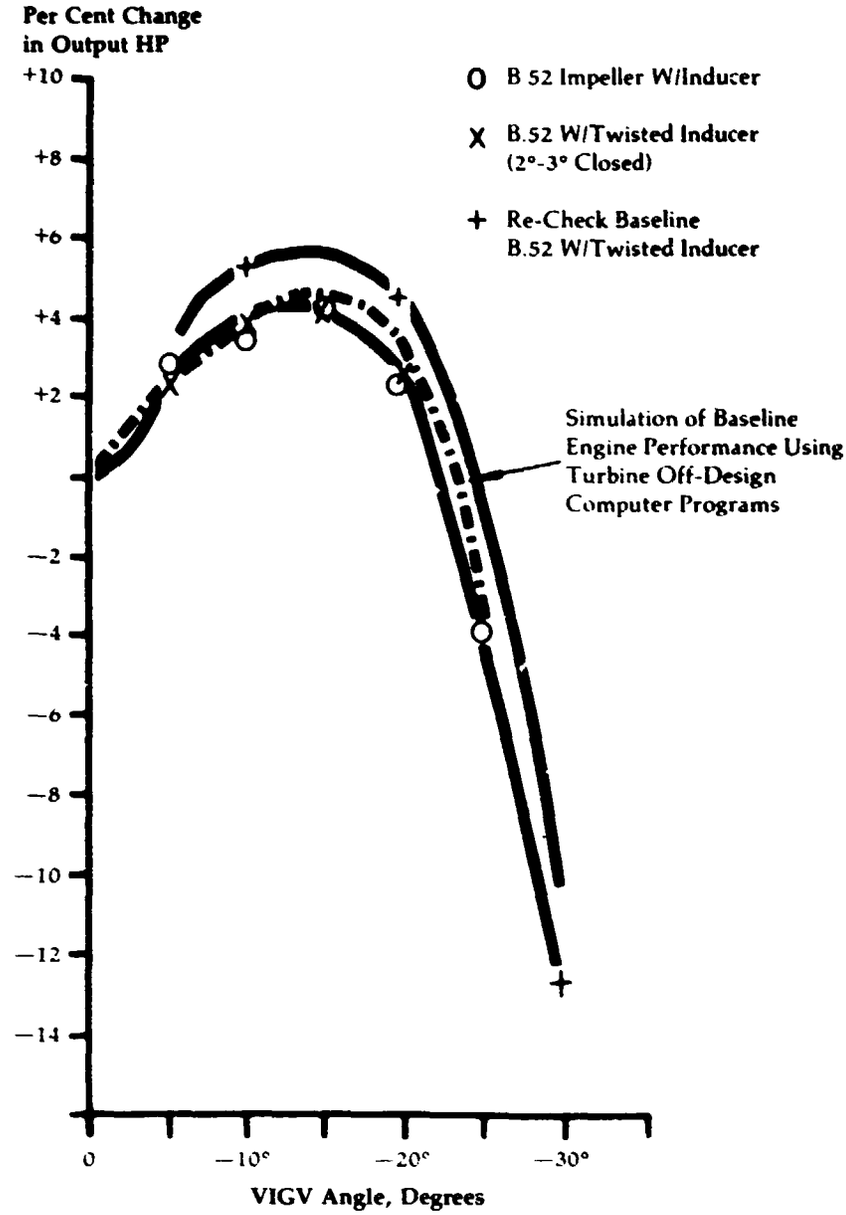

Figure 106

Variation of Turbine Efficiencies with VIGV Augmentation at 100% Speed

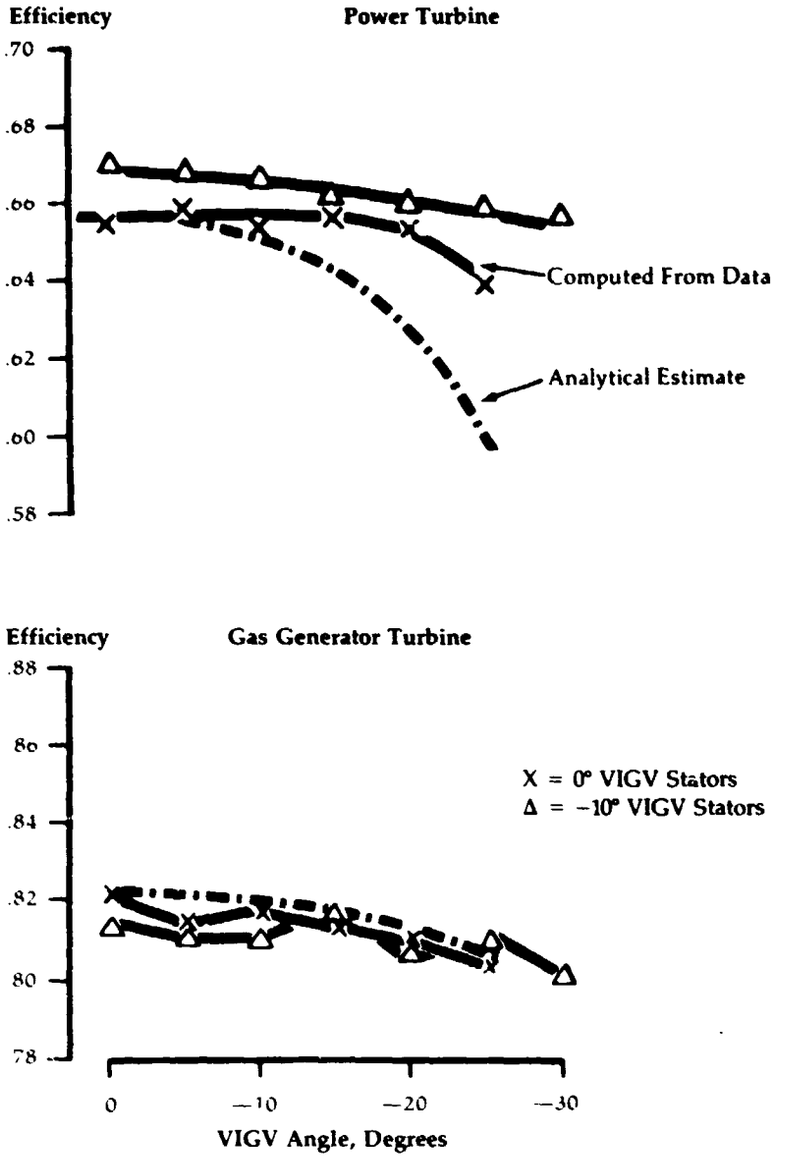

Figure 107

Finite Element Model of Baseline Engine Bulkhead-Quarter Section

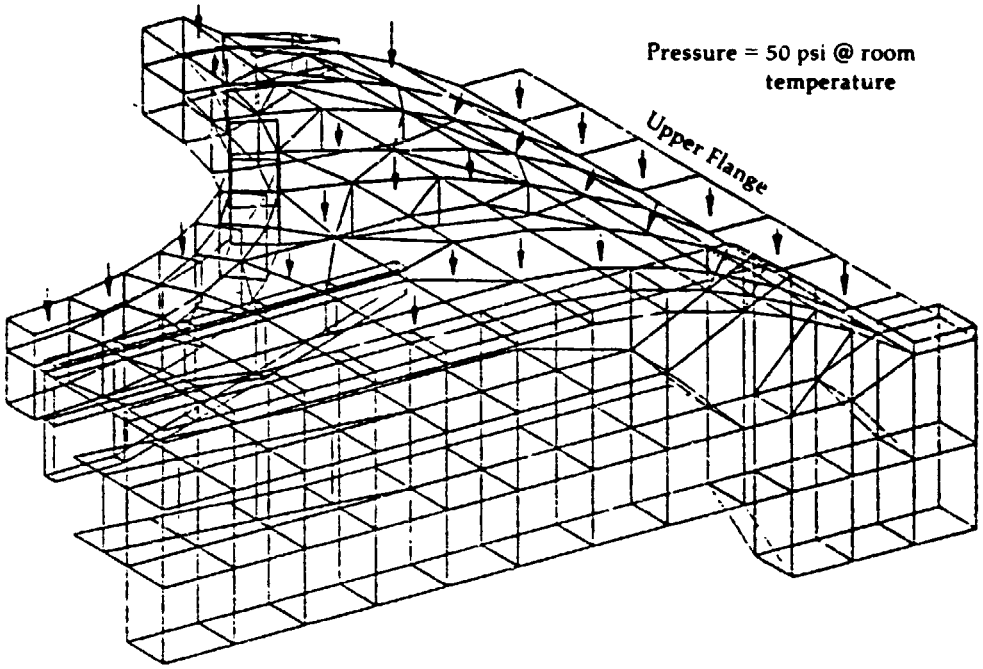

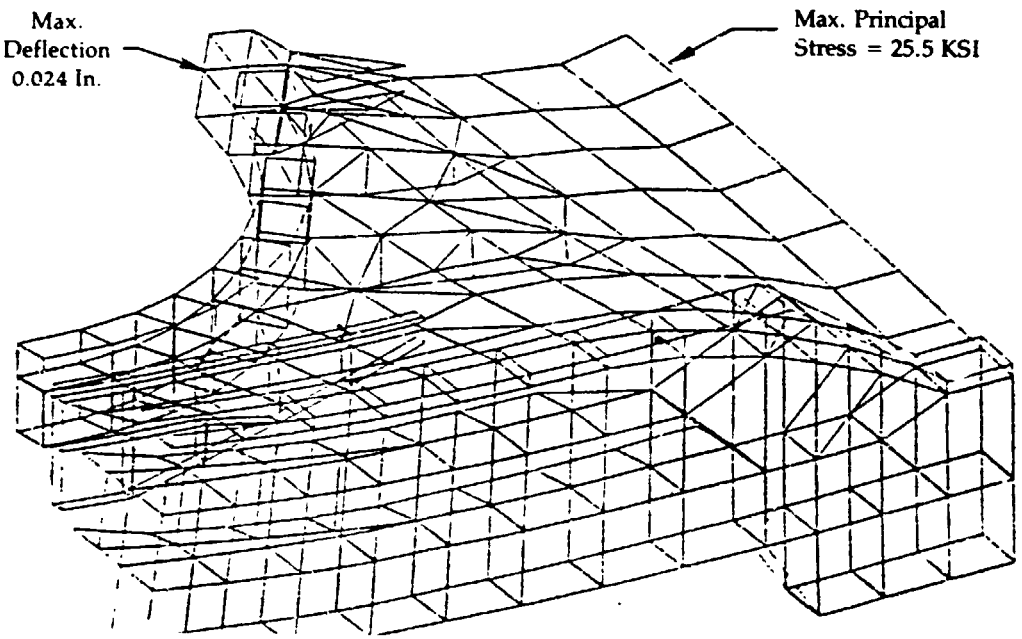

Figure 108

Summary of Baseline Engine Bulkhead Deflections

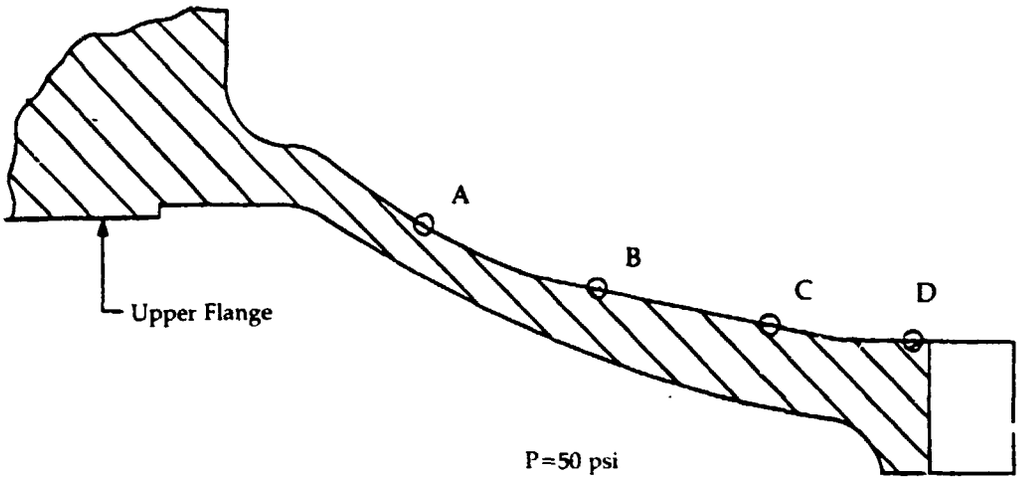

Location	Load (PSI)	Deflection - (In)		
		Nastran		
		Rigid	Guided Cantilever	Measured
A	50	.0080	.0120	.0118
B		.0120	.0170	.0190
C		0140	.0210	.0240
D		.0150	0240	.0265

Figure 109

Baseline Engine with Linerless Insulation

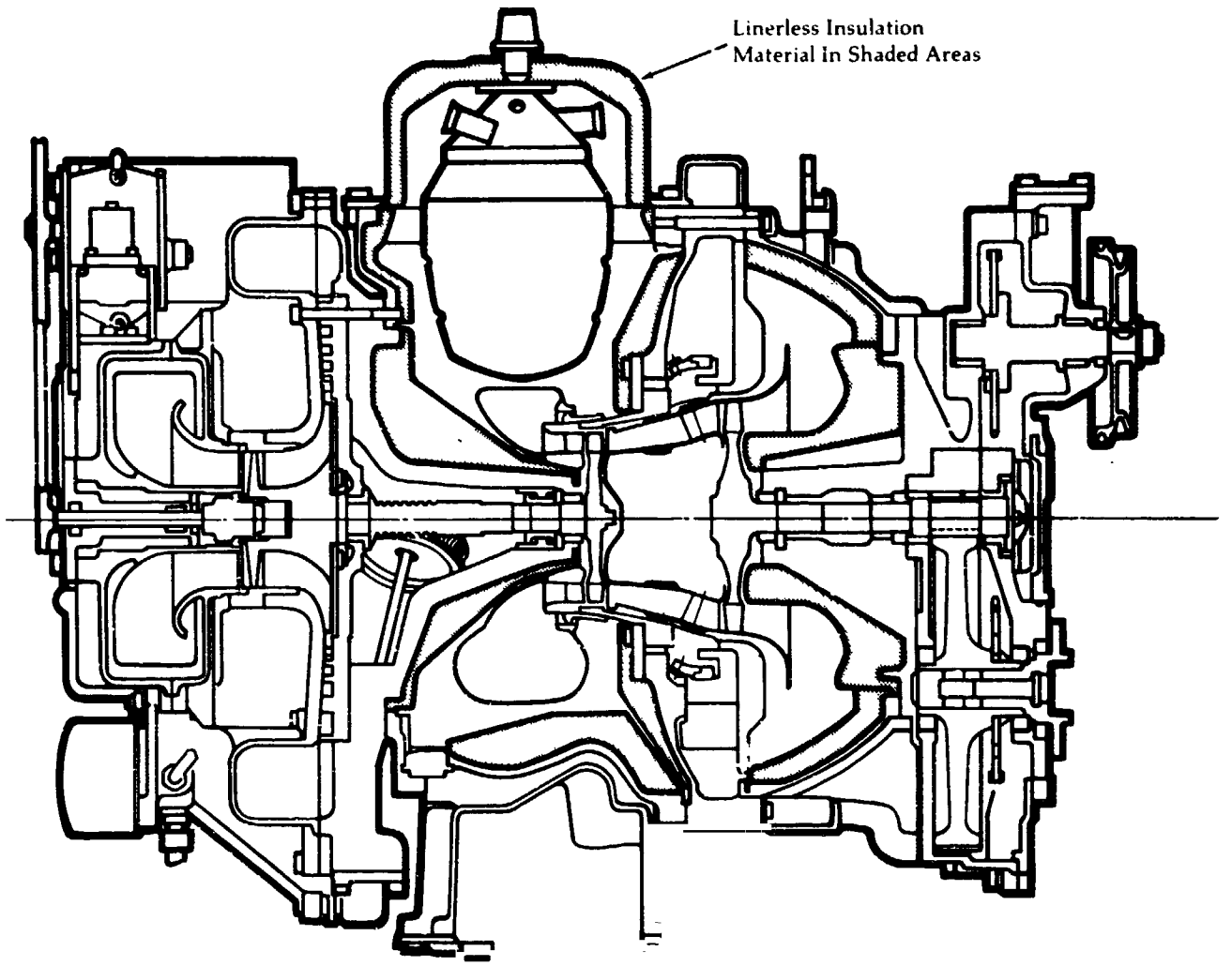

Figure 110

Linerless
Insulation in
Gas Generator
Assembly

Figure 111

Linerless
Insulation in
Power Turbine
Assembly

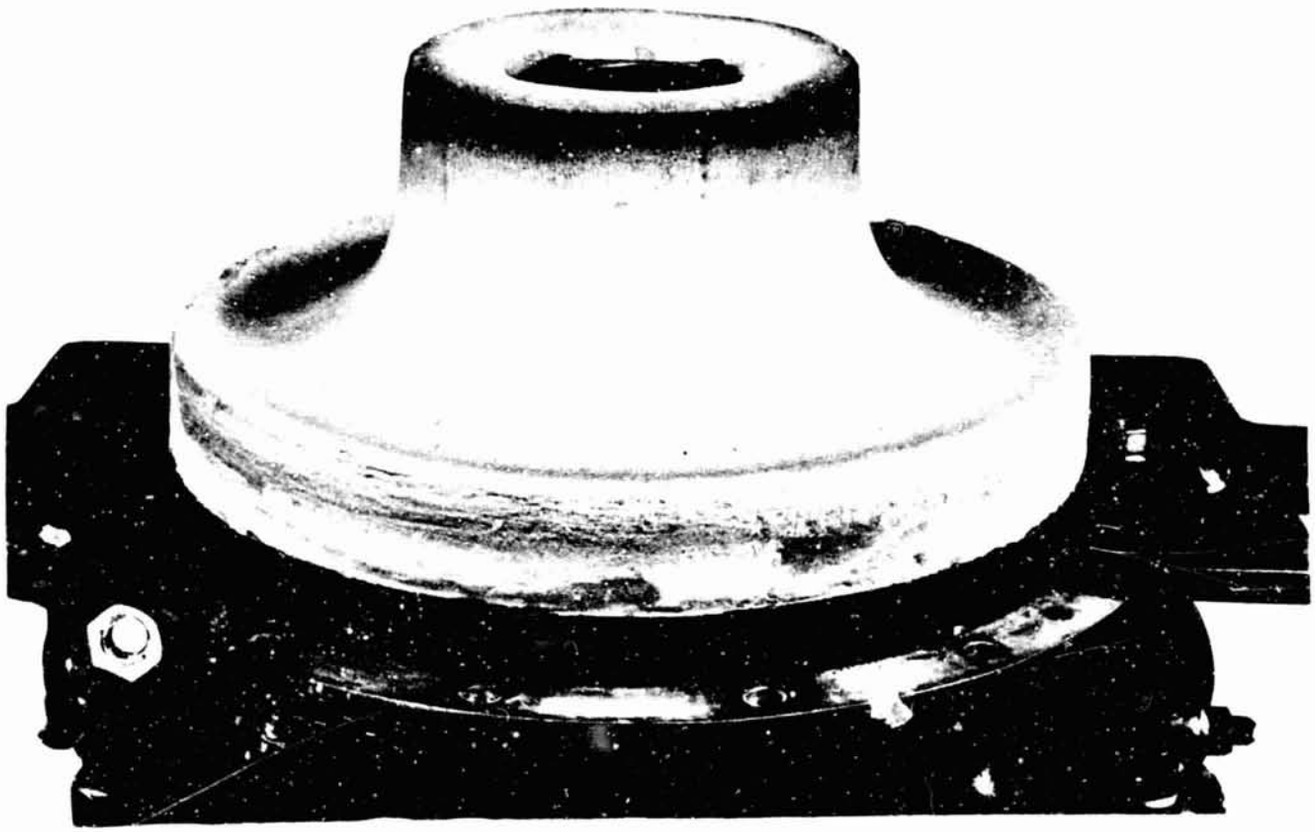

Figure 112

Effect of Insulation Type On Fuel Economy

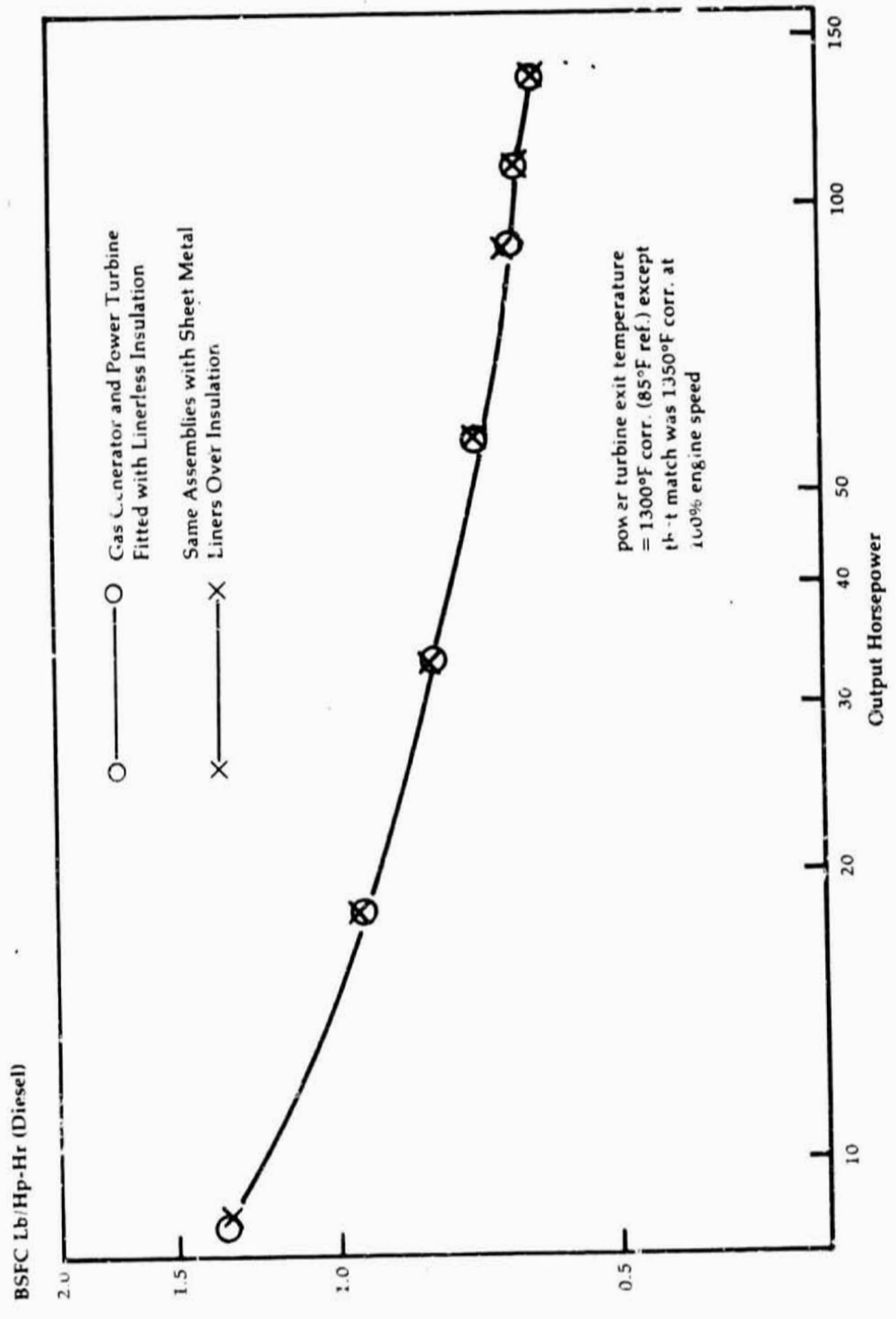

Figure 113

Linerless
Insulation in
Complete Baseline
Engine Housing

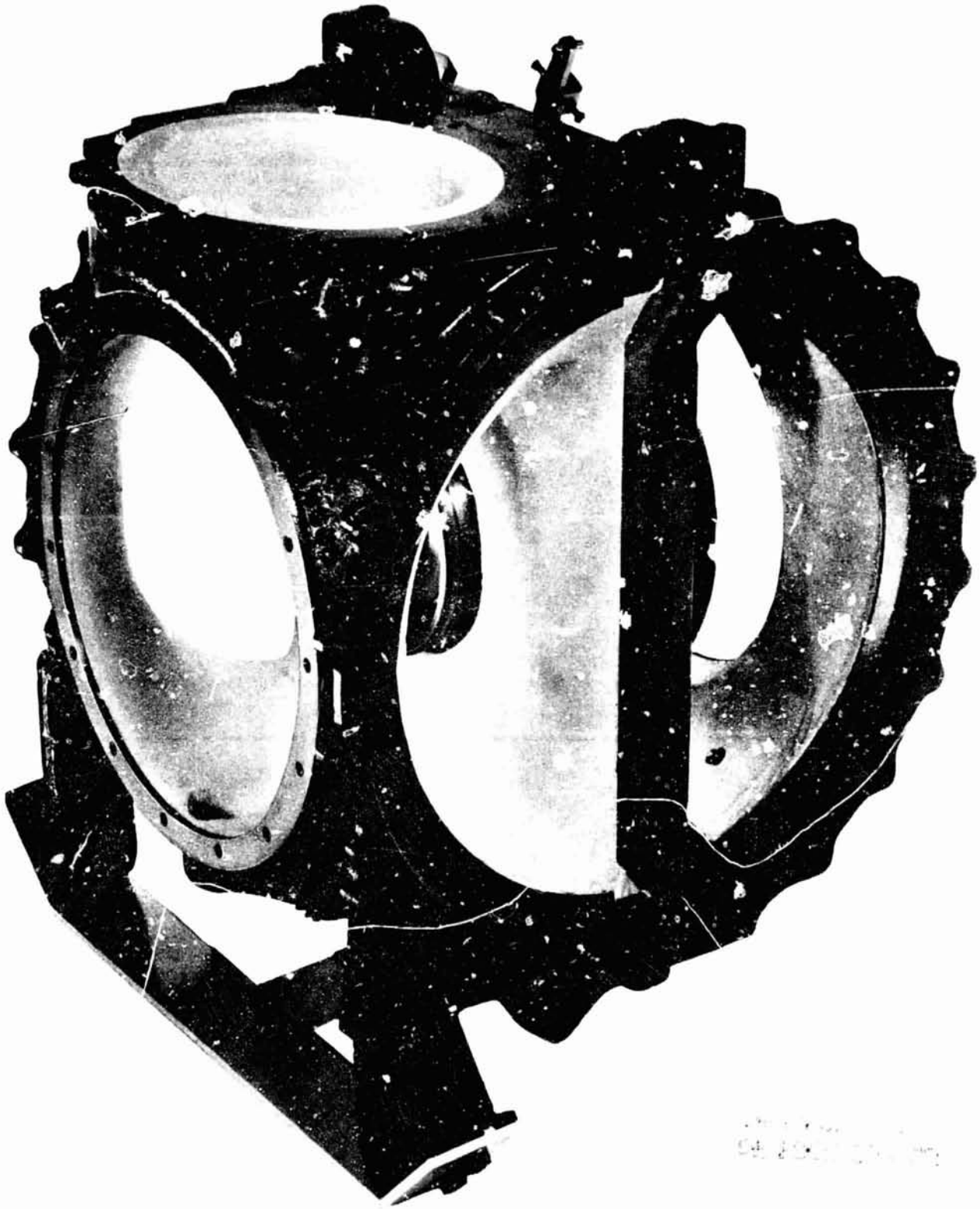

Figure 114